Southern African Climatic Anomalies, Summer Rainfall and the Angola Low

Henry Mubanga Mulenga

Oceanography Department
University of Cape Town, Cape Town

Thesis submitted to the Faculty of Science
for the Degree of Doctor of Philosophy

October, 1998

I declare that this thesis is my own, unaided work. It is being submitted for the degree of Doctor of Philosophy in the University of Cape Town, Cape Town. It has not been submitted before for any degree or examination in any other university.

CONTENTS

CHAPTER 3

MATHEMATICAL TECHNIQUES AND DATA

Glossary/ Acronyms

Definition of southern Africa

Southern Africa in this thesis is defined as the region south of 5°S. In this region most countries of Southern African Development Community are found (see figure 2.1(a) and 2.1(b)).

The following abbreviations are used in this thesis:

SADC	: Southern African Development Community
WMO	: World Meteorological Organisation
SST	Sea surface temperature
SSTA	: Sea surface temperature anomalies
ECMWF	: European Centre for Medium-Range Weather Forecasts
CLIVAR	: Climate Variability Research Program
TOGA	: Tropical Ocean Global Atmosphere
MJO	: Madden and Julian Oscillations
MAM	: March, April and May season
JJA	: June, July and August season
SON	: September, October and November season
DJF	: December, January and February
PCA	: Principal Component Analysis
PC	: principal component
r	: correlation coefficient
SOI	: Southern Oscillation Index
ENSO	: El Nino and Southern Oscillation
MSLP	: Mean sea level pressure
QBO	: Quasi-Biennial Oscillation
OLR	: Outgoing Longwave Radiation

Regional summer rainfall and sea surface temperature features

Significant features of southern African summer rainfall variabilities are revealed over Angola, Malawi, Zimbabwe and southern Zambia and the Eastern Cape in South Africa through principal component analysis (PCA). The Angola rainfall feature contributes most to interannual variability. A declining summer rainfall trend displays a north-west to south-east orientation over southern Africa with a rising trend over the north-east of the subcontinent. Decreasing DJF rainfall over southern Africa is linked to ENSO temporal characteristics through varying sea surface temperatures anomalies over the Central Indian Ocean. In a PCA of SST in the Atlantic and Indian oceans, four tropical and five subtropical features account for 27% and 16% of the total variance respectively. Warming/cooling in the subtropics and cooling/warming in the tropics lead to wet/dry summers over southern Africa.

Teleconnections

Finally, coherent spatial and temporal variabilities of SST, tropospheric circulation and convection anomalies through combined PCA reveal four significant features of variations and account for 62% of the total variance. It is found that summer droughts/floods patterns are associated with different sea surface temperature and circulation anomalies. Local forcing (internal, 21%) through the Angola Low contributes most to interannual variations of summer rainfall anomalies and is linked to warm water in the subtropics. The second feature (external, 16%) of the joint PCA is characterised by ENSO driven circulations and SST anomalies and thus making forecasting seasonal rainfall predictable.

Significant tropical teleconnection patterns are found to be more dominant than midlatitude patterns in tropospheric continuous monthly data. ENSO has a major impact on African climate. It can explain about 36% of the total variance of seasonal (DJF) 500hPa geootential height anomalies and 16% of the total variance of seasonal (DJF) OLR anomalies.

LIST OF FIGURES

LIST OF TABLES

Acknowledgements

This thesis could not have been written without the support and co-operation of the University of Cape Town Oceanography staff. I am very grateful to my supervisors Profs. Mark Jury and Geoff Brundrit who provided the guidance, endless encouragement and inspiration. Special thanks to Prof Brundrit for his inexplicable sympathy during my mother's bereavement. I thank Mark Majodina, Emmanuel Mpeta, Vuyisa Tanga and Annabela Brando for their assistance and lively sense of humour which, usually enervated the morbidity of a PhD study room. I am extremely indebted to Water Research Commission. This thesis was made possible by grants from the Carnegie Corporation of New York, the Rockefeller Foundation, the Ridgefield Foundation, and the Coca Cola Foundation, through the USHEPiA Programme. The statements made and views expressed are solely the responsibility of the author. The study leave, which the Zambia Meteorological Department granted me, is highly appreciated. I must also mention the professional advice I received from Profs. J.R.E. Lutjeharms, F.A.Shillington, B. Wang, R. Madden, D. Karoly, B.C. Weare and Drs. C. Reason and S.J. Mason.

I am grateful to my wife, Chao and the children, Idah, Mukuka and Chikumbutso for their understanding and patience during the period of study. Special thanks to my wife for practically sharing the burden of preparing the thesis.

To my parents Frank and Helen Mukuka Mulenga

CHAPTER 1

1 INTRODUCTION

1.1 Motivation

Anomalous climatic conditions have contributed to poverty, vulnerability and unemployment, which are major concerns of many southern African governments. Western countries continue to give food aid during drought periods and are looking for new and effective ways of supporting national food security plans (Walker, 1989a). Food security is a very difficult problem in Africa. A number of agricultural national programs have been planned to alleviate the problem but crop yields and living standards continue to deteriorate in many African countries. Unfavorable macro-economic conditions, debt repayments, civil war, political instabilities and mismanagement of resources make the situation more complex. It may be considered that anomalous climatic events (droughts or floods) are important factors, which contribute to acute food shortage.

Seasonal rainfall forecasts are an important management tool for donor countries as well as local farmers. The failure to utilize forecasts based on sound scientific knowledge would negate attempts at achieving food security (World Meteorological Organization, 1996). It is for this reason that rainfall is an important input parameter in attaining self-sufficiency in food. Rainfall varies in space and time over southern Africa (Preston-Whyte and Tyson, 1988; Walker 1989b; Mason, 1992; Rocha, 1992; Makarau, 1995). Further investigations of year-to-year variability of southern African summer rainfall are required in order to understand mechanisms and make accurate seasonal forecasts. Therefore, research work in climate should have high priority in African countries. The need to understand and predict the interannual variations of the atmosphere and the oceans has resulted in formation of global programs like the Tropical Ocean Global Atmosphere (TOGA) and World Climate Research Program (Climate Variability and Predictability, CLIVAR, 1995 and 1998).

Determination of the dynamics of droughts and floods continues to be a major problem. Correct prediction of extreme events such as droughts, floods, cold and warm spells involves knowing the mechanisms as well as the local and remote forcings. Several mechanisms have been suggested but more empirical research is required to understand and predict climate variability of southern African on intra-seasonal and inter-annual time scales. This study focuses on inter-annual and intra-seasonal variability of southern African climate with the view of identifying climatic regional and local features that influence summer rainfall and its fluctuations over southern Africa as whole. In order to achieve this, determination and refining of rainfall-SST anomaly relationships is carried out. Teleconnection patterns and coherent structure of interannual variability are revealed. Atmospheric mean meteorological features over Southern Africa and adjacent oceans have direct impact on summer rainfall. Thus determination of mean features using up-graded new and longer data sets provides a basis for investigating inter-annual and intraseasonal variability. This study presents mean characteristics of peak summer (December, January and February) based on 14 years ECMWF gridded data set.

This study is motivated by a desire to understand climatic controls of inter-annual summer rainfall variability over southern African. The intensity of summer rainfall is modulated on synoptic, intra-seasonal, interannual and decadal time scales. Previous empirical studies have examined inter-annual and intra-seasonal variability within national boundaries using averaged rainfall indices. Links between SST anomalies and specific countries have been determined (Walker, 1989b; Mason, 1992; Rocha, 1992; Makarau, 1995). However, these relationships may not be stable and thus continuous monitoring of links with longer and updated data is required. Determining and refining relationships between various fields in the climate system are important as they often suggest physical mechanisms that influence the system. The relationships can be exploited in climate prediction. No previous attempt has been made to use gridded rainfall data for the whole of southern Africa to find features of variability and then link them to SST anomalies. Other SADC countries have

not been included in the previous analyses. With the availability of new data sets and mathematical techniques, this study focuses on inter-annual and intraseasonal variability of southern African climate. There is a need to use gridded rainfall data and SST to investigate or re-confirm the relationship between SST anomalies and DJF rainfall in southern Africa and this study aims to fill that gap. It is the intention of this study to investigate the role of remote (e.g. SST's) and local (e.g. Angola heat low) forcing in modulating the summer rainfall.

1.2 Scientific issues

Some of the important scientific issues can be raised through questions such as:-

(1) To what extent do remote processes (teleconnections) affect the intensity and distributions of summer rainfall over southern Africa? The answer to this question can be found in combined teleconnection patterns and the coherent structure of variability in remote SST and local circulation variables.

(2) How do the local thermodynamics and circulation dynamics actively determine the summer convection? This is achieved through pentad composite analysis, which demonstrates the influence of the Angola low and its impact on the southern African climate. The quasi-geostrophic model demonstrates the mechanism of the formation of the inland trough and links the strength of the surface heating to the intensity of the Angola low.

Teleconnection patterns, which are also referred to as preferred modes of low frequency variability could persist for several months or years and have an impact on climate. This study investigates regional tropical teleconnections. Identification of SST-forced and internal dynamics-forced summer circulation anomalies is carried out. Links are established between the north-south SST gradient over the Indian Ocean and rainfall anomalies over southern Africa.

Over southern Africa, surface heating plays an important role in modulating the low -level circulation. Land processes may be important to the summer circulation. Warm conditions in early summer over southern Africa may be linked to regional or global circulations, which provide the land surface with

excess (or deficit) moisture relative to the long-term mean. Vegetation also plays an important part in modulating rainfall. In this study the role of continental surface heating and the contrast between land and oceanic regions is investigated. The influence of the heating anomaly over southeast Angola has not been given much attention. Currently most studies (Rocha and Simmonds,1997b; Rautenbach, 1997) emphasize the influence of SST anomalies. The effects of land-sea thermal contrast and other physical processes have been neglected in most studies. The Benguela upwelling leading to cold coastal temperatures and the heated plateau over Angola (Bie plateau, see **figure 2.1(b)**) provide a large meridional temperature gradient which is important in developing the Angola low. The Angola low has an important effect on the development of the onset and the subsequent nature of the summer season. The Benguela upwelling may affect the intensity of the heat low over Angola, which is closely related to summer rainfall.

Surface heating plays an important part in creating an inland low, which is important for 'drawing' moisture. The differential heating over land alone cannot maintain the summer rainfall patterns for a long time. The summer rainfall also depends on adjacent oceanic monsoons (e.g. moisture transport from the Indian sector and Atlantic Ocean, through recurved trade winds i.e. Congo air). Local heating may play an important part in controlling the strength of the low level moisture convergence. The presence of strong differential heating may support propagating and stationary modes but weak differential heating may be unable to support the low -frequency modes. Differential heating at the interannual time scale may be evident through the presence of upper level westerlies (cool dry conditions), in contrast with easterlies which favor upper level warming. The upper level warming associated with easterlies is hydrostatically more effective in inducing a low pressure area near the surface and may favor wet summers.

1.3 Objectives

It is the intention of this thesis to investigate the temporal and spatial variations of regional circulation and the influence of oceanic anomalies. This is achieved through the documentation of inter-annual variability of regional SSTA, which may represent remote forcing. Local forcing is also present and is revealed through the intra-seasonal study. Quasi-geostrophic modeling of the formation of a trough over southern Africa is carried out. The dynamics of the Angola low based on a quasi-geostrophic model will be revealed to explain some of the major processes involved in its formation. Heating distributions depend on temperature gradients; moisture convergence is controlled by the intensity of the Angola low. The absence of heating (both sensible and diabatic) over the plateau can result in the presence of upper level westerlies prevailing over southern Africa. Mean characteristics of the thermal and kinematic fields over southern Africa play significant role in determining the state of atmosphere (i.e. surface sensible fluxes, moisture convergence and convective of the mid-troposphere).

The main goal of this thesis is to establish the major climatic features, which influence summer rainfall and its variations over southern Africa as whole. In achieving this goal it is necessary to investigate the regional circulation features which are dominated by Angola low in summer, rainfall and climate anomalies over an extensive 1950 to 1989 period. The ECMWF data-set over limited period 1980 to 1993 provides better resolution. A quasi-geostrophic model is used to confirm a possible mechanism for the formation and intensification of the Angola low. The specific aims, which form the work-plan in achieving the goal of the thesis are as follows:-

(i) To describe the mean summer circulation of southern Africa and adjacent Oceans and provide an interpretation.

(ii) To document the spatial and temporal characteristics of southern African summer rainfall and Sea Surface Temperature (SST) anomalies in the adjacent tropical Atlantic and Indian oceans.

(iii) To identify and reconfirm some statistical associations between summer rainfall features and SST anomalies.

(iv) To identify summer SST, tropospheric circulation and convection anomalies associated with dry and wet seasons. To identify tropical teleconnection patterns with continuous monthly data and link them to ENSO.

(v) To document temporal and spatial characteristics of intra-seasonal oscillations. To determine thermodynamics and dynamic structure of the atmosphere associated with deep convective activities over Angola in order to demonstrate the role of the Angola low in modulating seasonal rainfall.

(vi) To model the formation of the inland surface trough using quasi-geostrophic theory.

1.4.Lay-out of the thesis and hypothesis

The above mentioned objectives and hypothesis are addressed in this thesis which consists of eight chapters. **Chapter 1** has provided an introduction, motivation and hypothesis. **Chapter 2** provides a literature review. It discusses observational, theoretical and modeling studies concerned with southern African rainfall. Characteristics of southern African rainfall and mechanisms are briefly mentioned. Southern African rainfall bearing systems and large-scale circulations (i.e. quasi-stationary, teleconnectionsa nd intraseasonal oscillations) are noted. Work on the importance of teleconnections and oceanic processes (e.g. SSTA, ENSO) is cited.

Chapter 3 is concerned with the mathematical techniques and data. Techniques that are useful in determining the spatial and temporal structure of variability in climate systems are: Spectral Analysis, Principal Component Analysis (PCA), Correlation and Composite techniques. These techniques are described. European Center for Medium-Range Weather Forecasts (ECMWF) atmospheric, CRU historical rainfall and UKMO SST data sets are briefly described.

Chapter 4 documents the mean summer circulation characteristics as a background to understand inter-annual variability. Mean fields of thermodynamic and kinematic parameters based on 14-years are computed.

Identification of significant features e.g. interior low (Angola) and interpretation of the mean fields are accomplished. Interpretation in terms of linear theory and simple climatic model is carried out.

Features of southern African summer rainfall and sea surface temperature variability are revealed in **chapter 5.** Determination and refining of relationships between summer rainfall and adjacent oceans' SSTA are done in chapter 5. Time and space structure of interannual summer rainfall is analyzed. Chapter 5 shows that Angola feature contributes most to inter-annual variability. The variability of standardized SST anomalies in the spatial and temporal domain is revealed.

Chapter 6 documents low frequency variability over southern Africa and adjacent oceans. It reveals summer coherent structure involving sea surface temperature, lower and upper tropospheric winds and convection of anomalies. The coherent structure provides knowledge on external and internal forcing of convection anomalies. Separation of internal and external forcing is important for seasonal rainfall forecasting and has not been done previously in southern Africa. Chapter 6 illustrates that summer droughts/floods are due to different mechanisms. The chapter also looks at atmospheric teleconnections, which are crucial in modulating weather systems. Midlevel pressure and convection seasonal anomalies are correlated to SOI. The aim of studying the time/lag correlation between different fields is to ascertain if any predictive relationship can be obtained. Low frequency propagating features associated with mid-level pressure-anomalies are revealed in this chapter.

Chapter 7 demonstrates importance of intra-seasonal variations in summer rainfall and the link to local forcing through the Angola low. Temporal characteristics of Angola convection anomalies need to be revealed. Thermodynamic and kinematic fields associated with Angola convective anomalies are revealed. Antecedent conditions before wet spells are required for forecasting purposes. Determination of temporal characteristics is done through Spectral Analysis. Composites of atmospheric variables associated with intra-seasonal convective activities over southeast Angola are presented.

Thermal forcing fields representing the heating contrast between land and sea are given. A final hypothesis to be tested in this thesis is that the formation and intensity of Angola low depends on local processes rather than remote forcing. Modeling of the formation of the heat low is carried out in this chapter in order to test the hypothesis.

The conclusions are presented in **chapter 8** in which significant findings are given greater prominence.

CHAPTER 2

LITERATURE REVIEW

2.1 Introduction

The objective of this chapter is to provide a literature review related to characteristics of southern African rainfall, rainfall-bearing systems, quasi-stationary waves and features associated with sea surface temperature anomalies. Statistical and modeling methods have been used to advance knowledge in understanding the mechanisms behind rainfall variations in the tropics including southern Africa. Major breakthroughs have been made. As a background to this study, this chapter deals with the relevant literature on characteristics of southern African rainfall and known mechanisms behind rainfall variations. The importance of low frequency disturbances (teleconnections or quasi-stationary standing waves), intra-seasonal oscillations are discussed in the literature review. The variability of rainfall anomalies over Africa has received considerable attention recently. Tropical theoretical and modeling work on equatorial wave dynamics is reviewed. The roles of moisture, basic flow and vertical shear in generating the tropical waves are emphasized. A brief review on the theory of teleconnection is presented in order to interpret some of the results.

2.2 Characteristics of southern African rainfall

The characteristics of southern African rainfall can be extracted from global, regional and specific country-scale studies. The distribution of rainfall over Southern Africa has been given in many papers (Lau and Sheu, 1988; Hulme, 1992; Diaz, 1996; Hulme, et al., 1996). Most regions in Southern Africa receive precipitation during the period November to March with the exception of some coastal areas in South Africa. A considerable amount of rainfall is concentrated in the DJF period. **Figure 2.2(a)** shows the distribution of the mean DJF rainfall over 40 years. Highest summer rainfall occurs in the northeast parts and gradually decreases towards the southwest. In this study the summer rainfall is defined as the

total amount of rainfall during the 3 months from December to February. The DJF rainfall standard deviations are shown in **figure 2.2(b)**. **Figure 2.2(c)** gives the ratio of annual rainfall to DJF total in percentage. **Figure 2.2(d)** shows the ratio of standard deviation to the mean (coefficient of variation) showing low values over central Africa and high values in the southwest desert of the subcontinent. Previous studies on inter-annual variability of global, continental and regional rainfall are addressed in the next section.

2.2.1 Inter-annual variability of rainfall :from global- scale analysis

Documentation of inter-annual variability of rainfall on global scale has been achieved (Ropelewski and Halpert, 1996; Diaz, 1996). In these studies the roles of ENSO and QBO in modulating rainfall are suggested. Contrasts between land and oceanic precipitation are identified.

Lau and Sheu (1988) applied Harmonic and Principal Component Analysis to monthly global precipitation. The first mode of PC analysis, which explained 9% of the total variance was linked to ENSO. The spatial loadings show wet areas over Eastern Africa (10°S- 20°N, 25°E- 40°E) and dry regions over Southern Africa during warm events. The time series of the first PC mode was decomposed into ENSO (3-7 years) and QBO (2-3 years) and it was found that 48.7% of the variance was due to ENSO and 22.8% to QBO. An amplitude modulation at 20 years was observed in the filtered time series.

Hulme (1992) described the global land precipitation based on 1951-80 monthly 5° latitude × 5° longitude grid resolution. A decreasing trend of -0.4 mm /year was found. Southern Hemisphere annual rainfall was linked to SOI (Southern Oscillation Index) with a correlation coefficient of 0.24.

Diaz (1996) examined large-scale rainfall characteristics for the period 1979 to 1993 using land stations as well as oceanic data (through satellite) at 5°×5° degree grid resolution. His results showed a decrease in mean monthly precipitation for the period 1979 to 1993 compared to 1951 to 1970. Global rainfall departures between land and ocean were out of phase between 1979 and 1993. The

correlation coefficient between land annual precipitation and oceanic was found to be -0.74 for the tropical regions. At global level for December, January and February season (DJF) the correlation coefficient was found to be -0.63. It was concluded that increased precipitation over water is associated with enhanced anticyclonic (drier) conditions over land. Conversely, enhanced cyclonic conditions in the continental regions appear to be associated with decreased precipitation over ocean areas. The first PC mode (5.6 %) of the rainfall (1979 to 1993) was found to be linked to ENSO (r = 0.42) at lag 2 seasons. The spatial loadings of the first mode exhibited a weak dipole between southern Africa and the Central Indian Ocean (0°S-20°S, 50°E-100°E). Gershunov and Michaelsen, (1996) analysed interannual variability of tropical ocean (30°N-30°S) rainfall using 15 years of monthly microwave sounding unit rainfall data. They examined 185 months from January 1979 to May 1994 at 2.5° × 2.5° grid resolution and found that ENSO and QBO dominated the interannual variability.

2.2.2 Inter-annual variability of rainfall: from Continental Africa-scale analysis

Temporal and spatial rainfall fluctuations at the continental scale have been examined by a number of researchers (Nicholson, 1986, 1997; Janowiak, 1988; Semazzi et al, 1996). Nicholson (1986) classified six spatial anomaly types of rainfall variability over Africa using monthly rainfall data for the period 1901 to 1973. The anomaly modes showed two preferred patterns i.e. precipitation anomalies of the same sign over the whole continent, or anomalies of opposite sign in the tropical versus subtropical latitudes. The temporal characteristics for southern Africa gave significant peaks at 2.2-2.4 and 3.3-3.8 years over Angola, East Africa, and southern Africa. Strong coherence was found with ENSO in the 2.2-2.4 period over the areas east of 30°E over southern and equatorial east Africa. A strong relationship with ENSO in the 5.0-6.3years oscillation was found over Angola, eastern Botswana, northern South Africa, southern Zambia and Malawi.

Janowiak (1988) applied PCA to annual and seasonal rainfall over Africa utilizing the same data set as Nicholson, (1986) for the period 1927 to 1973. Non-normalized data were used and the higher modes of the annual rainfall showed three areas of action namely West Africa (12.0%), East Africa (9.2%) and southern Africa (7.9%). The patterns had out-of-phase relationships between rainfall anomalies in equatorial and subtropical regions of the subcontinent. PCA analysis of December, January, February and March (DJFM) exhibited three major areas of variability. The first mode (14.5%) indicated large positive loadings over southern Africa and weak negative loadings over Central Africa and East Africa (10°S to equator). The second mode (13.3%) displayed large positive loadings over East Africa with weak negative loadings over southern Africa. The third mode (11.3%) had largest positive loadings over West Africa and indicated a possibility of alternating signs of the loadings in a meridional axis. It was found that during ENSO events, the DJFM rainfall tends to be 10% to 25% below normal over the region east of 20°E and between 15°S and 30°S, but above normal east of 20°E between the equator and 10°S.

Conceptualizing the mechanisms behind the rainfall variability is done in chapters 5 and 6. Rainfall and convective (OLR) anomaly patterns are linked to sea surface temperature anomalies and circulations in order to investigate the mechanisms.

2.2.3 Interannual variability of rainfall: from regional- scale analysis

Progress has been made in documenting temporal and spatial variability of regional and national rainfall in southern Africa. The discussion on rainfall will be confined to stations with longer records. More work has been done in South Africa than other Southern African Development Community (SADC) countries. Tyson (1980) examined rainfall anomalies in Africa south of 22°S using station data for the period 1910 to 1977. He found an 18-20 year cycle in the unfiltered raw data. Dyer (1981) used station data of annual rainfall (1921 to 1975) and applied PCA.

The first mode (32%) had highest loadings over central South Africa, and its time score had 10-13 year and biennial oscillations. The second mode (14 %) had large loadings over northern South Africa with spectral peaks at 10 and 2.7 years. The pattern of the third mode (10%) had large coefficients over Gauteng and the Western Cape and its scores had spectral peaks at 7, 3, 6, and 2.1 years. The fourth mode (6%) displayed high loadings over the former Cape Province and its time score had peaks at 10-13 and 4 years.

The interannual variability of rainfall over southern Africa has been found to be quasi-periodic and spatially coherent. The above discussion of rainfall variability suggests that for southern Africa the causes of inter-annual variability may be linked to ENSO and a dipole between oceanic and continental regions. Some of the rainfall patterns have not been explained. This thesis attempts to explain some of rainfall features in chapter 4 and 5. Importance of oceanic processes and differential heating (between land and adjacent oceans) is noted. The role of differential heating in formation of the heat low is taken up in chapter 8.

2.3. Southern African rainfall bearing systems

Major breakthroughs have been achieved in understanding rainfall bearing systems and rainfall variations through observational, theoretical and numerical studies. Most parts of southern Africa lie within the latitudes (0°N to 30°S see figure 1.1a) and hence it is affected by tropical (monsoon, ITCZ, easterly flow) and midlatitude (westerly waves, fronts) weather systems (Preston-Whyte and Tyson, 1988). In southern Africa Preston-Whyte and Tyson (1988) have described the synoptic circulation features for the areas south of 20°S. Some case studies exist for other areas such as Zambia (Mumba and Chipeta, 1984) and Zimbabwe(Makarau, 1995) describing particular summer episodes. The main synoptic systems which affect the weather over southern Africa during the rainy season (October-April) are Inter-tropical convergence zone (ITCZ), Congo Air Boundary (CAB), westerly waves (Kumar, 1978), easterly waves (Mumba and Chipeta, 1984; Okoola, 1989), tropical cyclones (Bhagare, 1978). Tropical cyclones have

been studied by Bhagare (1978), Mudenda and Mumba (1997), Parker and Jury (1995). The main synoptic feature of summer period is the ITCZ and the associated easterly waves, which are documented by Asnani (1993). The maintenance, development and decay of synoptic disturbances depend on barotropic, baroclinic and conditional instability of second kind (Charney and Eliassen, 1964; Kuo, 1978; Kwon, 1989; D'Abreton, 1992). Jury et al (1994) studied the ITCZ evolution and variability over the south-western Indian ocean. Precipitable water, OLR and wind data were used to define the ITCZ. The ITCZ was defined as an area with precipitable water >5 gm cm^{-2}, OLR values less than 220Wm^{-2} with convergent low level winds. The mean summer position of the ITCZ for the period 1987 to 1990 was found to lie over 15°S latitude over south-east Africa and Madagascar. The easterly winds to the east were driven by the south-west Indian Ocean anticyclone. Dry zones had OLR values >260 Wm^{-2} and precipitable water < 3.6 g cm^{-2}. A dipole between the southern western Indian Ocean and southern Africa was identified.

The propagation of the ITCZ over Africa is controlled by meridional gradient of moist static energy (Webster, 1983) and periodicities of the convective activities are governed by ground hydrological feedbacks (Webster, 1983). Srinivasan and Smith (1996) have suggested wind-evaporation feed-back mechanism may explain the meridional migration of the ITCZ. Other large scale systems are the Intra-seasonal (30-60 day) oscillation (Madden and Julian, 1971), and Hadley and Walker circulations (Harrison, 1986; Keshavamurty and Rao, 1992). At inter-annual scale sea surface temperature and the related El-Nino\Southern Oscillation (ENSO) (Lindesay, 1988) play an important part in modulating rainfall over southern Africa. Quasi-stationary standing waves play an important part in regulating summer rainfall (Harrison1986). Tyson (1981) found wet spells to be associated with the lowering of pressure over the interior of the subcontinent.

Interactions between midlatitude and tropical disturbances have impacts on rainfall. Miron and Tyson (1984) associated wet spells with negative pressure

deviations over the central parts of the subcontinent and positive anomalies over south-western ocean area in the region of Gough Island. For dry periods the anomalies were reversed. Tyson (1984) further examined the differences in annual geopotential heights at 850hPa and 500hPa levels between 16 stations over southern Africa and adjacent oceanic areas. It was found that the 500hPa circulation field was more important than its near-surface counterpart as a control of annual rainfall. Wet years in central and the northern interior parts of South Africa appeared to be caused by easterly waves with the trough axis occurring over Namibia, Botswana and central South Africa. It was found that regional variations in annual rainfall are linked to variations in low latitude forcing associated with easterly airflow. It was emphasised that the 500hPa atmospheric field of motion is responsible for year to year differences in annual rainfall totals.

Lindesay and Jury (1991) found interactions between tropical convection, easterly wave, South-west Indian Ocean anticyclone (high over Mozambique channel), and midlatitude westerly wave to the south which resulted in the flood of February 1988. Kumar (1978) observed an interaction between upper westerly waves and the intertropical convergence zone over Zambia.

Harrison (1986) emphasized the roles of the Hadley circulation, the semi-annual oscillation, ENSO and Walker circulation across the Tropical Indian Ocean in modulating rainfall. Higher rainfall in summer was associated with an intensified Hadley circulation.

Jury and Pathack (1991) correlated January-February rainfall amounts and 700hPa zonal wind over southern Africa and the south-west Indian ocean. Westerly winds were found over central Africa (10°S -20°S, 15°E to 30°E) and easterlies in southern Africa (20°S to 35°S) were found to be associated with wet spells.

Jury (1995) has done a useful review on mechanisms of southern African rainfall.

Much progress has been achieved on the description and understanding of Asiatic and Indonesia-Australian summer monsoons (Murakami, 1992; Asnani, 1993;

Keshavamurty and Rao, 1992). Little literature exists for summer monsoons over equatorial Africa. This has been due to a lack of interest and data. Southern Africa needs immediate attention to document the mean summer circulation in order to remedy this deficiency. With the availability of European Centre for Medium Range Weather Forecasting (ECMWF, 1994) data, this thesis sets out to describe African monsoon variability.

2.4. Importance of quasi-stationary waves

Quasi-stationary waves can modify the structure of upper and lower tropospheric wind patterns. During DJF the summer season, three major areas of large –scale precipitation are observed over southern Africa, Indonesia and south America (Liebman and Hartman, 1981). These regions have been identified with standing waves, which are forced by diabatic heating. Cloud bands oriented north-west to south-east have been observed to form in these areas (Harrison, 1986). The standing waves contribute to interannual variability of rainfall over southern Africa (Harrison, 1986). Harrison (1986) has identified an upper tropospheric westerly Atlantic wave that has an impact on southern African rainfall. The Atlantic wave has some influence on the position of the tropical –temperate troughs. It has been observed that below normal African rainfall occurs when the tropical- temperate trough overlies over Madagascar.

Karoly (1985) identified standing waves with large zonal and short meridional length scales. Maximum variance of the geopotential height, temperature and meridional winds was found at 20°S, at 200hPa and 850hPa levels and wave number one had largest amplitude in winter. Mo and Higgins (1997) confirmed the existence of wave number 1 and 3 in Southern Hemisphere using harmonic analysis and 500 hPa geopotential height monthly anomalies. Kiladis (1997) examined standing waves in the Southern Hemisphere associated with ENSO by applying composite analysis to 500hPa height anomalies. It was observed that during warm events DJF pressure anomalies were positive over southern Africa and negative over the midlatitudes (40-55°S). Most studies on teleconnection

patterns have been confined to midlatitudes and few exist for tropical regions. This study investigates tropical teleconnections and their impact on southern African climate. The teleconnection patterns may be explained as propagating Rossby waves.

2.5. Importance of oceanic processes

For southern Africa, the most important ocean-atmosphere-land interactions involve equatorial Pacific, Indian and Atlantic oceans. The seasonally varying climate of southern Africa is governed in part by pronounced seasonal variations in surrounding oceans. SST anomalies have been found to have a large impact on rainfall variability over southern Africa (Walker, 1989b; Lindesay, 1988; Mason 1992; Rocha, 1992). SST temperatures of the adjacent Mozambique, Agulhas and Benguela current systems were found to be linked to summer rainfall over South Africa (Walker, 1989b) in non-ENSO years. Warmer waters in those regions were associated with wetter summers. Mason (1992) identified SST anomalies in the western equatorial Indian Ocean as partly responsible for the longitudinal shifts in the African convective centres. Rocha (1992) has linked the central Indian and eastern Pacific SST anomalies to south-eastern African summer rainfall. Further investigations of SST fluctuations on interannual and decadal time scales are required to describe and understand southern African climate variability and ENSO influences.

ENSO is a low frequency phenomena which arises from the instability of the coupled tropical ocean-atmosphere system (Kuo, 1989). El-Nino is linked with large scale warming over the tropical eastern Pacific. It is quasi-periodic with periods ranging from 2 to 10 years. Its mean period since 1864 is 3.2 years (Quin and Neal, 1983). Large scale warming of water over the tropical Pacific Ocean has serious consequences on economical activities of SADC countries (Hulme, et al 1996). The Southern Oscillation (SO) is a large "see-saw" of atmospheric mass between the tropical eastern and western Pacific (Montgomery, 1940). The SO and El-Nino are closely related phenomena and are referred to as El-Nino/Southern

Oscillation (ENSO). The Southern Oscillation Index (SOI) which is the difference between Tahiti and Darwin sea level pressure anomalies quantifies ENSO. A warm event refers to low SOI values, which are associated with low pressure and above normal precipitation over the tropical eastern Pacific. Asnani (1993) provides an excellent review on ENSO. In southern Africa it has been observed that during warm events rainfall tends to be below normal (Janowiak, 1988; Nicholson, 1986; Matarira and Jury, 1992). Above normal SST are observed over the central Indian (Rocha, 1992). However, the physical mechanisms responsible for the teleconnection are not well understood. Upper air processes and SST anomalies in the Indian and Pacific oceans are some of the elements which play an important part in teleconnections. Other local factors like the Angola low or regional SST anomalies in the adjacent oceans (Mason, 1992) may play an important role in modulating the remote forcing. It has been observed that the teleconnections due to tropical SST anomaly patterns affect both the tropical and extratropical atmosphere.

Many studies have documented the theoretical and observational aspects of the teleconnections associated with ENSO (Hoskins and Pearce 1983; Wallace and Gutzler,1981; Cavalcanti, 1997; Casey, 1997; Kiladis, 1997; Mo and Higgins, 1997). These studies have shown the existence of teleconnection patterns. Casey (1997) examined the Southern Hemisphere teleconnection patterns and the East African rain season using 500 hPa geopotential heights. He identified DJF PC3 as being linked to MAM East African rainfall. The PC3 pattern had alternating anomalies, which propagate across the south Pacific into the high latitude South Atlantic where dissipation occurs in the form of baroclinic transients. Hastenrath et al (1993) have identified the dipole between East Africa and southern Africa rainfall anomalies

Recently Kiladis (1997) studied large-scale circulation anomalies of the Southern Hemisphere during extreme ENSO events. It was observed that during warm events strong convection developed over central and eastern Pacific which drives a

stronger than normal divergent circulation. Easterly and westerly wind anomalies prevail over East Africa and southern Africa, respectively at 200 hPa level during the DJF period. Large scale convection during ENSO events are the main forcing mechanism which modify the basic state.

2.6 General Circulation Model (GCM) Studies

Jury et al (1996) linked warm sea surface temperature over the central Indian Ocean to drought over South Africa using a General Circulation Model. Warm SST over central Indian Ocean were associated with latent heating and tropical westerlies over Africa resulting in lower divergence and upper convergence. It was found that low level moisture convergence was above normal over south-west Indian Ocean. Rautenbach (1997) applied Atmospheric General Circulation Model (AGCM) using the CSIRO-9. He utilized global SST for the period August 1995 to March 1996 to investigate the teleconnections between global SST anomalies and the summer 1995/1996 rainfall over southern Africa. Results of the simulation showed a thermal forcing caused atmospheric circulations favourable for good rain over southern Africa. Surface wind simulations indicated stronger than normal easterly winds to the east and south of southern Africa.

Reason et al (1997) used an Ocean General Circulation Model (OGCM) to study the mechanism associated with low-frequency climate variability in the South Indian Ocean. The observed inter-decadal wind anomaly was used as a forcing and results showed that changes in the south Indian gyre could lead to observed SST variability in the Agulhus current region and southern midlatitudes. It was also observed that the SST anomalies tend to be warm in the region of Agulhus and south Indian Ocean and cool in the central south Indian Ocean during periods when the semi-permanent subtropical anticyclone over the ocean is strengthened.

Rocha and Simmonds (1997a) examined the relationship between rainfall over Sahel and Kalahari regions and its association with SST. The Melbourne University General Circulation Model (MUGCM) with prescribed SST's and sea-ice coverage. Results showed a common period of 3.3 years for Sahel and

Kalahari. The 3.3 year period was also found in the SST forcing. When the SST forcing was removed the 3.3 year periodicity disappeared. This suggests that the 3.3 year periodicity is due to external oceanic forcing. The spatial correlations between rainfall and global SST indicated an ENSO structure.

Goddard and Graham (1997) examined the impact of prescribed SST of central Indian Ocean on southern African precipitation. Using a GCM they demonstrated that Indian Ocean SST's strongly influence the climate over southern Africa. The influence is due to local changes in convection and mean circulation.

Rocha and Simmonds (1997b) used the MUGCM to study the distinct modes of SST - forced rainfall variability over Southern Hemisphere continents. Unbiased internal and external (SST forced) forcings were applied. In southern Africa the forcing was observed over central southern Africa, suggesting that variations in the location and strength of the thermal low is the origin of convective rainfall in the region.

2.7.Importance of Intraseasonal Oscillations and wave- trains (10-60 days)

Lim and Chang (1983) used shallow-water equations with time-dependent forcing to demonstrate the influence of mid-latitude 'surges'. For slow forcing the atmospheric response was to generate Rossby and Kelvin waves while for fast forcing, mixed Rossby gravity waves and inertial-gravity waves were obtained. In the Rossby mode response, a belt of strong winds which is associated with strong pressure gradient moves from the midlatitudes to the equator. Lau and Lim (1984) used a linear model to study the propagation of waves from the tropics to midlatudes due to tropical forcing under westerlies and easterlies. In the westerly wind regime, barotropic Rossby waves propagate to the extratropics and this implies that extratropical teleconnections will be generated in equatorial westerlies. In easterly wind shear, teleconnections are confined to the tropics whereas in the westerly case, the characteristic Rossby wave train develops poleward and downstream of the forcing.

Blade and Hartman (1995) investigated the impact of tropical heating on the

extratropics using a simple model. An eastward moving dipole heating system (with period of 40 days) appeared in the area of tropical heating when non-linearity was allowed with a wave-train downstream. As the heating propagates eastward, the wave-train in the extra-tropics and the dipole in the subtropics propagate together with the heating dipole.

Simple numerical models have been utilised to study the influence of tropical thermal forcing on the tropics and extra tropics (Hoskins and Karoly, 1981; Webster, 1981). Results of the simulations indicated that stationary Rossby waves with low wave numbers are transmitted from low latitudes to high latitudes through thermal forcing. Waves with high wave numbers are confined to the tropics. Barotopic structure in lower and upper fields in geopotential and temperature appeared outside the tropics. It was concluded that the response of the atmosphere to tropical thermal forcing takes the form of Rossby wavetrains of alternating high and low pressure that are seen along a great circle route across the sphere in the upper levels. Most barotropic studies indicate that the heating of the upper levels of equatorial troposphere by release of latent heat is the driving mechanism of the Rossby wavetrain. Theoretical work of Hoskins and Ambrizzi (1993) shows possible areas of Rossby wave propagation, which includes the Southern Hemisphere sub-tropical jet.

In addition to low frequency oscillations (teleconnections), significant 20-30 day intraseasonal variations occur over southern Africa (Levey and Jury, 1996; Makarau, 1995). These waves are important in affecting the evolution of the seasonal cycle. In southern Africa Levey and Jury (1996) have identified westward moving modes which prevailed in 1986 to 1992 ECMWF data. Over the Indian Ocean region the westward moving modes have been identified as part of a self-sustaining system which consists of MJO (Madden and Julian Oscillation) and westward moving modes (Wang and Xie, 1997). Intraseasonal waves are important in regulating large-scale temperature and winds.

Madden and Julian (1971) first observed tropical oscillations with periods of 30-

60 days referred to as the Madden Julian Oscillation (MJO). Literature on observations, theories and modelling studies on MJO have been documented (Hayashi and Sumi, 1986; Neelin et al,1987; Lau and Peng, 1987,1990). Madden and Julian (1994) gave an excellent review on MJO. The MJO has been recognised as a fundamental mode of tropical atmospheric variability particularly over the east Indian and west Pacific. Observational studies by Knutson, Weickmann and Kutzback (1986), and Rui and Wang (1990) documented the characteristics of MJO. Kinetic energy of MJO is extracted from high frequency modes and annual cycle (Sheng and Hayashi, 1990). MJO loose kinetic energy to long-term time mean flow.

Several analytical and numerical models have been performed to study the response of the atmosphere near the equator and Kelvin and Rossby waves appear as solutions (Matsuno, 1966; Webster, 1972 and 1973; Gill, 1980).

The Rossby waves and Kelvin waves can be used to explain the MJO and some observed tropical synoptic disturbances (Chang, 1977; Hayashi and Sumi 1986). The interaction between convection and dynamics through mobile wave-cisk has been identified as the main mechanism of low-frequency oscillations (Lau and Peng, 1987; Chang and Lim, 1988). The vertical heating profile was found to be important in the determining the characteristics of the dominant unstable modes (Wang, 1988; Sui and Lau, 1989). It was found that for maximum heating in the lower troposphere result in unstable stationary mode. For maximum heating at the mid-tropospheric levels, eastward propagating waves were obtained and the mode is due to interaction between two internal modes, which are locked in phase vertically. Moist static energy, vertical shear and moisture play are important in the development of Rossby and Kelvin waves (Wang, 1988; Rui and Wang, 1990; Lau and Peng, 1990; Xie and Wang , 1996).

Vertical heating distribution (diabatic heating) was found to be a critical factor in determining the dominant unstable modes and heating in the lower troposphere slows down the wave-CISK modes (Sui and Lau, 1989). Lau and Peng (1990)

studied the interaction between the MJO and the large-scale monsoon circulation. They emphasised the role of vertical shear in generating the westward moving Rossby waves. Interaction between the mean flow and MJO led to the rapid development of westward propagating synoptic-scale cyclonic vortices. It was deduced that for tropical disturbances to form large wind shear was required but in the presence of moisture, weak vertical shear could induce similar unstable waves. It was also seen that increasing the moisture would result in decreasing the scale of the unstable wave. It was concluded that tropical Rossby wave instability could occur with relatively weak wind shear provided that the latent heat effect is included. Rui and Wang (1990) found that without sufficient moisture the Kelvin and Rossby waves were damped but Kelvin waves were selected when moisture increased. It is seen that the selection of Kelvin waves was due to frictional moisture convergence which produced about one third of the wave energy over the warm pool.

Xie and Wang (1996) demonstrated the role of vertical shear on equatorial Kelvin and Rossby waves. Moderate vertical wind shear has been found to have little impact on equatorial Kelvin waves. It was deduced that Rossby waves are affected by vertical wind shear, the westerly wind shear favors trapping of Rossby waves in the upper levels but the easterly wind shear confines the unstable waves in the lower troposphere.

2.8 Summary of literature review

Previous studies have revealed the temporal and spatial characteristics of African rainfall. PCA studies have identified ENSO characteristic as dry zones over southern Africa and wet areas over East Africa during warm phase. Dipole structure in rainfall anomalies between land and oceanic regions has been identified in global analysis. More analysis is required for southern African rainfall. Causes of rainfall variability have been linked to Hadley, Walker circulations, SST anomalies, ENSO, regional circulations, 30-60 day oscillations and synoptic features. Preston-Whyte and Tyson (1988) have given a model of wet

spell and dry spells for southern Africa. More investigations are required in order to re-confirm some of the previous findings. The influence of tropical teleconnections has not been investigated and it is the intention of this thesis to remedy this deficiency.

From previous studies on intraseasonal oscillations the following findings are significant namely moisture, basic state, vertical shear and heating. It has been observed that moisture plays a very important role in enhancing tropical instability (Lau and Peng,1990; Rui and Wang, 1990). Moisture transport depends on large-scale flow. The supply of moisture reduces the role of vertical shear in destabilising the waves (Lau and Peng, 1990). The role of the basic state is important in modulating the ITCZ and controlling the teleconnection (Lau and Lim, 1984). In easterly flow the evaporation-wind feedback makes the ITCZ propagate poleward and in westerly wind the ITCZ moves equatorward (Srinivanasan and Smith, 1996). The easterly shear destabilises and traps the Rossby waves 'insitu' and changes the Rossby-wave structure from symmetric to asymmetric with respect to the equator. In westerly wind shear barotropic Rossby waves resulting from tropic forcing can propagate to the extratropics (Lau and Lim, 1984). Teleconnections are confined to the tropics in easterly wind shear. In easterly vertical shear the unstable waves are restricted to the lower troposphere and in westerly vertical shear the unstable waves are confined to the upper troposphere (Xie and Wang, 1996). The preferred unstable wavelength increases with increasing vertical shear and decreases with increasing heating intensity. The tilting of the phase lines is useful for determining the stability of the waves. In an unstable Rossby wave, the phase increases with latitude and thus allows the transfer of energy from mean flow to the eddies. Maximum heating in the lower level results in a stationary mode while maximum heating in the middle levels produces an eastward propagating Kelvin wave (Chang and Lim, 1988).

Statistical and GCM studies have demonstrated the importance of external sea surface temperature anomalies forcing in modulating the rainfall over southern

Africa (Lindesay, 1988; Mason,1992; Rocha, 1992; Makarau, 1995; Jury et al, 1996; Reason et al, 1997; Rautenbach, 1997). Internal forcing has received less attention and the recent work of Rocha and Simmonds (1997b) have shown the importance of the internal dynamics over southern Africa. Further work is required in understanding the quasi-stationary low over southern Africa. The role of the quasi-stationary low in modulating rainfall through moisture convergence and maintaining the convective activities needs investigation.

Although several researchers regarding the summer rainfall in southern Africa have made many studies, there remain many unsolved problems. Identification of tropical teleconnection patterns needs to be carried out. Separation of remote and local forcing of circulation anomalies is important and requires investigation.

In order to meet the above stated objectives mathematical techniques and relevant data are required to carry out an empirical study. An empirical study includes the elaboration of spatial, temporal and multivariate relationships. Spectral, composite, correlation and principal component analyses techniques have been successfully used to determine the spatial and temporal structure of variability in most components of the climate system. In this thesis these techniques are applied and information about the techniques is given in the next chapter.

a

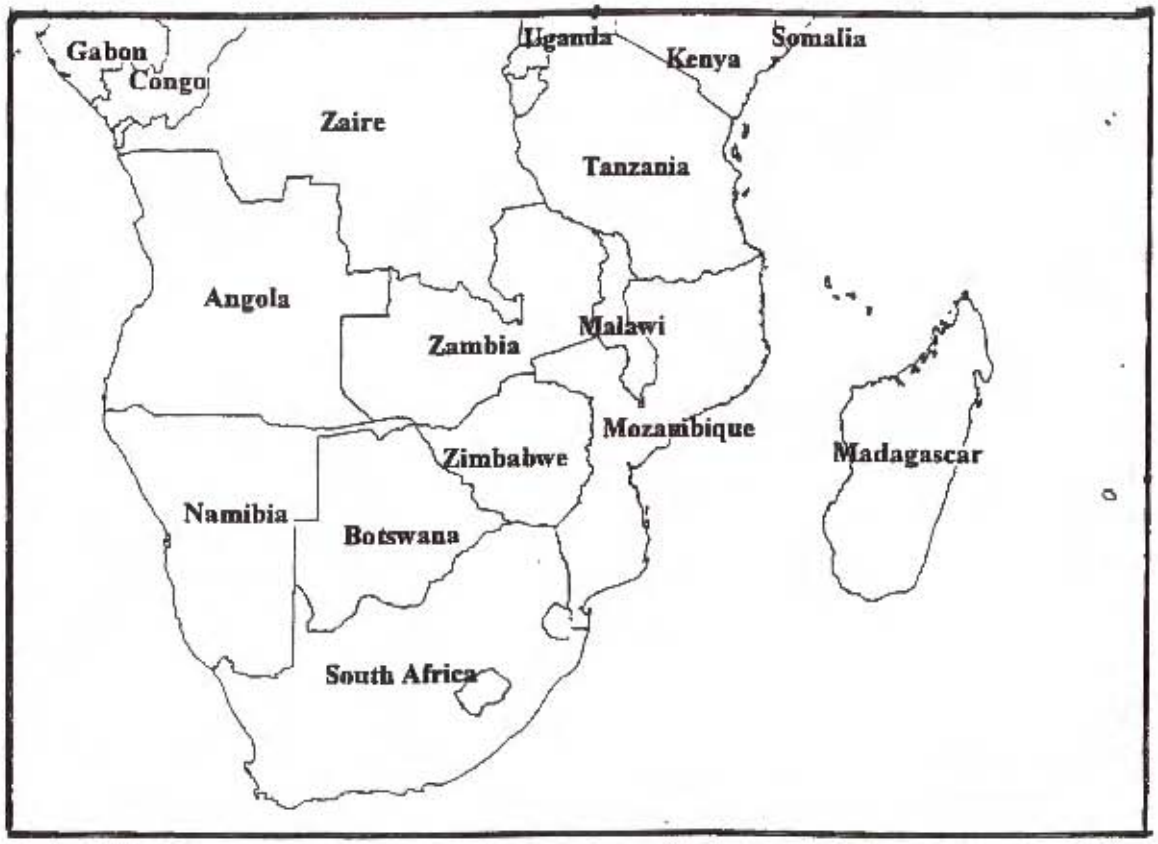

b

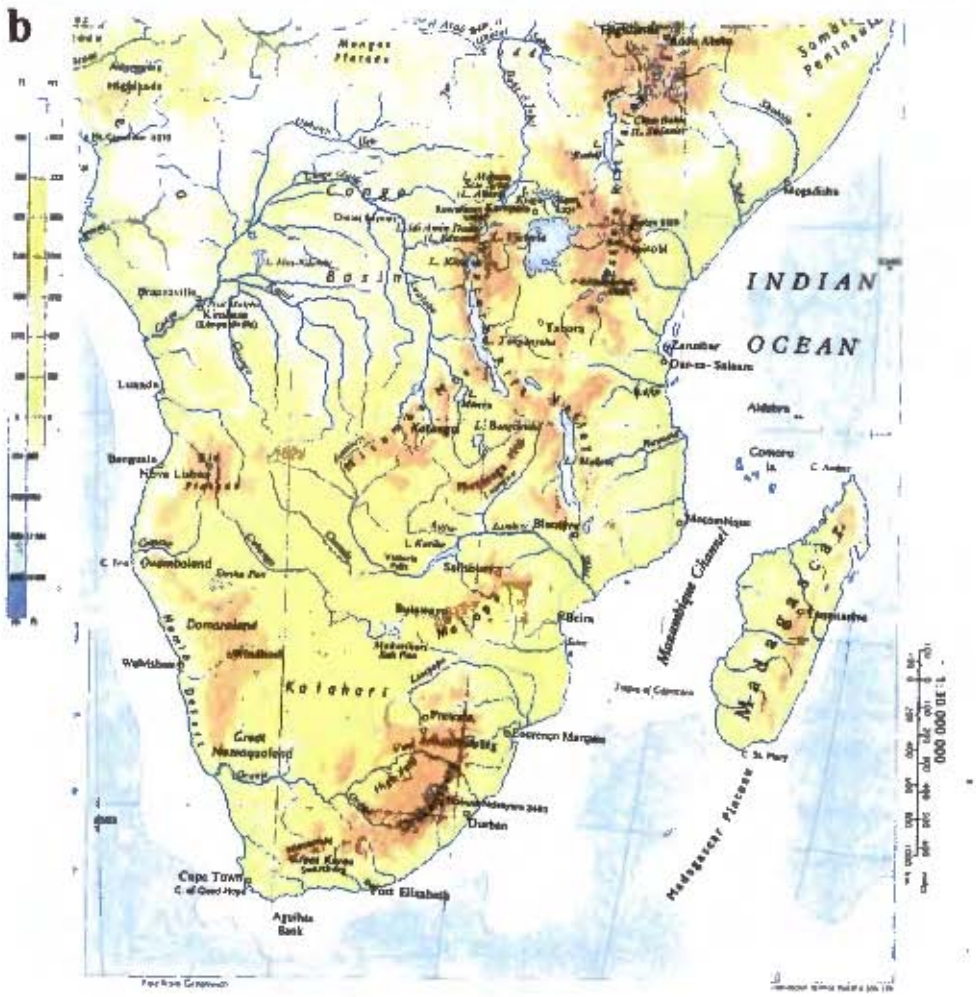

Figure 2.1 (a) Political map of Central, East and southern African countries.
Figure 2.1 (b) Topographical features of southern Africa. (From University Atlas , Fullard et al., 1975).

a

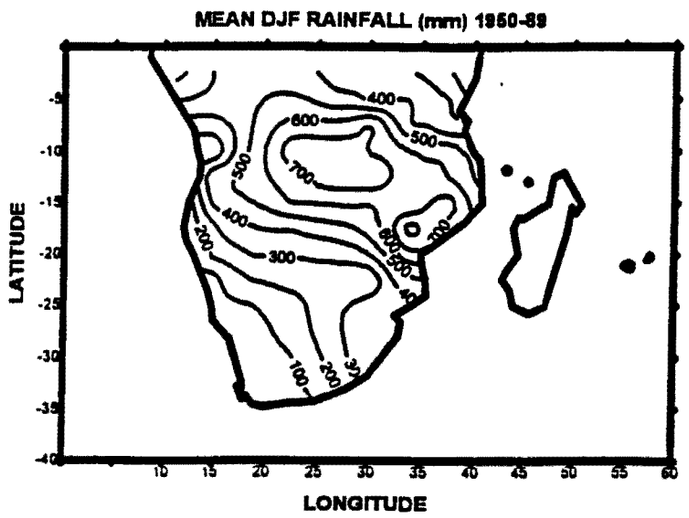

b

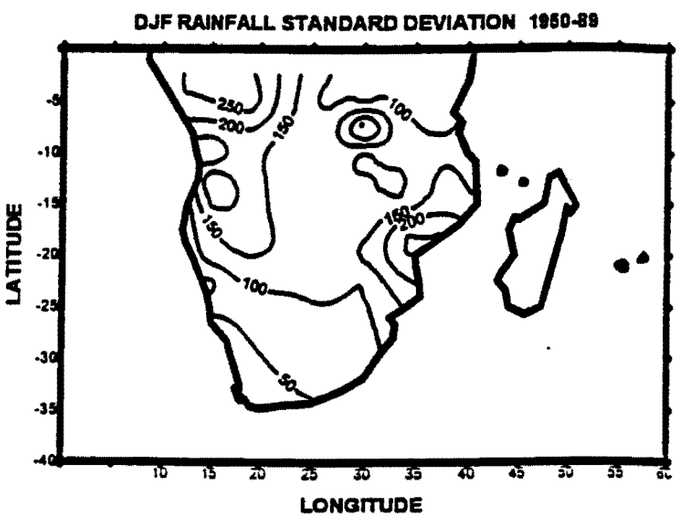

Figure 2.2 (a) Mean summer rainfall (December to February, DJF) in millimeters over Southern Africa based on the period 1950 - 1989. (b) DJF standard deviations in millimeters.

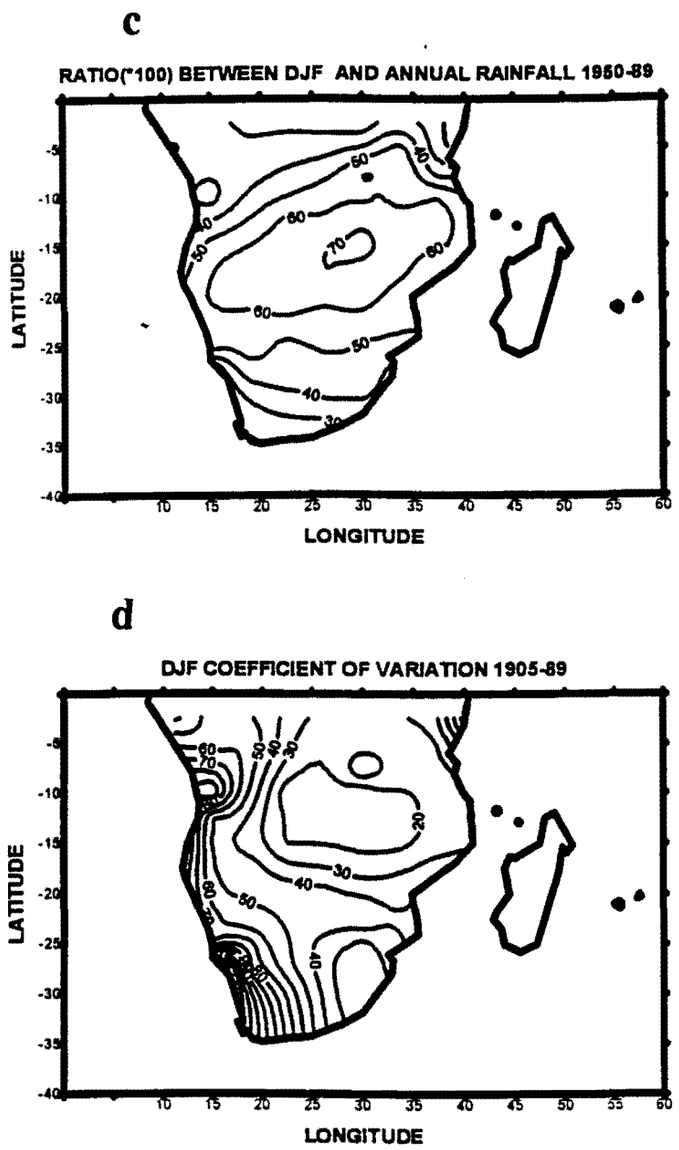

Figure 2.2 (c) Ratio between DJF and annual rainfall in percentage. (d) DJF Coefficient of variation (100* standard deviation / mean).

CHAPTER 3

MATHEMATICAL TECHNIQUES AND DATA

3.1 Introduction

Analysis of observed data is necessary in order to obtain maximum information for interpretation of climate dynamics. There are mathematical and physical models which, link reality with the mechanisms generating the pattern. Generally, there are three types of models namely deterministic, static and stochastic (random). In the deterministic model, time and space variables and model parameters determine the observations. In the static model, the observations can be determined with simple random components which, are due to measurement or sampling errors of unknowns in the mechanism. Stochastic models are random models and use memory (persistence) to explain the observations. In this case the observed signal depends on its predecessors in time or adjacent points in space. This study will concentrate on static models and the extraction of a deterministic part from observations. Elimination of the random component will be carried out in order to understand the generating mechanism. Spectral Analysis, Principal Component Analysis (PCA), and Extended Empirical Orthogonal Functions (EEOF) techniques will be utilised in this thesis. The next section deals with a brief outline of the theoretical aspects of the mathematical techniques.

3.2 Spectral Analysis

This technique has been widely applied in meteorology and oceanography to determine the temporal characteristics. More detailed description of this method can be found in Yuen and Fraser (1979). Other references are Jenkins and Watts (1968), Bloomfield (1976) and William et al (1997). Spectral Analysis relies on the representation of a time series as a sum of cyclical functions in time and identifies the correlation structure by the relative importance of cycles of different frequency. Fourier transform is used to obtain the coefficients of the sinusoids at a discrete set of frequencies.

3.2.1 Discrete Fourier Transform

In practice it is not possible to find continuous functions which are infinite so we consider the Discrete Fourier Transform (DFT). Let f_n be a sample taken from time series f(t), thus one needs to approximate the DFT to be close to FST of f(t), that is

$$G(\omega) = \lim_{\omega_0 \to \infty} \int_{-\infty}^{\infty} f(t) \left\{ \frac{e^{-2\pi i \omega t}}{2\pi i \tau} - \frac{e^{-2\pi i \omega_0 t}}{-2\pi i t} \right\} dt \qquad (3.1)$$

$$f(t_n) = f_n \qquad o \le n \le N-1$$

DFT is defined as $F_m = \frac{1}{N} \sum_{N=0}^{N-1} f_n e^{\frac{-2\pi i n m}{N}}$ (3.2)

The inverse DFT is given as $f_n = \sum_{M=0}^{N-1} F_m e^{\frac{2\pi i n m}{N}}$ (3.3)

where $\Delta t = \frac{I}{N-1}, f_n = f(t_n), 0 \le n \le N-1, t_n = n\Delta t$

F_m is a complex number. $F_M = A_m + iB_m$ where A_m is the real part and B_m is the imaginary part. The advantage of DFT is that there are no convergence problems. The equation (2.1) is defined for all $-\infty \le m \le \infty$ and is periodic in m with period N. The RHS of equation (2.2) is defined for all $-\infty \le n \le \infty$, and gives a periodic extension of the data outside the interval (0,T), with period $N\Delta t = T + \Delta t$, even though the original data may not be periodic.

Periods and Frequencies

$t_n = n\Delta t$ is time

$\omega_m = \frac{m}{n\Delta t}$ is frequency

(i) Lowest non-zero frequency is

$$\omega_1 = \Delta\omega = \frac{1}{N\Delta t} = \frac{1}{T + \Delta t} \text{ as } \Delta t \to 0,\ T \to \infty$$

(ii) Highest detectable frequency is $\omega_{\frac{N}{2}} = \frac{1}{2\Delta t} \to \infty$ as $\Delta t \to 0$

$\omega_{\frac{N}{2}}$ is called the Nyquist frequency

Period $T_m = \frac{1}{\omega_m} = \frac{N\Delta t}{m} = \frac{T+\Delta t}{m}, \quad \leq m \leq \frac{N}{2}$

The shortest resolved period is the Nyquist period $T_{\frac{N}{2}} = 2\Delta t$

F_m is complex number

$F_m = A_m + iB_m$

$F_m = \mathrm{Re}(F_m) + I_m(F_m) = A_m + iB_m, |F_m|^2 = A^2 + B^2$

$|F_m|^2$ and $R_e(F_m)$ are symmetric about $\frac{N}{2}$ but $I_m(F_m)$ is antisymmetric about $\frac{N}{2}$

A_m is symmetic $|F_m|^2$ is symmetric about $\frac{N}{2}$, but B_m is antisymmetric about $\frac{N}{2}$.

In practice we want F_m to be close to $dG(\omega_m)$ of the time series.

$$F_m = \int_{\infty}^{\infty} W[\mu] dG(\omega) \tag{3.4}$$

where W[μ] is the weighting function.

W $(\mu) = 0$ when $\mu = m$, an integer $0 \leq \mu \leq \frac{N}{2}$

F_m receives contributions of unit weight not only from $dG(\omega_m + j\omega_N)$. The frequencies $\omega_m + j\omega_N$ are called the aliases of ω_m and signals at these frequencies contribute to the DFT estimate F_m of $dG(\omega_m)$. This is called aliasing of high frequency signals onto lower frequencies. Aliasing is due to the fact that the time interval is finite and is not zero. Thus to avoid aliasing the time interval Δt and N are chosen such that there are no large amplitudes. The other problem of DFT is the leakage which is due to limited frequency resolution (T is finite and less than infinite). The weighting function brings in the problem of Leakage. Leakage is due to limited frequency resolution ($T < \infty$, $\Delta\omega > 0$) leakage can be reduced by Hanning the DFT or tapering the data.

Hanning the DFT

Hanning of the DFT is done by applying the differencing to the amplitudes

$$\tilde{F}_m = -\frac{1}{4}F_{m-1} + \frac{1}{2}F_m - \frac{1}{4}F_{m+1} \qquad 0 \le m \le N-1 \qquad (3.5)$$

and making use of $F_{-1} = F_{N-1}, F_N = F_0$ applying a second order difference operator to the spectral amplitudes F_m.

Tapering the data

The effect of multiplying the data by a scaling function or passing it through a window is called tapering the data. This is equivalent to Hanning the DFT.

$$\begin{aligned} \tilde{f} &= \chi f_n \\ \chi &= \frac{1}{2}\left(1-\cos\left(2\pi\frac{n}{N}\right)\right)f_n \\ \tilde{f} &= \frac{1}{2}\left(1-\cos\left(2\pi\frac{n}{N}\right)\right)f_n \end{aligned} \qquad (3.6)$$

Tapering the data or Hanning the DFT will reduce leakage. The tapering is usually applied to the first 10% and last 10% of the data.

3.2.2 Filtering

The word filter is borrowed from electrical engineering, where digital filters are commonly used to remove (filter out) unwanted frequencies in a time series. There are number of filters depending on the requirements. The main uses of filtering are, smoothing the time series, removing particular frequencies and studying a particular frequency band.

Smoothing the time series (low frequency)

The filter is used to smooth the series to reduce the high frequencies so that one can study the low frequencies. This can be achieved through running averages and transfer functions. The running average is given as:

$$f_n = \frac{1}{2L+1}\sum_{l=n-L}^{N+l} f_L \qquad \text{using (2L+1).} \qquad (3.7)$$

and the filtered data through the transfer function is given as:

$$\tilde{H}_m = H_m \chi_m \tag{3.8}$$

where χ_m is the transfer function which relates the amplitudes of filtered and the unfiltered data.

Pre-whitening (high frequency)

Prewhitening reduces low frequency so the spectrum is "white". To attain a white spectrum one should use a high pass filter i.e.

$$\hat{f}_n = -\frac{1}{4} f_{n-1} + \frac{1}{2} f_n - \frac{1}{4} f_{n+1} \tag{3.9}$$

applying this filter causes the loss of 2 data points.

Red-noise spectrum

In order to test the significance of the spectral periods, the red-noise spectrum is utilised (Lau and Sheu 1988). The red-noise spectrum is computed based on the lag one month correlation, r_1. The formula for red noise spectrum S_k is given as:

$$S_k = S^* \left\{ \left(1 - r_1^2\right) / \left[1 + r_1^2 - 2r_1 \cos\left(\frac{\pi k}{m}\right) \right] \right\} \tag{3.11}$$

where $S^* = \frac{1}{m+1} \sum_{k=0}^{m} S_k$ is the average of the total raw spectral estimates S_k.

Disadvantages of Spectral Analysis

According to Burroughs (1986), there are dangers in using spectral analysis as a statistical method for detecting periods or cycles in climatic data. Periods may be due to non-linearity or interactions between high frequencies. Sometimes, filtering introduces periods which, may not be in the data.

3.2.3 Covariance between time series.

In meteorology one would like to know the lag covariance between two time series say g(t) and h(t). The expression for the lag covariance can be written as:

$$C_{gh}(\tau) = \frac{\lim it}{\tau \to \infty} \frac{1}{2\tau} \int_{-T}^{T} g(t-\tau) h(t) dt \tag{3.10}$$

with finite set of samples, g_n, h_n

In terms of discreet data the lag correlation is given as: $C_{gh_L} = \frac{1}{N-L}\sum_{N=L}^{N-1} g_{n-L}h_n$

In order to seek relationships between variables over the set of observations, the correlation can be calculated. Correlations measure the strength of the linearly symmetric relationship and how much the explanation is due to the independent variable.

3.3 Multivariate analysis

3.3.1 Introduction

This section deals with methods for studying multivariate data-sets with several variables. Relationships between the variables are sought and these relationships may be principal components or factors. The aim of multivariate analysis is to identify groups of inter-correlated variables, reducing the number of variables being studied and to re-write the data -set in alternative form. Brief outlines of Principal Component Analysis (PCA), Extended Empirical Orthogonal Functions (EEOF), and Complex PCA are given. Complete details of these methods can be found in statistical textbooks Preisendorfer (1988), Jackson (1991), Johnston (1992) and William et al (1997).

3.3.2 Principal Component Analysis (PCA)

After obtaining the data, the issue of analysing data in order to identify coherent structures in the data is encountered. In most cases subjective sampling or composite analysis is applied to the data but this leads to different results and thus objective analysis is required. It is in such cases when PCA is most useful. PCA identifies coherent structure (common fluctuations) which, depend on the data rather than the researcher's a priori knowledge of the phenomenon of interest. Basically, PCA decomposes the multivariate time series that is from the original data into linear combinations of Empirical Orthogonal Functions (EOF). The EOF are also called principal components (PC). The PC's are calculated from the covariance or correlation matrix from the data matrix. Principal Component

Analysis (PCA) has been widely used by both social and natural scientists. These include meteorologists and oceanographers, who have used it to study temporal and spatial variability of meteorological and oceanic fields. EOF analysis allows the calculation of orthogonal linear combinations of variables that account for maximum possible amount of variance in a data-set. The technique offers several important advantages namely:

(1) Description of important patterns of data variability,

(2) Data-set can be compressed,

(3) Filtering the data by using only significant components,

(4) Orthogonality property of the components is useful for predictor variables

(5) Exploratory data-analysis allowing dominant inter-relationships between data to be highlighted.

3.3.3 Problems with unrotated PCA

The rotation of principal components has been discussed in a number of papers (Richman, 1986; Rinker and Young, 1996). Unrotated PC modes have some properties, which make physical interpretation more difficult. The major characteristics are domain shape-dependence, subdomain instability, sampling problems and inaccurate portrayal of the physical relationships embedded within the input matrix. To avoid such problems the number of rotation techniques have been proposed. Determination of the number of significant PC modes from the noise is also very important. There are many methods which can be used to determine the number of significant PC components (North et al, 1982). The methods are; Kaiser Criterion, Scree method, Logarithm of the eigenvalue (LEV) and use of sampling errors of eigenvalues.

(1) Kaiser Criterion

All PC modes with eigenvalues greater or equal to one are significant.

(2) Scree Test

In this test, a graph is plotted with eigenvalues associated with PC modes against the PC mode number in descending order. Small eigenvalues are linked with gradual slope while the large eigenvalues with steep slope. The regions with gradual slope are neglected as they are associated with noise. The explained variance is sometimes plotted against the component number (in ascending order). If PC variance approaches some constant value then the components are measuring random errors. Graphical plots of the component numbers versus the variance extracted in unrotated components are useful. The number of significant components according to the test are determined from the graph at the point where the graph starts to flatten.

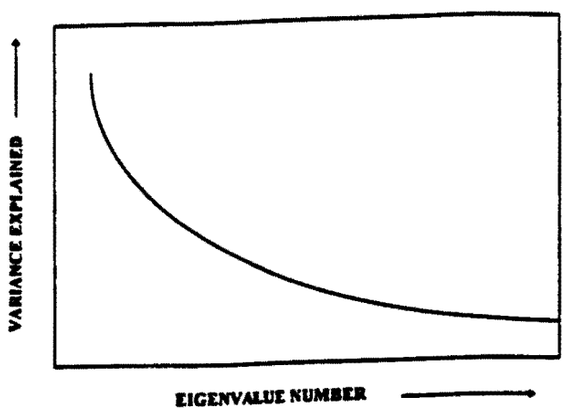

(3) Logarithm of the eigenvalue (LEV)

The logarithms of the eigenvalues are plotted as in (2) and the cut-off occurs where the curve becomes linear.

(4) Use of sampling errors of eigenvalues

In this method the sampling error is used to determine the significant components. Sampling error is the order of $(2/N)^{1/2}$ where N is the total number of the variables. Thus if the sampling error of a particular eigen value λ_i ie $(\delta\lambda_i=\lambda_i(2/N)^{0.5})$ is comparable to or larger than the spacing λ_i and λ_{i-1} a neighbouring eigenvalue, then the component associated with λ_I will be

comparable to the $\delta\lambda_I$. The cut-off point is when $\delta\lambda_I$ is $> \lambda_i - \lambda_{i-1}$. Details of these methods can be found in North et al (1982).

Rotation

PCA assumes that the records are orthogonal (independent) while many physical variables are not. Meteorological parameters like rainfall are influenced by synoptic and regional factors, giving some degree of similarities (non-orthogonality) between rainfall patterns of neighbouring locations. Such similarities are rejected in PCA solutions. Thus, some of the derived patterns may be physically unrealistic. Rotation of PC components makes the associated patterns more interpretable.

3.3.4 Practical Application of PCA

The starting point in PCA is to calculate the covariance matrix or the correlation matrix

$$\underline{C} = \begin{bmatrix} c_{11} \ldots c_{12} \ldots c_{1n} \\ : \\ c_{1n} \ldots\ldots\ldots c_{nn} \end{bmatrix} \tag{3.14}$$

or

where C_{ij} is the covariance between i^{th} and j^{th} variable.

S_{ij} is the correlation coefficient between I and j^{th} variable.

Thus $\underline{C}$ or $\underline{S}$ is a symmetric, non-singular matrix and may be reduced to a diagonal matrix λ by pre-multiplying and post multiplying it by a particular orthonormal matrix $\underline{U}^{l}$ such that

$$\underline{U}^{l} S \underline{U} = \lambda \tag{3.15}$$

The columns of $\underline{U}$ i.e. $\underline{u}_1, \underline{u}_2, \ldots \underline{u}_n$ are called eigen vectors. The diagonal elements of $\underline{\lambda}, \lambda_1, \lambda_2, \ldots\ldots, \lambda_p$ are called the characteristics roots, or eigen values of $\underline{S}$ or $\underline{C}$.

The eigen values are obtained from the characteristic equation $|S - \lambda I| = 0$ .where I is the identifying matrix. This involves solving a polynomial of degree n.

Use of Correlation or Covariance matrix

Sometimes the covariance matrix is used but it becomes difficult when the units vary i.e. the original variables are different in units. For example, if a variable is expressed in hPa and in another one in degrees centigrade. In this case the correlation matrix is superior.

Uses of Component Scores in Regression Analysis

The fact that the time series are orthogonal to each other implies that they are independent. The property of independence makes the scores useful in regression analysis or prediction models. The problem of co-linearity (Johnston, 1992) is avoided in multiple regression by using the component scores. Interpretation of the linear models obtained using the scores may sometimes be difficult. However the time scores are useful in interpretation of dynamical elements of climate.

3.3.5 Multivariate EOF Analysis (Combined PCA) and EEOF

In order to find the coherent structure of combined fields multivariate EOF analysis can be used (Wang, 1992). In multivariate EOF analysis two or more fields are combined together into one data field which is then subjected to PCA. This analysis extracts dominant patterns which are common in different fields. These patterns are useful in identifying the physical processes and teleconnections between ocean and atmosphere.

Extended Empirical Orthoganal Function Analysis (EEOF)

EEOF is an extension of PCA, which finds new variables that are linear combinations of the p variables. The description of EEOF can be found in Weare and Nasstrom (1982). This technique offers an alternative approach to describe moving features in spatial fields. A brief description is given below.

Let NP be the number of grid points and M the total (period) time.

Let $x_{i,j}$ be grid time series where i is the space index and j is the time index.

$$X_t = \begin{bmatrix} x_{1,1}, x_{1,2}, \ldots\ldots x_{1,M-2} \\ : \\ x_{Np,1}, x_{Np,2}, \ldots\ldots\ldots x_{Np,M-2} \end{bmatrix} \tag{3.16}$$

is a vector consisting of time-series of NP grid points at zero lag

$$X_{t+1} = \begin{bmatrix} x_{1,2}, x_{1,3}, \ldots\ldots\ldots x_{1,M-1} \\ : \\ x_{Np,2}, x_{Np,3} \ldots\ldots x_{Np,M-1} \end{bmatrix} \text{ at time t + 1} \tag{3.17}$$

at lag t + 2

Let $\underline{P} = \underline{x}_{t,t+1,t+2} = \underline{Q}\underline{Z} + \underline{E}_{t,t+1,t+2}, t = 1, \ldots\ldots M$ (3.18)

$\underline{E}$ is the error function

$\underline{Q}$ is the set of coefficients

$\underline{Z}$ is the desired empirical function

$$P = \begin{bmatrix} x_{1,1}, x_{1,2} \ldots\ldots\ldots x_{1,M-2} \\ : \\ x_{Np,1}, x_{Np,2} \ldots\ldots\ldots x_{Np,M-2} \\ x_{1,2}, x_{1,3}, \ldots\ldots\ldots\ldots x_{1,M-1} \\ : \\ x_{Np,2}, x_{Np,3}, \ldots\ldots\ldots x_{Np,M-1} \\ x_{1,3}, x_{1,4}, \ldots\ldots\ldots\ldots x_{Np,M} \\ : \\ x_{Np,3}, x_{Np,4}, \ldots\ldots\ldots\ldots x_{Np,M} \end{bmatrix} \tag{3.19}$$

P is the matrix of dimension 3 * NP by M-2. The eigen function Z is of dimension 3 * NP. Practically three successive maps are plotted. The correlation (covariance) matrix is obtained from $C = PP^T$ and eigen values are obtained from $CZ = \lambda Z$ where λ is the eigen value. C is the lagged covariance matrix.

The first NP elements of the eigenvector corresponds to the observations belonging to the period (t), and the next NP values belong to the period (t+1) and the last NP values refer to (t+2) period. The disadvantage of EEOF analysis is that the concurrent intercorrelations and the lag correlations are repeated. The

dimension of the covariance (correlation) matrix may be very large. The resulting elements of the eigenvector become smaller relative to the elements of PC's in standard EEOF.

The advantage of EEOF is the identification of 'hidden' structures in the atmospheric fields and quantification of the patterns towards the total variance of sequentially evolving fields. The EEOF is better for this than the complex EOF analysis.

3.3.6 PCA Analysis of wind as a vector

A situation can arise when quantitative descriptions of coherent structures in meteorology/oceanography may require analysis of complex variables. In such cases a different approach is used which is similar to PCA but for complex numbers. A description of the method is available in Legler (1983).

Let $U_j(t)$ be a complex vector data field. In matrix form let the field be represented by:

$$U_j(t) = \begin{bmatrix} u_{11}, u_{12} \ldots\ldots u_{1M} \\ : \\ u_{N1}, u_{N2} \ldots\ldots u_{NM} \end{bmatrix} \quad \text{which is the entire data field} \qquad (3.20)$$

To find the eigenvalues and eigenvectors one needs the covariance (correlation) matrix. In a complex data set the covariance (or correlation) matrix is the Hermittian matrix. The Hermittian matrix is a special matrix consisting of complex numbers such that the diagonal elements are complex conjugates of each other. It has real eigenvalues and complex eigenvectors.

$$[H] = \frac{1}{M}[U][U^{*T}] \qquad (3.21)$$

where U^{*T} denotes the complex conjugate of U

The eigenvector decomposition

$$[H][E] = [E][\lambda] \qquad (3.22)$$

where $[E]$ are eigenvectors and λ is the associated eigen value. The trace of H is the total variance of the original data set.

$$\text{TRACE } [H] = \sum_{i=1}^{N} \lambda_i$$

The eigenvalue of each of the eigenvectors indicates the proportion of the total variance accounted for by that particular mode of variation. Time-dependent scores $A_n(t)$ are given by

$$A_n(t) = \sum_j U_j(t) E_n(x_j) \tag{3.23}$$

where $U_j(t)$ is a complex data field, $E_n(x_j)$ are complex eigenvectors.

3.4 Composite analysis

Composite Analysis is one of the techniques used in studying the structures of synoptic disturbances (Keshavamurty and Rao 1992). This technique is similar to correlation analysis. The method has been applied in a number of studies locally (Levey, 1993; Majodina, 1995; Kabanda, 1996). Composite analysis technique assists in depicting relationships amongst meteorological variables. Individual cases may diplay different features due to different mechanisms but composite analysis identifies the common characteristics.

3.5 NAG Subroutines and STATISTICA Package

The following subroutines from NAG Fortran Library Routines (1990) were utilised in order to facilitate the computations in this thesis;

(1) G13DNF: This subroutine calculates the sample partial lag correlation of a multivariate time series.

(2) G02BAF: This computes means, standard deviations of variables, sums of squares and cross products of deviations. Pearson product moment correlation coefficients are also calculated.

(3) C06EAF: This computes the discrete transform of a sequence of real data values. This routine also performs an inverse using C06GBF and C06EBF.

(4) F02ABF: This calculates the eigenvalues and eigenvectors of real symmetric matrix.

(5) F02GJF: This calculates the eigen values and if required all the eigenvectors of the complex generalised eigenvalue problem.

(6) F02AXF: This computes the eigenvalues and eigenvectors of a Hermitian matrix.

(9) BESK and BESY calculates Bessel functions.

3.6 Data

3.6.1 Introduction

This section describes the data from the European Centre for Medium -Range Weather Forecasts atmospheric data, the Climatic Research Unit the historical rainfall data, the United Kingdom Meteorological Office sea surface temperature, and the National Centre for Environment Prediction Outgoing Longwave Radiation (OLR) data.

3.6.2 European Centre for Medium -Range Weather Forecasts (ECMWF) data

The European Centre for Medium -Range Weather Forecasts data set is a large collection of gridded surface and atmospheric data that has been available since 1979, in conjunction with the World Climate Research Program. The other data set, which has been used is the monthly and daily data set from NCAR. In this study the ECMWF data has been utilised extensively. In interpolating ECMWF values, four dimensional data assimilation is used. ECMWF continues to create and maintain an archive of surface and atmospheric data at standard tropospheric levels. The data is stored in form of classical spherical harmonic coefficients of horizontal winds, vertical velocity, temperature, moisture and geopotential heights. The resolution here is at 2.5 degrees latitude by 2.5 degrees longitude. It is important to note that geopotential heights are analysed quantities and temperatures are predicted by the model.

The optimum interpolation scheme employed at ECMWF uses observations to determine increments of geopotential height on model sigma levels. The hydrostatic temperatures are then added to the 6 hour forecast guess model-level temperatures to obtain the analysed temperatures. Analysed snow cover and SST's specify some lower boundary conditions for the model, while surface and near-surface temperatures over land are largely dependent on relevant physical parameterizations. Continuous improvements in the paramerisation are being undertaken. Postprocessing to standard pressure levels involves an interpolation of temperatures from the two nearest model sigma levels, or if the pressure level is below the model terrain, an extrapolation is involved using a standard lapse-rate. So one might anticipate larger uncertainties at 1000 hPa when surface pressures are less than that.

There are a number of shortcomings in processing the ECMWF data namely changes in forecast models, changes in the data assimilation system and unavailability of delayed mode data. Details of the quality and inconsistencies of the can be found in the literature (Bengtsson and Shukla, 1988; Trenberth and Olson, 1988; Hurrel and Trenberth, 1992). The ECMWF data set has been utilised in many institutions for research to document and analyse synoptic and large scale systems. For example, Hoskins et al (1989) constructed diagonotics of global atmospheric circulation based on ECMWF data.

Historical outline of ECMWF the temperature data

During the period 1979-1989, data were taken from the archived analyses and were produced from 12 hourly data excluding a few "bad" analyses where problems clearly existed. Prior to 1982, very large and physically unrealistic temperature variations at 1000 hPa are present in the ECMWF analyses. Standard deviation of ECMWF 1000 hPa monthly temperature anomalies are found to be large in 1979-1981 period. It is difficult to account for the source of the

uncertainties in the 1000 hPa data prior to 1982. Other uncertainties exist in the ECMWF 1000 hPa temperature analyses after this time.

Operational ECMWF analyses were not originally intended for climate studies, and there are many reasons why the analysed temperatures should not be appropriate for climate monitoring, particularly over Africa where observations are sparse.

As discussed by Bengtsson and Shukla (1988), the model-based ECMWF global date set is a very useful by-product of the operational forecasting missions. As such, discontinuities in the data arise from frequent improvements to the forecast model and the data assimilation system, and these discontinuities are manifested as apparent changes in climate. Bengtsson and Shukla (1988) have discussed the major changes in the ECMWF Forecast model. This study commenced prior to re-analysis data being available and care has been taken to avoid derivative parameters which, could be model dependent.

3.6.3 Gridded Southern African Rainfall data

Gridded rainfall data was obtained from Climate Research Unit (University of East Anglia). The Southern African historical monthly precipitation data set was extracted from stations across Africa from 1900 to 1993, gridded at 2.5 degrees latitude by 3.75 degrees longitude resolution. For full details on quality of the data refer to Hulme and Jones (1993).

3.6.4 UK Meteorological Office SST data

This data set is an extension of the Comprehensive Ocean -Atmosphere Data set (COADS) which is a very large collection of surface marine data available for the world ocean over the last 150 years (Woodruff et al, 1987). The data set consists of grid box SST time series for the global ocean from 1901 to 1992. Here, the UK Met Office version of the Historical Sea Surface Temperature (MOHSST) is used. The resolution is 5° x 5° latitude/longitude and the data has been quality

controlled. A window domain between latitude 47.5°W to 97.5°E, and longitude 17.5°N to 37.5°S was extracted. This window covers the Indian and the Atlantic Oceans. The data before 1950 contains a lot of missing values and thus only data after 1950 to 1992 was utilised in this study. This period coincides with the historical gridded rainfall data (Hulme, 1996). The details have been discussed by Mason (1992). Most of the problems have been dealt with and an historical development of the original COADS date set is available.

3.6.5 National Centre for the Environment Prediction (NCEP) OLR and Southern Oscillation Index (SOI) data

The Outgoing Longwave Radiation (OLR) data was obtained form National Centre for Environmental Prediction. A resolution of 2.5° x 2.5° longitude/latitude was utilised in the domain 70°W -100°E and 20°N-40°S. OLR data can be used as an approximation to deep convection in lower latitudes (Wang and Rui, 1990).

The Southern Oscillation Index was obtained from NCEP and is the difference between the normalised monthly mean sea level pressure at Tahiti (17.5°S, 149.6°W) and Darwin (12.4°S, 130.4°E).

3.7 Summary

The main purpose of the techniques is to investigate temporal and spatial characteristics of SST and atmospheric data. Spectral Analysis has been applied to study tropical synoptic features (Asnani 1993). In this study spectral analysis will be applied to rainfall, SST and atmospheric data. PCA will be applied to reveal both spatial and temporal variability. The advantage of this method in climate dynamics is to recognise teleconnection patterns, which can be helpful in identifying the mechanisms behind the variations. Many modes can be computed but only a few are significant. PCA is an inductive method and it can be used to compress data. In this study PCA is applied to rainfall, SST and atmospheric variables in order to reveal the modes and the time scores, which are later used for

prediction. The time scores are further utilised in identifying the links between the circulation modes and ENSO. In order to identify propagating features EEOF is applied to 500 hPa standardised monthly geopotential height anomalies. The combined PCA is applied to summer (DJF) OLR, SST and tropospheric wind anomalies. This method is quite helpful in finding coherent structures and previously it has been applied in investigating the ENSO structure (Wang, 1992). The combined PCA assists in separating external and internal forcing. The vector PCA has been previously applied in investigating the trade winds over the Pacific Ocean (Legler, 1983), but its use has been limited due to the fact that it requires large computing capacity. In this study it is applied to water vapour flux. The kinematic and thermodynamic atmospheric variables are used from ECMWF data set. The period of study is from 1980 to 1993. Pentad (5 day mean)and monthly values are utilised.

CHAPTER 4

MEAN CHARACTERICTICS OF SUMMER CIRCULATION OVER SOUTHERN AFRICA

4.1 Introduction

The purpose of this chapter is to provide mean characteristics of summer circulation based on 14 years of ECMWF data. Mean characteristics are a necessary background for examination of causes of rainfall variability. Large-scale and quasi-stationary features occur over southern Africa and the adjacent oceans during summer season (Harrison, 1989; Rocha, 1992; Makarau, 1995). Changes in position and intensity of these features may determine behavior of the atmospheric circulation and rainfall. The purpose of this chapter is to present thermal and dynamical characteristics of southern Africa and the adjacent oceans. Some mean characteristics of the thermal field over the continent may reveal the influence of local forcing in maintaining the summer circulation. Tropical sea surface temperatures are boundary conditions which can affect changes in the atmosphere and hence the climate. Fluctuations in the lower boundary can cause changes in the large-scale circulations like Hadley or Walker cells (Harrison, 1986). Hence changes in the basic state of the tropical oceans can lead to changes in the circulations and thus the rainfall over southern Africa. The mean SST fields are used to initialize coupled ocean-atmosphere models for understanding the physical processes and prediction. Continuous monitoring of sea surface temperature is important. Lower and upper tropospheric fields can describe the state of the atmosphere. Thermal fields are important for regions where weak geostrophic wind fields are prevalent. Changes in these fields can cause changes in rainfall bearing disturbances and hence influence the rainfall over southern Africa. Thus there is a need to better document and understand the mean summer thermodynamic and dynamic fields. It is also important to know the mean field before undertaking the interannual and intraseasonal variability studies.

The Southern Hemisphere has been found to be characterized by the semi-annual

cycle (van Loon, 1972) modulated by wave number 1 and 3 (Karoly, 1985;Mo and Higgins, 1997). Preston-Whyte and Tyson (1988) and Theron and Harrison (1990) have described mean distributions of meteorological elements for southern Africa. This section of the study describes the mean circulation, which is a useful point of departure for explaining the interannual variability. Pathack (1993), Rocha (1992) and Makarau (1995) have described southern African circulations. This work can be considered as an update to the previous work. With the availability of ECMWF data, some mean circulations are presented in this chapter. It is important to explain the mean fields in terms of the simple atmospheric models with only essential physical processes. The model of Wang and Li (1993) is presented in order to show the importance of different physical processes and the schematic diagram showing the model physics is given in **figure 4.0** (the list of the symbols in figure is given in the annex 2). The focus is on peak summer months, which are December, January and February (DJF). The results of the lower levels are given first. Data utilized here are described in chapter 3. The data sets include monthly fields at standard pressure levels. The DJF mean fields are computed for selected the atmospheric variables some derived parameters and SST.

4.2 Mean DJF thermal fields, trends in rainfall and SST

It is well documented that earth-ocean-atmosphere system is driven by differential heating (Das, 1986). Various circulations occur in order to reduce the differential heating. In the tropics latent heating (due to release of condensational heating) is closely related to vertical motions. Ascending regions (low-pressure regions, convergence) are associated with precipitation and hence are heat sources, whilst heat sinks and radiational cooling dominate descending areas. The oceans interact with the atmosphere through momentum, latent and sensible heat, evaporational and condensational processes. Thus knowledge of thermal fields is very important. The distribution of sea surface temperatures (SSTs) are presented first followed by lower (850hPa) and upper (200hPa) temperature field. Standard deviations of SST are also presented.

Mean DJF SST.

Figure 4.1(a) shows averaged DJF sea surface temperature field, tropical Indian Ocean has a large extent of warm water compared to Atlantic Ocean. High SST (over 27°C) are observed between 5°N-20°S in Indian Ocean and along the equator over Atlantic Ocean. Since deep convection is found over high SST, these regions with high SSTs play an important role in the diabatic forcing of the southern African circulation. Note that the high SST regions do coincide with the oceanic ITCZ (see figure 4.4(a)). In general SSTs decrease poleward in response to solar radiation. Strong SST gradients are associated with strong winds (see figure 4.4(a). Subtropical high-pressure systems overlie waters with temperatures ranging from 22°C-24°C.

Standard deviation of DJF SST

Standard deviation field is shown in **figure 4.1(b)**. Large values of variance are confined to the southwest Atlantic and southern Indian Ocean where ship observations are sparse. Figure shows the field of standard deviation for DJF for the period 1950-89. Large standard deviations are over midlatitudes (> 0.4) and relatively small values over the tropics. Central Indian Ocean and equatorial Atlantic Ocean have relatively small values and thus making predictability less difficult.

Summer rainfall trends (DJF)

Figure 4.1(c) displays the long-term trend of DJF rainfall. The DJF trend map illustrates a negative trend (-0.6 mm per year) over eastern Zimbabwe and central Mozambique. Many areas show a negative trend except the western Cape and east of 25°E and north of 15°S. Maximum positive trend (0.6 mm per year) occurs over eastern Zambia and Malawi. The trend distribution in this peak season is similar to the orientation of the cloud bands (Harrison, 1984) which are dominant during the rainy season. It is inferred that cloud bands over the south eastern interior are

Mean DJF SST.

Figure 4.1(a) shows averaged DJF sea surface temperature field, tropical Indian Ocean has a large extent of warm water compared to Atlantic Ocean. High SST (over 27°C) are observed between 5°N-20°S in Indian Ocean and along the equator over Atlantic Ocean. Since deep convection is found over high SST, these regions with high SSTs play an important role in the diabatic forcing of the southern African circulation. Note that the high SST regions do coincide with the oceanic ITCZ (see figure 4.4(a)). In general SSTs decrease poleward in response to solar radiation. Strong SST gradients are associated with strong winds (see figure 4.4(a). Subtropical high-pressure systems overlie waters with temperatures ranging from 22°C-24°C.

Standard deviation of DJF SST

Standard deviation field is shown in **figure 4.1(b)**. Large values of variance are confined to the southwest Atlantic and southern Indian Ocean where ship observations are sparse. Figure shows the field of standard deviation for DJF for the period 1950-89. Large standard deviations are over midlatitudes (> 0.4) and relatively small values over the tropics. Central Indian Ocean and equatorial Atlantic Ocean have relatively small values and thus making predictability less difficult.

Summer rainfall trends (DJF)

Figure 4.1(c) displays the long-term trend of DJF rainfall. The DJF trend map illustrates a negative trend (-0.6 mm per year) over eastern Zimbabwe and central Mozambique. Many areas show a negative trend except the western Cape and east of 25°E and north of 15°S. Maximum positive trend (0.6 mm per year) occurs over eastern Zambia and Malawi. The trend distribution in this peak season is similar to the orientation of the cloud bands (Harrison, 1984) which are dominant during the rainy season. It is inferred that cloud bands over the south eastern interior are

getting weaker. The pattern is similar to figure 11 of Ropelewski and Halpert (1996) in which during warm phase (negative SOI) conditions produces a deficit in precipitation.

The general decrease in peak DJF summer rainfall may be due to the absence of the cloud bands (Harrison 1986) or the frequent appearance of warm events (negative SOI) which result into the eastward shift of the Walker circulation. Wetter conditions in the SON season (not shown) may be linked to early development of convergence between the Zaire Air mass and the easterly trades.

In general it is considered that the thermal contrast between the continent and ocean is a possible factor causing moisture convergence during summer. The summer rainfall over Southern Africa is linked to central Indian Ocean SST (Rocha 1992). Increasing SST over Indian Ocean may result in declining thermal contrasts and a poor rain season. Land-atmosphere interactions (e.g.declining vegetation) may be a further cause for the downward trend in rainfall.

Trends

Figure 4.2(a) shows the monthly SST trend from 1950 to 1990. The trend was obtained by using the least square method. Large positive trends are found over the eastern Atlantic, southwestern Atlantic, south Indian (65°E, 35°S) and central north Indian Ocean (80°E, 0°S) where ship observations are dense. Negative trends are confined to the equatorial western Atlantic Ocean. The positive pattern over the eastern Atlantic show a northwest to southeast orientation along the shipping lane.

Persistence of the SST anomalies

The intensity and temporal nature of the sea surface temperature anomaly pattern are important. A large persistence anomaly can generate a large response. In order to find the areas with persistent SST anomalies, autocorrelation coefficients were calculated. The autocorrelations at lag 2,3 and 4 months are displayed in **figure 4.2(b), (c) and (d)**. The values show a northwest to southeast orientation over the Atlantic and a zonal orientation over the north Indian Ocean. The patterns of auto-

correlation coincide with the shipping lane due to data density. Highest auto-correlation coefficients are found over the eastern Atlantic and north Indian Ocean and this may provide useful areas for predictands.

Surface DJF Temperature

Figure 4.3(a) shows the distribution of 850 hPa surface temperatures. The 850hPa level coincides with some continental features over southern Africa and thus it can be considered as representing the surface in some regions with heights close to 1500 meters. The heated areas with high temperature (>20°C) are over the African continent due to 12UT(1400h LST) data being used, while the oceanic regions have lower temperature (<16°C). The highest temperature is found over the Kalahari Desert and lowest temperature (<10°C) over the southern oceans in the midlatitudes. The land and heat contrast can be explained by the different heat capacities of air and water. Over land most of the solar radiation is spent on heating the air temperature while for the sea the heating goes to the upper-mixed layer (depth of 200m) and this results in the land being hotter than the ocean. Considerable amounts of heat are required to raise the SST compared to air temperature over land, and this is particularly evident in the diurnal cycle. Differential heating results in the creation of the low pressure over land and high pressure over cool oceanic regions.

Mean Sea Level Pressure Field (MSLP)

Figure 4.3(b) shows the distribution of MSLP for DJF. For the peak summer season (DJF), the dominant features are the two anticyclones over the South Atlantic and Indian oceans with low pressure over the equatorial regions and the subcontinent. Low pressure areas with sufficient moisture result in release of latent heat and the warming of air on large-scale and hence the creation of a temperature gradient between non-cloudy areas and cloudy areas.

Lower tropospheric heating

Figure 4.3(c) displays the mean thickness (an approximate for mean temperature in layer) between 850 and 500 hPa. A warm layer (heights greater than 4360 m) is

over tropical Africa with cold layer in the midlatitudes. High thickness heights (>4320 m) are mainly found in equatorial regions (15°N - 25°S). The maximum value is found over eastern Namibia (20°S, 20°E). Low values are found over the midlatitudes. A strong meridional gradient exists in the midlatitudes (30°S - 60°S). Since the geostrophic winds are weak in the tropical regions, this field is important for thermal westerly wind production.

Upper tropospheric heating

Figure 4.3(d) exhibits DJF mean thickness between 500 and 200 hPa levels. Similar pattern to the 850 hPa - 500 hPa thickness emerges with relatively lower heights over the Atlantic Ocean. High values (>6500 m) are confined to the equatorial regions (20°S - 10°N), maximum values are found over southeastern parts of Angola (17°S - 20°S). There are high values of thickness over equatorial latitudes (20°S to 7°N) with maximum over southern Angola (20°S and 15°S) during DJF. Minimum values are found over mid-latitudes. A trough of thickness prevails over western parts of the Atlantic Ocean. The high thickness represents high upper level temperatures. The largest annual amplitude of thickness (40 gpm) is found over Angola. It has been observed that tropical weather systems have an upper tropospheric "warm core" structure. Upper level warming can lead to lowering of surface pressure through the hydrostatic equation.

4.3 Mean DJF kinematic fields

Convective heating over subcontinent and cooling over the adjacent ocean result in differential heating. The imbalance in heating field requires some dynamic processes to occur to re-distribute the heat. Hence the presentation of dynamic fields can throw some light on how heat and momentum is distributed. This may be associated with convergence in the lower troposphere (adiabatic cooling) and divergence in upper troposphere in heat source regions. In heat sink regions one would expect upper convergence and lower level divergence (adiabatic warming). The imbalance creates local and regional Walker and Hadley cell circulations in

lower latitudes with weak coriolis force

Low level circulation

Figure 4.4(a) is the field of 850 hPa wind. Large subtropical anticylones are prominent over the Indian and Atlantic oceans. An axis of anticyclonic flows separates the westerlies south of 30°S from easterlies to the north. A weak anticyclone is found over the equatorial Indian Ocean with the axis along 5°S. The region between 20°S and 20°N is a general region of easterlies except for the cyclonic flow over Angola and western Zambia. The ITCZ is recognized by the zone of convergence of winds along latitude 20°S over Zimbabwe and 15°S over the Indian Ocean. The tropical regions where quasi-stationary convergence is observed are important for diabatic forcing. Changes in the positions of these features may lead to changes in the Hadley and Walker circulations and hence influence rainfall over southern Africa. The center of continental cyclonic flow varies from year to year and contributes to inter-annual variability of summer rainfall (Rocha 1992).

850 hPa Vorticity Field

According to Charney and Eliasen (1964), the vertical velocity at the top of the barotropic boundary layer is proportional to relative velocity at the surface. Hence the field of vorticity can throw some light on the state of vertical motion. **Figure 4.4(c)** indicates the 850 hPa vorticity field with strong positive values (>0.8 x $10^{-6}s^{-1}$) over the southern Atlantic and Indian Ocean midlatitudes (30°S - 40°S). Negative values are found over Central Africa (10°S - 20°S), the Indian Ocean (20°S - 5°S) and extra tropical latitudes (50°S - 60°S). Note the regions of negative vorticity coincide with the cyclonic areas described in the 850hPa circulation. The advection of vorticity from the western Atlantic coast (through the recurved Zaire air) and the Indian Ocean (through the easterlies (20°S) into the subcontinent maintains the ekman-pumping of moisture from the boundary layer.

Upper level circulation

The prominent feature is a large anticyclone over southern Africa centred over Zimbabwe with diffluent easterly flow north of 20°S and westerlies south of this latitude **(see figure 4.4(b))**. There are year to year variations in the intensity and position of the upper level anticyclone. If the position is far to the north westerlies prevail over southern Africa and this results in below normal rainfall. If it is located further to the south eastelies will prevail over southern Africa resulting in above normal rainfall. Over the Indian Ocean weak easterlies are observed. An Atlantic wave (Harrison 1986) is observed over the central Atlantic Ocean. The position of this Atlantic wave plays an important part in modulating summer rainfall. Strong westerlies are observed over midlatitudes (30°S-50°S). **Figure 4.4 (d)** shows 200hPa mean DJF vorticity field. Negative (cyclonic circulation) values are found in equatorial latitudes (18°N- 18°S) and positive (anticyclonic circulation) in subtropical regions (20°S- 50°S).

Divergence

The mean DJF 200 hPa divergence is displayed in **figure 4.5(a)**. This field indicates strong divergence over northeast Brazil, southern Africa and Madagascar, which coincides with strong convective regions. Large areas of convergence are over the northern Atlantic, eastern Atlantic, southeast Indian Ocean and the northern Indian Ocean.

4.4 Mean DJF heat sources and sinks

Heat sources and sinks can be inferred from thermodynamic parameters. Water vapor flux, precipitable water and OLR parameters are presented in order to identify the areas of heat source (convergence WVF regions, high precipitable water and low values of OLR) and heat sinks (regions with divergent WVF, low precipitable water and high values of OLR).

Mean DJF precipitable water

Figure 4.5(b) displays the precipitable water field. High precipitable water (> 50 mm) is found over north-east Brazil, central Africa and over the central Indian Ocean while low precipitable water (<30 mm) is located over the central Atlantic, southern midlatitudes and the areas north of 10°N. The field is consistent with the positions of the stationary convective cells and the planetary ITCZ. Low values are associated with subsidence regions.

Mean DJF water vapor flux

Vertically integrated atmospheric water-vapor flux is shown in **figure 4.5(c).** There is a prevailing atmospheric moisture flux divergence over oceanic regions south of 20°S. Moisture flux convergence is largest over land with a closed cyclonic circulation over Angola (10°S - 20°S). There is a line of flux convergence along 15°S over the Indian Ocean between the southeast and northwest trade winds. In general atmospheric moisture flux convergence is strongest over southern Africa. The source of water vapor for southern Africa is from the central Indian Ocean through the easterly winds.

Mean DJF convective activities OLR

The mean field of this parameter is similar to the precipitable water as can be seen in **figure 4.5(d)**. High values (260 W m^{-2}) are found over the Sahara and Kalahari deserts and the subtropical high-pressure areas. Low values (< 220 W m^{-2}), which are associated with convective systems, are observed over Brazil, central Africa and the central Indian Ocean monsoon trough.

4.5 Interpretation of mean summer circulation

The horizontal structure of tropical mean motions can be explained by linear shallow water equations (Matsuno, 1966; Gill, 1980). Tropical circulations are mainly forced by large-scale diabatic heating (Gill, 1980; Matsuno, 1966). In the Gill model a heat source is associated with stationary Kelvin waves to east of the

heat source and Rossby waves to the west. The response to large-scale heating depending on the position of the heating can be either a Rossby or Kelvin response. The mean location of maximum heat source during the summer season is found over Zambia (15°S, 30E) and Zimbabwe (see OLR figure 4.5(d), and upper level divergencel divergence figure 4.5(a)). At lower levels (850 hPa circulation see figure 4.4(a)) a cyclonic flow over Angola lies southwest of maximum heating and easterlies occur over the Indian Ocean. The response at upper levels (200hPa winds see figure 4.4(b)) is two large anticyclones, one centred over Botswana and Ethiopia with easterlies in the equatorial band. Strong easterlies occur over the Zambia. These patterns are similar to the theoretical linear patterns obtained by Gill (1980) except for the eastward movement of the Ethiopian anticyclone due to non-linear factors.

4.6 Forcing mechanisms for mean thermal trough

Most of the dynamical processes can be explained by shallow water equations in the tropics. In order to explain the mean DJF features of Southern Africa and the adjacent oceans, it is important to use the equations of motion and the thermodynamic equation as stated by Wang and Li (1993). It should be noted that the simple model is good for describing the fundamental features and the necessary physics. Assuming linear hydrostatic motion on a beta plane and using pressure co-ordinates the equation of motions for baroclinic mode of ϕ can be written as (Wang and Li 1993):

$$\frac{\partial}{\partial}\left(\vec{V}\right)+y\vec{k}\times\vec{V}=-\nabla\phi-\varepsilon\vec{V} \tag{4.1}$$

$$\frac{\partial\phi}{\partial}+N\phi+(1-\delta I)\nabla.\vec{V}=-NG\left(T_s-\overline{T}_s\right)+d(\delta B-1)\nabla.V_B-\delta F\left|V_B\right|\left(T_s-T_*\right) \tag{4.2}$$

$$-y\vec{k}\times\vec{V}_B=-\nabla\phi+A\nabla T_s-E\vec{V}_B \tag{4.3}$$

Where ϕ and $\vec{V}$ represent the non-dimensional geopotential and horizontal velocities in the lower free troposphere.. The nine non-dimensional parameters in the equations are:

$$\varepsilon = \frac{\varepsilon_*}{\sqrt{\beta C_0}}, N = \frac{\mu}{\sqrt{\beta C_0}}, I = \frac{RL_c b}{C_p P_2 S_2 \Delta p}\left(\bar{q}_3 - \bar{q}_1\right), B = \frac{RL_c b}{C_p P_2 S_2 \Delta p}\bar{q}_e, G = \frac{\Delta p}{2p_2} r, d = \frac{p_s - p_e}{\Delta p},$$

$$F = \left(\frac{C_0}{\beta}\right)^{0.5} \frac{\rho_s g L_c b}{2C_p p_2} C_E K_q, A = \frac{p_s - p_e}{2p_e}, E = \frac{\rho_s g K_D}{\left(p_s - p_e\right)\sqrt{\beta C_0}}$$

ε represents the Rayleigh friction coefficient, N is the Newtonian cooling coefficient, I the heating coefficient due to free - troposphere moisture convergence, B is the heating coefficient due to boundary layer moisture convergence. G is the coefficient of long wave radiation forcing, d is depth of boundary layer, F is the coefficient of evaporation forcing, A is the coefficient of SST gradient forcing and E is Ekman number in the boundary layer. The full list of symbols is given in annex 2. **Figure 4.0** is the schematic diagram illustrating the physics of the above model (Wang and Li, 1993).

For the mean circulation motion may be considered steady,

For steady motion $\frac{\partial}{\partial} \to 0$ Equation (4.2) becomes

$$N\phi + (1 - \delta I)\nabla.\vec{V} = -NG\left(T_s - \bar{T}_s\right) + d(\delta B - 1)\nabla.\vec{V}_B - \delta F\left|\vec{V}_B\right|\left(T_s - T_*\right) \qquad (4.4)$$

Where $\phi = \frac{1}{2}\left(\phi_3 - \phi_1\right)$ is the thickness between 850hPa and 500hPa levels

or between 500 hPa and 200hPa levels.

It can be seen that ϕ is a function of the radiational forcing, moisture convergence heating and evaporational forcing. The geopotential can be considered to be lower troposphere geopotential anomalies with upper level geopotential anomalies of opposite sign. Thus the forcing mechanism for lower tropospheric low-pressure system can qualitatively be taken as radiative forcing, moisture convergence and higher surface temperature.

Radiational Forcing

Radiational forcing is represented by $-NG\left(T_s - \bar{T}_s\right)$, a deviation from its domain mean. A higher than domain-mean surface temperature can result in lower pressure at 850hPa. Thus, in summer the radiation forcing is highest over the

southwest of the subcontinent (figure 4.3(a)).

Moisture Convergence Heating

Moisture convergence-induced heating will enhance the low pressure at 850hPa. This is represented by the expression $d(\delta B-1)\nabla.\vec{V}_B$, which is associated with free tropospheric moisture convergence and boundary layer moisture convergence. The large values of thickness are associated with high moisture content. The contribution due to this term is maximum over the interior of the subcontinent in summer season. Figure 4.5(c) shows large moisture convergence over southern Africa, the Indian Ocean along 10°S, Gulf of Guinea and northeast of South America.

Evaporational Forcing

Higher surface temperature will result in more surface evaporation (only if soil moisture is high) which in turn will enhance the low pressure at 850hPa. This is represented by the expression $-\delta F|\vec{V}_B|(T_s-T_*)$. The thickness heights will increase if the difference between T_s and T_* is large and frictional velocity is large.

4.7 Summary and discussion

The mean summer structure of southern Africa and the adjacent oceans has been presented in this chapter and the following characteristics have been revealed:

(i) SST field shows high SST in equatorial regions and low SST in midlatitudes. Trend of SST anomalies indicate warming over most parts of oceans for the period 1950 to 1990. Strong persistence of SST anomalies was found over eastern Atlantic and Tropical Indian Oceans, but could be data dependent. The trend in rainfall over southern Africa for the period 1950 to 1989 is negative trend over eastern Angola, Botswana, Zimbabwe and eastern South Africa.

(ii) MSLP field shows the presence of St Helena, Mascarene high-pressure cells and low pressure over the interior of the subcontinent. Associated with this is convergence over the continent and divergence over the oceanic regions.

(iii) Equatorial continental convergence represents the Northern ITCZ and the

convergence over southern Africa and Madagascar symbolizes the Southern ITCZ

(iv) High temperatures are observed over the continent and low temperature over the ocean with 12UT data. Upper tropospheric heating over southern Africa is due to the release of latent heat and divergence at 200 hPa. The land-sea temperature contrast is a major source of energy for the southern African circulation. Direct circulation results from warm air rising in the middle troposphere over land and cold air sinking over the sub-tropical oceanic regions.

(v) Moisture is advected from the Indian and Atlantic Oceans. Most of the moisture originates from the Indian Ocean.

(vi) The mean SSTs are relatively higher over the Indian Ocean compared to the Atlantic Ocean. SST gradients in the subtropical Atlantic Ocean are due to upwelling in the Benguela. The highest SST's over the Indian Ocean coincide with the ITCZ that extends zonally along 15°S - 5°N. The meridional temperature gradient over the midlatitudes supports a zonal thermal flow. High variability of SSTs are found over the southwest Atlantic Ocean and south Indian Ocean where data are sparse. Warm pool dynamics may occur in the central Indian and cold pool dynamics in the Atlantic and the Southern Ocean.

High sensible heating over Angola may play a crucial role in warming the lower troposphere and allow more intake of moisture. The heat low over the subcontinent will be taken up in chapter 7.

(vii) The mean water vapor flux field shows the presence of the vortex over Angola and the adjacent areas. This vortex plays an important role in the importation of moisture mainly from the Indian Ocean. The moisture convergence over this area contributes to raising the thickness and further amplification of the low. Moisture convergence, evaporation and sensible heat maintain the low-level vortex.

The location of the low-level cyclonic and upper level anticyclonic flow may contribute to rainfall variability. It has been observed by Rocha (1992) that during most dry southern African summers positive pressure anomalies occur over the

subcontinent and negative anomalies over south-east Madagascar. At upper level westerly anomalies are observed over southern Africa.

Several surface and tropospheric features appear in mean summer circulations that are consistent with previous findings (Rocha, 1992; Makarau, 1995). The features are quasi-stationary. These features are modulated by external (remote SST) and internal (topographic weather systems) forcings to produce anomalous summer circulations, which contribute to inter-annual variability. Prediction of seasonal positions and intensity of major features can be helpful in seasonal forecasting. Seasonal rainfall forecasting is difficult due to internal dynamics, which cannot be predicted beyond 2 weeks. Separation of forcings is important so that the influence of SST can be known and an attempt is made in chapter 6.

There is year to year variations in the location and intensity of the main features. More needs to be learnt about the influence of SST anomalies and the link to southern African summer rainfall anomalies.

The knowledge of mean state of atmosphere and underlying sea surface temperature will better inform the study of interannual variability and ocean atmosphere coupling mechanisms which are the focus of the following chapters 5 and 6.

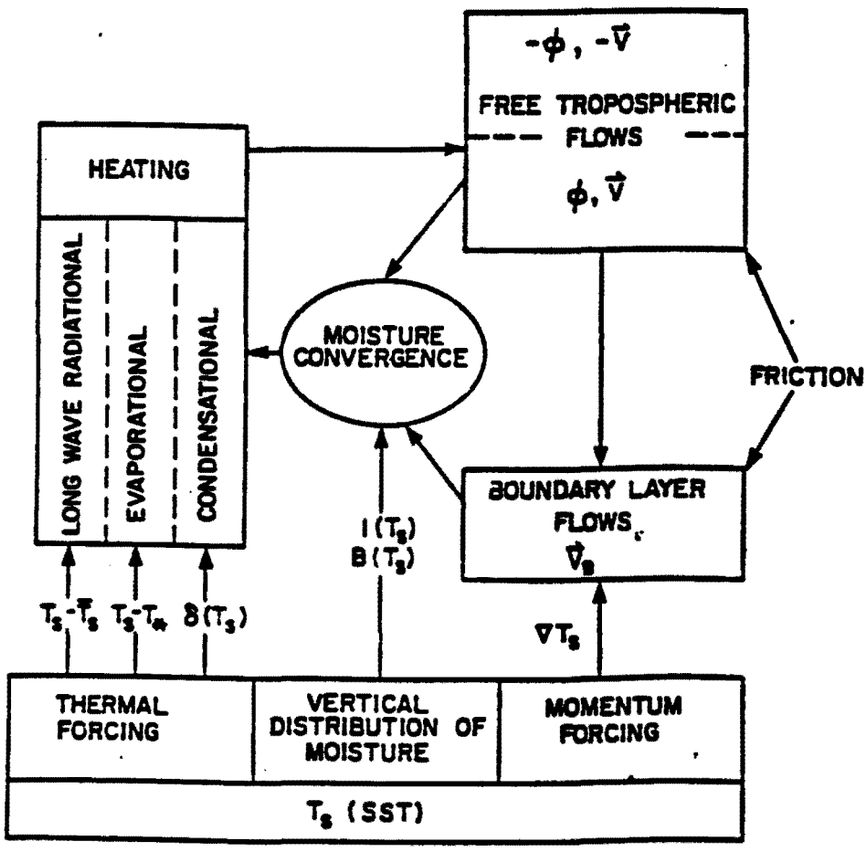

Figure 4.0 Schematic diagram illustrating how SST influences the atmosphere in a linear model (From Wang and Li, 1993).

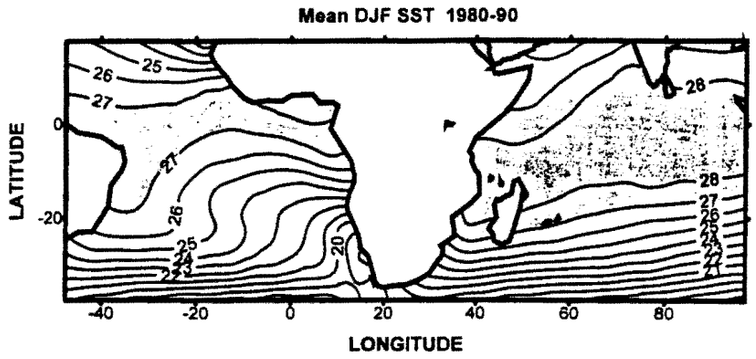

Figure 4.1 (a) Mean DJF SST 1980-90. Contour interval is 1°C.

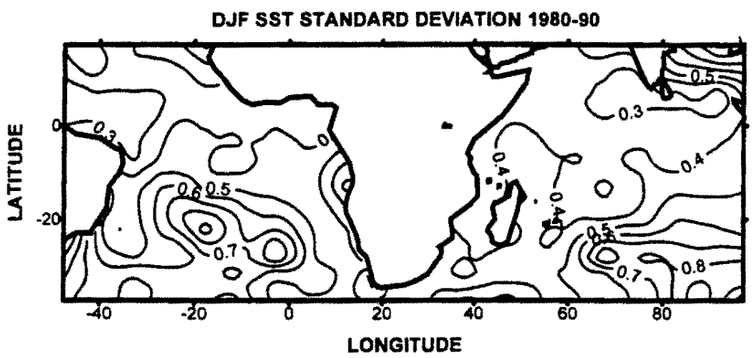

Figure 4.1 (b) DJF Standard deviation 1980-90 Contour interval is 0.1°C.

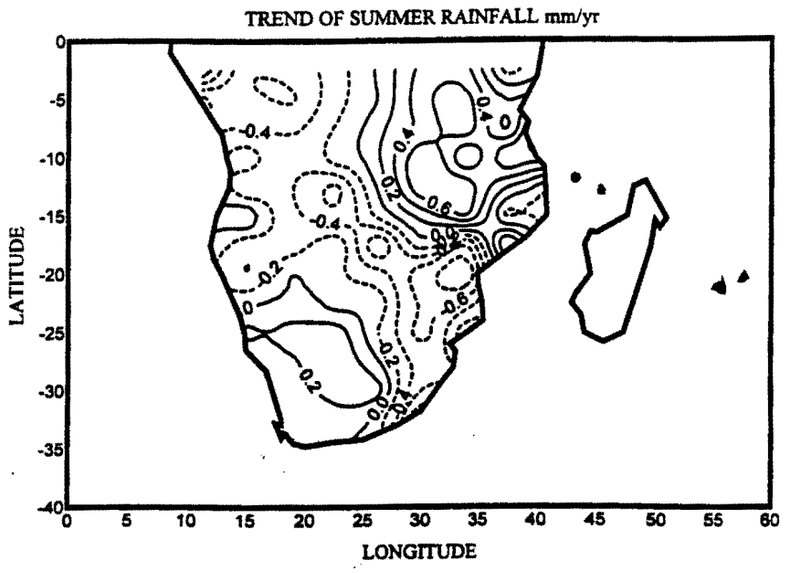

Figure 4.1 (c) Trends for DJF rainfall in millimetres per year.

a

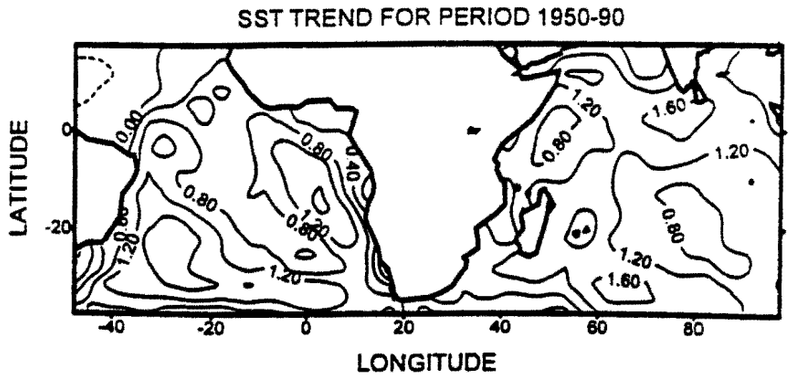

b

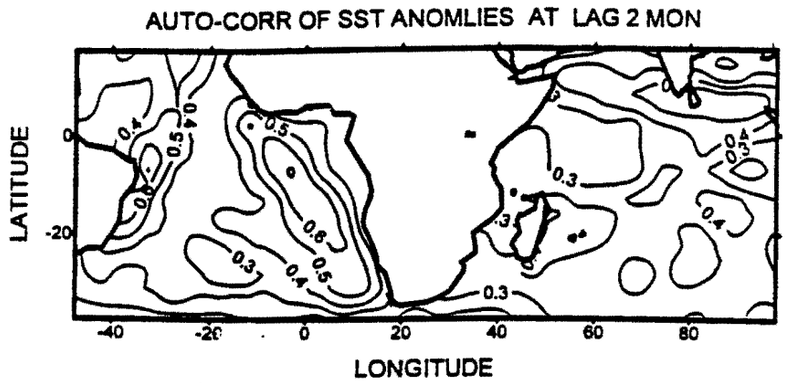

c

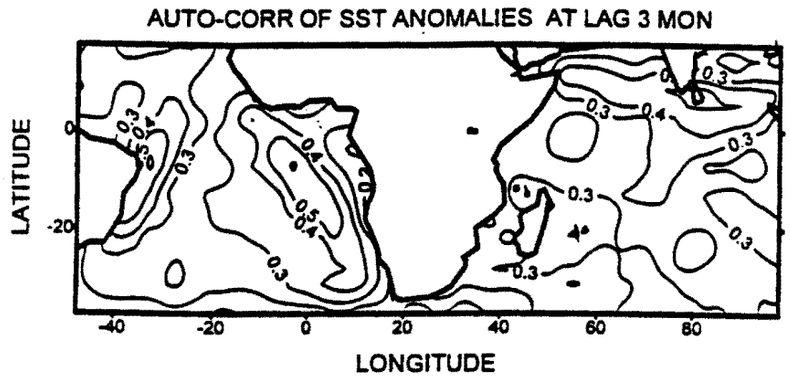

d

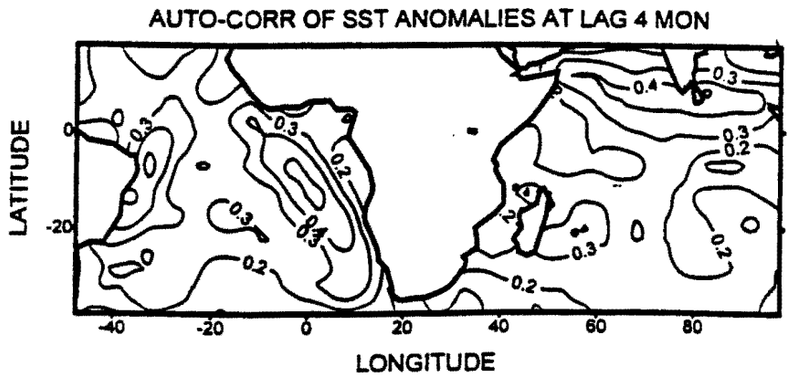

Figure 4.2 (a) SST trend for the period 1950 to 1990. (b) Autocorrelations of SST anomalies at lag 2 months. (c) Same as (b) but at lag 3 months. (d) Same as (b) but at lag 4 months.

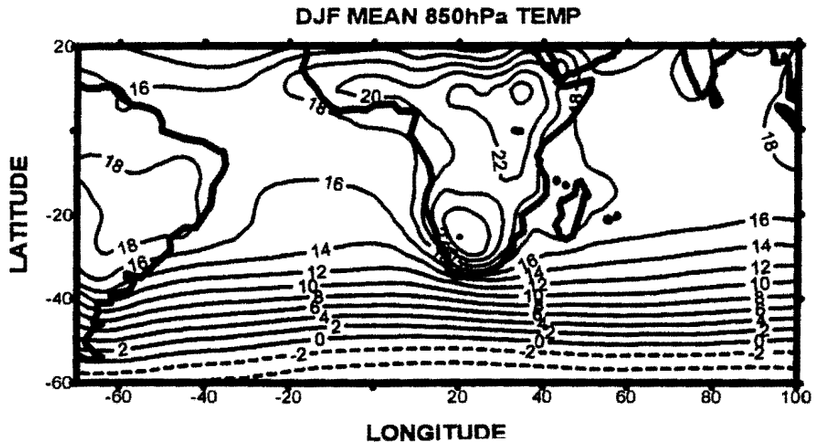

Figure 4.3 (a) Mean DJF 850 hPa temperature, contour interval is 2°C.

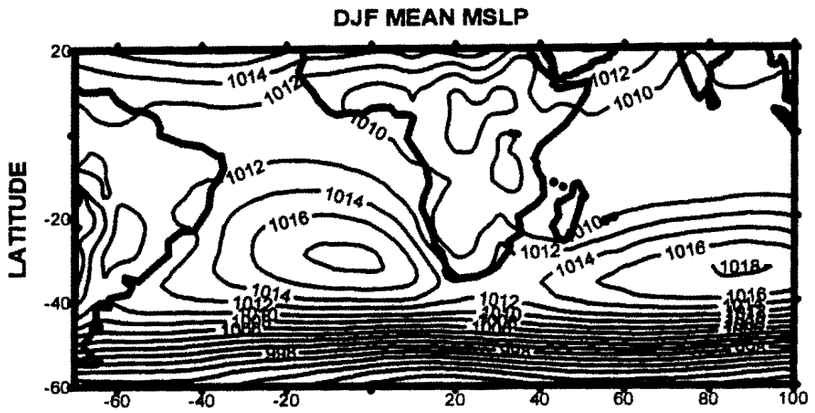

(b) As in figure 4.3(a) but for sea level pressure. Contour interval is 2 hPa.

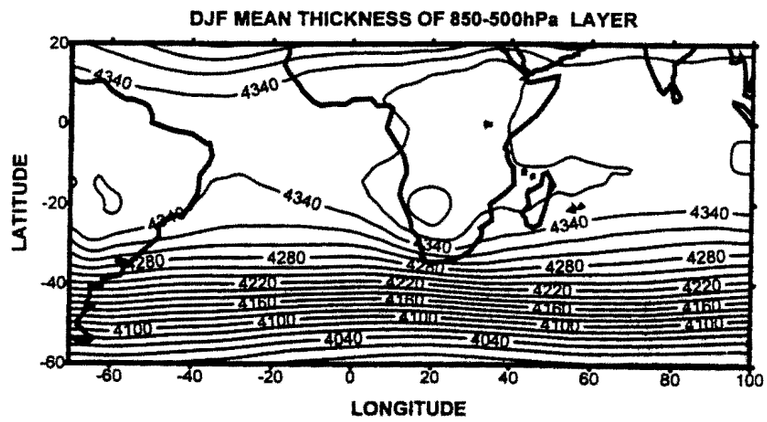

(c) As in figure 4.3(a) but for 850-500 hPa thickness in geopotential meters, contour interval is 20 meters.

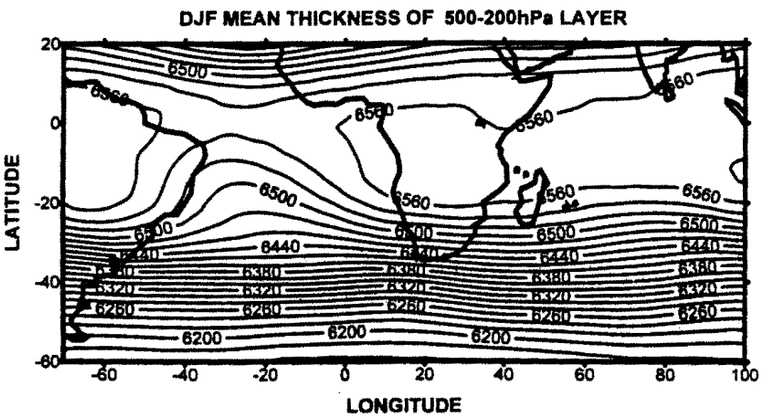

(d) As in figure 4.3 (a) but for 500-200 hPa thickness in geopotential metere, contour interval is 20 meters.

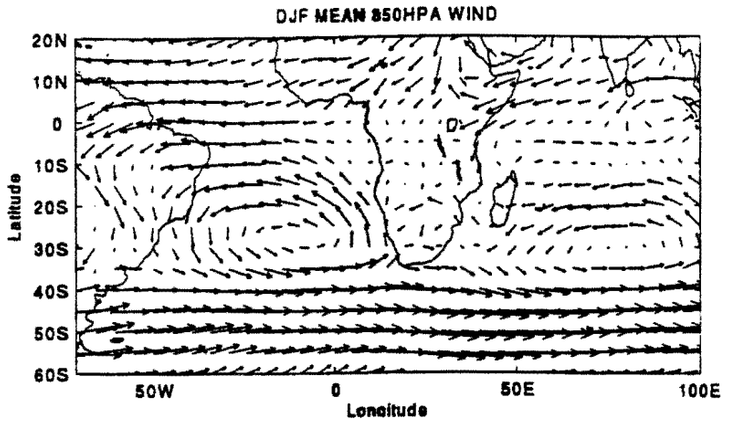

Figure 4.4 (a) Mean DJF 850hPa vector winds.

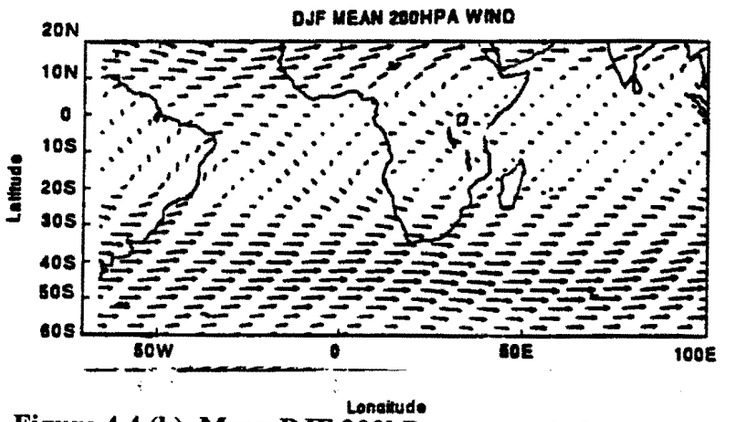

Figure 4.4 (b) Mean DJF 200hPa vector winds.

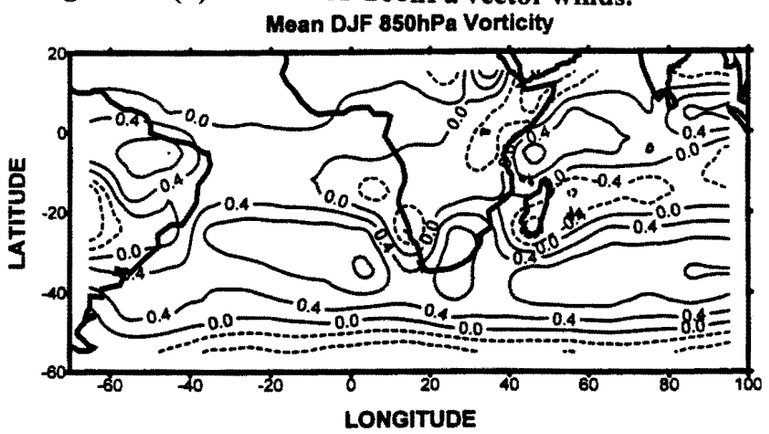

Figure 4.4 (c) As in figure 4.3(a) but for vorticity, contour interval is 0.4 x 10^{-5} s^{-1}.

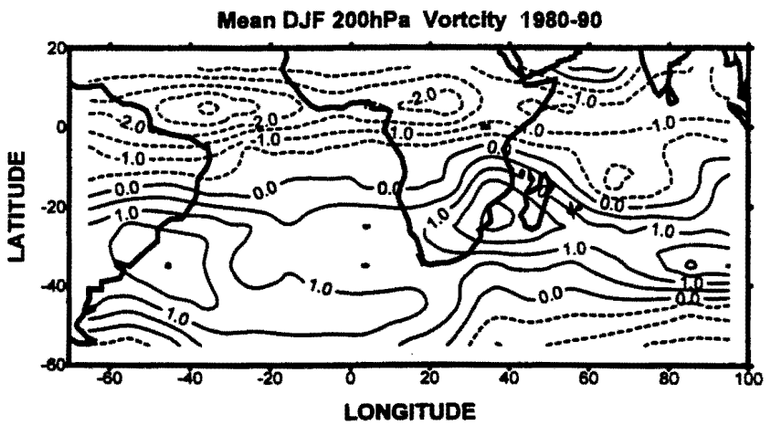

Figure 4.4 (d) As in figure 4.3(a) but for 200hPa vorticity, contour interval is 0.4 x 10^{-5} s^{-1}.

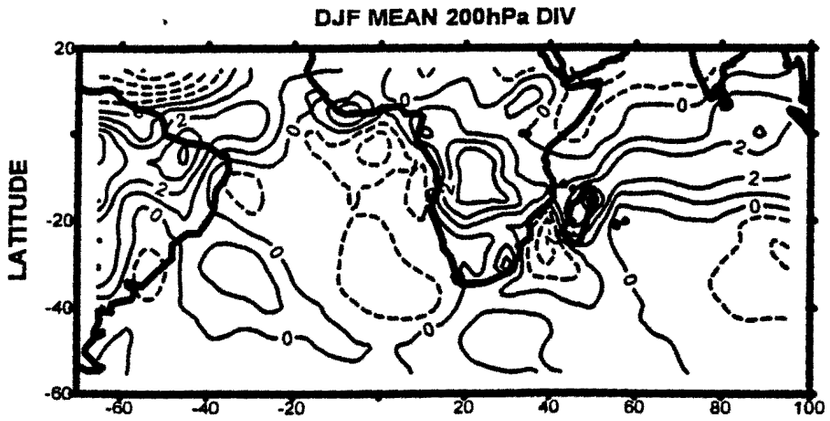

Figure 4.5 (a) Mean DJF 200 hPa divergence, contour interval 1.0 x 10^{-5} s^{-1}.

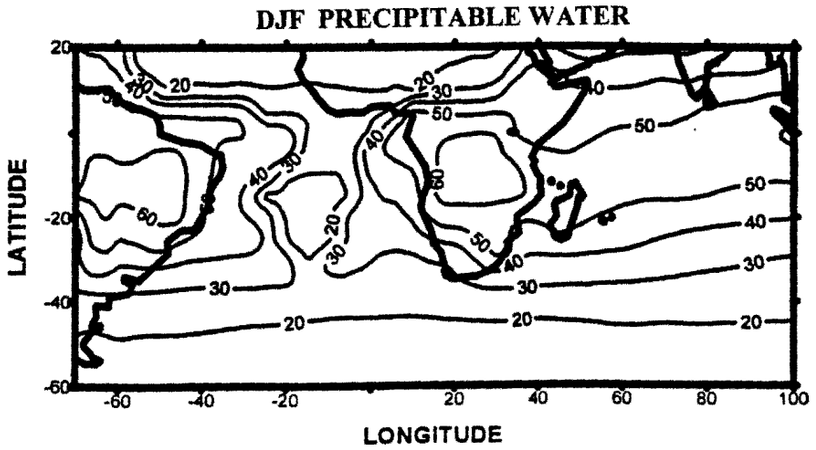

(b) As in figure 4.5 (a) but for precipitable water, contour interval is 10 mm.

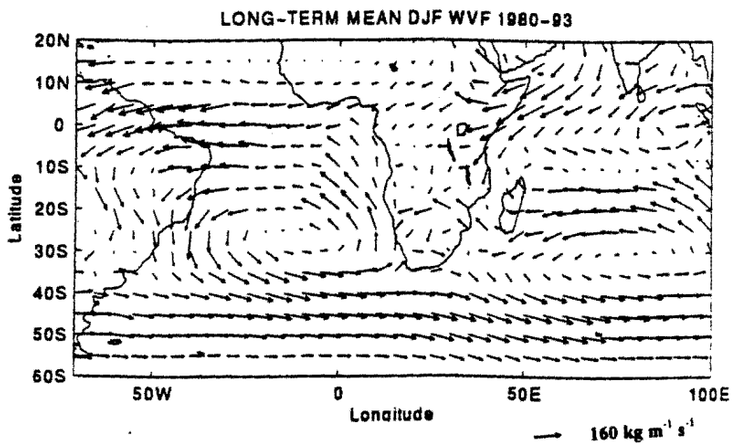

(c) As in figure 4.5 (a) but for DJF water vapour flux in kg kg^{-1} ms^{-1}.

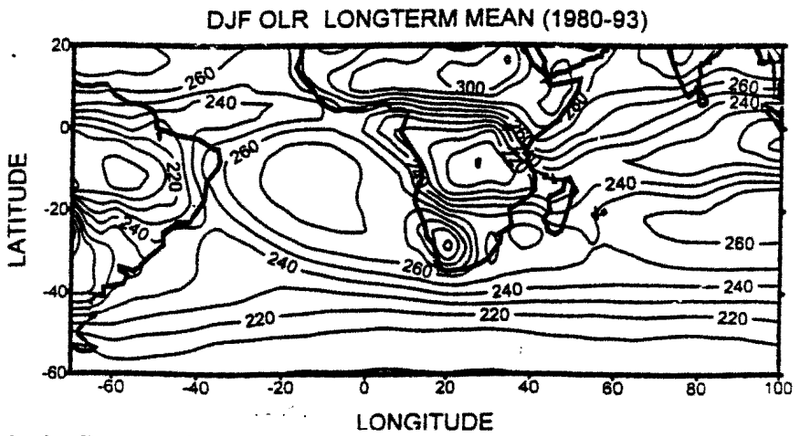

(b) As in figure 4.5 (a) but for DJF Outgoing Longwave Radiation, contour interval 10 Wm^{-2}.

CHAPTER 5

INTERANNUAL VARIABILITY OF SUMMER RAINFALL AND SEA SURFACE TEMPERATURE ANOMALIES

5.1 Introduction

The purpose of this chapter is to investigate the role of regional sea surface temperature anomalies in modulating rainfall anomalies over southern Africa. The main objective is to identify key SST regions that are related to summer rainfall anomaly patterns especially in regions where summer rainfall has not been linked to SST anomalies. Identifying the key SST areas over Atlantic and Indian Ocean is useful for prediction. If existence of SST-rainfall links are established, then key predictive indices can be developed or SST anomaly pattern can be predicted and hence rainfall. To make a seasonal rainfall forecast, the key areas of SST anomalies must be understood. Lag correlations assist in long range forecasting with SST leading. It is logical to identify DJF rainfall and monthly SST features of variability before investigating the link between them. In this chapter the objectives are achieved by applying principal component, correlation and spectral analyses techniques to rainfall and sea surface temperature data.

Many researchers have indicated a linkage between summer rainfall and several indices of atmospheric circulation. In previous studies no attempt has been made using gridded data most have used area-averaged rainfall (Rocha, 1993; Walker, 1989b; Makarau, 1995) to link to SST anomalies. Composite technique has been applied (Miron and Lindesay, 1983; Tyson, 1984) and is subjective unlike principal component analysis which is objective. The significant PC modes should give areas with common rainfall and SST anomalies. The obtained spatial patterns through PCA may throw some light on forcing mechanism by correlating the time scores with some known climatic indices (e.g. SOI, or QBO). In this chapter the time scores of DJF rainfall PC modes will be correlated to seasonal SST anomalies. The influence of Pacific ENSO on rainfall over southern Africa has been noted (Matarira and Unganai,

1995). However, there have been few investigations so far for inter-annual variations over the whole of southern Africa. The purpose of this chapter is to gain some understanding of the time and space structure of inter-annual variations of rainfall over southern Africa.

The historical monthly rainfall data set obtained from Climatic Research Unit (Hulme, 1994) was used. This monthly precipitation data set for 76 grid points is already described in Chapter 3. **Figure 2.1(a)** and **(b)** show the distribution of the mean and standard deviation of rainfall over 40 years of summer rainfall. Much summer rainfall occurs over Zambia and decreases southwestwards and northeastwards. The distribution of the standard deviations shows large variability over the southern Mozambique and Congo Basin. The year to year variability is smaller over the interior part of the subcontinent.

To investigate the spatial and temporal characteristics PCA, as described in Chapter 3 is applied to the standardized summer rainfall. The Genstat package was utilized to compute the rotated PC modes and time coefficients. To estimate the dominant periods, Spectral Analysis was applied to tapered and detrended time scores. The Statistica package was utilized in computing the spectral density functions.

5.2 Structure of low-frequency variation in the southern African summer rainfall

In many national meteorological services, rainfall zones have been classified using principal component analysis. A larger data set is utilized and the accumulated seasonal December, January and February rainfall amounts are considered in the study. This analysis is confined to the 1950 to 1989 period. **Table 5.1(a)** displays the PC modes and the associated percentage variance explained by each mode. The first 8 PC modes account for about 68% of the total variance. Only the first four modes are significant according to Scree test criteria and only these modes will be discussed.

TABLE 5.1(a) Summer PC modes and their center of location

Mode	Percentage Variance	Locations(Lat/Long)
PC1	24	Angola, 15°S 15°E
PC2	14	S.Tanzania, 10°S 35°E
PC3	8	N. Botswana 17°S 25°E
PC4	6	K. Natal 32°E 30°S

The spatial distributions of the amplitudes of the first PC four modes are shown in the figure 5.1(a), (b), (c) and (d).

PC1 (24%) (Angola mode)

Figure 5.1(a) shows the spatial loadings and the associated time series. PC1 indicates large positive values concentrated over Angola at 15°S with a narrow band elongated along 15°E longitude over Namibia. This mode is similar to the intraseasonal composite as discussed in chapter 8. This mode can be referred to as the Angola mode. It has highest loadings over the Bie Plateau. When the time coefficient is positive/negative then rainfall is enhanced/suppressed over Angola, Namibia and western Zambia. PC1 mode shows a slight decreasing trend from 1950 to 1989. Large positive amplitudes are observed in 1952, 1958, 1969 and 1978. Negative values are reported in 1967, 1973, 1980, 1983 and 1987.

PC2 (14%)

Figure 5.1(b) displays PC2 loadings and the time scores. This mode yields high positive loadings over northern Zambia and southern Tanzania. The loadings extend zonally along 10°S over the eastern side of the highlands of southern Tanzania. The time coefficient associated with this mode has large amplitudes in 1956, 1962, 1968, 1973, 1979 and 1989 with negative large values in 1953, 1961, 1967, 1975 and 1988.

PC3 (8%)

PC3 loadings and its associated time scores are displayed in **figure 5.1(c)**. PC3 is similar to the first mode described by Janowiak (1988) for DJFM PC1. The largest positive values are found over central parts of Zambia and northern Zimbabwe. It is associated with a zonal ITCZ over the Zambezi valley and is important for water resources. This pattern resembles the mean DJF summer rainfall. Large negative time coefficients are observed in 1974, 1976 and 1989 (wet years).

PC4 (6%)

Figure 5.1(d) shows PC4 loadings and time coefficients. PC4 displays large negative loadings over eastern parts of South Africa i.e. Kwazulu Natal region. Positive loadings are seen over northern Mozambique, NW Congo Basin. Large time coefficients prevail in 1962, 1968, 1970 and 1982; negative values in 1953, 1967, 1972, 1974 and 1978. Highest amplitude occurs around 1970. This pattern is found in an area that produces about 50% of food in the SADC.

In order to find temporal characteristics of time coefficients Spectral analysis was applied. The time series were detrended and tapered before applying spectral analysis. **Figure 5.1(e) to (h)** displays results and most of the series show significant spectral peaks at 2.0-2.8 years. In order to test for white noise the distribution of periodogram values was calculated and compared. If the time series is white noise with respect those frequencies (i.e., if there are no significant periodic cycles of those frequencies) then the distribution of the periodogram values should follow an exponential distribution (Statistica, 1995). **Figures 5.1(i) to (l)** show the histograms of periodogram values for PC1 to PC4 time series. It can be seen that the periodogram values do not fit the exponential distribution.

Four summer rainfall areas have been identified in Southern Africa using PCA and gridded rainfall data. The first PC mode is associated with Angola low and spectral peaks at 2.4 to 4 years and 5.2 years (see **figure 5.1(e)**). East African rainfall is identified with PC2 whose time series has periods ranging from 2.0 to 2.5 and 5 to 7 years (see **figure 5.1(f)**). The central African rainfall is linked to PC3, which is centered over northern Botswana and has dominant periods of

2.0 to 2.4 years (see **figure 5.1(g)**). The fourth mode is found over Kwazulu Natal with spectral peaks at 2.0 to 2.6 and 13 years (see **figure 5.1(h)**).

Since the SST anomalies have been suggested as controlling the summer rainfall, the next section of this study considers spatial and temporal variations of the SST anomalies in the adjacent oceans

5. 3 Structure of low-frequency variations in the regional SST

Previously Rocha (1992) has applied PCA to global seasonal SST for the period 1951 to 1989 using 8°latitude by 8° longitude areas. Fifteen anomaly patterns were identified. The first PC mode was identified with ENSO and explained 9.9% of the total variance. Walker (1989b) used a smaller domain (0°N to 35°S, 20°W- 70°E) in the Atlantic and Indian Oceans for the period 1949-1985. Seasonal SST anomalies in Indian and Atlantic separately were subjected to PCA and nine components were extracted from two oceanic basins. The first Indian PC (15%) was identified with Mozambique/Agulhas Current region and the second was situated in the tropical Indian Ocean. For the Atlantic basin the first and second PC were over central Atlantic and the third over in the eastern equatorial region. Mason (1992) combined both basins and extracted 8 principal components. The first PC (17%) was linked to the Benguela system, second PC (13%) to Agulhas and Mozambique Channel systems. The fourth principal component (7.5%) was located in western Indian Ocean.

In this study grid-box SST monthly time-series data from the Hadley center, United Kingdom Meteorological Office (UKMO) were subjected to PCA analysis. Missing values were replaced by interpolating in time. The SST data for the Atlantic and Indian basins were extracted in the domain: 17.5°N to 37.5°S, and 47.5°W to 97.5°E. This involved a total of 289 grid points at 5° x 5° grid resolution. The period of observation was from January 1950 to December 1991. This involved 516 months (43 x 12 months). Values were standardized, as for rainfall. The use of standardized anomalies reduces the influence of areas with poor observational coverage or high SST gradients.

SST's are used in operational long-range forecasting and thus the first nine PC modes will be retained. **Table 5.1(b)** gives the variance, and the area of highest loadings associated with each PC mode.

TABLE 5.1(b) SST PC modes and their center of location

PC	Variance	Location
1	15.9	C.Indian 80°E,0°N
2	6.5	Atlantic 0°E,5°S
3	4.8	N. Atlantic 20°W, 10°N
4	4.1	SW Indian Ocean 40°E, 30°S
5	3.0	off Somali Coast 50°E, 0°S
6	2.7	S.Indian 30°S, 80°E
7	2.4	SWAtlantic 20°W, 32°S
8	2.2	SW Atlantic Ocean 20°W, 17°S
9	2.0	Benguela Coast 30°S, 10°E

It can be seen that the first four PC modes explain a total of 31% of the total variance. Figures 5.2 to 5.4 show the results of rotated EOF analysis of standardized SST based on UKMO data set.

Figure 5.2(a), (b) and (c) exhibit the spatial loadings and their associated time-scores for PC1, PC2 and PC3 respectively.

PC1 (16%) (Figure 5.2(a))

The spatial loadings of this PC mode are focused on the Indian Ocean north of 20°S between 50°E and 90°E. There is a downward trend in the time scores which implies increasing SST over the Indian Ocean. After 1982, the score are generally negative implying warmer than normal SST. This is consistent with evidence for the declining rainfall over southern Africa, since southern African rainfall is negatively correlated to SST over the Central Indian Ocean (Rocha, 1992; Pathack, 1993; Makarau, 1995). This mode corresponds to global PC1 of Rocha (1992) where Pacific SST anomalies are coherent with the SST anomalies over the Indian Ocean. The years 1958/1959, 1964/1965, 1972/1973, 1982/1983, 1986/1987, 1991/1992 have negative score implying warm events in the central Indian and cooling over the southern zone. Cold years favoring above normal rainfall are 1951/1952, 1956/1957, 1965/1966, 1967/1968, 1971/1972, and 1976/1977. A meridional gradient of SST over the south Indian Ocean is seen to be an important feature. The correlation coefficient between the PC1 time score and September, October and November (SON) SOI is found to be 0.4, which is significant at 99% level. Warm and cold events modify the rainfall over southern Africa through a direct relationship by modifying the circulation on the equatorial side of the Mascarene high and hence the ITCZ over the central and western Indian Ocean.

PC2 (6%)(Figure 5.2(b))

This PC mode explains about 6% of the total variance. The key area with highest loading is found over the over the Gulf of Guinea and in the equatorial Atlantic Ocean (5°N to 10°S and 20°W to 10°E). The time scores are positive between 1950 and 1972. Highest scores were reported in 1964 and lowest in 1978-79. Significant warming took place between 1962 and 1970. Cold events are observed between 1976 and 1984. A correlation coefficient of 0.12 was obtained between the PC2 scores and SON SOI. This mode has influence on West Africa (Sahel) and East African rainfall (Folland et al., 1991). The warm and cold events associated with this mode can modify the midtropospheric easterly jets centered at 700 hPa height (Mass, 1979). Mid level easterly jets are

important energy sources for easterly waves. In barotropic processes, the kinetic energy of the jet is converted to easterly waves (Kwon, 1989). This mode may also affect southern and East African rainfall by modifying the Congo Air (north – westerlies current).

PC3 (5%)(Figure 5.2(c))

This pattern has larger positive loadings over the northern Atlantic Ocean (30°W, 10°N) and negative loadings over the central south Atlantic Ocean (0°E, 12.5°S). There is north-south SST gradient over the Atlantic Ocean. The respective time-score indicate high positive scores in 1959, 1970 and lowest in 1986. This mode is referred to as the Atlantic dipole, which controls Sahel and north-east Brazil rainfall (Folland et al., 1991). This mode can also affect West African rainfall by changing the basic flow and the north-south position of the ITCZ. Kushnir (1994) has observed decadal to interdecadal variability in the Atlantic Ocean.

Figure 5.3(a), (b) and (c) exhibit the spatial loadings and their associated time-scores for PC4, PC5 and PC6 respectively.

PC4 (4%)(Figure 5.3(a))

This PC mode shows large loadings over south-western parts of the Indian Ocean. This mode identifies the area influenced by the Agulhas gyre (Lutjeharms and Ballegooyen, 1988). Major warm events are reported in 1969, 1973, 1985 and 1988 while cold events occur in 1951, 1965, 1967 and 1976.

PC5 (3%)(Figure 5.3(b))

There are three centres of action in this PC mode, a major positive one over the south-west Atlantic Ocean (40°W, 25°S) and eastern Indian Ocean (85°E, 20°S), and negative loadings are found off the East coast of Somali and Kenya. The zonal temperature gradient plays an important part in modulating East African rainfall (Hasternrath et al., 1993). A correlation coefficient of 0.20 was found between the PC5 time scores and the SON SOI. The western subtropical Atlantic and eastern Indian are in sympathy.

PC6 (3%)(Figure 5.3(c))

This PC mode has its highest positive loadings over the south Indian Ocean (50°E to 90°E and 20°S to 30°S). It has been demonstrated through modelling that the Indonesian throughflow can modify the southern Indian Ocean on interdecadal time scale (Reason et al., 1996). The response of the GCM model to dynamical forcing (wind anomalies) resulted in the correct SST anomalies over the South Indian Ocean. Significant cold events are in 1958, 1967, 1978 and 1983. The correlation coefficient with SOI is found to be -0.20. This mode may have an influence on advection of moisture from the Indian Ocean.

Figure 5.4(a), (b) and (c) exhibit the spatial loadings and their associated time-scores for PC7, PC8 and PC9 respectively.

PC7 (2%)(Figure 5.4(a))

Largest negative loadings are exhibited over the south-west Atlantic Ocean (40°W to 0°W, 20°S-37.5°S). This PC mode has an upward trend from 1966 to 1990. This mode is likely to affect the midlatitude westerlies, hence the jet stream and its baroclinic disturbances.

PC8 (2%)(Figure 5.4(b))

The spatial loadings of this mode are positive over the western Atlantic Ocean (40°W - 0°E, 5°S-25°S) and negative over the central Indian Ocean (70°E, 10°S). This mode can influence the development of frontal systems and it has a strong correlation with SOI (r = 0.48). Cooling occurs over the western Atlantic during warm ENSO events and warming during cold events. This mode could alter midlatitudes storm tracks. The time scores show large negative values in 1958, 1966, 1979 and 1980. Large positive values occur in 1971 and 1984.

PC9 (2%)(Figure 5.4(c))

Highest positive loadings are confined over south-eastern parts of the Atlantic Ocean (10°E, 30°S) and negative over south-west parts of the Indian Ocean

(60°E, 30°S). This PC mode could modify the subtropical high pressure over the Benguela current and thus the intensity of south-easterly trades. There is a meridional dipole in the Indian Ocean, which could play an important role in the strength of zonal winds over south Indian Ocean. The link between SOI and the time scores is relatively weak (r = -0.26).

The standardized time scores and SOI time series were subjected to spectral analysis in order to find the dominant period of oscillation. The anomalies were detrended and tapered (the first 10% and last 10%). The **table 5.1(c)** below gives the major spectral peaks. The test for white noise was not carried out since the record length was long enough.

TABLE 5.1(c) Major periods of oscillation of SST PC time coefficient and SOI (figures are given in years)

Parameter	1st Peak	2nd Peak	3rd Peak	4th Peak
SST PC1	5.0	3.3	2.5	20.0
PC2	20.0	5.0	1.6	-
PC3	10.0	13.3	5.8	3.3
PC4	5.0	3.3	2.5	-
PC5	6.6	13.3	4.2	2.1
PC6	7.0	2.1	4.2	-
PC7	1.6	2.1	7.0	-
PC8	17.0	3.3	1.6	-
PC9	3.3	5.8	1.6	20.0
SOI	5.0	3.3	2.5	20.0

5.4 Statistical links between summer rainfall anomalies (PC patterns) and regional seasonal SST anomalies

The main objective of this section is to investigate the link between the summer rainfall PC modes and south Atlantic and Indian Ocean SST seasonal anomalies. This section will give statistical evidence of the relationship between Southern African rainfall and monthly SST's over Indian and Atlantic Ocean. Conditions of the SST's with rainfall especially when SST leads the

rainfall are very useful for forecasting. Seasonally averaged SST of SON and DJF were correlated to rainfall PC mode time scores.

Prospects for seasonal rainfall prediction in the tropics have advanced considerably with the use of SST data (Jury, 1996; Thiao, 1996). Spring season values of mean sea level pressure, QBO values, key SST areas, winds and Southern Oscillation Index (SOI) show strong relationships with seasonal rainfall. Predictability of southern African rainfall is high because of the link between rainfall and ENSO. When SST anomalies in central and eastern tropical Pacific Ocean increase above normal, westerly upper level winds are enhanced over the tropical Atlantic Ocean and there is a reduction of easterly winds (Rocha, 1995; Harrison, 1986) over southern Africa. This may result in the strengthening of the high pressure over Botswana. The tropical Indian ocean becomes warm and resulting in increased cyclogenesis over Indian Ocean and reduced rainfall over southern Africa (Jury et al, 1996). In this case reversal of the Walker circulation is responsible for drought. Tropical SST anomalies have been found to be better predictors than midlatitudes because of their longer memory. Mean SST's in the midlatitudes and south Atlantic are colder but equatorial Atlantic and Indian SST's are warmer and make an impact on diabatic forcing of the atmospheric circulation In this study Tropical Indian and Atlantic monthly sea surface temperatures are considered.

Figure 5.5 and 5.6 are lag correlation patterns of seasonal SST's and the DJF rainfall PC modes. Correlations >0.26 are significant at the 95% level.

Angola Mode - PC1 (24%)

Figure 5.5(a) and **(b)** are spatial correlations between PC1 rainfall mode and grid point SST in SON (3 months before) and DJF (zero-lag). In SON season, above normal rainfall requires below normal SST over the central Indian Ocean (75°E, 10°S) and south of 10°S over the Atlantic Ocean. Warming is anticipated over the south-west Indian Ocean (40°E, 20°S) and in the west African Gulf (5°E, 5°S). A similar situation is found for zero lag correlation (DJF) except for the warming over central Indian Ocean (75°E, 15°S).

Significant correlations (r = -0.3) are found over the Atlantic (0°E, 22.5°S) and Indian Ocean (70°E, 0°S).

From the thermal wind concept the SST pattern and the associated SST gradient would induce a westerly thermal wind to the west of 25°E, and easterly thermal wind to the east of it. This implies that there is upper level convergence.

The sign of the correlation implies surface divergent flow over Southern Africa. PC1 of summer rain will have negative loadings implying below normal rainfall when SST are warm in the tropical Indian Ocean.

PC2 (14%) - Northern Malawi and Zambia

Figure 5.5(c) and **(d)** display correlation patterns between PC2 rainfall mode and the SST at grid points. During SON the spatial correlation associated with this mode are generally positive around the subcontinent with maximum correlation (>0.3) over 65°E, 10°S and off the coast of Namibia (Benguela). Negative correlations are found in the eastern Indian Ocean (75°E, 10°S). There is a meridional SST gradient over the Atlantic and central Indian Ocean.

At zero lag (DJF), a strong north/south gradient prevails over the Indian Ocean. Large correlations (>0.3) are found over the central Indian Ocean (65°E, 10°S). The meridional gradient is greater than the zonal gradient. Large negative correlation (<-0.3) are found south 20°S over the Indian Ocean. The SST gradient associated with this pattern implies that during the periods of above normal rainfall, westerlies prevail over the subcontinent.

PC3 (8%)- Botswana Mode

Figure 5.6(a) and **(b)** are spatial correlation coefficients fields obtained between PC3 rainfall mode and SON and DJF SST's. For above normal rainfall over the central interior of Southern Africa (25°E, 17°S), below normal SON SST are found north of 10°S over the Atlantic Ocean, east of 80°E (near Western Australia) and over the south-west Indian Ocean. Negative correlations (<-0.3) are found off the coast of northern Angola, Zaire and Gabon. There is north-south temperature gradient in both basins.

During DJF the key areas are found over the central Indian Ocean (>0.3, see figure 5.6(b)), south-west Atlantic (r =-0.3) for above normal rainfall.

PC4 - Kwazulu Natal(SE South Africa)

Figure 5.6(c) and **(d)** are spatial correlation coefficients fields obtained between PC4 rainfall mode and SON and DJF SST's. During periods of above normal rainfall, SON and DJF spatial correlation indicate that low SST are required over the central Indian Ocean.

Since correlation analysis may not be the only appropriate statistical tool to establish the association between SST anomalies and rainfall anomalies, combined PCA is applied in order to give more statistical evidence. In order to explain the rainfall variability in terms of sea surface temperature anomalies, combined PCA (see methods in chapter 3) was applied to DJF standardized rainfall and sea surface temperature anomalies at zero lag. Previous statistical studies have used correlation techniques and have linked the central Indian SST anomalies to summer rainfall for South Africa and south-east Africa (Mozambique, Malawi and Zambia).

GCM simulations and simple modelling can bring out physical mechanisms of the variability of southern African rainfall on inter-annual time scale. These studies have given further evidence for the influence of central Indian Ocean SST anomalies on summer rainfall (Jury et al., 1996; Rocha,1992). Reason and Lutjeharms (1998) have shown the importance of South Indian ocean sea surface temperature variability on southern African rainfall.

This is a statistical study which is different from previous studies by using a larger gridded data-set and employing a different technique. In this study, the different anomaly patterns of SST will be considered as the forcing and response is the rainfall anomaly pattern. Thus the role of the SST anomalies will be examined. It has already been shown that warm tropical SST can generate convergence of moisture in the boundary layer and hence enhance rainfall locally. Depending on the location of the tropical SST anomaly, Kelvin or Rossby wave trains can be generated.

PC1(20%)Tropical Central Indian Ocean forcing (figure 5.7(a),(b) and (c))

Highest negative loadings (greater than 0.8) are confined to the Tropical Indian ocean (10° S- 5°N) with weak (less than 0.2) positive loadings over southern Indian ocean and western Atlantic Ocean. This SST anomaly pattern is associated with above DJF normal rainfall over Zambia, Angola, northern Namibia, Lesotho and eastern Cape. The ITCZ in the north and frontal systems in the south may responsible for this pattern. Negative rainfall anomalies are found over the Congo basin and southern Tanzania. The time scores show a link with the global El-Nino\Southern Oscillation (ENSO) with suppressed rainfall in 1964/65, 72/73 and 82/83. Spectral analysis of the time scores shows peaks at 5.0 and 2.5 years (see figure 5.10(a) and figure 5.11(a) for white noise test). There is a downward trend in the time series. SST patterns have an east-west orientation indicating the meridional gradient of SST implying the influence of zonal thermal wind over Indian Ocean. Negative SST anomalies over central Indian ocean may result in suppressed convection over central Indian Ocean and increased convection over southern Africa. This is consistent with the previous statistical and GCM studies (Rocha, 1992; Jury et al, 1996). The cooling over the western Indian Ocean may be due to advection of colder waters from the north -west and evaporation (Hastenrath and Lamb 1979).

PC2 (9%) Subtropical forcing (figure 5.7(d), (e) and (f))

Large negative values of the SST loadings are found in the subtropics over southwest Atlantic and south Indian oceans (20°S-40°S). There are weak positive loadings over the eastern Atlantic. There is a meridional gradient over the Atlantic and a zonal gradient over the Indian Ocean. The associated rainfall anomaly pattern has meridional orientation with maximum positive values over Zambia, Zimbabwe and Mozambique. Here the Walker circulation may play a part in modulating rainfall anomalies. Quasi-stationary cloud bands (Harrison 1986) may be associated with this rainfall pattern. The cooling of the SST may be due to strong winds in the midlatitudes. Reason et al(1997) indicate that SST anomalies over south central Indian Ocean tend to be warm (cool) when the semi-permanent subtropical anticyclone over the ocean is strengthened. The

time scores show a downward trend and large amplitudes from 1950 to 1968. Spectral analysis of the time scores shows peaks at 4.0 and 9.5 years (see figure 5.10(b) figure 5.11(b) for white noise test).

PC3 (6.3%) Atlantic dipole (figure 5.8(a), (b) and (c))

This pattern explains 6.3% of total variance and exhibits a decadal time scale. There is dipole between north (equator to 20°N) and south-eastern Atlantic (10°S-40°S). This may result in increased thermal westerly wind over the Atlantic (e.g. Walker Cell) and synoptic disturbances. Rainfall anomalies associated with this pattern have maximum loadings over western Zambia, north-east Botswana, Zimbabwe, northern South Africa, and southern Mozambique. It has a north-west to south-east shape in the Zambezi valley. In west Africa this pattern has been linked to Sahel rainfall (Folland et al 1986). The time series shows large positive value 57/58, 69/70, and 79/80 and 87/88 with low values in 73/74, 75/76, 85/86 and 88/89. Periods of 2.5 and 13.0 years are found with large spectral peaks (see figure 5.10(c) figure 5.11(c) for white noise test).

PC4 (6.3%) Atlantic (figure 5.8 (d), (e) and (f))

This anomaly pattern has negative loadings over the Atlantic Ocean with largest values over the western Atlantic. It explains 6% of total variance. The cooling of the Atlantic results in above normal rainfall over Angola, southern Mozambique and Swaziland. There is an upward trend in the time series. Large positive values are observed in 50/51, 65/66, 67/68, and 81/82 and negative values in 51/52, 56/57, 63/64, 76/77 and 88/89. Spectral peaks are at 6.5 and 2.5 years (see figure 5.10(d) figure 5.11(d) for white noise test).

PC5 (5.4%) Central Indian and eastern Atlantic forcing (figure 5.9(a), (b) and (c))

This pattern reflects cooling off Angola and in the central Indian Ocean and warming of the Agulhas current and western Atlantic Ocean. There is a reversed meridional temperature gradient between longitude 40°E-60°E over the eastern Indian Ocean implying an easterly thermal wind anomaly. Over the Atlantic Ocean an easterly thermal wind anomaly is also supported. This

enhances tropical easterly disturbances over north-east South Africa associated with positive time scores. The rainfall anomaly pattern has positive loadings over north eastern South Africa with opposite sign zonally to the north over Angola, Zambia, Malawi and Mozambique. There is an increasing trend in the time scores. Spectral analysis of the time scores shows peaks at 5.5 and 2.0 years (see figure 5.10(e) figure 5.11(e) for white noise test). The Hadley circulation may be the main contributor to rainfall bearing disturbances here. Note that the zonal position of highest negative rainfall and SST loadings over the equatorial Indian and eastern Atlantic coincide.

PC6 (4.8%) (figure 5.9(d), (e) and (f))

This pattern is associated with warming over central Indian and western Atlantic Oceans. Weak cooling occurs along the Benguela associated with negative rainfall anomalies over most parts of sub-continent with large values over Zimbabwe, Namibia and South Africa. Positive values are observed over southern Tanzania. Time scores show positive large values in 53/54, 67/68, 70/71 and 83/84. Negative values of time scores occur in 52/53, 67/68, 69/70 and 78/79. Spectral analysis of the time scores shows peaks at 2.4 and 9.5 years (see figure 5.10(f) figure 5.11(f) for white noise test).

5.5 Summary and discussions

Four DJF summer rainfall PC modes (see figure 5.6(f)) were identified and account for 52% of the total variance. The first mode is linked to the Angola trough that links the tropics to the midlatitudes. This suggests that the Angola pattern is most related to inter-annual DJF rainfall variability over southern Africa. A downward trend is observed in the time scores and this implies increasingly unfavorable conditions for the development of the low pressure over Angola. Periods of 2-7 years and 18-20 years have been identified in rainfall time series (Tyson, 1980, Nicholson 1986, Rocha 1992,) and thus the above spectral results are consistent with the previous findings. The 2-7 year periods can be linked to tropospheric quasi-biennial oscillations and ENSO.

The second anomaly pattern is over north-east Zambia and Malawi with periods at 2 and 6 years. The third pattern is identified with southern Zambia and the Atlantic dipole. Eastern South Africa is the focus of the fourth pattern.

Features of sea surface temperature anomalies

Nine PC modes major PC modes have been identified in Atlantic and Indian Oceans (see figure 5.6(e)). The 9 PC patterns account for 43% of the total variance. The first mode in this study is important and has been linked to Southern African rainfall, and its time series illustrates warming taking place in the central Indian for the past 40 years. It is also linked to ENSO since it has almost the same period of oscillation. The first 3 PC modes explain about 27% and are tropical modes. PC mode 2 may influence both East and West African rainfall. Mode 5 may be linked to East African rainfall (Hastenrarth et al, 1993). PC4 can be identified with the Agulhas Current. The rest of the modes from PC6 to PC9 are mid-latitude and may modulate baroclinic disturbances.

Spectral analysis of the time coefficient has revealed several periods of oscillations that are consistent with Mason's (1992) results. PC1 has been found to have the same spectral peaks as SOI showing that the two are coherent in time variation. Longer periods (10-18) years have been found in PC2, and PC8 time series. The 3-5 year period is quite evident in most PC scores.

Link between SST anomalies and DJF rainfall anomalies

Determination of key SST regions and associated rainfall regions has been carried out. From correlation analysis for the period 1950-89, Angola rainfall DJF PC1 (figure 5.1(a)) was negatively related to DJF SST anomalies over central Indian Ocean (10°S-5°N, 65°E-75°E) and Atlantic ocean (5°W-5°E, 18°S-22°S). It was positively correlated to standardised sea surface temperature anomalies in the Mozambique channel, some areas of the Agulhas current system, along east Atlantic coast and West African Gulf. Warm Agulhas current system and cold waters over Atlantic and central Indian Ocean coincided with wetter summers. A decreased north-south temperature gradient over the Indian Ocean is associated with positive rainfall pattern.

DJF rainfall anomalies over northeast Zambia and Malawi (PC2, figure 5.1(b)) were associated with DJF sea surface temperature anomalies of central Indian (0°N- 18°S, 60°E-70°E).

Western Zambia, Zimbabwe and southern Mozambique summer rainfall anomalies (PC3, figure 5.1 (c)) were positively correlated to DJF SST anomalies over tropical Indian Ocean (60 °E- 80°E, 0° N-5°S) and SST in subtropical latitudes (35°S-40°S). Increased north-south temperature gradient in the Indian Ocean was consistent with an above normal rainfall pattern.

Eastern South Africa summer anomalies (PC4, figure 5.1(d)) were associated with Central Indian Ocean (10°N-20°S, 60°E-70°E), Mozambique Channel and Agulhas current SST anomalies. Warm central Indian Ocean and cold waters over Mozambique Channel and Agulhas current region were associated with below normal summer rainfall season.

Combined PCA

Key regions in Atlantic and Indian Oceans have been identified. Results from combined PC analysis for the period 1950-89 indicated that above normal summer rainfall anomalies over most parts of southern Africa co-occurred with negative SST anomalies over the Central Indian Ocean. Western Zambia, Lesotho and south-eastern South Africa wet summers (due to this pattern) were negatively correlated to SST anomalies over the Central Indian Ocean (5°N-15°S, 50°E-100°E). Decreased north south SST gradient over the Indian Ocean was observed in the SST PC mode. The pattern is linked to ENSO. Spectral peaks were obtained at 4.4 and 2.2 years.

Eastern Botswana, southern Zambia, Zimbabwe and southern Mozambique rainfall positive anomaly pattern (PC2) was linked to cold subtropical waters over the Atlantic (40°W-15°W, 22.5°S-40°S) and Indian Ocean (50°E-75°E, 30°S-40°S) and warming in the Atlantic and Mozambique Channel. A strong meridional SST gradient in the Indian Ocean was evident in this SST PC mode. Temporal characteristics showed peaks at 3.8 and 9.2 years.

The Zambezi river valley (PC3) rainfall pattern was linked to an Atlantic dipole pattern (20°N-0°N, 50°W-20°W; 18°S-25°S, 7°E-15°E). Increased north-south temperature gradient over the Atlantic Ocean was associated with a positive rainfall anomaly. The associated time series had spectral peaks at 2.4 and 6.2 years.

Angola and Mozambique summer rainfall anomalies (PC4) were negatively correlated to SST anomalies over the Atlantic Ocean (0°N-25°S, 15°E-40°W). Cool SST over the Atlantic resulted in a positive rainfall anomaly pattern over Angola and Mozambique. Spectral peaks occurred at 2.4 and 6.2 years.

PC5 rainfall pattern exhibited a dipole pattern between southern (Lesotho and southeast South Africa) and northern regions (Angola, Zambia, Malawi and northern Mozambique). A positive rain anomaly over South Africa were negatively correlated to SST anomalies over Indian Ocean (0°N-5°S, 50°E-62°E) and positively with the Agulhas current system. Dominant spectral peaks occurred at 5.2 and 2.0 years. Southern African negative rainfall anomaly pattern (PC6) coincided with positive central Indian (5°S-5°N, 60°E-80°E) SST anomalies.

From this analysis it is not possible to know whether rainfall and SST anomalies respond to common atmospheric forcing or whether the rainfall anomalies are forced by SST. Tropical SST anomalies can drive the atmospheric circulation directly than SST anomalies in the midlatitudes. The combined PCA has identified coherent structure of SST and rainfall anomalies. The associated SST patterns may influence summer circulation in a number ways. The factors could include internal dynamics, which may not be evident in such an analysis. The central Indian Ocean plays a role in combined PC1, 5 and 6 and in the pair-wise correlation analysis for PC1, 2, 4 in the earlier section. The Atlantic Ocean is significant for combined PC3 and 4 and in the pair-wise correlation analysis for PC1 and 3. Tropical features, except for combined PC2 (mid-latitude) and PC4 (Atlantic dipole) dominate most of these PC modes. The influence of SST external forcing may be observed through:

(i) development of a continental high and subsidence

(ii) locally confluent moisture advection

(iii) tropic to mid-latitude SST gradient, hence thermal winds

(iv) extent of trade winds and position of the ITCZ

(v) zonal SST gradient which may enhance easterly waves.

The role of the Indian Ocean is quite evident in most of the rainfall anomaly patterns and this has been documented. In general, warm waters over the Mozambique Channel and Agulhas current and cold waters over central Indian Ocean lead to above normal summer rainfall. However the role of the Atlantic Ocean is not so clear. It may modulate rainfall patterns with north-west to south-east orientation. Wetter summers over Angola, western Zambia, northern Botswana, Zimbabwe and southern Mozambique are associated with cold waters over the Atlantic Ocean (PC3 and PC4).

Significant features of summer rainfall and SST anomalies have been identified and the links between them have been established. The distinctive wet and dry periods may be modulated by global and regional SST variations occurring over the Pacific, Central Indian and Atlantic Oceans. For the period 1950 to 1989 different patterns (rainfall PC modes) of droughts/floods occurred and were linked to specific mechanisms or SST patterns (SST PC modes) that together produced anti-cyclonic/cyclonic circulations over southern Africa. This shows that drought cannot be linked to a single SST pattern. Causes of rainfall variability are complex and diverse in various parts of southern Africa. The Angola PC rainfall pattern has been found to contribute most to inter-annual summer rainfall variability and SST anomalies over central Indian Ocean play an important role. More need to be learnt about how the rainfall anomalies are related to circulation as well as SST anomalies. The role of external forcing (direct SST) and internal (indirect) need to be investigated in order to see the influence of SST anomalies and this is taken up in the next chapter. This knowledge is useful to understand predictability of seasonal rainfall.

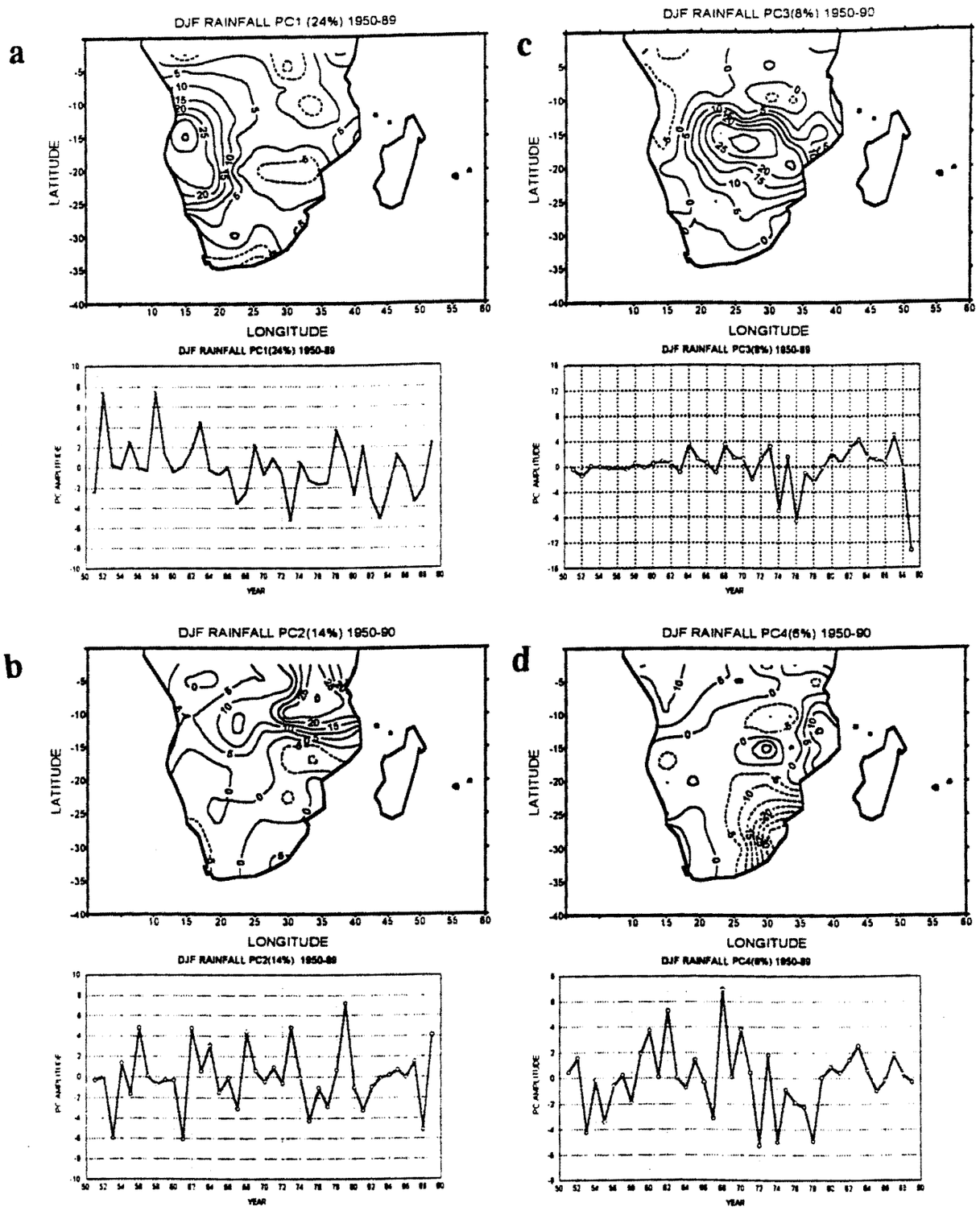

Figure 5.1 (a) Distribution of rotated PC1 of normalised DJF rainfall and the associated time series. (b) As in figure (a) but for PC2. (c) As in figure (a) but for PC3. (d) As in figure (a) but for PC4. The contour interval is 5.

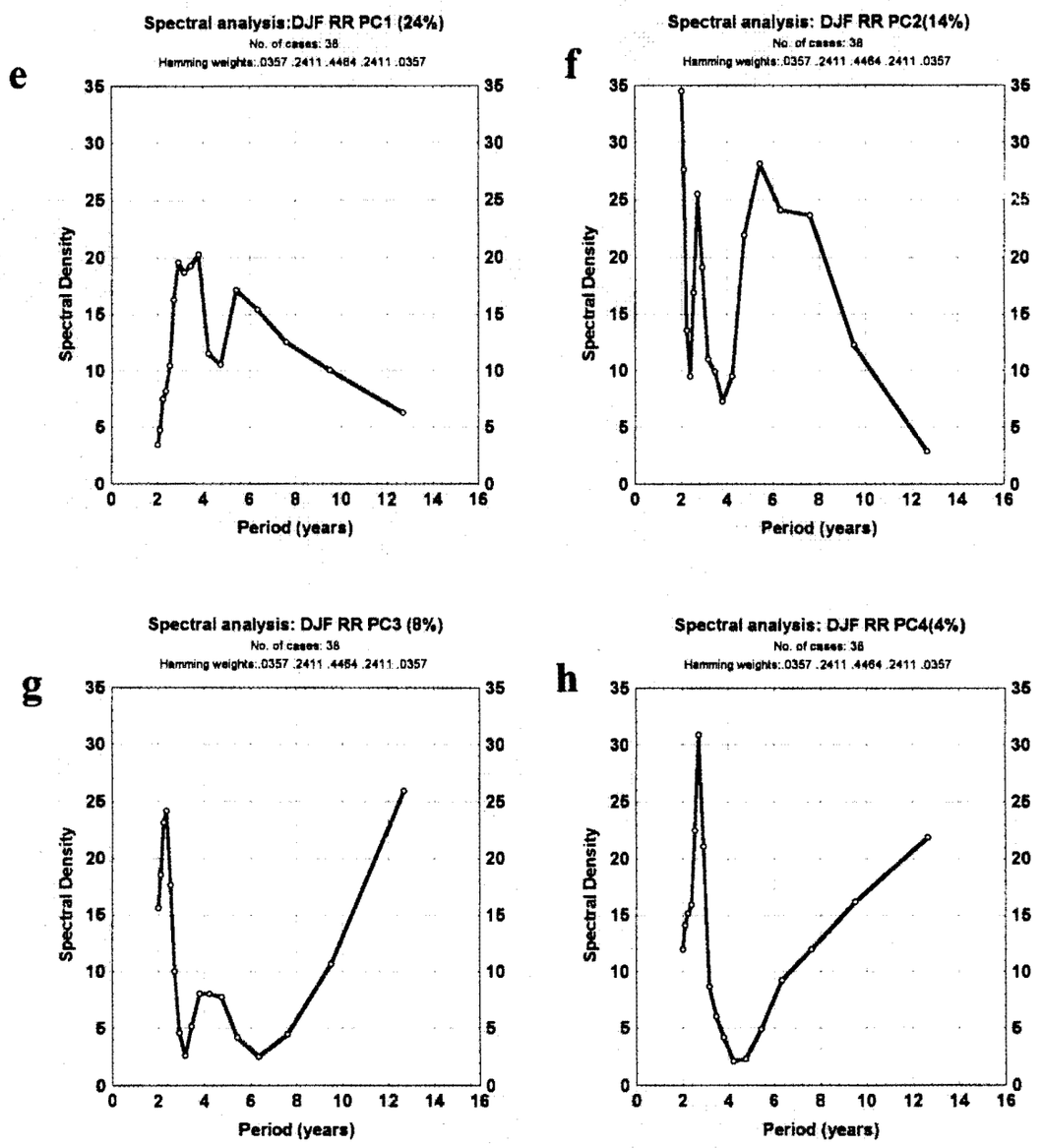

Figure 5.1 (e) Specral Analysis of PC1 (24%) pattern. (f) Spectral Analysis of PC2 (14%) pattern. (g) Spectral Analysis of PC3 (8%) pattern. (h) Spectral Analysis of PC4 (4%) pattern.

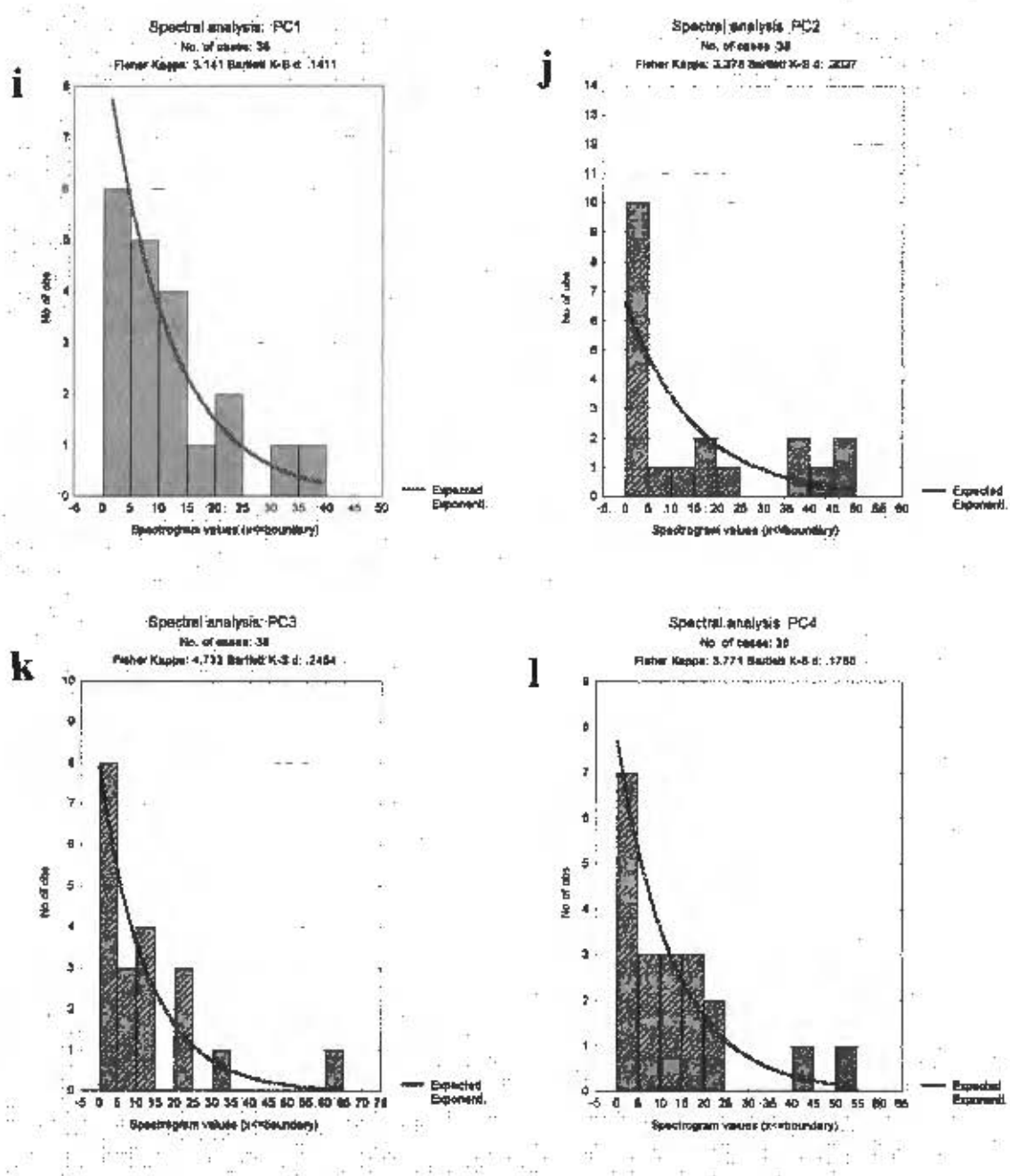

Figure 5.1 (I) PC 1 periodogram values , testing for white noise. (j) Same as in figure 5.1(I) but for PC2 . (k) Same as figure 5.1(I) but for PC3. (l) Same as figure 5.1 (I) but for PC4.

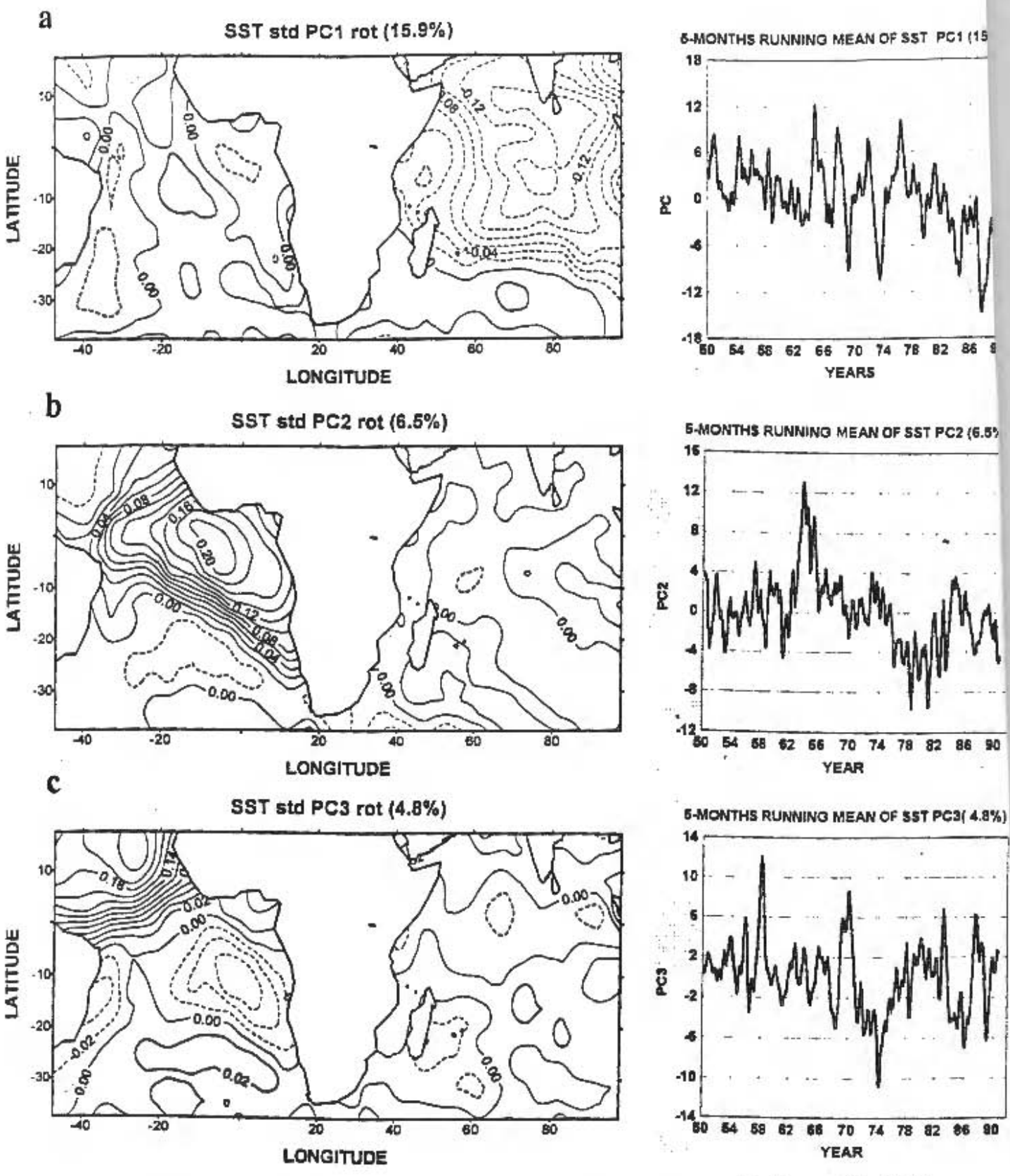

Figure 5.2 (a) Distribution of the spatial loadings of standardised monthly SST anomalies PC1 and the associated time scores. Contour interval is 0.02. (b) As in (a) but for PC2. (c) As in (a) but for PC3.

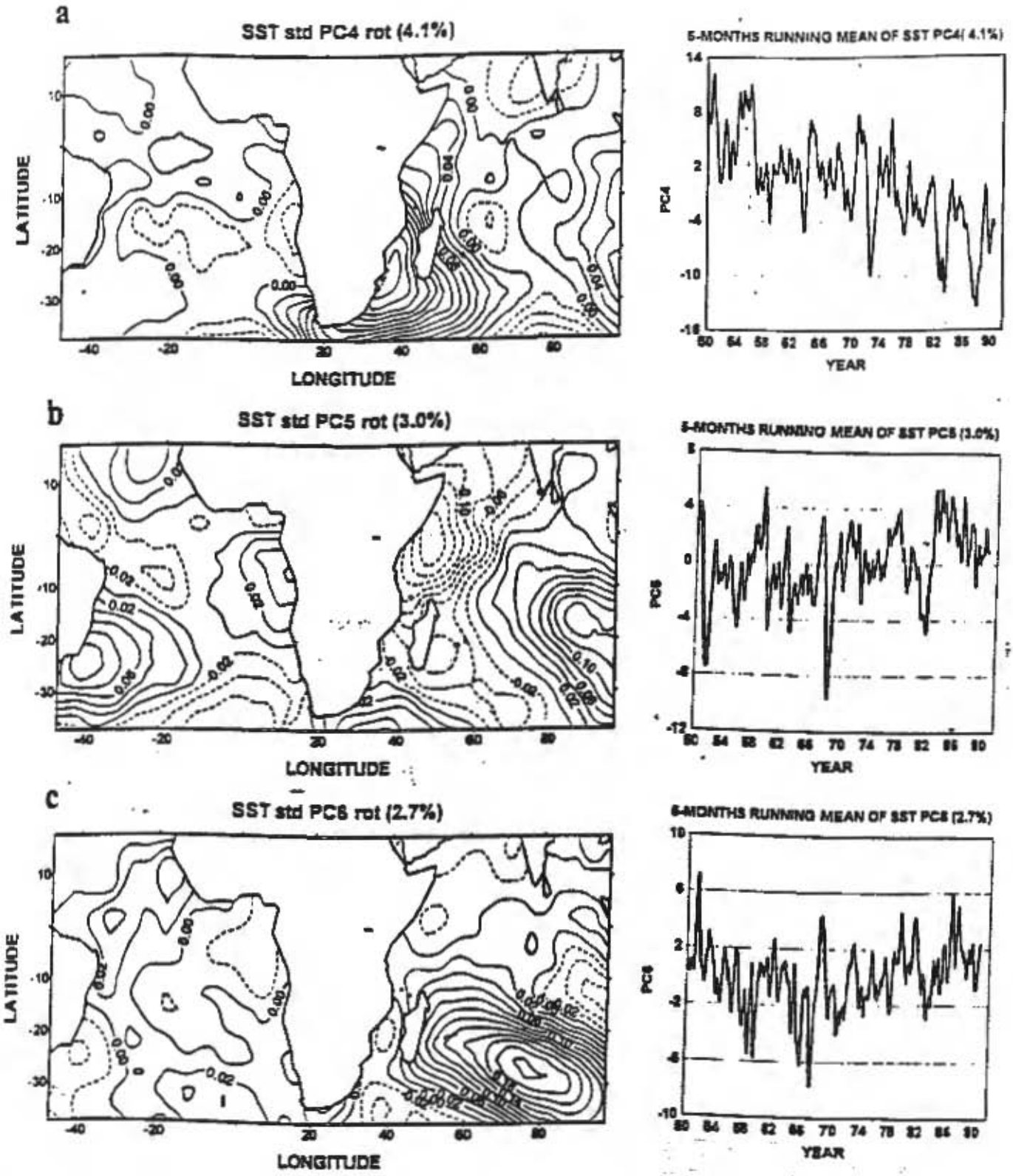

Figure 5.3 (a) Distribution of the spatial loadings of standardised monthly SST anomalies PC4 and the associated time scores. Contour interval is 0.02. (b) As in (a) but for PC5. (c) As in (a) but for PC6.

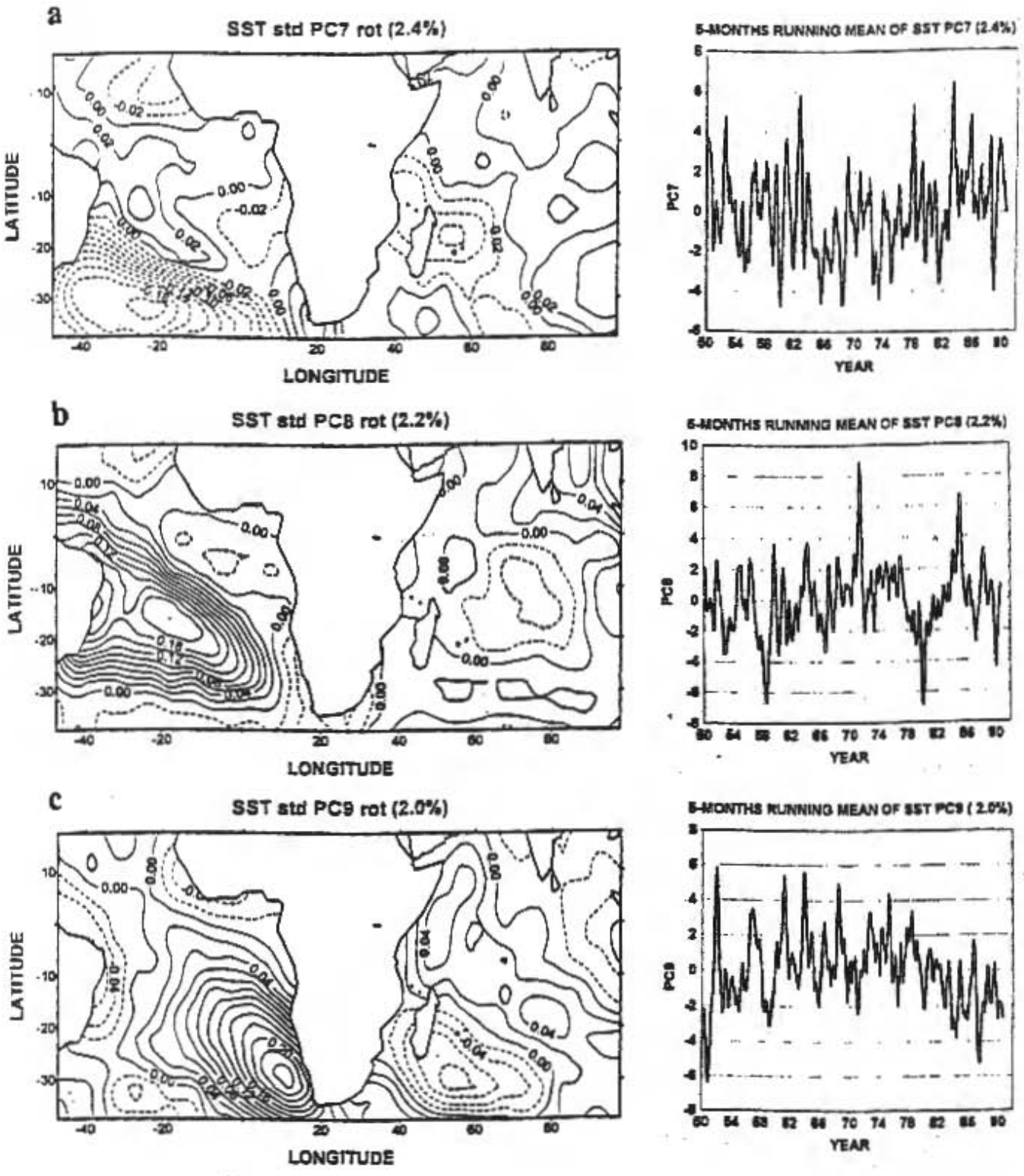

Figure 5.4 (a) Distribution of the spatial loadings of standardised monthly SST anomalies PC7 and the associated time scores. Contour interval is 0.02. (b) As in (a) but for PC8. (c) As in (a) but for PC9.

a

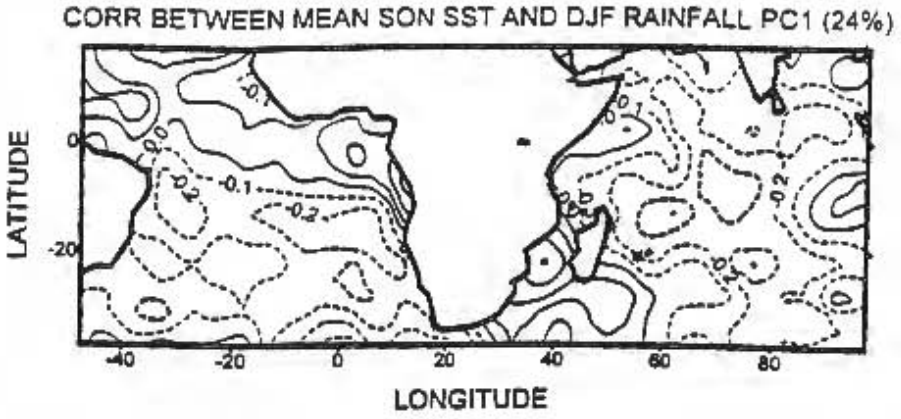

b

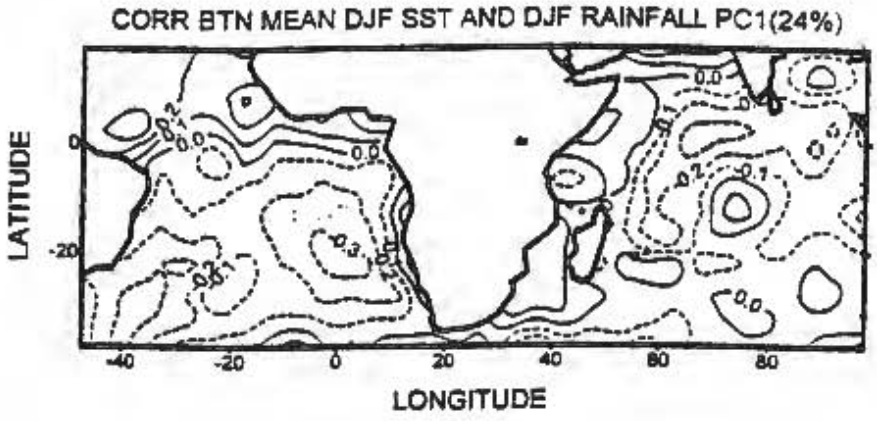

c

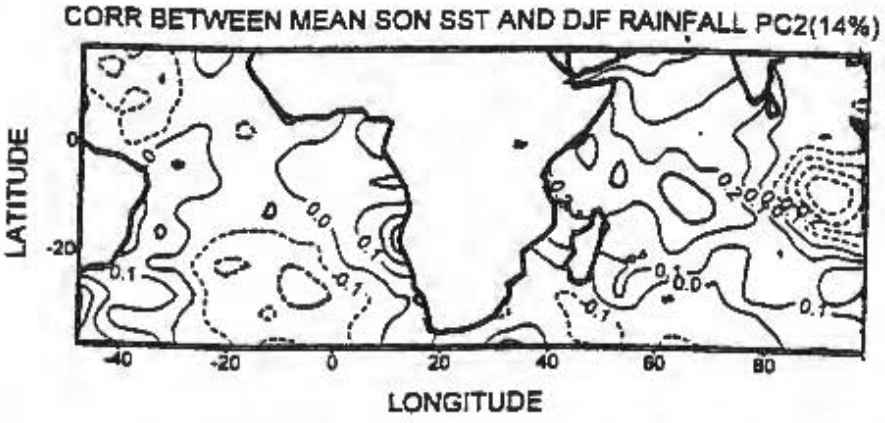

d

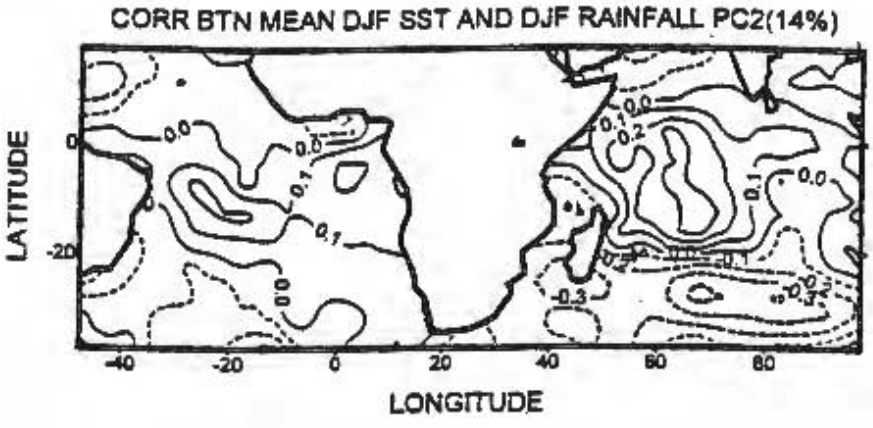

Figure 5.5 (a) Lag correlation pattern of SON SST anomalies and the first Principal Component of DJF rainfall. (b) As in (a) but for DJF SST's. (c) Lag correlations pattern of SON SST anomalies and DJF PC2. (d) As in (c) but for DJF SST's.

a

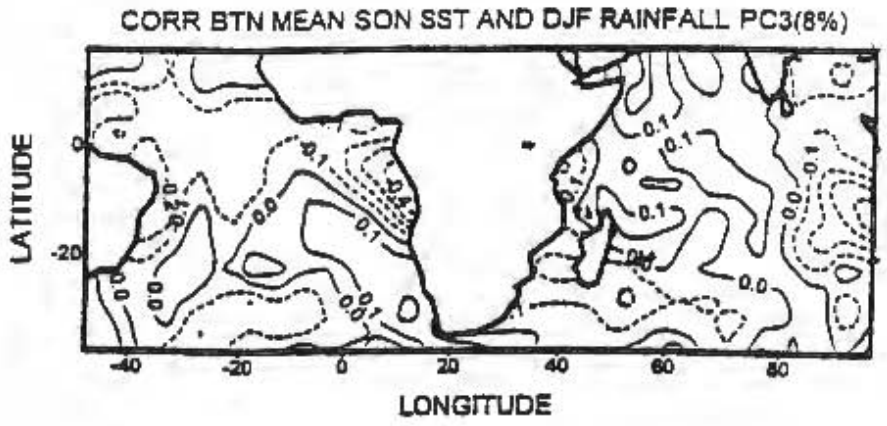

b

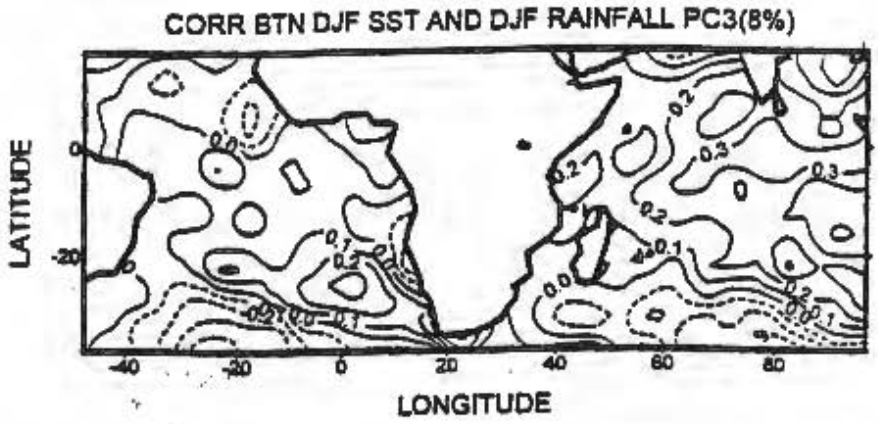

c

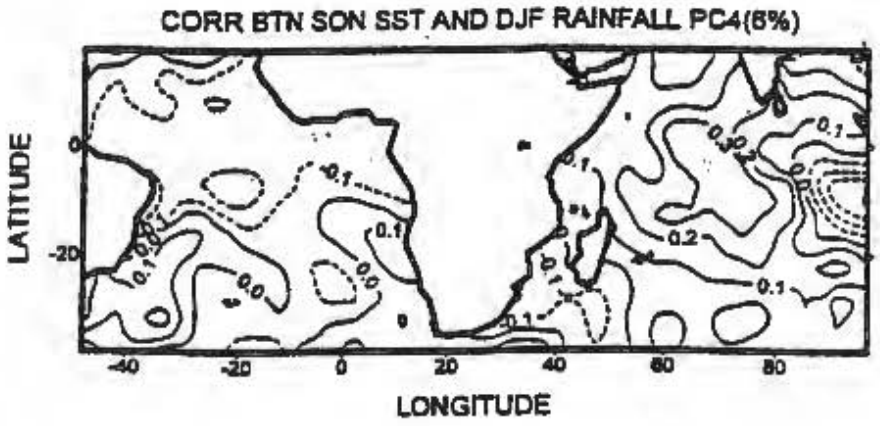

d

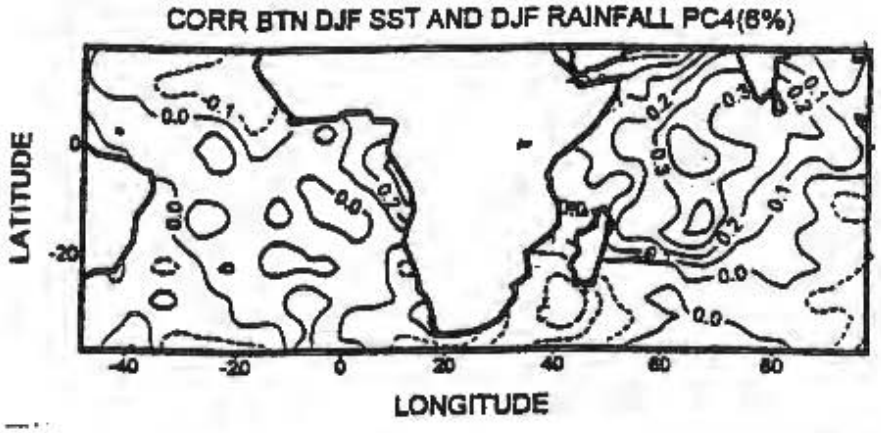

Figure 5.6 (a) Lag correlation pattern of SON SST anomalies and the third Principal Component of DJF rainfall. (b) As in (a) but for DJF SST's. (c) Lag correlations pattern of SON SST anomalies and DJF PC4. (d) As in (c) but for DJF SST's.

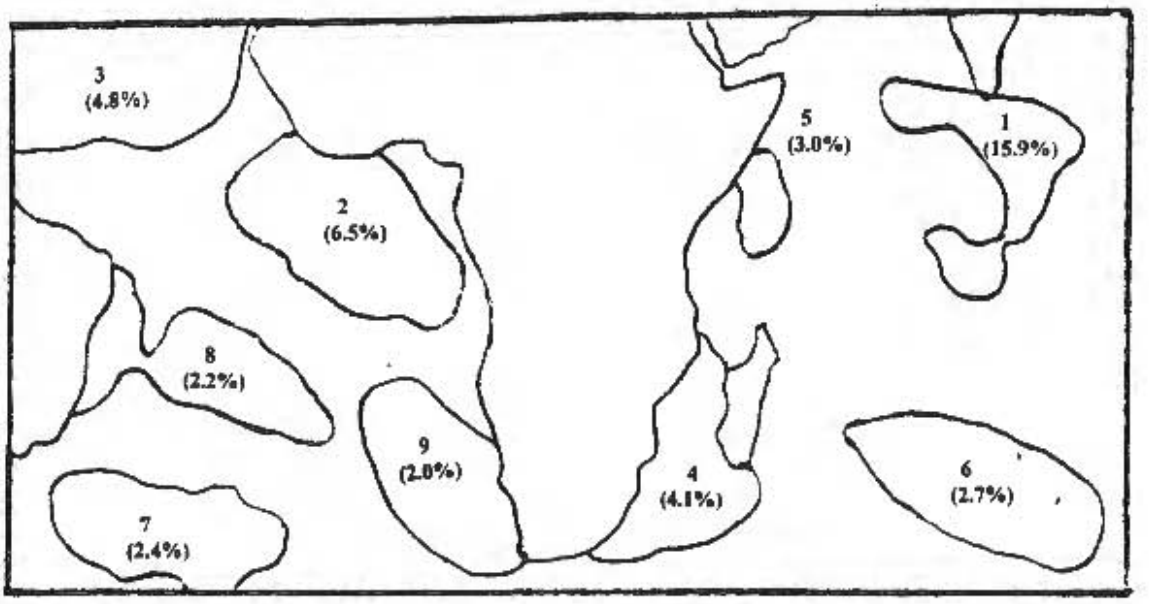

Figure 5.6 (e) Major SST features obtained from PCA . The percentage of total variance explained by each PC mode is in brakets. Cut-off contour is 0.16.

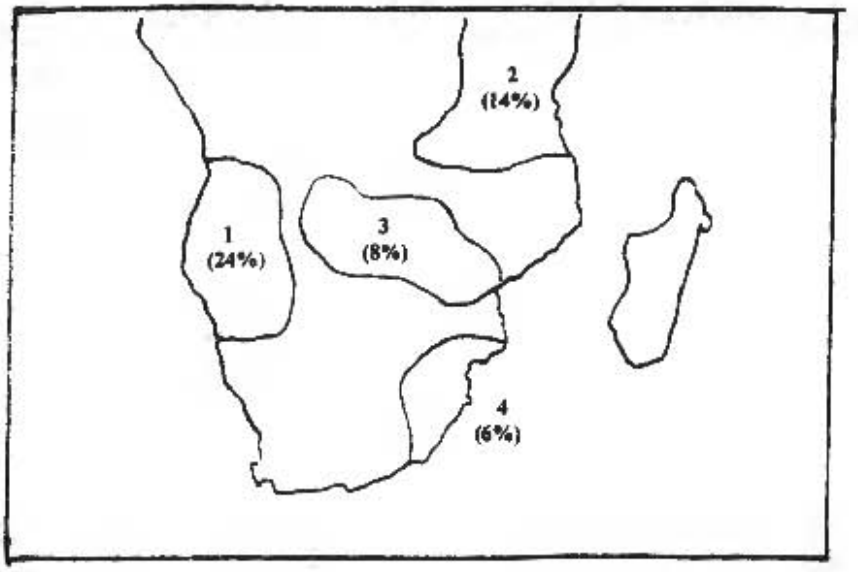

Figure 5.6 (f) Major DJF rainfall features obtained from PCA . The percentage of total variance explained by each PC mode is in brakets. Cut-off contour is 0.20.

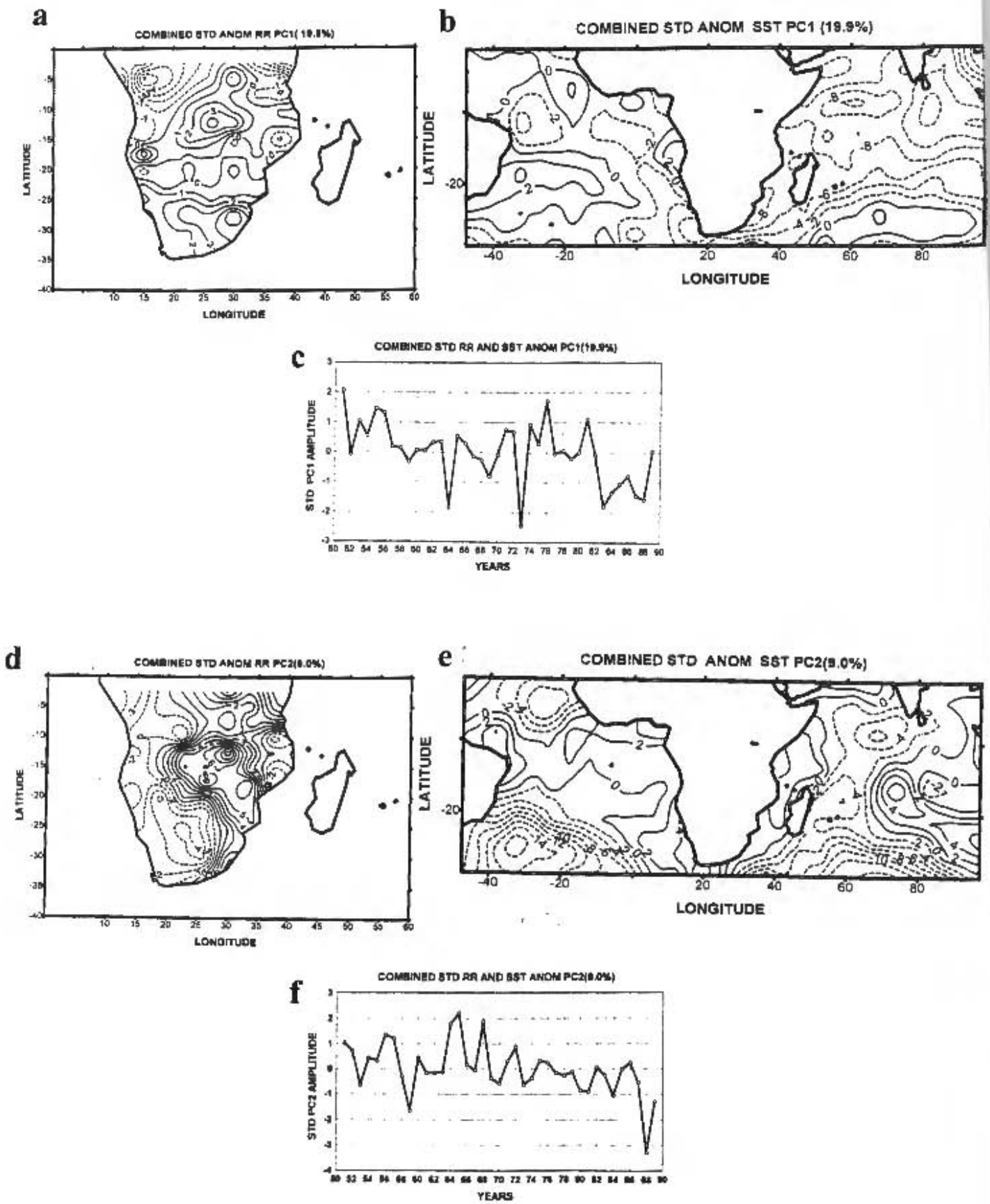

Figure 5.7 (a) Combined PC1 of DJF rainfall. Contour interval is 1. (b) Associated pattern for SST. Contour interval is 2. (c) Associated time scores for PC1 (19.9%). (d) Same as figure 5.7(a) but for PC2 (9.0%). (e) Same as figure 5.7(b) but for PC2. (f) Same as figure 5.7(c) but for PC2.

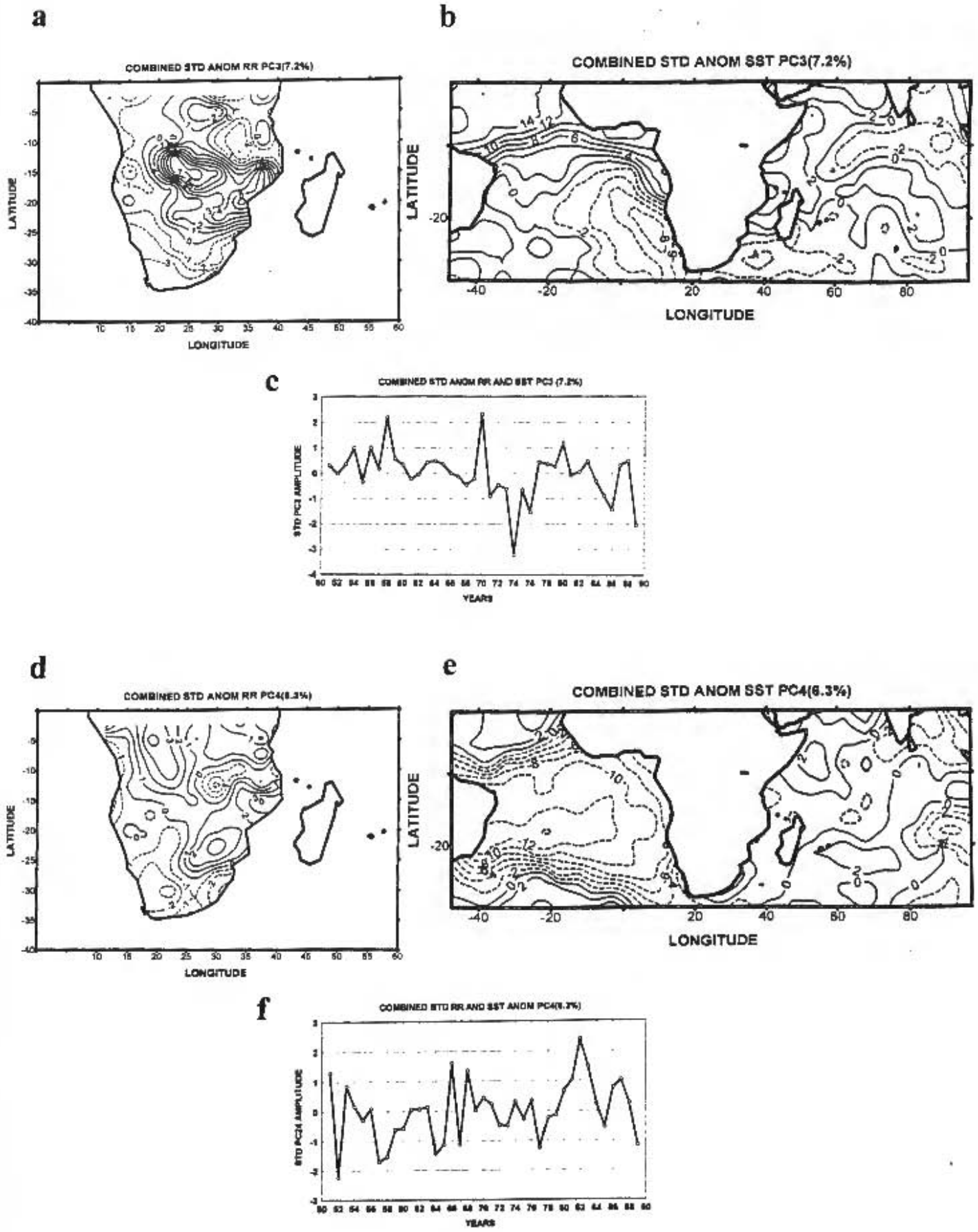

Figure 5.8 (a) Combined PC3 of DJF rainfall. Contour interval is 1. (b) Associated pattern for SST. Contour interval is 2. (c) Associated time scores for PC3 (7.2%). (d) Same as figure 5.8(a) but for PC4 (6.3%). (e) Same as figure 5.8(b) but for PC4. (f) Same as figure 5.8(c) but for PC4.

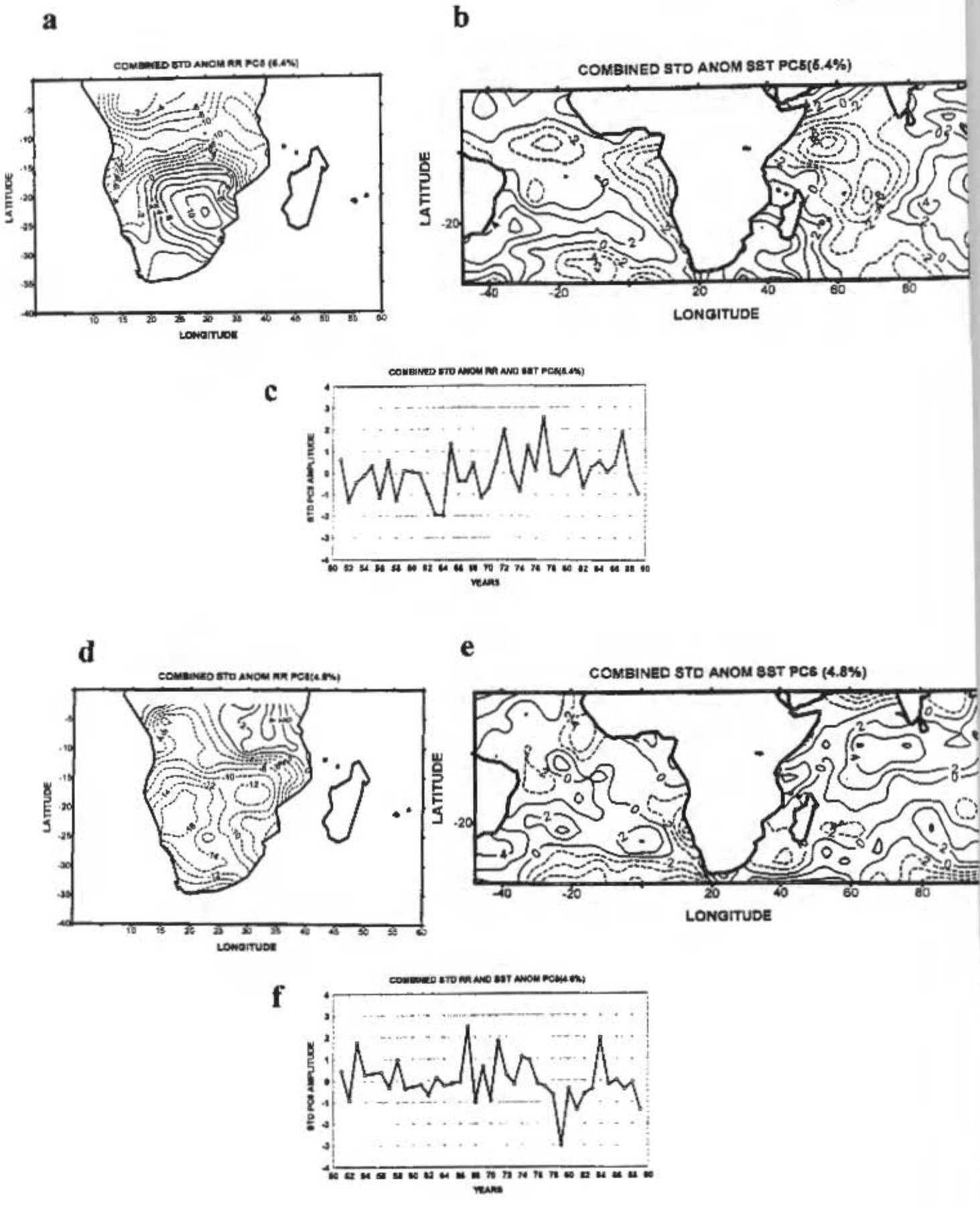

Figure 5.9 (a) Combined PC5 of DJF rainfall. Contour interval is 1. (b) Associated pattern for SST. Contour interval is 2. (c) Associated time scores for PC5 (5.4%). (d) Same as figure 5.9 (a) but for PC6 (4.8%). (e) Same as figure 5.9 (b) but for PC6. (f) Same as figure 5.9 (c) but for PC6.

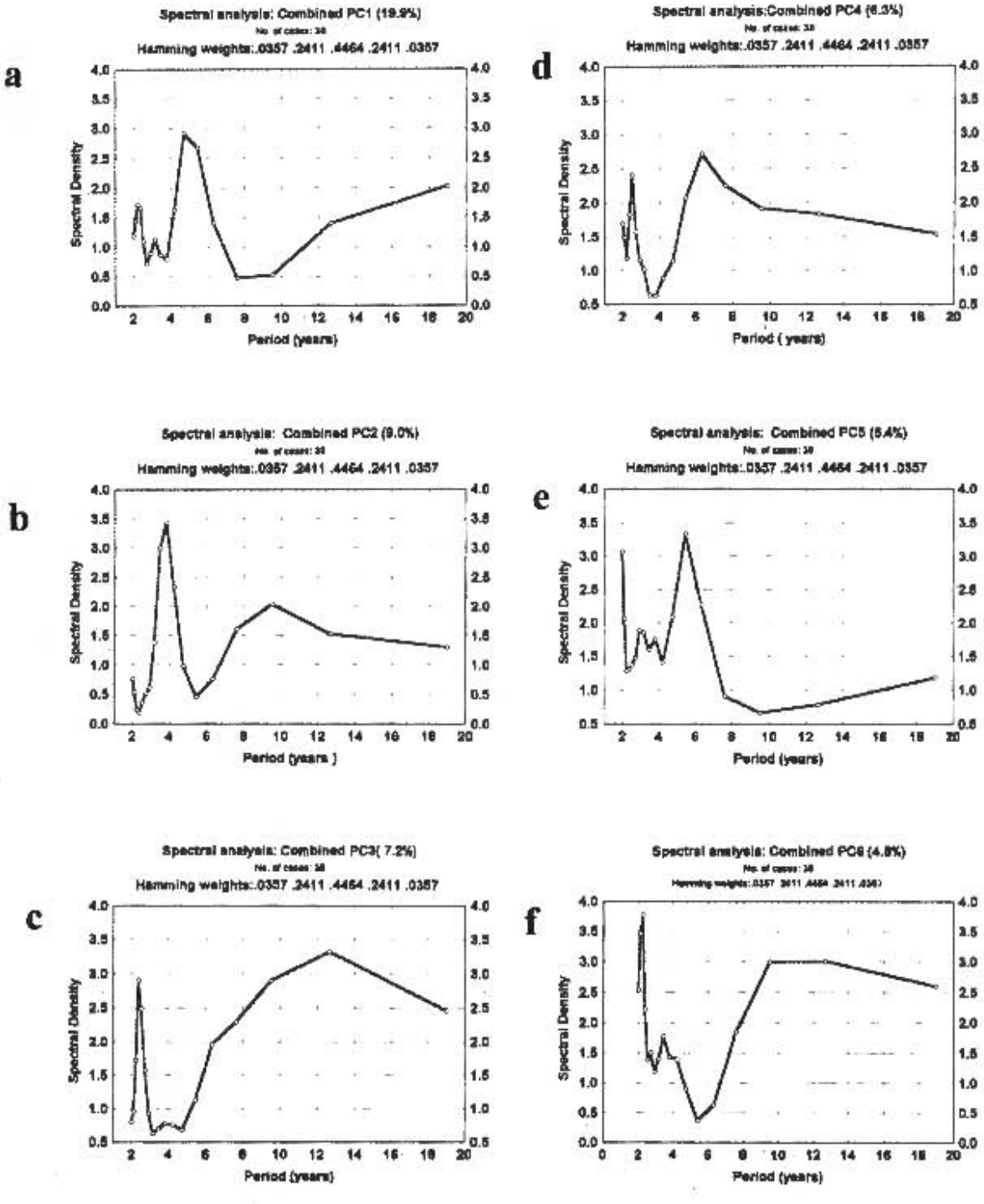

Spectral Analysis of Combined PC scores

Figure 5.10 (a) Specral Analysis of combined PC1 (19.9%) pattern. (b) Spectral Analysis of PC2 (9%) pattern. (c) Spectral Analysis of PC3 (7.2%) pattern. (d) Spectral Analysis of PC4 (6.3%) pattern. (e) Spectral Analysis of PC5 (5.4%) pattern. (f) Spectral Analysis of PC6 (4.8%) pattern.

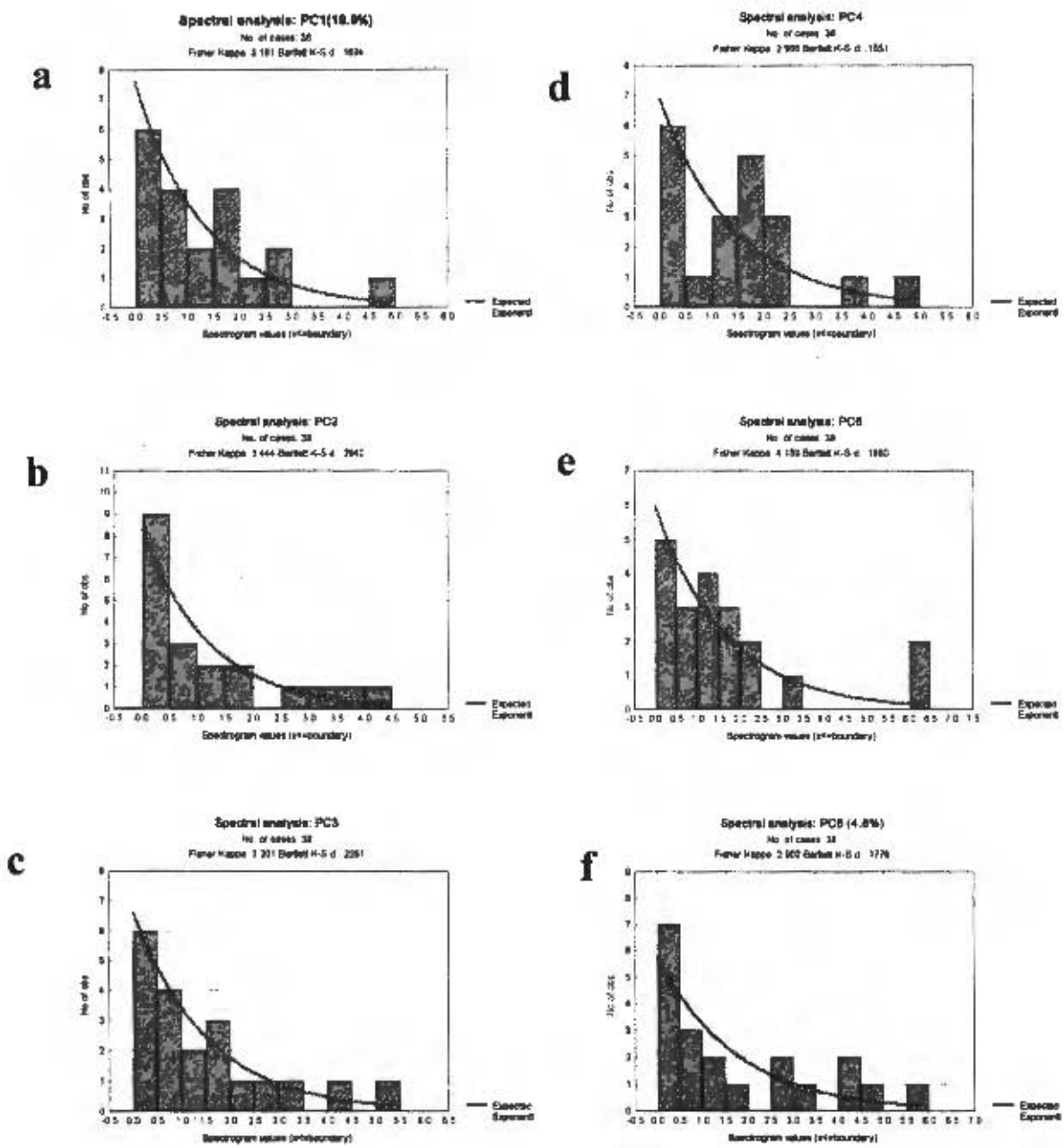

Figure 5.11 (a) PC 1 periodogram values , testing for white noise. (b) Same as in figure 5.11(a) but for PC2 . (c) Same as figure 5.11(a) but for PC3. (d) Same as

CHAPTER 6

STRUCTURE OF LOW-FREQUENCY FLUCTUATIONS

6.1 Introduction

The objective of this chapter is to identify regional SST, atmospheric and convective anomalous features associated with flood/drought summers during the period 1980 to 1990. The second objective is to investigate important atmospheric monthly anomaly patterns (tropical teleconnections) using continuous monthly data. The third objective is to find relationships between atmospheric features and the Southern Oscillation Index (SOI). The aim of studying the time/lag correlation between the fields is to ascertain if any predictive relationship can be obtained.

This chapter is divided into three sections and first deals with coherent structure of summer SST, tropospheric wind and convection anomalies. The second section is on teleconnection patterns and the third on relationships between teleconnection patterns and SOI.

6.2 Coherent structure of SST, tropospheric winds and convection anomalies

6.2.1 Introduction

The goal of this section is to identify coherent circulation anomalies by analysing concurrent variations of SST, convection, and lower and upper tropospheric winds. This type of work helps to describe and understand coupling occurring in natural environments. It also describes phenomenological relationships within fields and among fields of different variables. Many statistical analyses and GCM models have linked specific country rainfall to SST anomalies and tropical circulations. Few studies exist dealing with southern African convective, SST and atmospheric wind anomalies. This study will help in understanding the link between SST, circulation and convection anomalies. Separation of external (SST forcing) and internal dynamics can also be achieved through this analysis. Relationships

between observed SST, tropospheric circulations and convective anomalies are not completely understood. The purpose of this chapter is to identify large-scale coherent structure of DJF SST, tropospheric circulations (200hPa and 850hPa winds) and convection (OLR) anomalies. This study can help us understand the contribution of SST (direct) forced and internal dynamics (indirect SST) convective anomalies. The role of lower tropospheric circulation anomalies maintaining SST anomalies is investigated. Do local low level circulation enhance or dampen SST anomalies? Tropical SST anomalies have a greater impact on tropical atmospheric mean state than midlatitude SSTA. For example, in the tropical atmosphere, anomalous positive SST (external) forces widespread anomalies in convection and large scale Hadley and Walker circualtions. Convective regions are associated with low level convergence and upper level divergence. Teleconnections are created through Rossby waves (Gill, 1980; Webster, 1981) and interact with stationary waves. Changes are induced in the circulation and hence rainfall. According to linear theory, the atmospheric response to fixed SSTA is to generate vertical motion above the area of forcing, cyclonic and anticyclonic circulations occur in lower and upper levels respectively. In this case SST thermal forcing dominates internal forcing in tropical regions where advection processes are neglected. For midlatitude SST anomaly, advective processes dominate and thus internal dynamics (internal flow instabilities) occur.

In general rainfall anomalies depend on external (SST forcing) and internal (synoptic systems) forcings. In external forcing, the SST thermal forcing dominates internal dynamics, while for internal forcing it is synoptic or weather systems (flow instabilities) that are more prevalent. The SST-rainfall dependence is usually embedded in the 'noise' of natural variability (synoptic-scale systems). The rainfall anomalies due to SST anomalies can potentially be predicted by predicting SST anomalies given a good statistical or dynamical model. Rainfall anomalies due to flow instabilities are unpredictable on longer time scales. It is important to separate the internal dynamics and SST driven

convection anomalies. Knowing areas where convection anomalies are dominated by external (SST anomalies) forcing can be useful in long-range forecasting. This chapter will attempt to determine convective patterns, which are associated with external forcing (SST) versus those internally forced.

This chapter focuses on the structure of convective, sea surface temperature and circulation anomalies during summer season (DJF) for the period 1980 to 1990. No previous study has attempted to document anomalous structure of southern Africa and adjacent oceans using combined PC analysis.

From chapter 4, Angola low is associated with internal dynamics and land processes. It is observed that mean summer circulation over Southern Africa is characterized by low level moisture convergence over Angola and anticyclones over Indian and Atlantic oceans. The location and intensity of the thermal low over the subcontinent plays an important role in controlling moisture and stability of the atmosphere.

Spatial movements of oceanic anticyclones are crucial in determining the position of the ITCZ. SST variations may control the anticyclones. In the upper troposphere (200hPa), the mean circulation is dominated by a large anticyclone with prominent easterlies to its north. The anticyclone is located 10° to 20° degrees of longitude southwest of maximum convective center as indicated by low OLR (200 Wm^{-2} or less) over northeast Zambia. The strength of the upper level anticyclone depends on low level moisture convergence and non-linear factors. Variations in upper level circulation can contribute to inter-annual variability of summer rainfall. Standing waves as discussed in the literature review play an important role. Thus low level convergence, upper level divergence and several surface and tropospheric features characterise the mean summer circulation. From chapter 5, cold waters over the equatorial Indian Ocean and Atlantic Oceans with warm waters over Mozambique Channel and Agulhas current system are linked to wetter summer seasons for the period 1950 to 1990. The mechanisms for SST-rainfall associations may be demonstrated through GCM modeling. However, it is not the intention of this

study to test the associations this way. The aim of this chapter is to gain some insight into the importance of SST, OLR and circulation changes and how they are related over southern Africa and adjacent oceans. The roles of internal forcing and direct SST forcing will be revealed. SST forced convection are expected to be associated with increased evaporation, moisture convergence increased cloudiness and precipitation which results in release of latent heat in the neighborhood of the SST anomaly. According to Gill (1980) Kelvin waves occur to the east of a heating anomaly and Rossby waves to the west. Convection anomalies over cold SST anomalies are assumed to be induced by internal dynamics. Warming the over equatorial Indian and Atlantic oceans are likely to result in inducing anomalous precipitation due to the high background temperature compared to midlatitude regions.

In order to identify the structure of convective, SST and circulation anomalies combined PCA was applied to standardized DJF sea surface temperature, OLR and wind anomalies. This analysis will help in understanding the link between the atmosphere and sea surface temperature anomalies. Identifying the key SST anomalies and the associated lower and upper tropospheric circulation patterns of variability is being addressed and it is important to separate internal and external mechanisms for convection anomalies. Examining linkages between dynamic and thermodynamic variables should help in interpreting and fostering diagnostic studies leading to better understanding the roles of sea surface temperature anomalies. Combined PCA has been successfully used to study the vertical structure and development of ENSO anomaly mode (Wang, 1992). Nigam and Shen (1993) utilized combined PCA to study the structure of oceanic and atmospheric low-frequency variability over the Tropical Pacific and Indian Ocean. Care should be taken when interpreting this analysis due short to duration of the data set.

6.2.2 Data and method

Standardized DJF SST anomalies for 144 grid points for domain 20°N to 40°S, and 50°W to 100°E were used for the period 1980 to 1990 at resolutions 10°

latitude by 5° longitude. For tropospheric DJF winds, 850hPa and 200hPa level were chosen to represent lower and upper troposphere respectively. Standardized DJF wind and OLR anomalies were calculated at 10° by 10° for the domain 20°N to 40°S, 40°W to 90°E. Six variables namely, SST, 850hPa zonal wind, 850hPa meridional wind, OLR, 200hPa zonal wind and meridional wind were considered. OLR and wind fields each had 91-grid points. A total of 599(144+(5x91)) standardized time series were subjected to rotated PC analysis. The matrix of 599 x 10 elements was used and GENSTAT statistical package (1993) was applied to calculate the principal components and time scores. The PC loadings were multiplied by 100 to facilitate contouring.

6.2.3 Structure of coherent principal component patterns

PC1 (21%) Continental (figure 6.1)

The SST loadings shown in **figure 6.1(a)** indicate warm waters over most parts of oceans except over the central equatorial Indian Ocean. Large values were found over the southern Indian Ocean and thus implying weak north-south tropical and subtropical temperature gradients over the Indian Ocean. From thermal wind concept this may imply the presence of easterly winds over Indian Ocean in the latitude band from equator to 30°S. High temperature induces evaporation and may be due to solar radiation and adiabatic heating. The lower (850hPa) circulation loadings associated with this structure are shown in **figure 6.1(b)**. An anticyclonic circulation (with center 70°E, 30°S) overlies the SST heating over south Indian Ocean controls northeasterly flow over eastern parts of southern Africa. Over Atlantic Ocean and anticyclone (with center 20°S, 15°E) controls southerly flow over western parts of southern Africa. A vortex is evident over southern Africa. Thus moisture convergence is expected over southern Africa and divergence over anticyclonic flow regions. The anticyclones are warm implying they can intensify with height. The associated OLR loadings are negative values over southern Africa and midlatitudes with positive values over western Atlantic equatorial latitudes and subtropical Indian Ocean (see **figure 6.1(c)**). Southern African convection anomalies are out of

phase with Indian and Atlantic Oceans along latitude 20°S. The 200hPa wind loading anticyclonic ridge axis along 30°S with easterlies to the north and westerlies to the south. Strong easterly anomalies are observed over southern Africa (see **figure 6.1(d)**). The lower and upper flow anomalies are consistent with wet summers over southern Africa. The associated time scores are shown in **figure 6.4(f)**. Periods with negative scores may be associated with dry summers over southern Africa and wet summers over the Indian Ocean. This pattern is consistent with the dipole found by Jury (1992). The convective activities are land-based during wet season and oceanic forced in dry seasons. The heating of the Angola plateau is crucial in determining the differential heating between land and ocean. Internal local dynamics are important during wet summers.

Weak anomalous winds are observed over the warm regions and thus little advection, but northerly meridional winds over Mozambique channel suggest warm advection. Southerly meridional cold advection is observed along latitude 10°S over the Indian Ocean and may maintain cold waters over central Indian Ocean. It may be observed that the anomalous low-level winds in the region of large SST anomaly may enhance the pattern there.

PC2 (16%) ENSO, Quasi-stationary waves (figure 6.2)

Combined PC2 SST pattern exhibits positive loadings in the subtropical Atlantic (0°S-20°S) and south Indian Ocean (see **figure 6.2(a)**). Maximum negative loadings occur over the equatorial and south Atlantic Ocean. Anomalous lower cyclonic flow occurs in the Mozambique Channel, Madagascar and the adjacent areas (see **figure 6.2(b)**). Anticyclonic flow is over the southern Atlantic Ocean. Negative OLR PC loadings are negative over southern Africa, southern Indian Ocean and equatorial Atlantic Ocean (see **figure 6.2(c)**). Strong anomalous easterly winds are observed over equatorial regions (key area) see **figure 6.2(d)**. An axis of anticyclonic flow occurs along latitude 28°S. Flow patterns and OLR anomalies are dynamically consistent. Maximum negative loadings of SST over the Indian Ocean are associated with

cyclonic lower level and positive loadings in the south with cyclonic circulation, which is also found over the equatorial Atlantic. The OLR loadings pattern and large area of cyclonic flow suggest that this PC pattern may be associated with quasi-stationary waves and cloud bands (Harrison 1989). The convection anomalous over southern Africa and the equatorial Atlantic are SST forced while convection over the equatorial Indian is internally forced.

The time scores indicates large negative magnitudes in 1982/83 and 1986/87 known ENSO years (**see figure 6.4(g)**). Lindesay (1988) found that the SOI explains 16% summer rainfall over South Africa. Rocha and Simmonds (1997) suggest that rainfall anomalies linked to ENSO in southern Africa are SST-forced. Reason et al (1998) has found that the response of atmosphere to imposed subtropical SST anomalies is at interdecadal timescale. A cyclonic anomaly in the lower atmosphere is generated near and downstream of the warm SST anomaly in southern midlatitudes of the Indian Ocean. Over the Indian Ocean the anomalous circulation will enhance the SST anomalies.

PC3 (14%) Continental eastern Africa (figure 6.3)

Combined PC SST mode is associated with negative loadings over most parts of the Indian and Atlantic oceans (see **figure 6.3(a)).** Maximum cooling occurs over Agulhas, and along the east Africa coast. Large anticyclonic flow is exhibited over the central Indian Ocean with convergent flow over the southern Indian ocean in the lower troposphere (850 hPa) (see **figure 6.3(b)**). Anomalous divergent flow prevails over southern Africa. OLR PC loadings show positive values over the eastern parts of Africa with maximum values over southern Africa. A dipole between Madagascar and southern Africa is quite evident (Jury, 1992) (see **figure 6.3(c)**). Strong easterly anomalies are associated with negative OLR loadings over Madagascar and the south Indian Ocean with convergent flow over southern Africa in the upper troposphere (see **figure 6.3(d)**). The lower level flow favours warm air advection over the south Indian Ocean and cold advection over southeastern Atlantic Ocean. The time scores show dry summers due to this pattern in 1982/83,1983/84, 1984/85 and

wet summers 80/81, 87/88 and 89/90 (**see figure 6.4(h)).** It appears to be forced by SST anomalies over the Indian Ocean and adjacent southern Africa. Cold areas are associated with anticyclonic flow in the lower troposphere.

PC4 (11%) figure 6.4

Maximum values of combined PC4 SST are found over the Atlantic (10°S-30°S,) and Indian Ocean (0°S-20°S, 50°E-70°E). Negative SST loadings over Mozambique Channel and Agulhas current (see **figure 6.4(a)**). Anomalous diffluent flow prevails over regions south of 20°S with convergent flow over eastern Zambia, Malawi and Mozambique (see **figure 6.4(b)**). Large areas of convergent low-level winds are observed over the Indian Ocean. Negative loadings of OLR are found over the Indian Ocean and adjacent Mozambique, Malawi and eastern Zambia. The rest of the continent has positive loadings (reduced convection) (see **figure 6.4(c)).** In the upper troposphere a large anticyclonic flow centered over northeast Madagascar prevails (see **figure 6.4(d)**). Convergent flow is evident over southern Africa and the southeastern Atlantic Ocean. The anomalous circulation in the lower troposphere enhances the existing SST anomalies over the Indian and Atlantic Ocean. Since positive SST are associated with low level convergence, negative OLR and upper level divergence, it can be suggested that the system is SST forced over the Indian Ocean but internally driven over the Atlantic Ocean. The time series of scores show dry summers over the Indian Ocean due to this mode in 87/88 with maximum wet summers in 84/85, 81/82 and 83/84(see **figure 6.4(i)).**

6.2.4 Summary and discussion to section 6.2

Four large-scale features of coherent structure of DJF SST, circulation and OLR anomalies have been identified. They account for 62% of the total variance. Convective anomalies are associated with low level convergence and upper level divergence. For external SST forcing (direct), warm (positive) SST anomalies are associated with low level cyclonic and upper level anticyclonic circulation hence convective anomalies. In case of cold (negative) SST anomalies anticyclonic flow develops in the lower troposphere for SST induced

circulation. For internal dynamics (indirect), warm (positive) SSTs are associated with low level anticyclonic flow and upper level cyclonic flow. Cold (negative) SST anomalies are associated with low level cyclonic and upper level anticyclonic flow. Generally the low-level flow enhances the SST anomaly pattern through anomalous temperature advection.

The first OLR PC illustrates the importance of land based convection and also contributes most to DJF SST, circulation and OLR variability as shown in the previous chapter. The dipole nature of this pattern is noted between southern Africa and the southwest Indian Ocean. This PC shows the link between tropical and midlatitude disturbances. The internal dynamics play an important part in generating this anomaly pattern. This pattern is associated with reduced north-south temperature gradient over the Indian ocean, strengthened subtropical high pressure systems, intensified low level circulation (displaced Angola), deep convection and strong upper level easterlies over southern Africa during wet spells. During dry spells, the convection shifts to the Indian Ocean and is associated with increased north-south temperature gradient there implying the importance of baroclinic disturbances. The origin of southern African convection (Rocha and Simmonds, 1997b) depends on the location and strength of thermal low over southern Africa. Thus internal dynamics play an important role through differential heating in the formation of the thermal low over southern Africa. The role of differential heating in the formation of Angola low will be taken up later in chapter 7.

The second combined OLR PC, which explains about 16% of total variance, is SST-forced over the southwest Indian Ocean but internally-forced over central Indian Ocean. It has been noted in GCM model results by Reason et al (1998) that imposing warm SST anomaly in southern midlatitudes of the Indian ocean results in a cyclonic anomaly in lower atmosphere near and downstream of the SST anomaly. It can be linked to cloud band (Harrison 1986). Weak north-south temperature gradients occur over the in Indian Ocean but are strong over the Atlantic Ocean. It also illustrates some inter-hemispheric link in the Indian

Ocean, which is associated with ENSO. Wet summers over southern Africa are associated with cold waters over central Indian Ocean and warm Agulhas current system. Strong upper level easterlies are noted over the West African Guinea Gulf. This key area will be discussed in the next section.

The combined pattern OLR PC3 exhibits a dipole structure between southern Africa and the Indian Ocean. Cooling of oceanic waters in both basins results in dry summers over southern Africa. Cooling over Arabian Sea, Mozambique channel and Agulhas current results in lower level divergence and upper convergence over southern Africa. This is SST-forced over the Indian Ocean but internally driven over the Atlantic Ocean. During dry spells, southern Africa acts as sink region for convection over Madagascar.

PC4 represents a dipole between central Indian Ocean and southern Africa convective anomalies. It is SST-forced over Indian Ocean but internally over Atlantic Ocean. The SST-forced disturbances also contribute rainfall over Northeast Zambia, Malawi and Mozambique. Dry summers due to this pattern may be linked to warming over the southwest Indian Ocean and cooling futher south. This is associated with anticyclonic flow over southern Africa in lower the troposphere and cyclonic flow in upper troposphere.

This analysis shows that both internal and SST-forced mechanisms play an important part in summer convective anomalies. The importance of internal dynamics is seen in PC1, where land based thermal low (Angola low) is revealed. Some of SST-forced circulations are linked to ENSO. Dipole patterns (PC1, PC3 and PC4) contribute a total of 46% of the total variance for the first 4 PC modes considered.

6.3 Low-frequency atmospheric variability over southern Africa and adjacent oceans

6.3.1 Introduction to teleconnections

The contribution of SST anomalies to inter-annual variability of southern African summer rainfall has been discussed in the previous chapter, which has confirmed links between SST anomalies and rainfall anomalies. Summer

rainfall also depends on internal dynamics, which are transmitted through the tropospheric circulation. Motivated by the availability of data this chapter investigates the role of tropospheric circulation anomalies by revealing significant patterns and relating them to ENSO. Although the atmospheric memory is shorter than oceanic memory some PC patterns may contain key areas which may be used in predicting summer rainfall. Hence the purpose of this study is to identify key regions from which regional indices can be developed for seasonal rainfall prediction in southern Africa. The other reason for studying inter-annual variability or low frequency variations is that weather systems evolve and develop in preferred regions for example in southern Africa the seasonal heat low develops over Angola or Botswana and frontal systems have preferred tracks. Low frequency features may influence positions of these features.

Numerical predictability of atmospheric motions is less prone to errors up to about two weeks. Beyond that times the detailed predictability of atmospheric parameters (e.g. rainfall, temperature) at any given instant is reduced. Thus quantitative analysis of meteorological fluctuations on seasonal time-scales will assist in establishing the potential for "memory" in the coupled ocean-atmosphere system to help extend the practical range of Numerical Weather Prediction (NWP) through determination of statistical associations. Weather systems are believed to evolve and develop in preferred regions. In Southern Hemisphere the frequency maximum of surface fronts is usually located along 40°S (Preston-Whyte and Tyson, 1988). Majodina and Jury (1996) studied the structure of the cyclones between latitude 30° to 50°S. The large-scale and synoptic disturbances are associated with atmospheric conditions, which support their growth. The mean tracks or the preferred regions of these disturbances may be constant or variable and their tracks can exhibit seasonal shifts resulting in anomalous regional weather.

In this section PCA is applied to monthly geopotential thickness heights, winds, 500hPa geopotential heights, water vapor flux, and Outgoing Long wave

Radiation (OLR). The main focus of this study is the teleconnections of the atmospheric anomaly patterns and their temporal characteristics over Africa and the adjacent oceans. Statistical associations between PC tropospheric patterns and ENSO are carried out in order to identify which key areas are associated with ENSO and those which are non-ENSO. The domain of study includes the Atlantic and Indian Ocean and the subcontinent of Africa. The region extends from 70°W to 100°E, 20°N to 60°S. Data are at regular intervals of 2.5°. The period of study extends from 1980 to 1993. This study is different from the previous cited studies because of the data characteristics i.e. period and domain. In general PC analysis of various meteorological parameters has not been done for the African domain. Comparison with previous studies is therefore difficult.

In this section the anomalies evident in the ECMWF data are identified using rotated Principle Component Analysis (PCA). The description of the technique is found in chapter 3. The focus will be on the first three PC modes, which explain the largest percentage of the variance. It is generally considered that the first PC mode (PC1) indicates large-scale features of a scale similar to the domain under scrutiny. Thus the first mode may not show local features of interest. In order to remove the high frequency variations the time series of the PCA modes are presented as five months running means.

6.3.2 Data and method

The data consists of monthly values of meteorological parameters from ECMWF. A full description of the data can be found in chapter 3 of this thesis. A total of 168 monthly fields are included in this analysis with no missing values. For PCA the matrix size was reduced to 595 by considering a resolution of 5° longitude. PCA was applied to normalized data (temperature, geopotential etc.) with the seasonal cycle removed.

The Genstat package was used to compute the eigenvalues and the associated principal component score. The eigen values and eigenvectors were computed from the correlation matrix (595 x 595). Generally the first PC is the dominant

mode of the variance of the sample of data fields. Only three PC patterns will be retained to avoid many diagrams although the Scree test of significance allows more than three.

6.3.3 Vertical structure of the geopotential height anomalies

The objective of this section is to determine which areas have barotropic or baroclinic behavior. It is important to understand the vertical nature of pressure anomalies. In order to determine the spatial variations of monthly geopotential height anomalies in the vertical, correlation coefficients between 850hPa and 200 hPa geopotential height anomalies were computed. The calculations are based on all months. The autoregressive nature (Greenhut, 1979) was not taken into account when calculating the significance levels due to the large number of the data points. Using 166 (168-2) degrees of freedom, values of r greater than 0.20 are siginficant at 1% level (Underhill, 1981).

In **figure 6.5(a)** are shown the spatial distributions of correlation coefficients between 200hPa and 850hPa consecutive monthly geopotential height anomalies. Highest values (>0.4) occur in the midlatitudes (30°S - 60°S), the West African Gulf and the tropical Atlantic. Generally positive values are observed except for a broad zone in the subtropics (18 - 21°S, 50°E - 100°E). Small values of the coefficients are observed over the equatorial zone.

At the climatic scale the entire region appears barotropic. The strong (>0.6) positive correlations over the middle latitudes (35°S - 60°S) shows the barotropic behavior of inter-annual fluctuations in this region. This test has ambiguities associated with it and one has to be cautious about the results.

6.3.4 Thermal structure of low-frequency variations in the lower troposphere

The use of thickness patterns is an economical representation of the tropospheric temperatures and thermal wind flow patterns. In order to examine the lower tropospheric thermal anomalies the 850 to 500 hPa geopotential thickness was subjected to PCA. The discussion of the PCA patterns will emphasize the relevance to the Southern African circulation.

Figure 6.5(b), (c) and (d) display PC loadings and their associated time scores for PC1, PC2 and PC3 of standardized thickness anomalies.

PC1 (31%)(figure 6.5(b))

PC1 explains 31% of the total variance and is characterized by large negative (cold) loadings, which extend from northeast Brazil, through West Africa and the Indian Ocean. Strong negative coefficients are mainly along the equator (15°N - 15°S). The center of the maximum variability is over West Africa and Northeast Brazil. Positive (warm) loadings are observed along the subtropics (20°S - 40°S).

The time score shows warming in tropical latitudes in 1982/83 and 1986/87 periods which are ENSO events but cooling in 1984 and 1993. This mode is of specific importance for southern African climate and implies a positive anomaly pattern over the equatorial region would destroy northeasterly flow and induce southwesterly flow over southern Africa. The north-south gradient is more pronounced than the east-west gradient.

PC2 (8%) (figure 6.5(c))

The pattern has a wave-train structure emanating from South America. Thermal anomalies over southern Africa are weakly anti- phase with the southwest Atlantic Ocean (40°- 60°S, 60°W 20W°). The time series has an upward trend with the highest magnitude in 1988 and lowest in 1982.

PC3 (6%) (figure 6.5(d))

This pattern has highest negative loadings (cooling) over the subtropical latitudes (15°S - 20°S) of the south Atlantic Ocean and in the north Atlantic around 16°N. Warm anomalies are found over Brazil and the southern midlatitudes (20°W to 100°E, 40°S - 50°S). This pattern induces a shearing deformation pattern over southern Africa due to thermal wind circulation. The time series indicate a declining trend. Shearing deformation (Preston-Whyte and Tyson 1988) is one of the basic flow configurations, which can lead to frontogenesis.

6.3.5 Structure and propagation of low-frequency variations in a mid-tropospheric circulation

The 500hPa-geopotential height is a good representative of the physical processes that are important in weather and climate systems. It indicates the mass of the atmosphere and gives knowledge on the circulation. It should be noted that geopotential heights are the result of differential heating due to land - sea locations and seasonal variation in net radiative heating. The 500hPa level is the steering level for many low-level weather disturbances. Tropospheric geopotential heights have become more popular in operational long-range weather forecasting centers in Japan, China and USA (WMO, 1994). Thus the 500hPa geopotential was chosen as a convenient quantity to analyze.

Figure 6.6(a), (b) and (c) show the first four PC modes for 500 hPa standardized monthly anomalies of geopotential height. The first two modes are tropical and centered over the Atlantic and Indian Ocean. The next two modes all have centers over the midlatitudes.

PC1 (32%) (figure 6.6(a))

The leading mode explains 32% of the total variance and shows three centers of action. The largest amplitudes are found over the equatorial Atlantic Ocean. This mode has strong zonal gradient over continental Africa and Brazil. The zonal gradient is negligible over the Atlantic Ocean compared to the meridional gradient. Weak negative anomaly centers are located over the Indian Ocean (80°E - 40°S, and 10°N, 75°E).

Based on geostrophic consideration (30°S - 20°N) excluding the equatorial region (10°S - 10°N), the distribution of height anomalies in PC1 is associated with above normal westerly flow over the latitude band (10°S - 30°S) over the Atlantic Ocean and southerly flow over continental Africa. This mode suggests an anticyclonic circulation anomaly associated with periods of large positive time scores. This mode may modify wave number 1.

This mode covers some of the relatively dry areas of the tropics (Asnani, 1993). These areas include Northeast Brazil, and the Equatorial East Atlantic. This mode may also be associated with the Dynamical valley effects of the equator as described by Asnani (1993). The principal causes of the dryness may be due to cool sea-surface temperature (SST) and horizontal velocity divergence. The time scores show a downward trend and have an ENSO character. The center of the mode coincides with the SST PC2 mode.

PC2 (10%) (figure 6.6(b))

This mode is characterized by large values of negative loadings over the tropical Indian Ocean (0°, 80°E) and weakly positive loadings over the Atlantic Ocean in the region west of Greenwich. This loading can induce above normal northwesterly flow over continental Africa. The pressure anomalies can be linked to SST. It has both zonal and meridional gradient, the former is more pronounced over continental Africa. Kelvin waves may play an important part in generating this anomaly field. There is an increasing trend implying the deepening of low-pressure systems. This is in agreement with SST PC1 mode.

PC3 (8%) (figure 6.6(c))

This mode has three centers of action and all are located in the midlatitudes. The largest negative values are located in areas where subtropical anticyclones are positioned. The tilt of the anomalous trough and ridge axes is northwest-southeast. This is similar to unstable Rossby waves whose constant phase lines tilt eastward with latitude (Xie and Wang 1996). The structure of these waves is conducive for transferring potential energy from mean flow to eddies. This mode has some influence on both tropical and midlatitude barotropic and baroclinic waves. An upward trend is observed in the time series.

In order to investigate propagating features in the 500-hPa geopotential height anomalies, the extended empirical orthogonal function technique is applied. This technique reveals moving patterns in the data and has been described in chapter 2. The Genstat statistical package was used to calculate the EEOF

modes. The first four EEOF modes are discussed. The analysis is based on the 1980-1993 period.

Figure 6.7(a) and **(b)** show the EEOF1 at zero lag and at lag 2 months. The mode explains about 25% of the total variance and its largest values move from the tropical Indian Ocean to the South-west Atlantic. **Figure 6.7(c)** and **(d)** represent EEOF2 at 0 lag and 2 months lag respectively. The second mode EEOF2 explains 8.7% and describes a dipole pattern between the Atlantic and the Indian Ocean at zero lag. The largest magnitudes are over the equatorial region. This pattern is similar to PC1 and PC2 500 hPa gpm. After two months the positive values have shifted southwards from the equatorial region to the south Atlantic Ocean. The negative values over the Indian Ocean have extended westwards and cover most parts of the African continent. This pattern can be linked to high SST over the tropical Indian Ocean and low SST over the sub-tropical Atlantic Ocean. The interesting feature is the propagation of the negative anomalies that amplify and spread both eastwards and westwards. The speed of westward movement is approximately 1° longitude per day. The southward shift of positive anomalies is 0.82° per day.

Figure 6.7(e) and **(f)** represent EEOF3 at 0 lag and 2 months lag respectively. The third EEOF3 is mainly an Atlantic mode with the highest loading over the equator at zero lag. It is similar to PC1 of 500 hPa geopotential heights and mean sea level. At lag 2 months the negative anomalies amplify and extend eastwards at a speed of 0.66° per day along 0- 20°S.

Figure 6.7(g) and **(h)** represent EEOF4 at 0 lag and 2 months lag respectively. The fourth EEOF4 has a wave train pattern along 40°S and the trough and ridge axes tilt backwards (north-west to south-east), giving the possibility of conversion of mean available potential energy into eddy potential energy (Xie and Wang, 1996). The zonal gradient is more pronounced. At lag 2 months the EEOF pattern has a meridional gradient which is quite evident in the midlatitudes. There are positive loadings along 30°S with highest values over the southwestern Atlantic Ocean. Southward movement of negative values are

noted over the Atlantic while eastward movements of negative values are observed over the Indian Ocean. Positive values over the Southwest Indian Ocean shift northeastwards.

6.3.6 Structure of low-frequency variations in the water vapor flux

Water vapor flux is an important thermodynamic parameter and the convergence of it leads to precipitation. The availability of moisture is important in CISK and the destabilization of both Kelvin and Rossby waves (Wang and Rui, 1990). Thus knowing the sources and sinks of moisture is essential. Departures were not standardized in order to gain some insight of the actual values. Since moisture is the important parameter in both midlatitudes and tropics, vector wind PCA is applied. Figure 6.8(a), (b), and (c) display the spatial loadings and the time coefficients of PC1, PC2 and PC3 respectively.

PC1 (10.2%) (figure 6.8(a))

This is an equatorial Atlantic mode with easterly anomalies over the Gulf of Guinea and Northeast Brazil. The strong easterlies may be linked to a mid-level easterly jet, which is found in northern summer. An inflow is identified over Southern Africa and it is located over Angola. The convergence zone is seen along 10°S over the Central Indian Ocean. There is a decline in the time series, which has a possible decadal oscillation.

PC2 (6.4%) (figure 6.8(b))

This is a midlatitude mode with deformation zones over the south Indian and Atlantic Oceans. Strong westerlies occur near Cape Town. The time scores shows below normal values between 1982 and 1987. An upward trend is evident from 1988 to 1994. There is weak vortex over Angola and this may contribute to southern Africa rainfall. The structure of the mode indicates a good interaction between the tropics and midlatitudes systems.

PC3 (5.6%) (figure 6.8(c))

This mode is dominated by vortex over the south Atlantic Ocean and Indian ocean. A weak outward flow is over southern Africa. Relatively strong easterlies are over the Democratic Republic of Congo and Gabon. Four major

positive peaks are observed in the time series i.e. 1981, 1986, and 1992. Inflow circulations are possible in 1981, 1984, 1987 and 1990.

6.3.7 Structure of low-frequency variations in 200hPA winds

For the past few years research has increased on low-frequency variability of zonal mean circulation of Southern Hemisphere. Spatial and temporal characteristics of zonal-mean circulation variability has been documented by Shiotani (1990) and Rashid (1997). Most studies have been confined to the surface and 500hPa level. In this section some aspects of low-frequency variability of the 200hPa monthly zonal wind departures are described. In figure 6.9 (a), (b), and (c) are shown the distributions of PC modes for 200hPA zonal wind departures.

PC1 (18%) (figure 6.9(a))

The first PC mode is characterized by large negative loadings within the tropical band (20°N - 15°S). Largest negative values are found over West Africa (10°W, 10°N), the central Indian Ocean (75°E, 20°S) and east Brazil (50°W, 25°S). Positive (westerly) loadings are confined south of extra-tropical regions (40°S to 60°S, 70°W to 20°W, 18°S - 25°S, west of 20°E, and 20°S - 40°S east of 50°E). This mode is a tropical mode with little variation in the zonal direction. The orientation of the pattern south of the equator is slightly north-west to south-east. The time scores have an ENSO character. Upper level westerly wind anomalies are observed during the ENSO episodes and easterlies in anti-ENSO events. Increased tropical easterlies suggest convective outflows over southern Africa (Levey and Jury, 1996).

PC2 (9%) (figure 6.9(b))

This mode has elongated zonal anomalies along the southern middle latitudes (30°S -45°S) with largest values over the South Atlantic (20°W, 40°S) and south Indian Ocean (80°E, 40°S). The time shows large values in 1983 and 1987.

PC3 (8%) (figure 6.9(c))

The rich structure of this mode is confined to western South Atlantic Ocean with alternating centers of a meridional nature. The pattern has a wave train emanating from the south Atlantic Ocean into the West African Gulf. This mode has a stationary time series with periodic events.

Meridional wind components play an important role in generating Rossby waves in the atmosphere and hence some knowledge on meridional wind anomalies is essential to understand regional circulations. In order to determine the spatial structure of the principal modes of variability PCA was applied to the meridional wind component. The characatristics of Rossby wave-trains have been noted by Hoskins and Pearce (1983).

The following PC modes are dominated by midlatitude Rossby waves. Figure 6.10(a), (b) and (c) display PC loadings and their associated time scores for PC1, PC2 and PC3 of meridional wind departures.

PC1 (12%) (figure 6.10(a))

This mode is characterized by six alternating centers of action which describe a wave train over the tropical Atlantic and midlatitudes to the east. The phase tilts are north-east to south-west, west of 20°E, and north-south further east. This pattern suggests the external Rossby wavetrains that are stationary. The stationarity may be due to the horizontal scale. The wave train emanates from the equatorial Atlantic and has turning latitude around latitude 40°S. By comparing standard deviation maps with the PCA1 mode, it can be seen that the centers of action south-west of Africa corresponds to a region of maximum variability in 200 hPa meridional winds. It should also be noted that the westerly jet is found near the axis of this wave train during the peak summer season. The tilts of axes of the troughs and ridges is westward with increasing latitude over the Atlantic Ocean but eastward over the Indian Ocean. This implies that potential energy is being transferred from mean flow to eddies over the Indian Ocean and the reverse over the Atlantic Ocean. The time series shows decreasing trend from 1980 to 1990.

PC2 (11%) (figure 6.10(b))

This mode has four centers of action and the loadings tilt north-west to south-east. Maximum amplitudes are observed off the coast of South America (45°S, 65°W). The loadings remain within the 45 - 35°S latitude band. Rossby waves can grow in this mode since the mean potential energy can be transferred to the waves. There is a downward trend in the time series.

PC3 (6.3%) (figure 6.10(c))

This is characterized by six centers of action. The mode is similar to PC1 with the major active centers shifted eastwards over the south Indian Ocean. Turning latitude is found at 40°S. This mode may not support growing Rossby waves because of the tilt. Large positive amplitudes are observed in 1982 and 1989 with low amplitudes in 1984, 1986 and 1992.

6.3.8 Structure of low-frequency variations in convection

Rainfall is an important determinant of climate and any meteorological element, which indirectly measures it, is of useful value. The OLR is used as proxy for rainfall over Africa and the adjacent oceans. Temporal and spatial variations of convection over southern Africa and the adjacent oceans are discussed in this section. Figure 6.11(a), (b), (c) and (d) display OLR PC modes and their associated time scores.

PC1 (11%) (figure 6.11(a))

The most dominant feature of PC1 is the large negative values over the continental deserts of southern Africa and the Sahara. Positive loadings are found over the Central Indian Ocean. An area of negative loadings is seen leeward of the Andes. A downward trend is observed from 1980 to 1986, thereafter an upward from 1986 to 1993. This implies increasing rainfall over southern Africa from 1986 to 1993 due to this pattern.

PC2 (6%) (figure 6.11(b))

PC2 reflects the monsoon trough over the western Indian Ocean. This band may be identified with active convection over the Indian Ocean and the main axis of the monsoon circulation. There is also a narrow band along 40°S, which

joins the major band over the south Indian Ocean. This pattern is similar to mode 2 found in the 500 hPa geopotential height PCA analysis. The time scores have an oscillation near four years.

PC3 (4%) (figure 6.11(c))

This mode features the tropical Atlantic Ocean where a large negative loading appears. Positive loadings are found over Central Africa and the south Atlantic midlatitudes. This pattern is consistent with PC1 of 500 hPa geopotential height anomalies. The amplitude of the time score is low in 1982-1983, 1986-1987, and 1991-1992 periods, which coincide with ENSO events.

PC4 (3.9%) (figure 6.11(d))

PC4 shows the Atlantic under positive loading with Southern Africa and central South America under negative values along 20°S latitude. This pattern may be identified with Southern African summer convection and its time scores have an ENSO character. A wave train is present which is consistent with figure 6.1 (c).

6.3.9 Summary and discussion to section 6.3

PCA has been applied to selected atmospheric standardized variables in order to study the inter-annual climatic teleconnection patterns. Tropical and midlatitude centers of action have been revealed. In 500 hPa geopotential heights, and water vapor flux two tropical and two midlatitudes modes have been observed. The tropical modes are more dominant than the midlatitude modes possibly because of standardising. ENSO characteristics have been revealed in some of the time series of the modes. The first PC pattern of thickness identifies a tropical mode. During ENSO events the thermal structure of the tropical band (10°S - 10°N) is found to be warmer in the upper troposphere implying above normal rainfall in those tropical areas. It should be noted that the two tropical modes in 500-hPa gpm are similar to the first two modes of SST found in chapter 4. Three zonal water vapor flux modes are found in the tropics implying the origin of water vapor to be mainly from the tropical oceans. Upper-tropospheric westerly wind anomalies are identified

with warm ENSO events. The OLR PC modes are dominated by tropical modes, the first being continental, the second the central Indian and the third over the Atlantic. The fourth OLR mode is linked to southern Africa and has ENSO characteristics in its time scores.

An important key area over equatorial Atlantic has been identified as being associated with large values of loadings (PC1, 850-500hPa thickness heights, 500hPa geopotential height, and water vapor flux) and this region may be useful to develop an index for seasonal forecasting. The pressure anomalies are barotropic in nature. The second region is the equatorial Indian Ocean (PC2 OLR and 500 hPa geopotential heights PC2) can also be utilized in preparing seasonal rainfall forecasts. Large variations of pressure in these key regions may have an impact on rainfall over southern Africa through Walker and Hadley circulations.

EEOF has been applied to 500hPa geopotential height anomalies and five modes explaining 46% of the total variance are extracted. The first mode (25%) is the Indian mode and is associated with a southwestward movement of pressure anomalies from the central Indian ocean to the southwest Atlantic ocean. The second mode (7.7%) which has highest loadings over the central Indian Ocean shows westward propagation of pressure anomalies to Africa. The third mode is the Atlantic and has some eastward propagation to Africa. The fourth mode is more difficult to interpret.

The prediction of SST and circulation anomalies over key areas is required in order to improve seasonal forecasts. National meteorological services should be encouraged to include these areas in their forecasting models.

6.4 Association between SOI and regional teleconnection features.

6.4.1 Introduction

The purpose of this section is to investigate relationships between ENSO and regional circulation anomalies. The ENSO phenomenon has great influence on inter-annual variations of meteorological parameters in tropical regions. Links between rainfall and SOI, which measures the ENSO phenomena, have been

found in East and Southern Africa (Ogallo, 1988; Matarira and Unganai, 1995). Local forecasting centers are now using the SOI index to predict seasonal rainfall (Harare, Nairobi). It has been documented that during warm events rainfall tends to be 15% more over East Africa and 15% less in southern Africa i.e. south of 15°S and east of 30°E. (Janowiak, 1988). Southern African rainfall has also been linked to central tropical Indian Ocean SST changes (Jury et al, 1996; Tennant, 1996) which are correlated with ENSO. During ENSO warm events it has been found that there is a dipole between southern Africa and Madagascar-Mauritius, and rainfall tends to increase over the ocean and decrease over the interior of the southern African subcontinent. Cloud bands (Harrison, 1984) which are manifestations of the interaction between the tropical disturbances and midlatitude system shift eastwards and their locus is observed to be over Madagascar. Regional tropical Atlantic and Indian Ocean SST have been related to rainfall (Mason, 1992; Rocha, 1992). Warming of Atlantic and Indian Oceans occur during warm ENSO events and this may result in modifying the local Hadley circulation. Changes in large scale Walker circulations modulates easterly flow which is conducive to rainfall over southern Africa. Changes in Walker circulations are related to changes in SST anomalies over the Pacific Ocean (Harrison, 1983). It has been observed that during ENSO warm events 200 hPa tropospheric westerly winds increase over southern Africa (Preston-Whyte and Tyson,1988; Rocha, 1992) and this reduces moisture advection from the Indian ocean. It has been observed that during warm ENSO events a high pressure develops over Botswana (Makarau, 1995) and inhibits convective activities thus resulting in reduced rainfall. Tropical transmissions have not been documented and the origin of the Botswana 500hPa high pressure is not clear whether it is the descending part of the Indian Walker cell or part of the South Atlantic Standing wave.

Knowledge on propagation of ENSO signals to southern Africa may throw some light on different kinds of droughts that occur. Some droughts due to ENSO are different in extent and intensity. In order to investigate ENSO effect

on southern Africa, correlation analysis is applied to SOI, 500hPa standardized geopotential height and Outgoing Long Wave Radiation seasonal anomalies. Time scores of selected PC patterns of the first two of 500gpm height and the fourth pattern of Outgoing Long Wave Radiation are correlated to SOI in order to investigate the relationship to equatorial Atlantic key region.

6.4.2 Relationship between mid-troposphere circulation anomalies and SOI

In order to establish the precursor patterns in OLR and 500 hPa geopotential fields, lagged correlations are required. These patterns are useful for prediction purposes. Lagged correlation coefficients between 3 month seasonal (MAM, JJA, SON and DJF) SOI and DJF regional OLR and 500hPa geopotential height were constructed. Standardized seasonal values were used. Figures 6.12 and 6.13(a), (b), (c) and (d) are the fields of correlation coefficients. Correlations greater than 0.36 are significant at 10%, correlations greater than 0.45 are significant at 5% level and above 0.61 are significant at 1% level (N-2 i.e. 12 was used as the degree of freedom ignoring the autoregresive nature).

Figure 6.12(a) displays spatial correlation patterns between MAM SOI (6 months before) and DJF 500hPa geopotential height anomalies. Highest values are found in the midlatitudes i.e. south of 40°S maximum (r = 0.4) being confined to the South Indian Ocean (40°E -100°E, 40°S - 60°S). Negative values (r = -0.4) are observed over southeast South Africa and the Indian Ocean (60°E, 30°S). This illustrates that 6 months before DJF, pressure is above normal over the midlatitudes and below normal over southern Africa during anti-ENSO years. The reverse is true for warm ENSO years, so atmospheric "memory" is present and may offer some predictability.

Figure 6.12(b) exhibits the correlation field between JJA SOI (4 months before) and DJF 500hPa geopotential hieghts. High negative values (> - 0.4) are found over most parts of the continent. Largest values (> - 0.6) are over southern Africa, Somali and eastern parts of the Indian Ocean.

Figure 6.12(c) shows the correlation field of SON SOI and DJF 500hPa geopotential heights. Strong links (r = -0.6) are observed over most parts of

Africa, with maximum negative values over the Southeast Atlantic Ocean. Highest positive values (>0.8) are in the midlatitudes.

Figure 6.12(d) is the field of correlation coefficients at zero lag. A similar pattern as in the previous figure 6.12(c) is noted. Westwards moving positive values are evident over the southeast Indian Ocean. The highest negative correlation (r = -0.6) covers most parts of Africa.

6.4.3 Relationship between convection anomalies and SOI

In order to investigate the link between SOI and convection anomalies (OLR), lag correlation coefficients were computed.

Figure 6.13(a) displays the correlation patterns of MAM SOI and DJF OLR. Highest coefficients (> 0.4) are over northeast Brazil, Central Latin America and over the southeast Atlantic Ocean. Negative values greater than -0.4 East of Madagascar. There is out-phase relationship between the Mozambique Channel, East Africa, Central Indian Ocean and west of 25°E over Angola and the adjacent southern African countries.

Figure 6.13(b) displays the correlation patterns of JJA SOI and DJF OLR. Largest negative values (-0.4) are confined to the West African Gulf and Equatorial Atlantic Ocean adjacent to Brazil and South of the Mozambique Channel.

Figure 6.13(c) displays the correlation patterns of SON SOI and DJF OLR. Positive correlation coefficients are mainly in the midlatitudes and Western parts of the Indian Ocean, Atlantic and eastern parts of South America. Negative values cover the Equatorial Atlantic, Gulf of Guinea, southern Africa and south of Madagascar in the Indian Ocean.

Figure 6.13(d) displays the 0 lag correlation patterns of DJF SOI and DJF OLR. High values of negative correlations are found over the Equatorial Atlantic Ocean, the Gulf of Guinea and southern Africa. Most parts of the Atlantic Ocean, midlatitudes, East Africa, Central and Eastern Indian Ocean have positive correlation coefficients. There is a dipole between the central

Indian Ocean (80°E, 25°S) and southern Africa including the Mozambique Channel.

Eastward movement of negative OLR anomalies is observed over the equatorial Atlantic (key area) between MAM and JJA. Both westward movement of negative OLR over Madagascar and southern Africa and eastward propagation over the southwest Indian Ocean occur. It appears the OLR signal can originate from equatorial Atlantic and SW Indian Ocean producing a NW-SE axis in consistent with a the edge of the S. Atlantic wave (figure 4.4(b)).

6.4.4 Association between tropical mid-tropospheric features and SOI

The 500hPa circulation has been found to exert control on annual rainfall (Tyson 1984) and thus it is important to see how the 500hPa circulation anomalies are related to ENSO. The first and second PC patterns of 500hPa geopotential height anomalies found in the previous chapter are correlated to SOI. In order to take into account the autoregresive nature of the data, an effective number of degree of freedom was computed according to Greenhut (1979). The effective degrees of freedom is given as: $N_{eff} = N\Delta t/\tau$ where Δt is time resolution of data and τ is obtained from the formula of Greenhut (1979).

Figure 6.14(a) shows the cross-correlation function between SOI and GH5 PC1 (32%). Significant correlations are observed at 13 months (r = 0.32) when SOI leads PC1 patter and 3 months (r = - 0.538) when SOI lags the PC1 pattern. For GH5 PC1 and SOI, τ was calculated as 10.17 and thus reducing the degrees of freedom to 16. Values of r greater than 0.317 are significant at 10%.

This may suggest that the SO is a forcing mechanism. According to Greenhut (1978), there is a relationship between a given frequency of oscillation and lead and lag times when the lag correlation is negative and the lead correlation is positive. The frequency of oscillation is found to be twice the sum of the lag and lead times. In this case the period of oscillation is 32 months (2* (13+3)).

The lag and lead relationship between 500hPa PC2 (10%) and SOI is given in **figure 6.14(b)**. SOI leads PC2 by 9 months (r = 0.2655 significant at 20% with

τ= 7.7, the new degrees of freedom = 20). Significant correlation at 6 months when PC2 pattern leads SOI (r = -0.336, values of r greater than 0.2842 are significant at 10% level). The oscillation period is deduced as 30 months. Spectral analysis of SOI indicates significant periods at 3.5 years and 2.0 years (see **figure 6.15 (b)**). Lead and lag correlations may suggest some feedback mechanism between SOI and 500hPa PC2 pattern.

The fourth PC of OLR which has high loadings over the south Atlantic Ocean and southern Africa was correlated to SOI and is found to lead SOI by 2 months (see **figure 6.14(c)** r = 0.68, τ=1.22, N = 138, values of r greater than 0.19 at 1% level).

This shows that 500hPa PC1, PC2 and OLR PC4 are all related to ENSO.

6.5 Summary and discussion

One of the purposes of the chapter was to document and identify regional SST, atmospheric and convective anomalies associated with drought/flood summers over southern Africa and adjacent regions. The following features have been observed for the period 1980 to 1990 in connection with combined PCA:

(1) The first anomaly pattern (20%) is associated with internal dynamics (refer to figure 6.1). A low level vortex over the subcontinent (20°S, 25°E) drives the circulation with subtropical warming (20°S- 30°S), anomalous anticyclonic circulations over the Atlantic (20°S, 0°E) and Indian (30°S, 60°E) Oceans. Above normal convective anomalies over southern Africa are opposed over Mauritius (20°S, 60°E) and the western Atlantic (10°S, 30°W). Upper level anomalous easterly winds occur over southern Africa.

(2) The second (anomaly pattern (16%) may be associated with SST-forcing the over southern Indian Ocean (refer to figure 6.2). The warm waters (30°S-40°S, 70°E-85°E) were associated with cyclonic flow, which extended into the Mozambique Channel and southern Africa at low level (850hPa). There is a decreased north-south temperature gradient over the Indian Ocean but an increased north-south temperature gradient over Atlantic. Most parts of southern Africa observe above normal convection.

Strong easterlies occur over most parts of Africa. The time series of this pattern suggests links to ENSO. The anomalous upper level easterlies are part of the Walker circulation, which is the dynamic link between ENSO and weather over southern Africa. Note strong easterly wind anomalies over the Gulf of Guinea.

(3) The third pattern (14%) is SST-forced over the Indian Ocean but internally forced over the Atlantic Ocean (refer to figure 6.3). Anomalous negative SST over the central Indian Ocean are associated with low level divergent flow, which extends into southern Africa, where convection was inhibited. Anomalous convection is found over Madagascar and east Atlantic. Upper level flow is convergent over southern Africa.

(4) The fourth pattern (11%) is SST- forced, positive SST anomalies over the Indian (20°S-10°S, 50°E-90°E) and Atlantic (10°S-30°S, 10°W-15°E) Oceans co-occurred with cyclonic circulation in the lower troposphere (refer to figure 6.4). Above normal widespread convective anomalies occur over the Indian Ocean and adjacent region in Mozambique and Malawi. Southern Africa experiences suppressed convection due to this anomaly feature. Upper level anomalous anticyclone occurs over the western Indian Ocean.

The above features show that various types of summer droughts/floods are due to different mechanisms i.e. some are internally or externally (SST) driven.

Using all the monthly data for the period 1980 to 1993, PCA was applied to standardized 850-500hPa thickness heights, 500hPa geopotential heights, winds and OLR. Vector PCA was applied to departures of water vapor flux in order to identify key regions. An important key area over the equatorial Atlantic (PC1) has been identified by the loadings (PC1, 850-500hPa thickness, 500hPa geopotential height, and water vapor flux). EEOF analysis of 500hPa geopotential height anomalies has revealed the eastward and westward propagation of the Atlantic mode (PC1 in 500hPa gpm) and Indian mode (PC2 in 500hPa gpm) respectively. These regions may be useful to develop indices

for seasonal forecasting. The pressure anomalies are barotropic in nature. The second region is the equatorial Indian Ocean (PC2 OLR) which can also be utilized in preparing seasonal rainfall forecasts. Large variations of pressure in these key regions may have an impact on rainfall over southern Africa through Walker, Hadley circulations and the development of an inland low pressure.

Relationships between regional circulation features, convection and ENSO have been investigated through correlation analysis. Seasonal lag-correlations fields of 500hPa height anomalies and SOI indicate a 'see-saw' between the tropics and midlatitudes. There is a tendency for below normal pressure over tropics and above normal pressure over midlatitudes during anti-ENSO events. In the OLR correlation field, negative values occur over southern Africa and positive values over the central Indian Ocean and western Atlantic Ocean occurred during anti-ENSO events. Convection teleconnections exist between Northeast Brazil, the Equatorial Atlantic Ocean and southern Africa. There is a possibility of a feedback mechanism between ENSO and tropical geopotential height anomalies. Some regional mid-tropospheric circulations have been identified and are linked to ENSO. Anomalous upper level westerlies are associated with warm ENSO events over most parts of the subcontinent. In this chapter important features associated with drought/flood summers have been identified. The role of the inland vortex (first feature of concurrent variations in the lower troposphere i.e. PC1) and the mechanism of the formation of continental troughs are taken up in the next chapter.

a

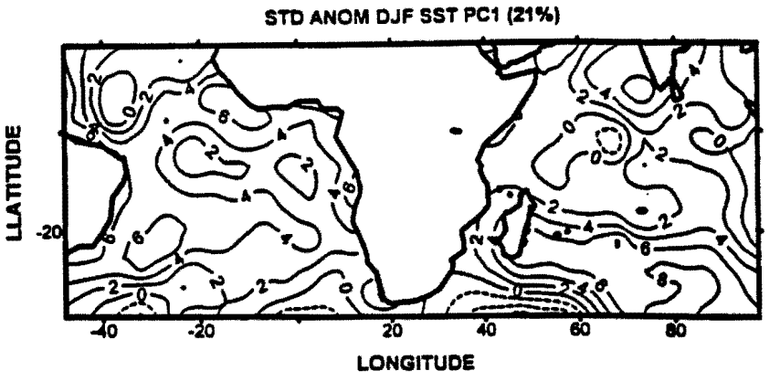

b

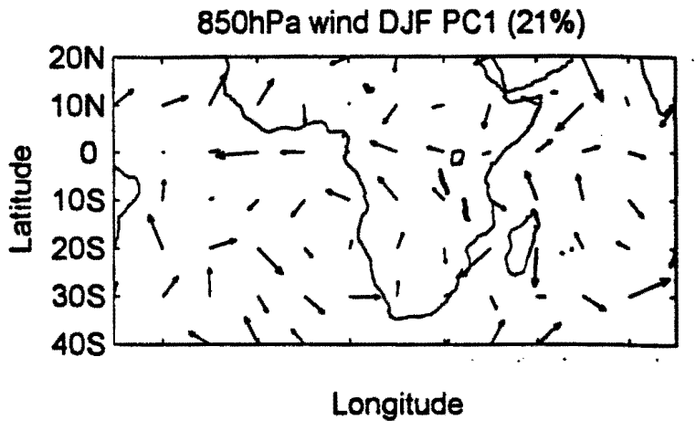

c

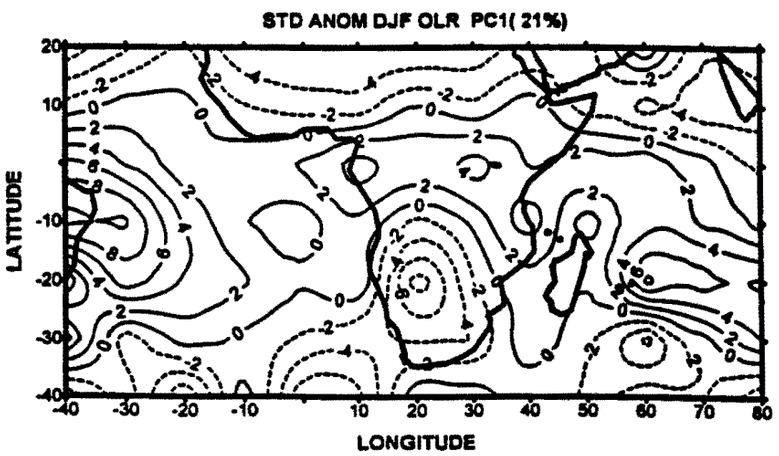

d

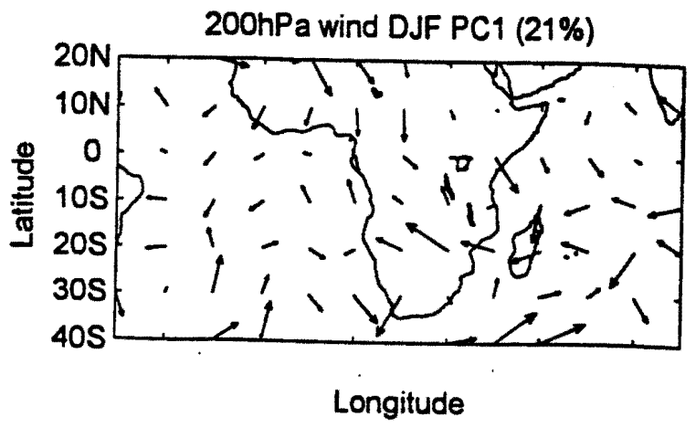

Figure 6.1 (a) Combined PC1 (21%) for SST pattern contour interval is 2. (b) for 850hPa wind pattern (c) OLR pattern contour interval is 2. (d) 200hPa wind pattern.

a

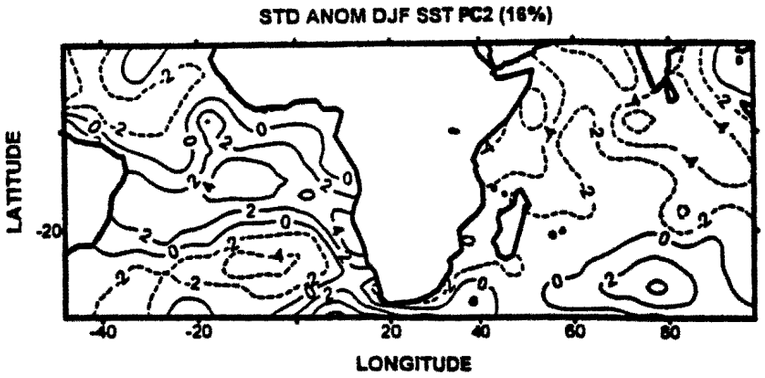

b

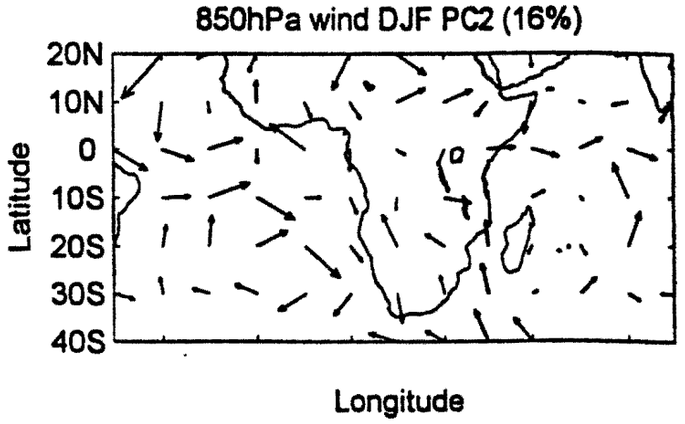

c

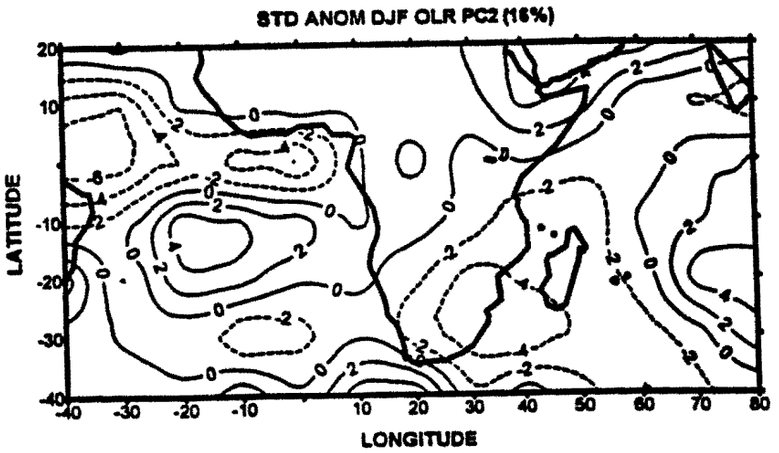

d

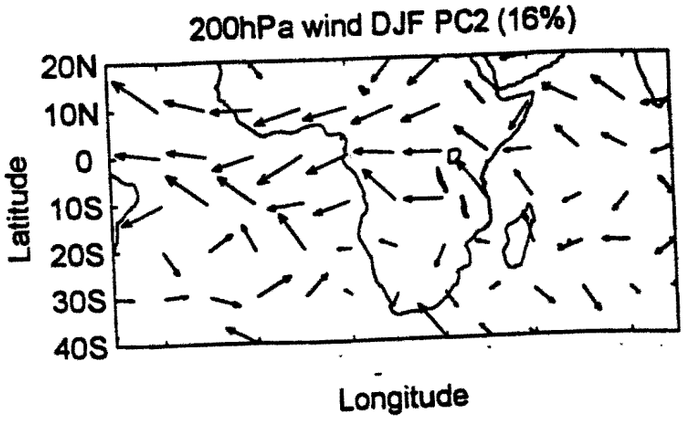

Figure 6.2 (a) Combined PC2 (16%) for SST pattern contour interval is 2. (b) for 850hPa wind pattern (c) OLR pattern contour interval is 2. (d) 200hPa wind pattern.

a

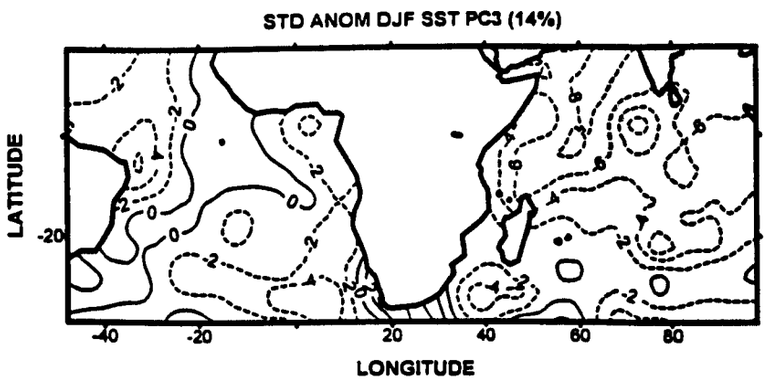

b

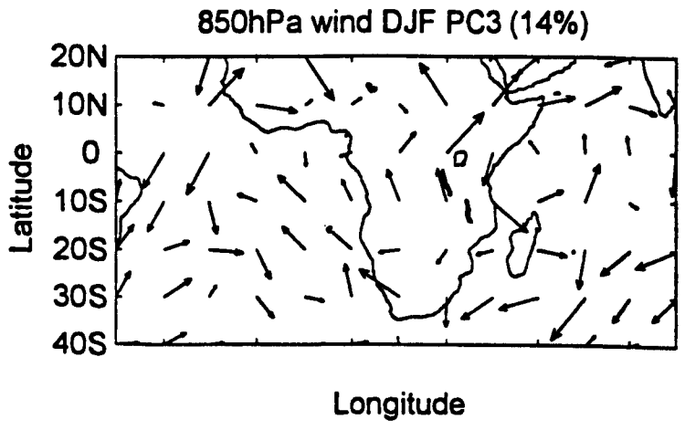

c

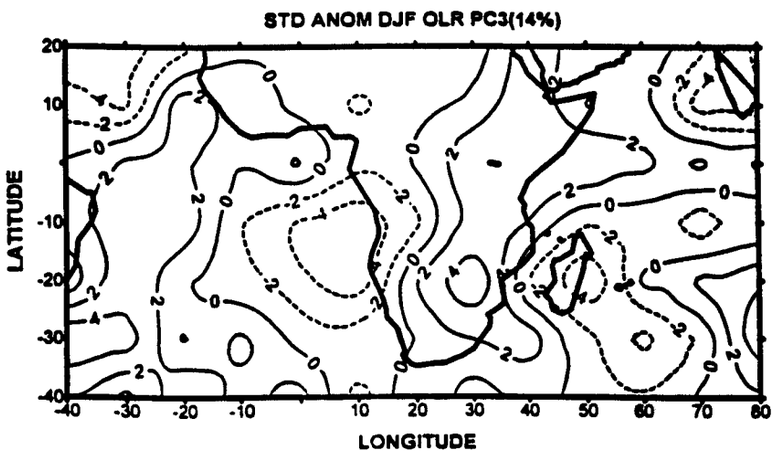

b

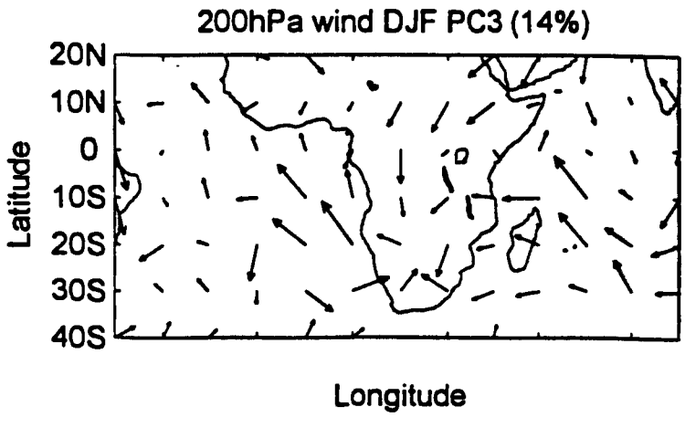

Figure 6.3 (a) Combined PC3 (14%) for SST pattern contour interval is 2. (b) for 850hPa wind pattern (c) OLR pattern contour interval is 2. (d) 200hPa wind pattern.

a

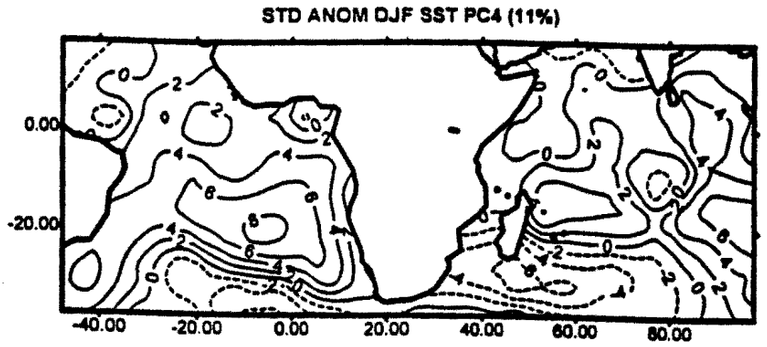

b

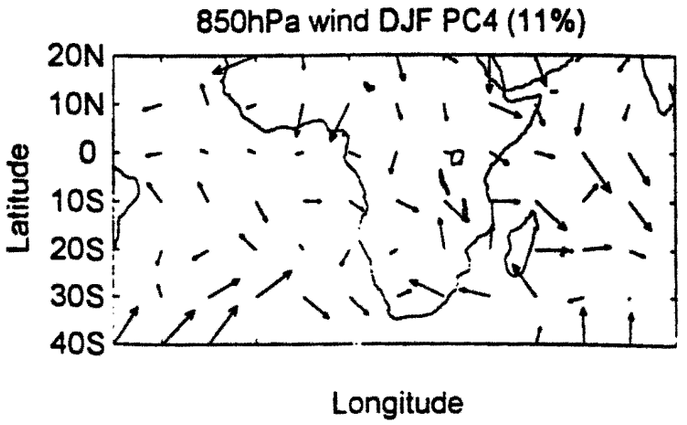

c

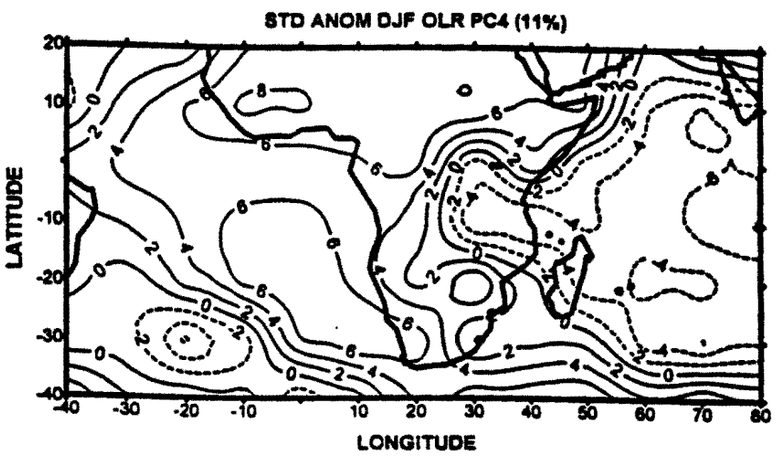

d

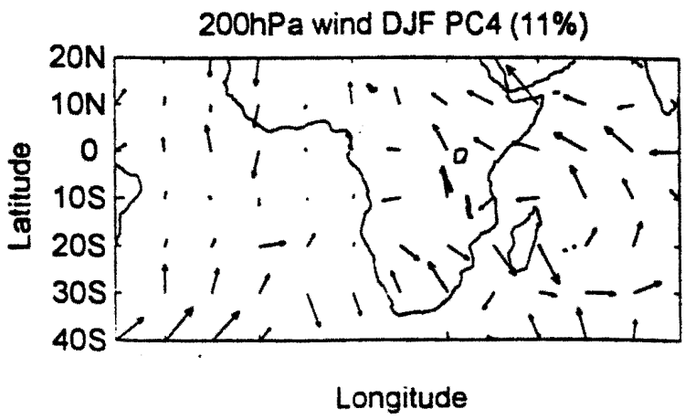

Figure 6.4 (a) Combined PC4 (11%) for SST pattern contour interval is 2. (b) for 850hPa wind pattern (c) OLR pattern contour interval is 2. (d) 200hPa wind pattern.

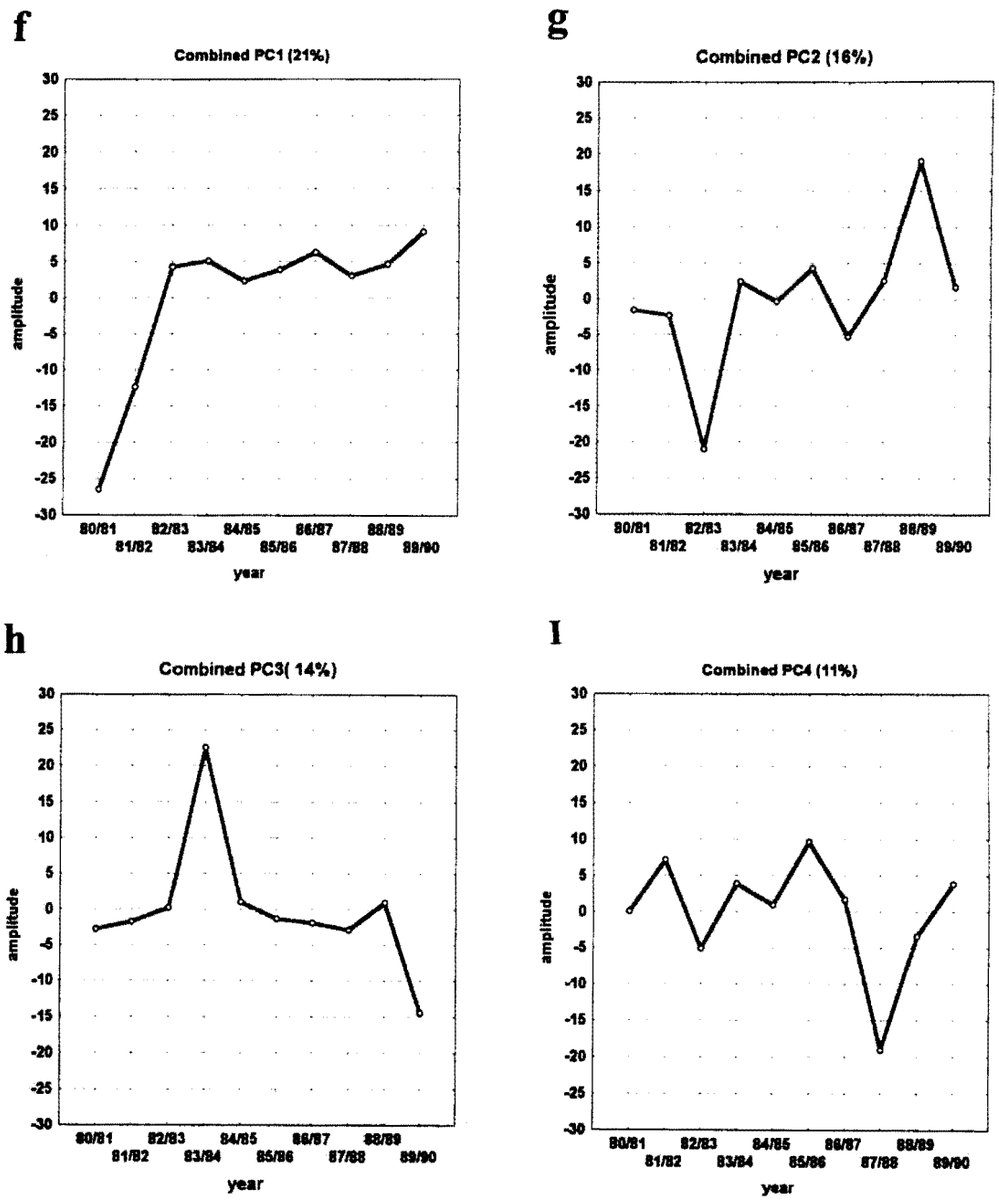

Figure 6.4 (f) Time series of combined PC1 (21%). (g) Time series of combined series of PC2(16%). (h) Time series of combined PC3(14%). (I) Time series of combined series of PC4 (11%)

a

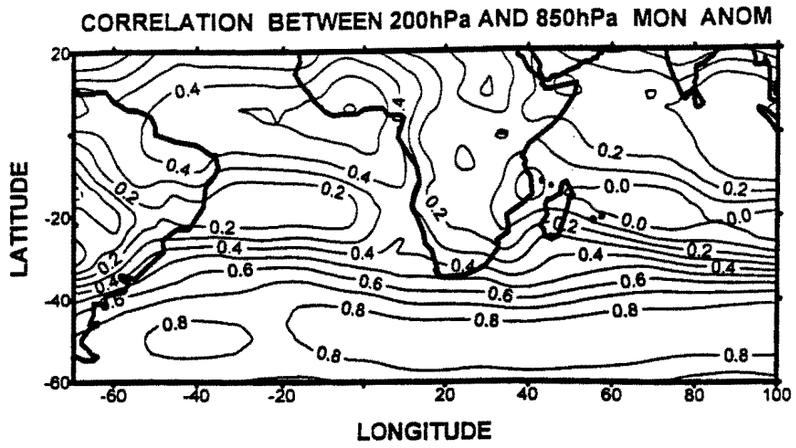

Figure 6.5 (a) Correlation between 200 hPa and 850 hPa monthly geopotential height anomalies.

b

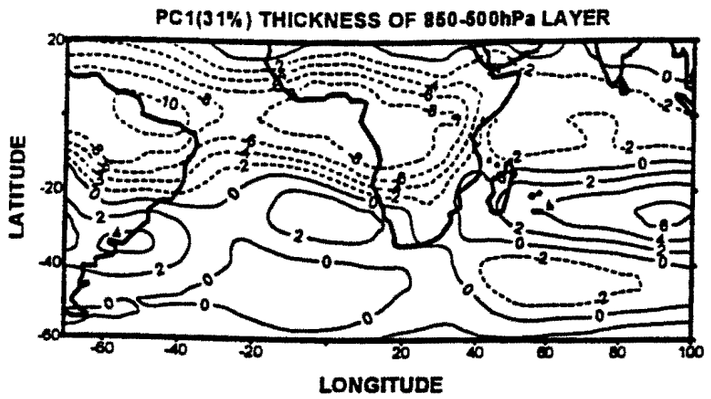

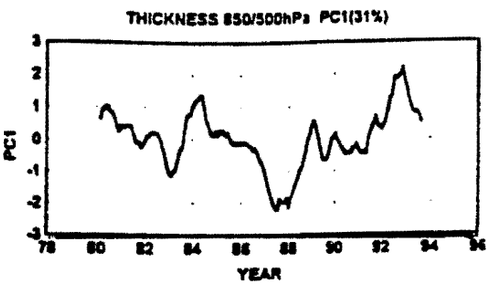

c

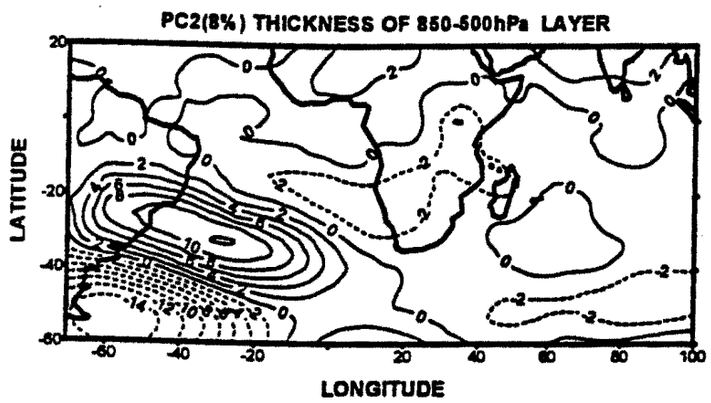

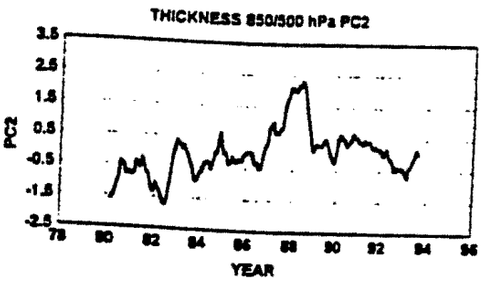

d

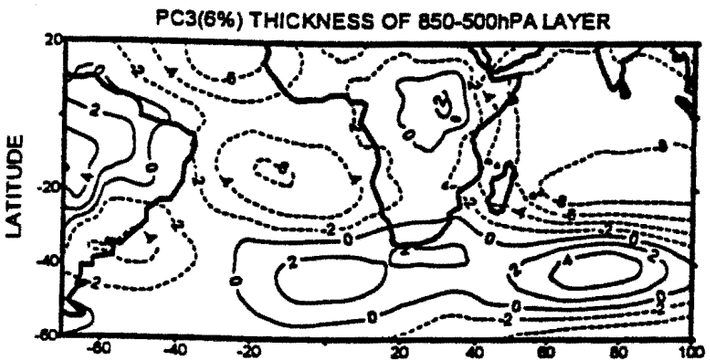

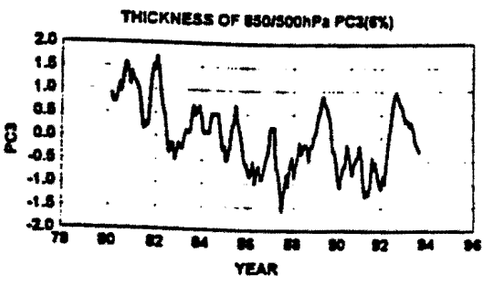

Figure 6.5 (b) PC1 loadings of standardised monthly 850/500 thickness height anomalies and the associated time scores. (c) Same as in (a) but for PC2. (d) Same as in (a) but for PC3. Contour interval 2.

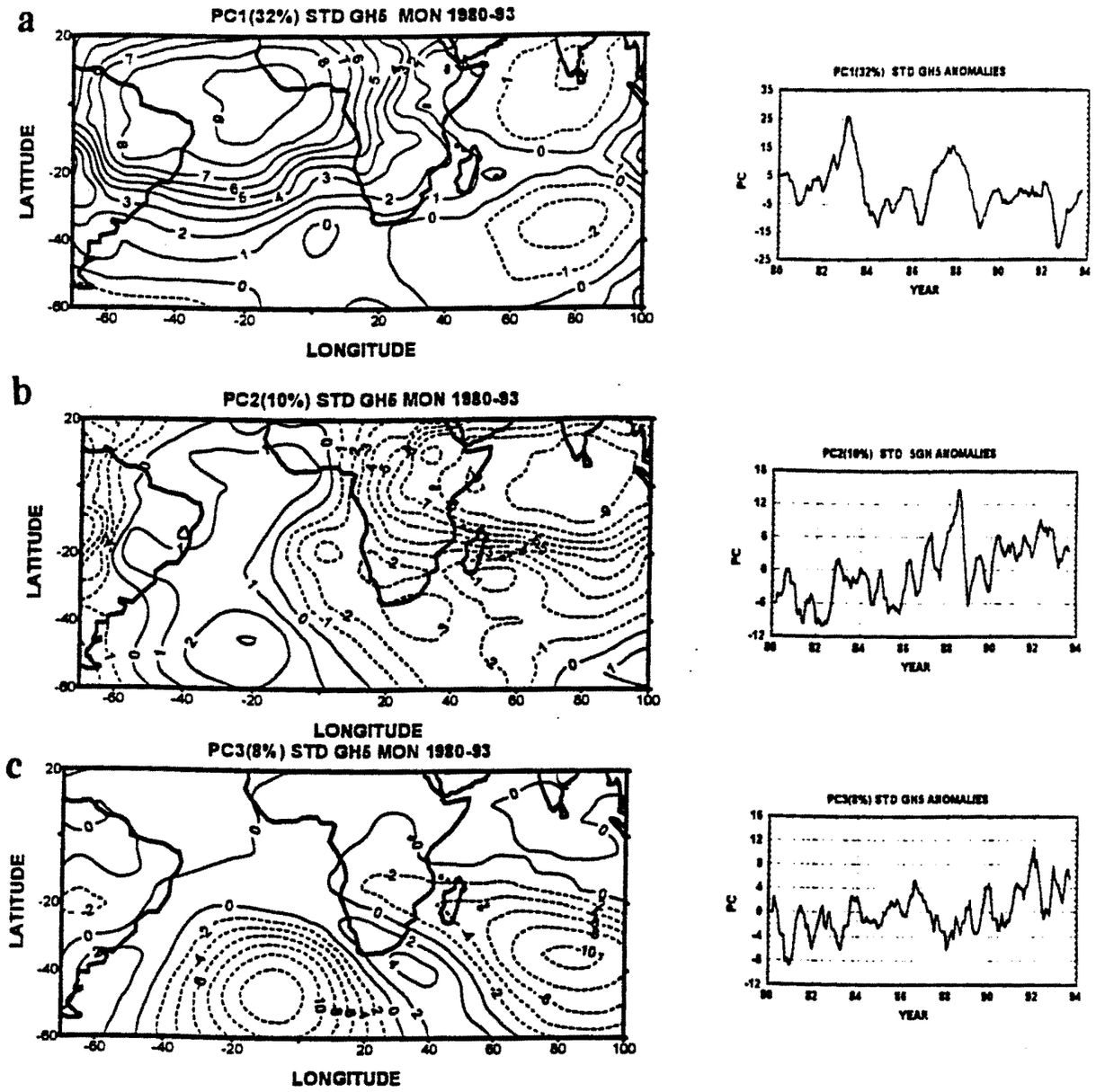

Figure 6.6 Same as in figure 5.5 but for 500 hPa gpm. Contour interval is 1.

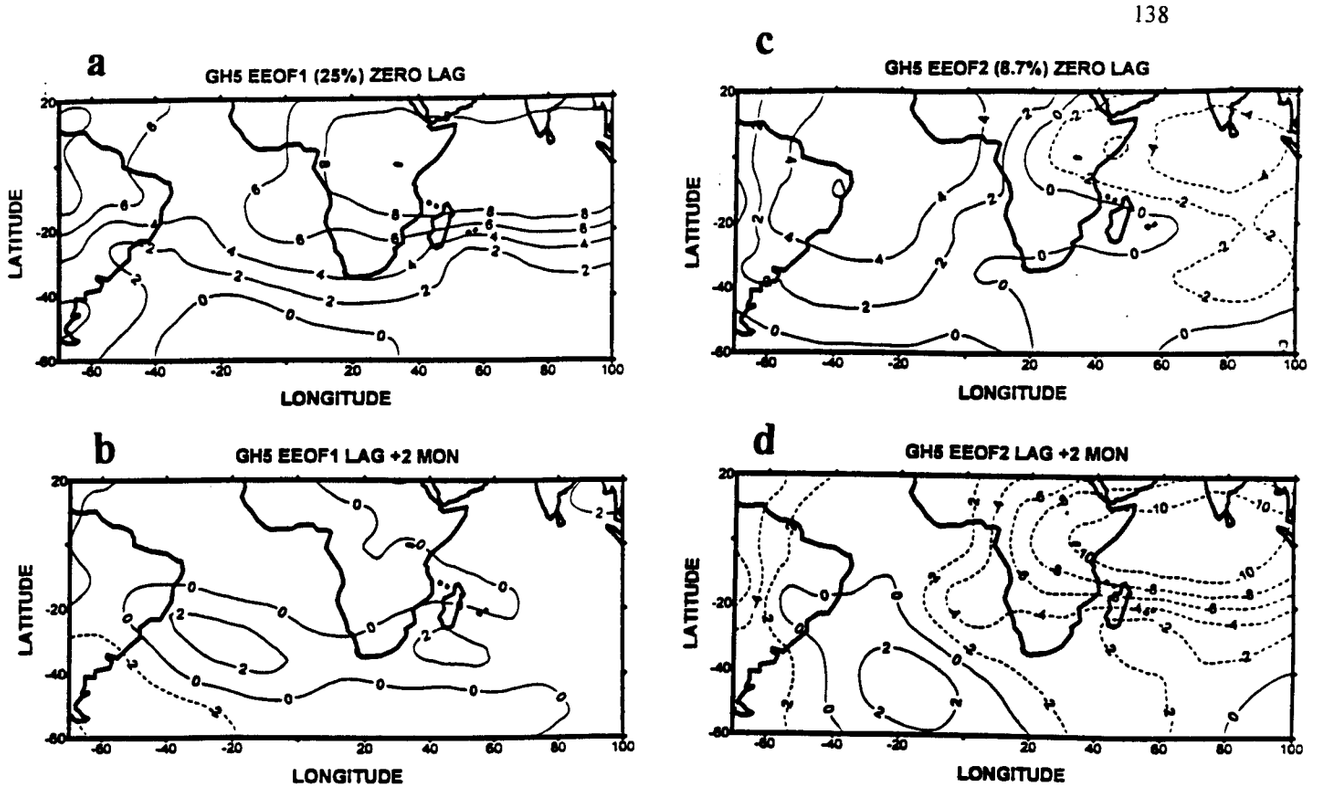

Figure 6.7 (a) Extended empirical orthogonal functions loading of 500 hPa gpm PC1 at lag zero. (b) As in (a) but at lag 2 months. (c) As in (a) but for PC2 at lag zero. (d) As in (c) but at lag 2 months.

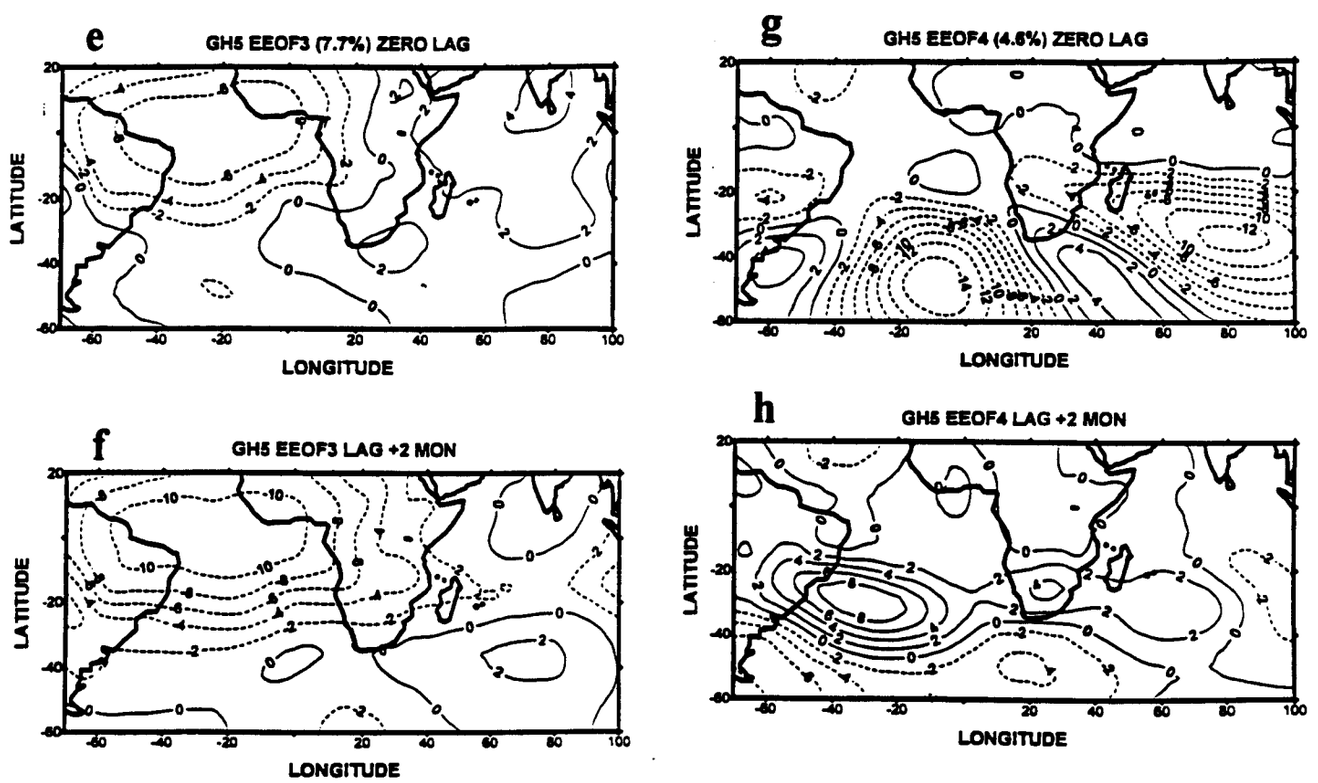

Figure 6.7 (e) As in (a) but for PC3 at lag zero. (f) As in (a) but for PC3 at lag 2 months. (g) As in (a) but for PC4 at lag zero. (h) As in (a) but for PC4 at lag 2 months.

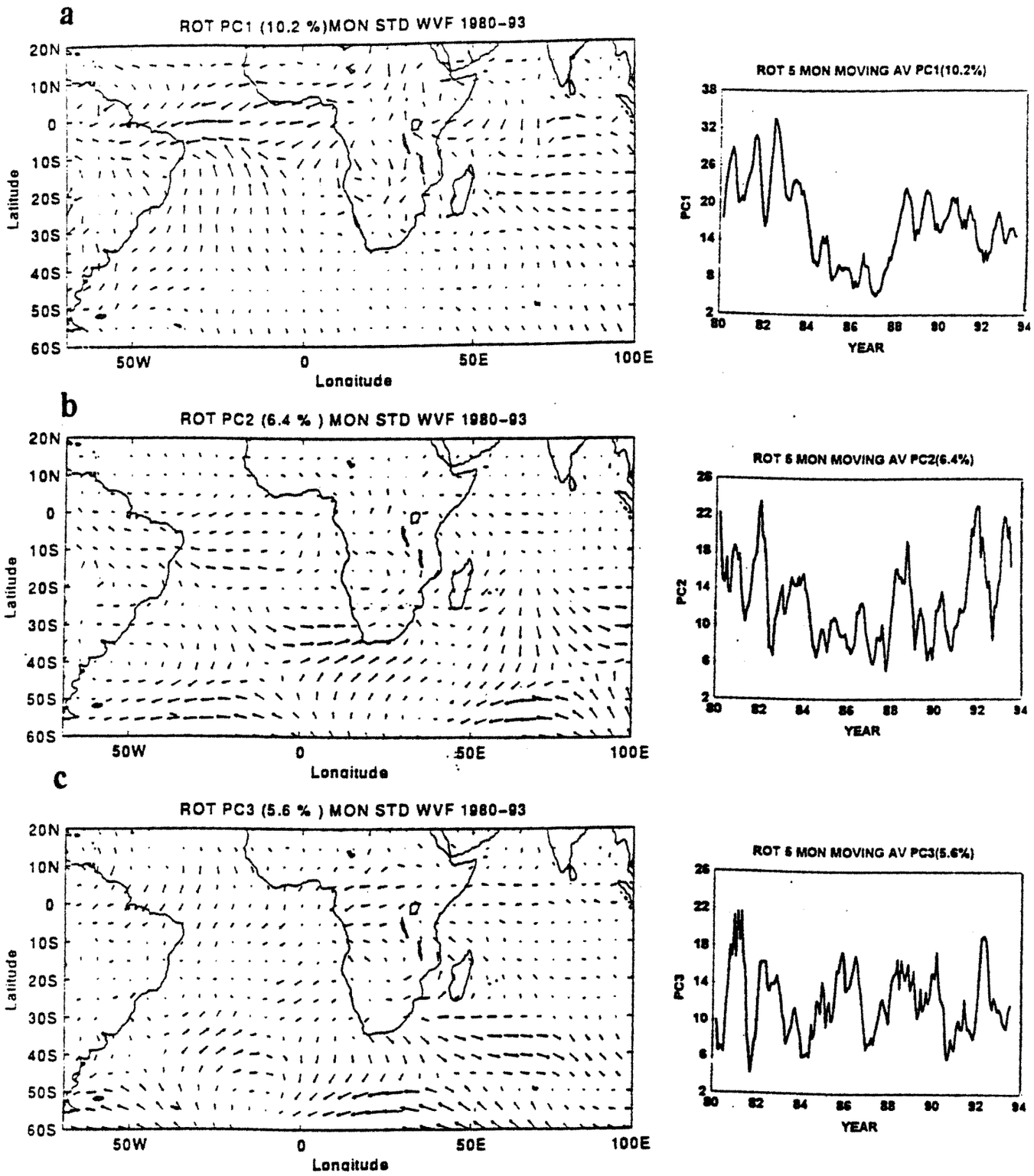

Figure 6.8 (a) Vector loadings for water vapour flux of PC1 and the associated time scores. (b) Same as figure (a) but for PC2. (c) Same as figure (a) but for PC3.

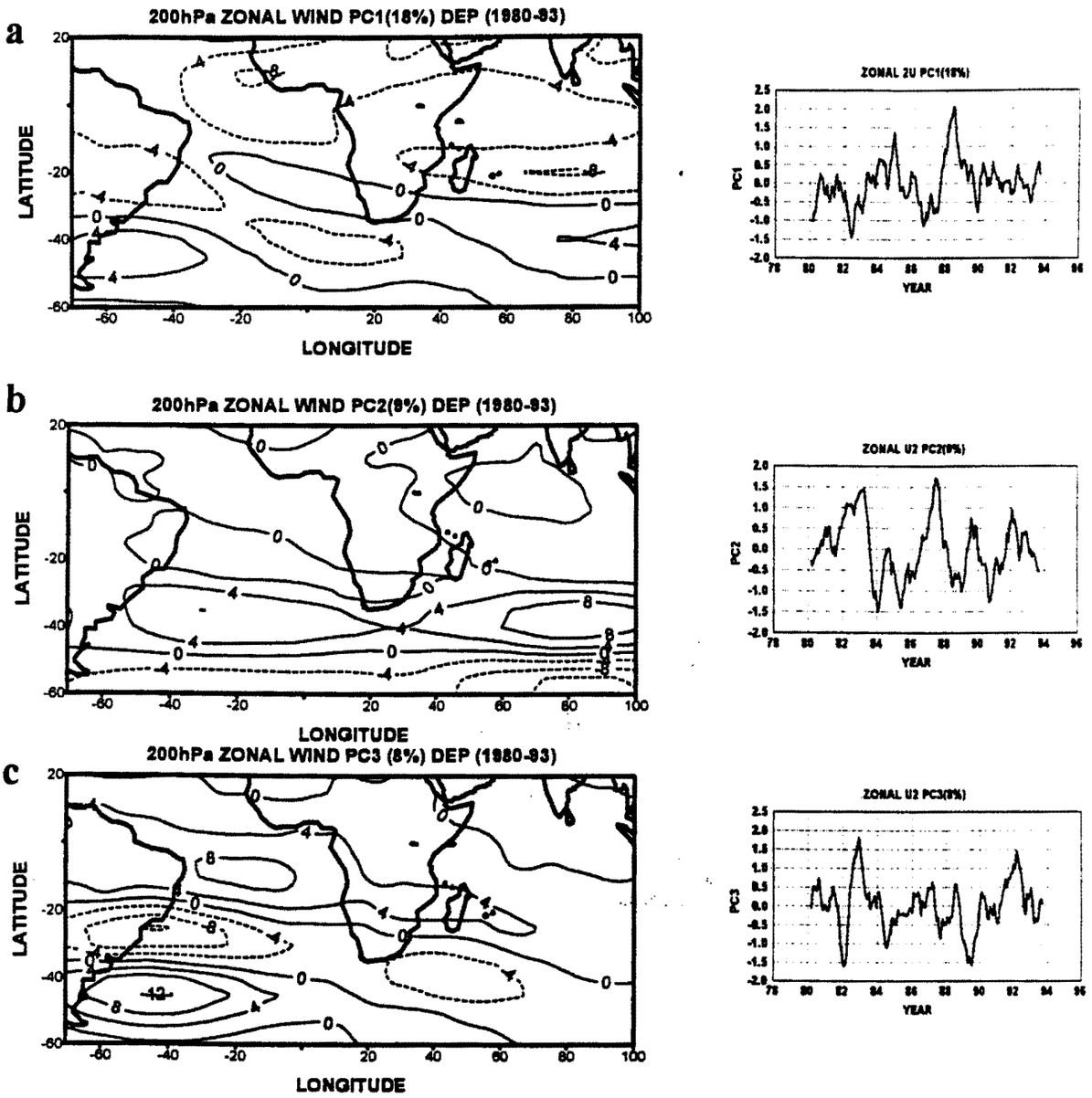

Figure 6.9 Same as in figure 6.6 but for zonal wind component. Contour interval is 4.

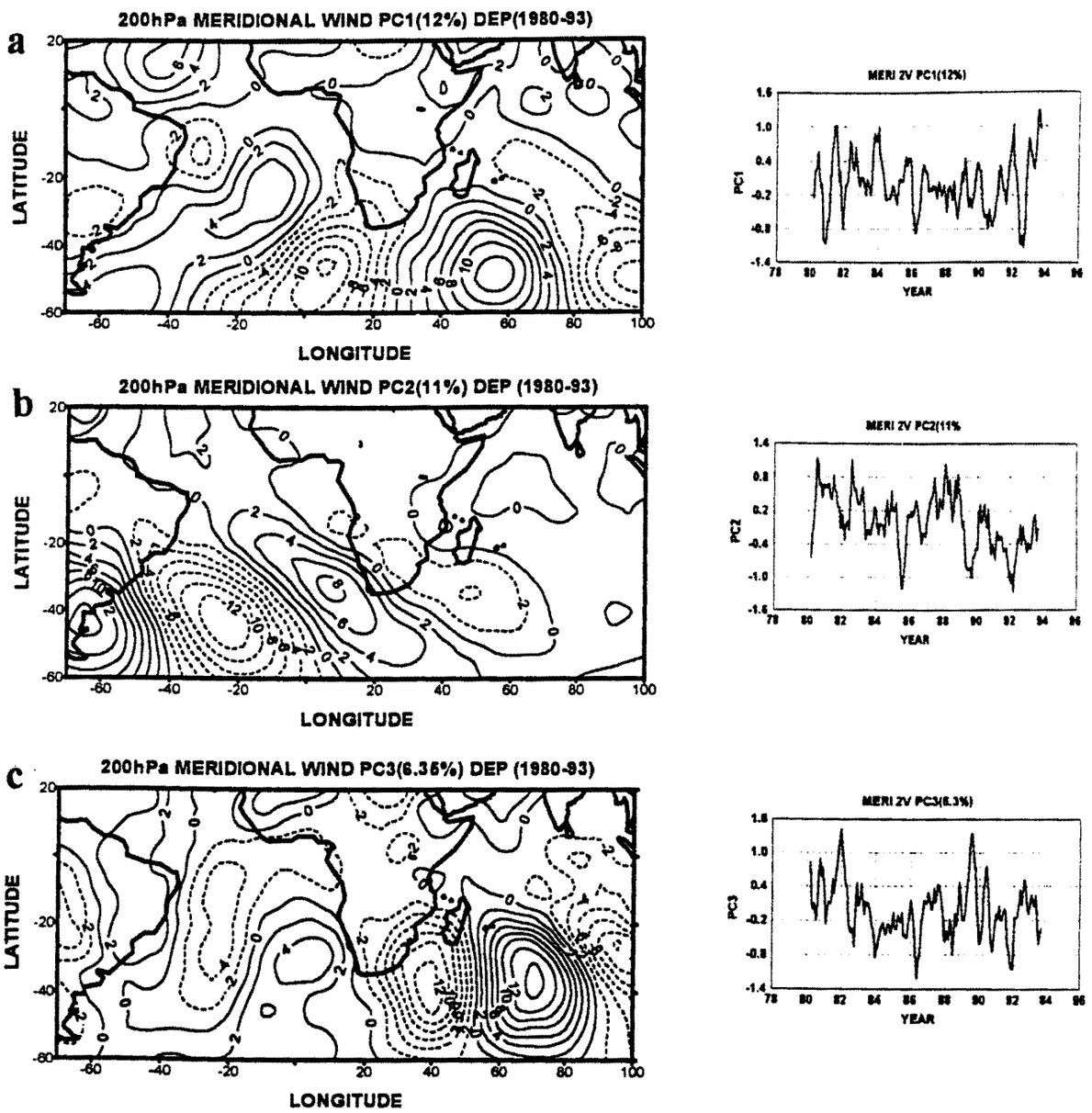

Figure 6.10 Same as in figure 6.6 but for meridional wind component. Contour interval is 2.

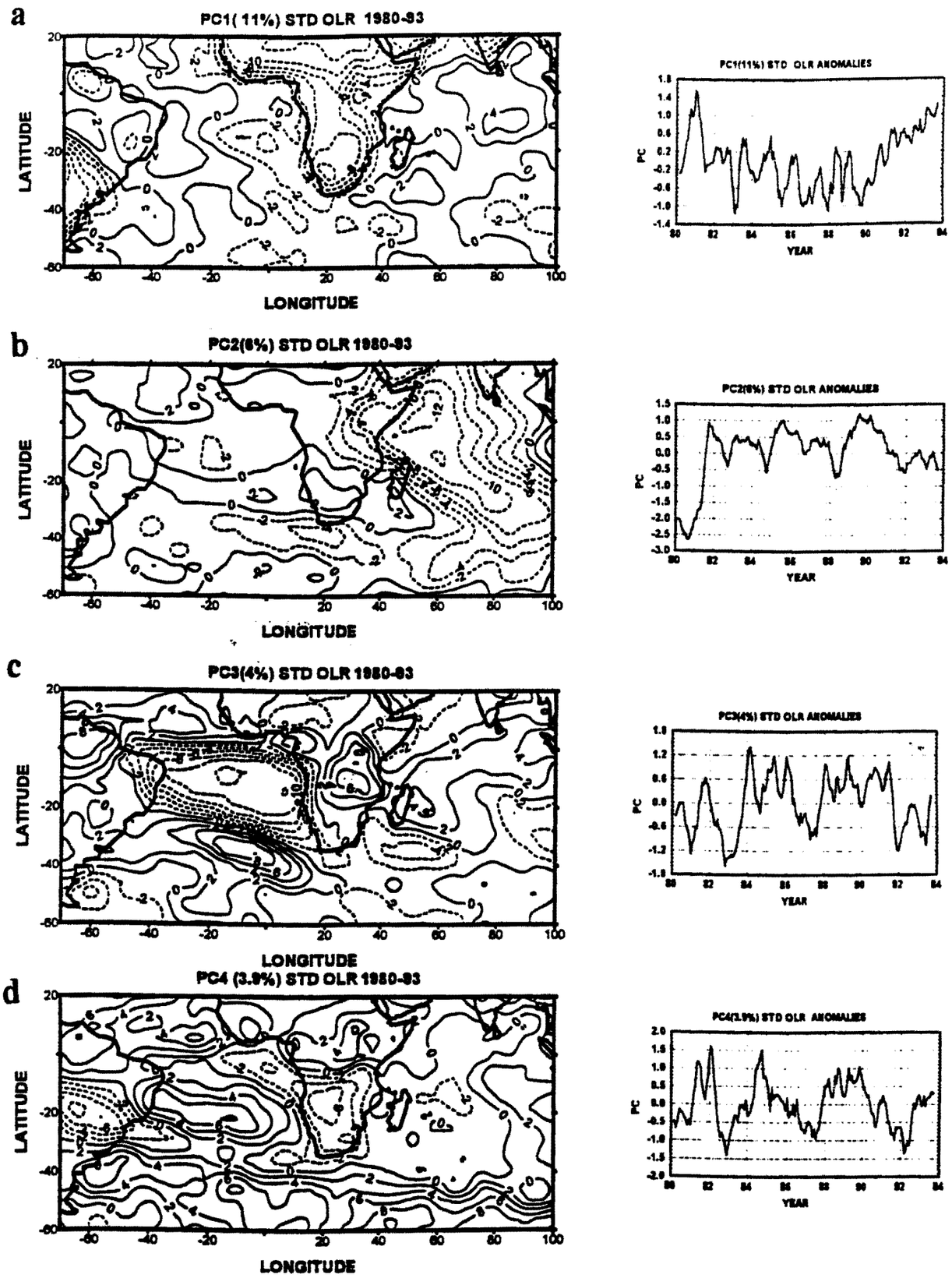

Figure 6.11 Same as in figure 6.6 but for OLR. Contour interval is 2.

a

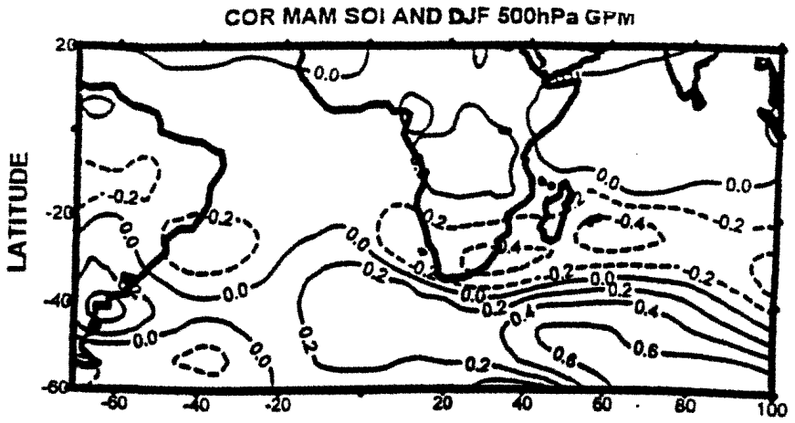

b

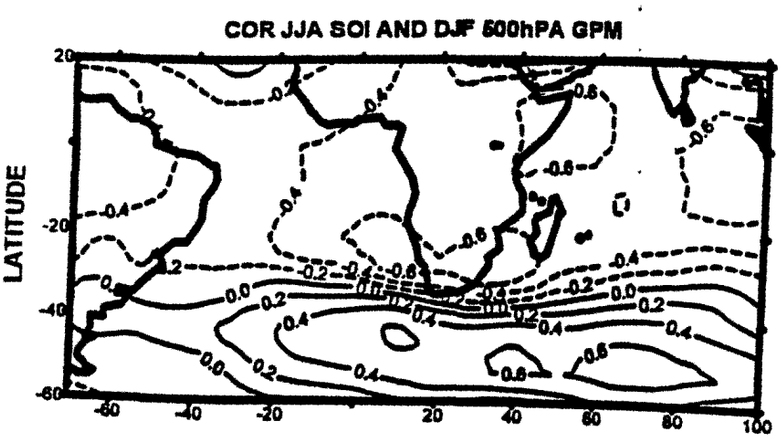

c

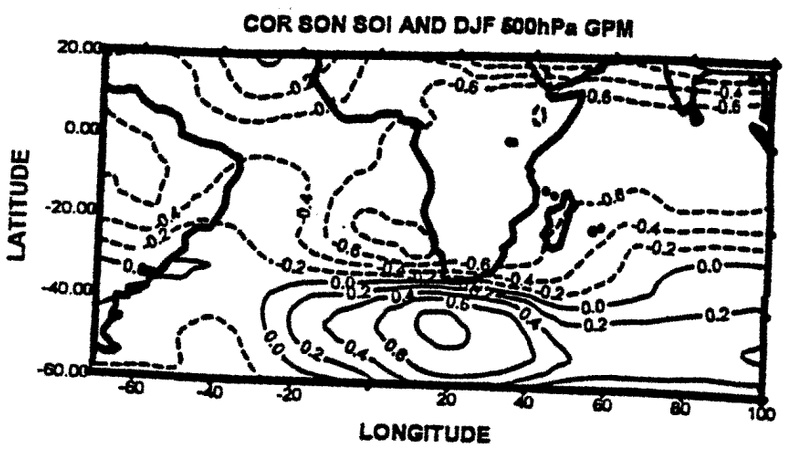

d

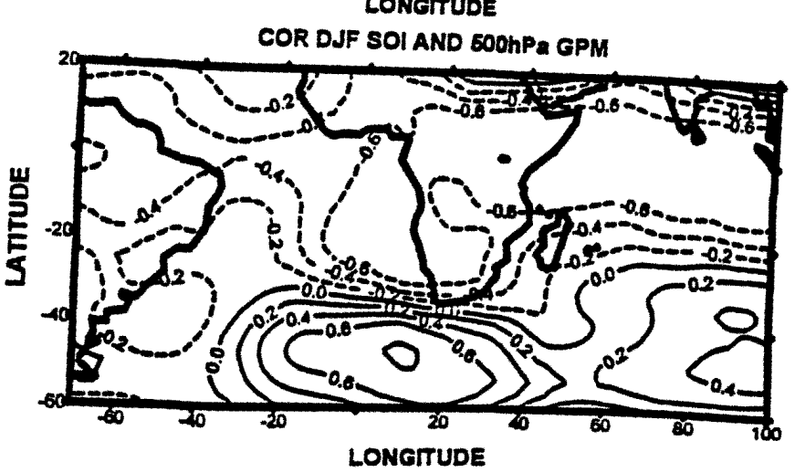

Figure 6.12 (a) Spatial distribution of the correlation coefficients ob between March, April, May SOI and DJF 500 hPa gpm. (b) Same as for JJA SOI. (c) Same as (a) but for SON SOI. (d) Same as (a) but SOI.

Figure 6.1
correlation
SOI and OI

...tween

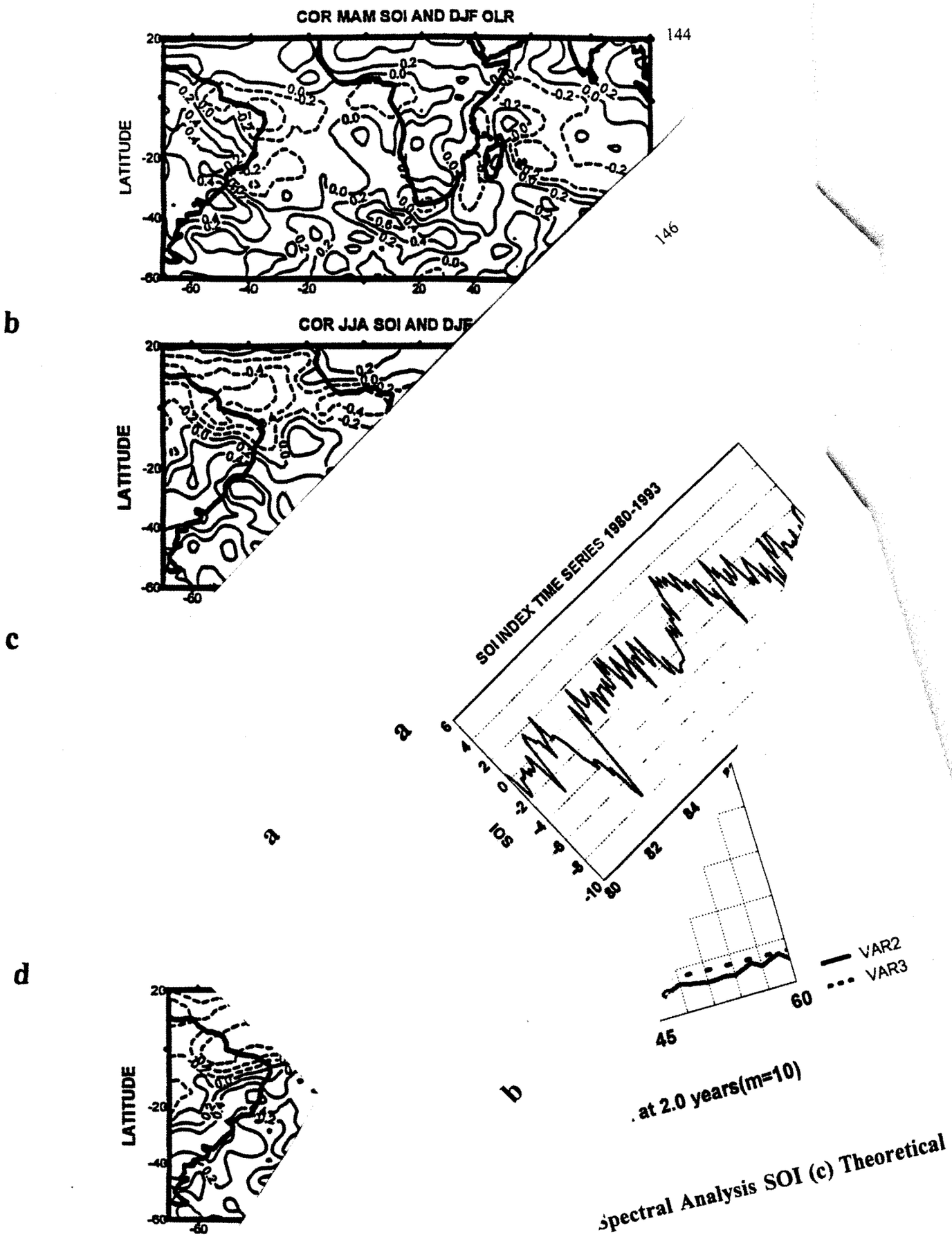

Figure 6.13 (a) Sr
between March,
SOI. (c) Same r

a

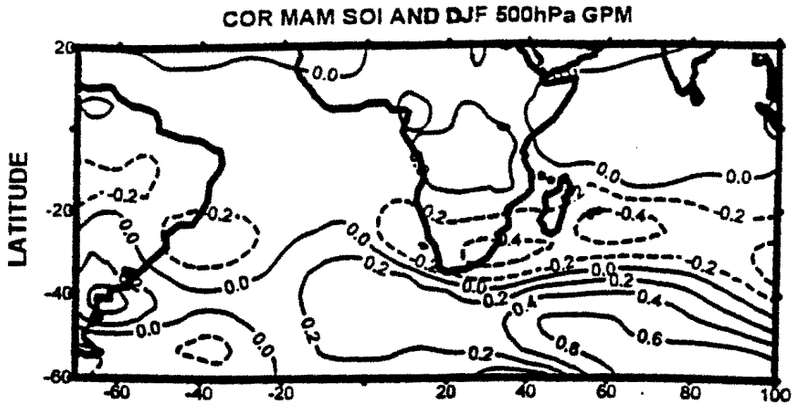

b

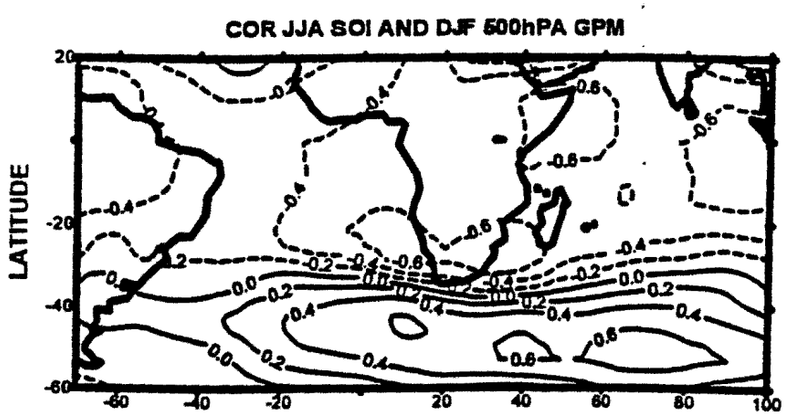

c

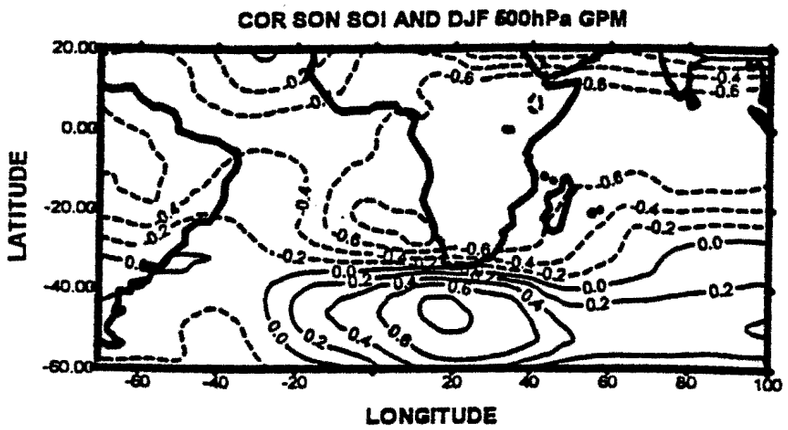

d

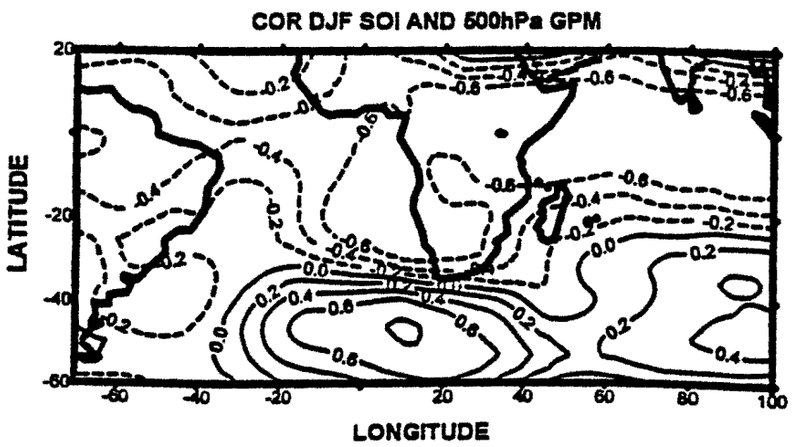

Figure 6.12 (a) Spatial distribution of the correlation coefficients obtained between March, April, May SOI and DJF 500 hPa gpm. (b) Same as (a) but for JJA SOI. (c) Same as (a) but for SON SOI. (d) Same as (a) but for DJF SOI.

a

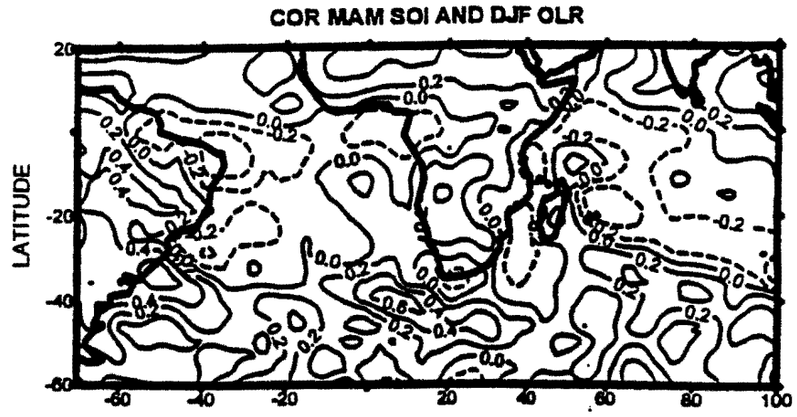

b

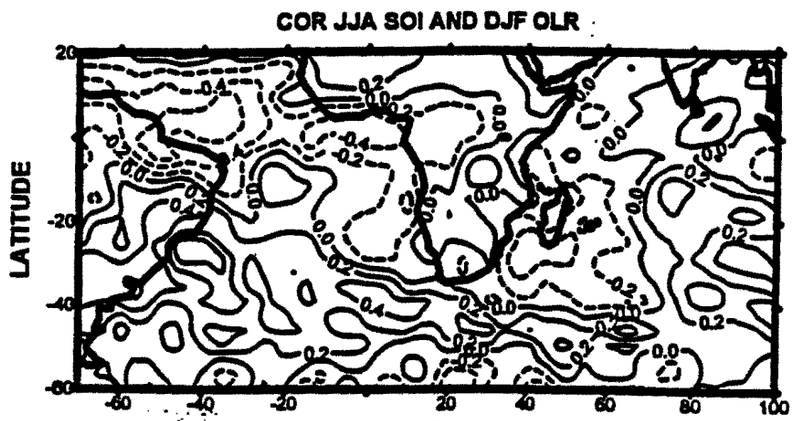

c

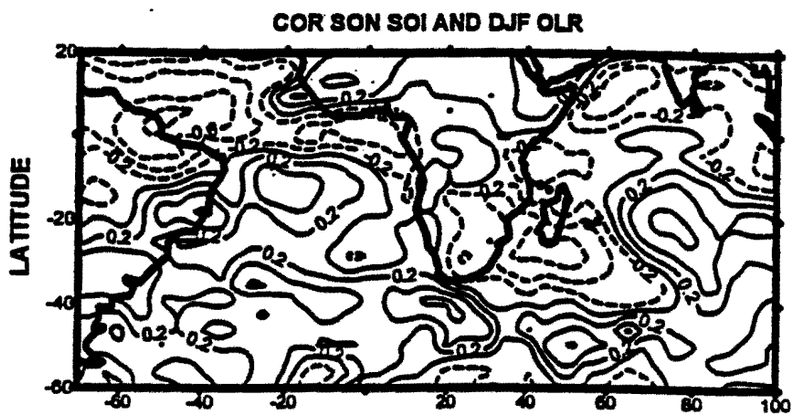

d

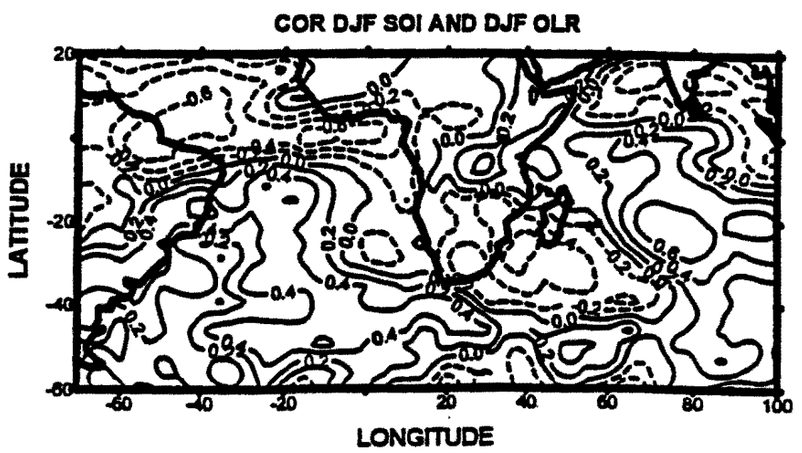

Figure 6.13 (a) Spatial distribution of the correlation coefficients obtained between March, April, May SOI and DJF OLR. (b) Same as (a) but for JJA SOI. (c) Same as (a) but for SON SOI. (d) Same as (a) but for DJF SOI.

a

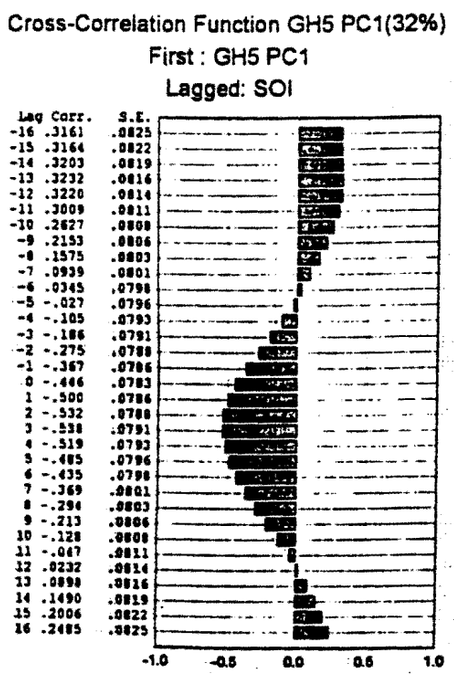

b

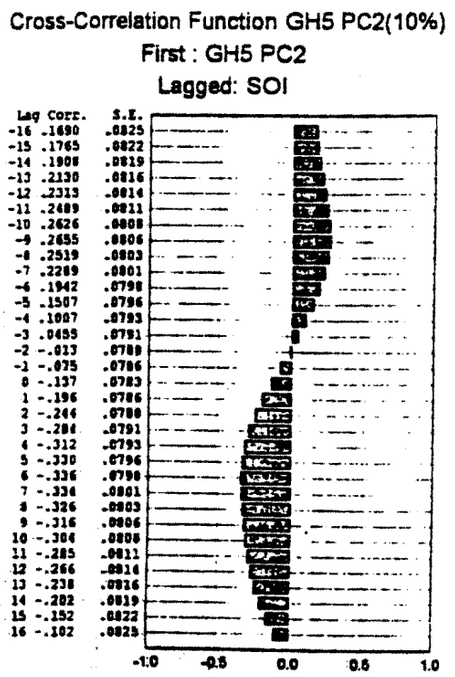

c

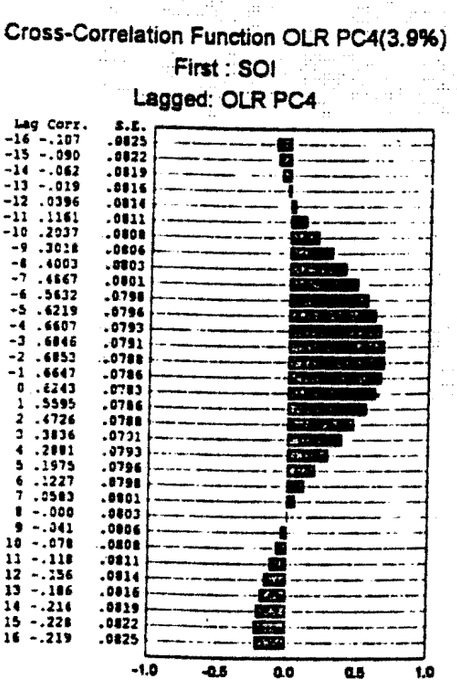

Figure 6.14 (a) Lag correlation between SOI and 500 hPa gpm PC1. (b) Lag correlation between SOI and 500 hPa gpm PC2. (c) Lag correlation between SOI and OLR PC4.

a

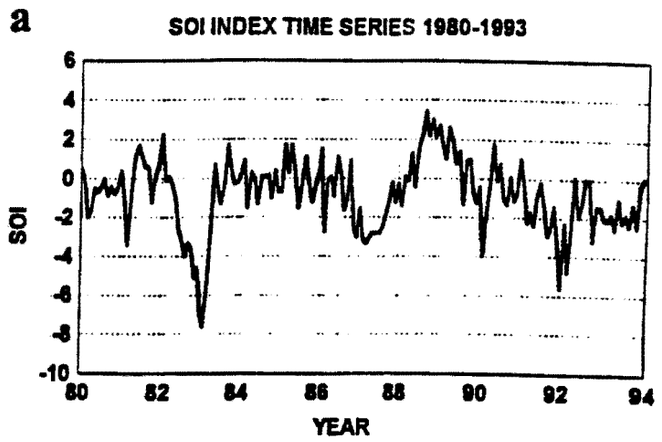

b

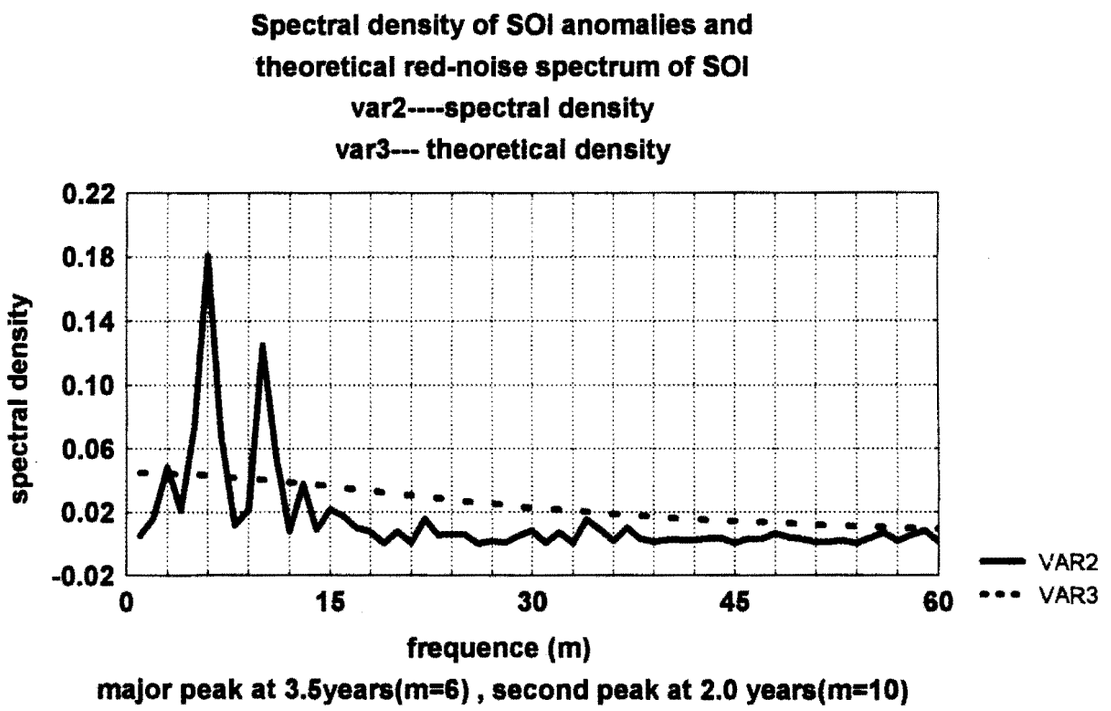

Figure 6.15 (a) Time series of SOI. (b) Spectral Analysis SOI (c) Theoretical Red noise spectrum of SOI.

CHAPTER 7

INTRA-SEASONAL DYNAMICS AND QUASI-GEOSTROPHIC MODELLING OF THE FORMATION OF INLAND TROUGH

7.1 Introduction

The purpose of this chapter is to document atmospheric structure associated with anomalous convection over southeastern Angola on intra-seasonal scales and to perform quasi-geostrophic modelling of this surface inland low. In southern Africa the peak rainfall period occurs in December to February (DJF). During this period well-defined synoptic scale stationary or propagating disturbances appear (Kumar, 1978; Acharya et al., 1981; Harrison, 1986; Preston-Whyte and Tyson, 1988; Levey, 1993). Easterly waves, heat- lows, intraseasonal oscillations (MJO) and westerly waves interact. Multiplicity of scales makes it difficult to understand the individual disturbances and their contribution to peak summer rainfall. Knowledge of the mechanisms underlying the disturbances is limited.

The most significant feature during summer months is the inland low (Angola or Botswana low) over the interior of the subcontinent. However, basic questions remain to be answered i.e. What are the physical and dynamical processes which determine the position and intensity of the Angola low? The hypothesis that heating plays an important part in formation of heat low is demonstrated by modelling, using the quasi-geostrophic theory.

There are periods (greater than 5 days) when some regions of southern Africa are characterised by extreme convective activity in the form of widespread moderate to heavy rainfall. Such situations are have been linked to intra-seasonal oscillations. Makarau (1995) has documented characteristics of southern Africa pentad rainfall. He has observed that the season consists of 5 wet spells alternating with 4 dry spells. The dynamics of such wet spells are linked to the intensity of the thermal low. Dynamic and thermodynamic anomaly fields linked to Angola convective activities needs critical examination. Without any significant changes in dynamic and thermodynamic

important to understand the factors controlling the dynamics of the Angola low. It has been speculated but not documented that surface heating and orography play an important part in the formation of the Angola thermal low. The interannual variability of the inland heat low may affect rainfall over southern Africa through anomalous land surface conditions and hence differential heating between land and adjacent oceans. Land surface conditions may due to vegetation changes or midlatitude /tropical air systems brought about by global

fields, there are periods when some regions of southern Africa may experience dry conditions. Thus dynamics and conditions before and after onset of Angola wet spells need to be determined. Chapter 5 and 6 have discussed teleconnection patterns that may be associated with abnormal summer rainfall such as abnormally high or abnormally low rainfall. Interactions between the inland low and intra-seasonal oscillations (ISO) are not well understood and require further investigation. The intraseasonal variability of summer rainfall can be linked to local forcing by the Angola low (inland low) as illustrated in

or regional circulation anomalies. Differential surface heating can modulate heat budgets, temperature and moisture between southern Africa and adjacent oceans. In this process, the effect of sensible heat flux over the subcontinent is important in regulating the onset and strength of the thermal low.

Heating over the continent is influential in determining when and where anomalies develop (e.g. anchoring). The Angola low may act as an anchor point for convection during wet years. Easterly waves propagating from Madagascar may intensify this quasi-stationary thermal low. Thus a study of the Angola low and the associated thermal and dynamic fields is important. The aim of this chapter is to provide evidence for the existence of the thermal low, which may be explained using the quasi-geostrophic theory.

Summer surface low-pressure systems have been observed and studied over Northern Africa (Ramage, 1971), Saudi Arabia (Smith, 1986), West Pakistan and Northern India (Ramage, 1971; Chang, 1972), Australia (Leslie, 1980) and Southwestern USA and Mexico (Rowson and Colucci, 1992). The major findings from these studies are:

(1) These low -pressure systems are quasi-stationary over heated regions

(2) They are usually confined to levels below 700hPa and are 500-2500 km in horizontal extent.

(3) The requirement for convergence caused by differential heating causes these systems to be positioned mostly over land.

Orography plays an important part in the formation of stationary waves (Asnani 1993).

7.2 Existence of thermal low over Angola

From the mean distributions of the 1980-93 ECMWF data the following points should be noted concerning the existence of the low over Angola and the adjacent areas :

(a) Water-vapour flux DJF vortex and cyclonic low level flow is over located Angola (20°E, 17°S)(figure 4.4(a) and 4.5(a)).

(b) DJF mean 850hPa temperature shows maximum heating over southern Angola (20°E, 17°S)(figure 4.3(a)).

(c) DJF mean 850-500 hPa layer thickness is maximum over North-east Namibia (20°E, 20°S (figure 4.3(c)).

(d) Mean DJF MSLP field shows an area of low pressure over south-western parts of the Southern Africa (Angola, Namibia, Botswana 20°E - 30°E, 12.5°S - 30°S) (figure 4.3(b)).

In order to quantify the Angola low an OLR index is formed based on the observed existence. A key area bounded by the latitudes 12.5°S and 17.5°S and longitude 17.5°E to 22.5°E was chosen to represent the Angola low as shown in **figure 7.1(a)**. It was based on the area where highest DJF mean-thickness is found as previously discussed. The low pressure over Angola is parameterised by an OLR-Index. The choice of index is supported by the DJF rainfall PC1 loading pattern (see figure 5.1(a)) which explained 24% of field variance over sub-equatorial Africa.

The data used in this study are pentads of meteorological elements from ECMWF analyses for the peak rainy season i.e. DJF. The pentads are formed from the period 2nd December to 24 February (see the appendix **Annex 1 (a)** for the calendar of pentads). Anomalies are defined as the departures of the pentad OLR data from the corresponding long-term seasonal mean (DJF) based on 15 years of data (See the appendix for the calendar of the pentads).

The region of study was taken as 0°N - 50°S, 0°E - 60°E and is shown in **figure 7.1(a).** The limited area was chosen in order to focus on terrestrial aspects at the intra-seasonal scale. It should be noted that the summer tropical atmosphere consists of the ITCZ, which has limited meridional extent. The mean winds are very weak during the summer season implying that horizontal advection is also weak and thus large-scale vertical motion dominates. The vertical motion may be directly related to the heating distribution, which is confined to the land.

In general the 500-hPa vertical motion (ascent) is associated with the heat source and subsidence with the heat sink. The areas covered by the heat source and sinks are also limited and the associated upper-level divergence and low-level convergence have limited spatial extent.

It has been observed from the mean summer surface wind flow that the north-easterlies from East Africa, easterlies from the Indian Ocean, north-westerlies recurved from the Atlantic Ocean converge over the interior of the subcontinent. The intensification of a high-pressure system over the midlatitudes influences the wind system. It is necessary that the domain of study region should include part of the subtropical high-pressure areas. The other reason for study area to be focused is the need to evaluate variability of the convective system and links to internal processes i.e. orographic forcing etc. The domain also considers the influence of mid-latitude features. Thus the choice of the domain was based on these physical considerations.

7.3 Seasonal and Intraseasonal Variability

The focus of this section is to reveal temporal characteristics associated with anomalous convective activities over Angola quantified by OLR as defined in previous section. Spatial and temporal characteristics of mean historical mean summer pentads are determined through rotated PCA.

Figure 7.1(b) gives the mean pentad OLR pattern for the period 2nd November to 21st March. This study will focus on the period 7th December to 24th February, which ranges from pentad 7 to 29 (as given appendix **Annex 1(a)**). The highest values of 240 W m^{-2} is found at pentad 7 and the lowest at pentad 25 and the standard deviation has largest value at pentad 7, 12 and 16, the lowest standard deviations being observed at pentad 23, 31 and 34.

Figure 7.2(a) and **figure 7.2(b)** display the spatial distribution of the mean and standard deviation of OLR based on the 12-year period (1983 - 1994). The mean distribution exhibits lowest values (<220 W m^{-2}) over central Africa and highest values (>280 W m^{-2}) over south-west Africa. The highest standard deviations are found over the Mozambique Channel and the lowest over the Congo and oceanic regions. Highest standard deviations (>12 Wm^{-2}) are confined to the eastern interior in a zonal narrow band (12°S - 20°S).

7.4 Temporal characteristics of convection over Angola (OLR index)

In order to find the major periods for convection over Angola, spectral analysis was applied to the time series of pentad OLR data. The time series were

detrended and tapered before subjecting them to Spectral Analysis. The results (see **table 7.1**) should be treated with caution since the data period is short (N=30).

Table 7.1 Major periods of oscillations of convection anomalies over Angola.

Year	First Peak(days)	Second Peak(days)	Third Peak(days)
1982	31	12	15
1983	31	15	10
1984	27	41	11
1985	41	23	15
1986	14	35	11
1987	35	11	20
1988	22	13	
1989	27	19	13
1990	41	13	27
1991	20	11	35
1992	31	15	
1993	27	19	13
1994	19	35	12.5

The primary convective cycle is found to be between 20 and 40 days. This finding is similar to that of Levey (1993) and Makarau (1995).

Explanation of the Period

The period found in this OLR - index may be linked to the convective waves propagating from the adjacent ocean. The easterly waves may be the primary driver of 10-25 day oscillations. A number of studies (Jury, et al., 1996; Mason, 1996; Tennant, 1996) have pointed out that sea surface temperature anomalies can induce fluctuations of southern African summer convection. The thermal

state of the adjacent oceanic regions may play an important part in modulating or in determining the period of oscillations over southern Africa. Thus the observed period of 20 - 40 day oscillation may be linked to what is happening over the Indian Ocean. Theoretical local theory of the 30-50 day oscillation has been given by Krishnamurti et al (1992). They proposed that the 30-50 day oscillation may be due to an ocean-atmosphere interaction in which atmospheric mixing transports horizontal momentum from aloft to the sea-surface, thereby enhancing the wind-driven mixing of the surface layer of the ocean. In this theory periods of oscillation are found to depend on the depth of surface mixed layer of the ocean, surface friction velocity and surface temperature.

Surface hydrology can also influence the period of oscillation. Nanjundiah et al (1992) emphasised the role of ground hydrology in explaining the life span of the locked continent convection. The lifespan of the phase locking depends on how long the soil in the region of the ITCZ takes to dry. The soil characteristics will determine the rate of evaporation. It has been shown that period of drying is 10 days for a field capacity of 10 cm and 30 days for 50 cm.

7.5 Spatial and temporal characteristics of mean intraseasonal oscillations (pentad OLR)

In order to reveal temporal and spatial characteristics of 11-year mean season PCA was applied to historical mean pentad OLR data. Mean pentads were calculated from $x_p = \sum x_{pi}$ for I=1 to 11 (i.e. 1983 to 1993) I is the year, p is the pentad number from 7 to 36. Departures from long term mean were calculated and subjected to PCA. The OLR is used as a proxy for rainfall over the tropical regions and the adjacent oceans. The historical mean pentads for the period 1983 to 1993 were computed to analyse components of the seasonal cycle. The long-term mean was removed from the data before applying PC analysis. **Figure 7.3** displays the results of PCA where negative loadings are associated with above normal convective activities and positive loadings with dry periods.

PC1 (50%)

Figure 7.3(a) displays the first PC mode and associated scores. It explains 50%

of the total variance. Highest loading are found over northern Mozambique and Madagascar (5°S - 12°S). From the time coefficients of this pattern, pentad 15 to 30, are associated with wet spells over northern Mozambique and Channel due to this pattern. The areas with highest loadings coincide with the mean position of the ITCZ. The pattern has a zonal structure with a strong meridional gradient. This mode is associated with the northeast monsoon trough and it is most convective in early February.

PC2 (15%)

Figure 7.3(b) displays the second PC2 pattern and explains 15% of total variance. This PC mode has large loadings over the central interior of the subcontinent. The centre of the negative highest loadings is found over northeastern Botswana (20-30°E, 15-22°S). Large positive loadings are found over the Mozambique Channel (40°E, 15°S). The time-series associated with this mode suggests that early summer (pentad 7 - 18) continental wet spells are mainly reflected in the pattern.

PC3 (5%)

The third PC3 pattern is given in **figure 7.3(c)** and explains 5% of total variance. The pattern is mainly zonal and may be associated with the ITCZ emanating from southern Angola (17°S, 17°E) where the stationary seasonal thermal low develops. Largest positive loadings are found over Angola. It is inferred from the loadings and corresponding time-scores that, this mode may be associated with wet spells over Angola, Namibia, Zambia, Zimbabwe, Botswana, southern Malawi and central Mozambique during the pentads 7 - 14 and pentad 29 - 36 at the beginning and end of summer.

7.6 Roles of Angola low in maintenance of southern African rainy season.

7.6.1 Introduction

Dynamic and thermodynamic fields linked to Angola convective activities are examined in this section to demonstrate the role of Angola low. Structures of thermodynamic and dynamic fields before and after the wet spell are determined through composite analysis. Conditions antecedent to wet spells are

important for forecasting purposes. The composite analysis technique is applied to selected ECMWF data in order to reveal the structure. The composite analysis technique has been discussed in Chapter 3.

Method of defining cases

Generally the choice of the pentads were based on certain threshold values and based on the OLR - index. First the wet periods (designated as P_0) were defined as the period (or pentad) which had a value of OLR less than 200 W m^{-2}. The criteria of choosing P_{-1} was the pentads before P_0 which had a value of 225 W m^{-2}, P_{-2} with the value 250 W m^{-2}. P_{+1} was chosen as the pentad after deep convection (P_0) with the value of 225 W m^{-2}. P_0 is considered as the deep convection stage, P_{-2} is onset, P_{-1} wet stage and P_{+1} is decay case. The chosen cases and their respective pentads are given in **table 7.2** below:

Table 7.2 shows the number of cases used in the study (NC means no case)

Year	P_{-2}	P_{-1}	P_0	P_{+1}
OLR(Wm^2)	240	220	200 – 175	220
75	20	21	22	24
76	NC	24	25	26
77	NC	NC	NC	NC
78	19	20	21	22
79	20	23	24	25
80	NC	NC	NC	NC
81	NC	NC	NC	NC
82	NC	NC	NC	NC
83	19	22	23	26
84	23	25	26	28
85	NC	22	23	26
86	23	24	25	28
87	25	26	28	29
88	20	21	22	25
89	23	24	25	26
90	NC	NC	NC	NC
91	21	NC	23	25
92	NC	NC	NC	NC
93	22	23	24	NC
94	NC	16	17	18

NC = no case

7.6.2 Structure of the intraseasonal oscillations associated with Angola wet spells.

It is important to test the significance of the anomaly fields but this was not done due to large amount of computation involving many parameters. A student 't' test, defined by parameter: $t = [(x_1-x_2)/S]^* (1/n_1+1/n_2)^{-0.5}$ where x_1 and x_2 are two sample means and $S = (n_1-1)s^2_1+(n_2-1)s^2_2)/(n_1+n_2-2)$, n_1 and n_2 are number of sample means, $s_1$and s_2 are two standard deviations (Lighthill, 1981).

7.6.3 Lower-tropospheric anomaly fields

Temperature Composites

Figure 7.4(a), (b), (c) and (d) show the sequence of composite maps of 850 hPa temperature anomalies for P_{-2}, P_{-1}, P_0 and P_{+1} respectively.

P_{-2}

During P_{-2} (see figure 7.4(a)) the cold pool indicating cloud and rain is found north of 17°S. The region between 17°S and 35°S is mainly under warm conditions. Maximum cooling is found at 20°E, 12.5°S and 30°E, 12.5°S. Largest warming occurs over western South Africa. This pattern has a reversed temperature gradient over the subcontinent and from the thermal wind principle easterly winds can be induced over the region between 15°S and 25°S with a cyclonic thermal wind over Zambia, northern Angola and Congo. The cooling may be linked to evaporation and diabatic effects. As per theory of Webster (1983) and Srinivasan and Smith (1996), this configuration may lead to the southward movement of the ITCZ. This pattern shows a strong meridional gradient of temperature over land and a zonal gradient south of 35°S implying the presence of baroclinicity.

P_{-1}

Figure 7.4(b) displays the temperature anomalies at P_{-1}. The cooling extends from 5°S to 25°S over the subcontinent. In this pattern both zonal and meridional gradients prevail implying the presence of both meridional and zonal thermal circulations. The warming occurs over most parts of the oceanic regions.

P_0

Large negative temperature anomalies (see **figure 7.4(c)**) are observed southwest of the OLR - index box and cooling occurs over most parts of the subcontinent. Maximum warming is observed over the south Indian Ocean (55°E, 35°S). The cool area has two axes, one extending eastward to Malawi and another one southeastward to Lesotho.

P_{+1}

The intensity of cooling due to evaporation of rainfall reduces but the pattern is similar to P_0 (see **figure 7.4(d)).** The largest negative anomalies are observed over the OLR Index box and the high plateau.

850 hPa Geopotential Height

Figure 7.5(a), (b), (c) and (d) show the composite maps for 850 hPa geopotential height anomalies for P_{-2}, P_{-1}, P_0 and P_{+1} respectively.

P_{-2}

At P_{-2} a dipole pressure pattern is evident with high pressure west of the 30°E and low pressure east of 30°E over southern Africa. Zonal pressure gradients are large over the midlatitudes (35°S - 50°S, see **figure 7.5(a)).** There are small pockets of low pressure to the northwest of the target box. Large pressure falls (>40 gpm) occur over the southern Indian Ocean (50°E, 47°S), and large rises (>5 gpm) occur over the southern Atlantic Ocean (42.5°S, 2.5°W). The target box is under pressure rise.

P_{-1}

Pressure falls are observed between the latitude 5°S and 20°S. Highest falls (>5 gpm) are reported just to the south of the target area, east of Madagascar and over the Southern Ocean (see **figure 7.5(b)).** Pressure rises are confined to the Congo, southern Atlantic and south Indian Oceans (east of 25°E between latitude 25°S - 35°S). The pattern is mainly zonal in structure suggesting that the Hadley cell is relatively stronger than the Walker cell. The meridional gradient is more evident north of 40°S. There is also slow propagation of the high pressure in the midlatitudes (35°S). The build up of the low pressure over the interior and the appearance of the high pressure over the south Indian ocean and Congo favours convective activity over the central interior.

P_0

There is intensification of the high pressure over southeast parts of the

subcontinent and over the Congo (see **figure 7.5(c)**). Deepening of the low pressure east of Madagascar (50°E, 25°S) is quite evident. Pressure falls (>4 gpm) are found in the OLR Index box. The pattern is quite similar to P_{-1} apart from the changes over the southern oceans. The high pressure over the southern oceans has a meridional structure implying a blocking effect or a slow rate of propagation. The location of this positive pressure anomaly coincides with wave number 3 (Preston-Whyte and Tyson, 1988).

P_{+1}

At P_{+1} there is an eastward retreat of the deep low east of Madagascar and the appearance of a zonal circulation over the middle latitudes (30 - 40°S, see **figure 7.5(d)**). This implies suppressed westerlies in the middle latitudes, which may be associated with high-pressure systems. There is a contraction of the high pressure over Congo. It can be observed that at P_{-2}, the isotherms are more zonal north of 25°S but the isobars are meridional implying that the pressure and temperature surfaces are intersecting and thus there is generation of potential energy.

850 hPa Divergence

In order to show areas of near-surface convergence and divergence the 850-hPa circulation was considered. Figure 7.6 (a), (b), (c) and (d) displays the composite maps for 850 hPa divergence anomalies for P_{-2}, P_{-1}, P_0 and P_{+1} respectively.

P_{-2}

At P_{-2} convergence is revealed over southern Congo, Zambia, Malawi and northern Mozambique, convergence is also found over Lesotho and central Namibia (see **figure 7.6(a)**). Divergence regions are over northeast Namibia and southern Tanzania.

P_{-1}

Strong convergence ($<1.0\times10^{-4}s^{-1}$) prevails over Zimbabwe, Botswana, eastern Namibia and the Western Cape (see **figure 7.6(b)**). Divergence ($>1.0\times10^{-4}s^{-1}$) is evident over northern South Africa, Madagascar and East Africa.

P_0

Areas of convergence are confined to Namibia, southern Angola, Botswana, southern Zambia and Zimbabwe in a zonal axis (see **figure 7.6 (c)**). Divergence is over the Congo and Madagascar.

P_{+1}

Pockets of convergence are observed over southwest South Africa, Namibia, eastern Botswana and southern Mozambique (see **figure 7.6 (d)**). Divergence is found over the Mozambique Channel.

7.6.4 Mid-troposphere anomaly fields

500 hPa Temperature

In order to understand the importance of upper level warming which is necessary for direct circulation, middle level temperature composites were constructed. Direct circulations maintain tropical disturbances through warm air rising and cold air sinking. Figure 7.7(a), (b), (c) and (d) show the composite maps for 500 hPa temperature anomalies for P_{-2}, P_{-1}, P_0 and P_{+1} respectively.

P_{-2}

The major feature is the cooling in the middle latitudes (40°S, 50°S) and between 15°S and 25°S (see **figure 7.7(a)**). Warming is evident over the areas confined between 25°S, 40°S latitude and the areas to the north of 15°S i.e. northern Zambia, northern Angola and the Congo.

P_{-1}

Warming dominates most parts of the subcontinent except over East Africa and the extreme parts of Southern Oceans where cooling takes place (see **figure 7.7 (b)**).

P_0

Warming takes place in most parts of the subcontinent with maximum over the Cape Province in a zonal axis along 30°S (see **figure 7.7(c)**). Cooling is confined to areas north of 15°S.

P_{+1}

Areas to the north of 20°S latitude are under cooling with warming south of

this latitude (see **figure 7.6 (d)**). Maximum warming (>1.5°C) occurs off the coast of eastern South Africa.

500 hPa Vertical motion

Figure 7.8(a), (b), (c) and (d) show the composite maps for 500 hPa vertical motion anomalies for P_{-2}, P_{-1}, P_0 and P_{+1} respectively.

P_{-2}

Ascending motion prevails over northern Angola, southern Congo, Zambia, Malawi and central Mozambique including the Mozambique Channel (see **figure 7.8 (a)**). Maximum vertical motion is found over northeast Angola, and eastern Zambia. Descending motion is evident over northeast Namibia, Botswana, Zimbabwe and South Africa.

P_{-1}

Most parts of the subcontinent are under ascending motion except northwestern parts of the Congo, western Namibia and Mozambique where downward motion occurs (see **figure 7.8 (b)**). The major descending areas are Madagascar and south Indian Ocean.

P_0

Maximum upward vertical motion (<-0.4) is observed over Southeast Namibia and northwest Botswana (see **figure 7.8 (c)**). Most parts of the subcontinent is under upward motion except the northern Congo, Mozambique and the northern parts of South Africa. The major regions of downward motion are over the Atlantic Ocean (0°E, 37.5°S), Indian Ocean (32°E, 37.5°S), and northern Madagascar (45°E, 15°S).

P_{+1}

Ascending motion is observed over southern Congo, Tanzania, northern Zambia, Malawi and the eastern parts of South Africa (see **figure 7.8 (d)**). Downward motion is over Angola, Botswana and Zimbabwe along latitude 15°S. There are two major oceanic areas of descending motion namely; Atlantic Ocean (15°E, 45°S) and Indian Ocean (45°E, 25°S).

Water Vapour Flux

Figure 7.9(a), (b), (c) and (d) displays the composite maps for water vapour

flux anomalies for P_{-2}, P_{-1}, P_0 and P_{+1} respectively.

P_{-2}

An anticyclone with centre at 15°E, 30°S controls the flow over southern Africa (see **figure 7.9(a)**). The major feature is the southwesterly anomaly field, which prevails over the midlatitudes. An easterly flow is observed between 22°S to 12°S.

P_{-1}

Two vortices are identified at P_{-1} with centres over northeast Namibia and Indian Ocean (50°E, 20°S see **figure 7.9(b)**). Strong convergence of water vapour flux between north-westerlies and south-easterlies exist along latitude 17°S over the eastern parts of the subcontinent. Strong north-westerly flow prevails north of 15°S and easterlies south of 22.5°S. The anticyclonic anomaly with centre over the south Indian Ocean (40°E, 35°S) controls the easterly flow over South Africa.

P_0

The inland vortex remains in the same position with strong westerly flow over the regions north of 15°S (see **figure 7.9(c)**). The strong convergence region is maintained along 18°S. The centre of the anticyclone is over the Indian Ocean (52°E, 47.5°S). A second anticyclone is observed over the central Indian Ocean (45°E, 5°S). Convergence is noted along an axis from the Angola low to Marion Island.

P_{+1}

The cyclone centre is found to be over western Zimbabwe and the flow south of 25°S is controlled by an anticyclone over the Southern Ocean (see **figure 7.9(d)**). Southwesterly flow is observed along 10°S over northern Angola, Congo and East Africa.

Precipitable Water

Figure 7.10(a), (b), (c) and (d) show the precipitable water anomalies for P_{-2}, P_{-1}, P_0 and P_{+1}. At P_{-2} relatively high precipitable water anomaly of greater than 2 mm is found over central parts of the subcontinent (Zambia, Malawi)

and Mozambique Channel. Negative anomalies are confined to south of 15°S and north of 5°S over the subcontinent.

At P_{-1} large values (>4 mm) of precipitable water anomaly are found over the subcontinent and east of Madagascar over the Indian Ocean. The highest positive values are situated over western Zambia and eastern Angola.

At P_0, most parts of the subcontinent are under positive anomalies with the highest being confined to Botswana, Namibia and South Africa. There is a decrease in precipitable water at P_{+1} and the highest values are found over Malawi, northern Mozambique and central Namibia.

7.6.5 Upper tropospheric anomaly fields

Composite of 200 hPa Winds

Upper-level wind anomalies for P_{-2}, P_{-1}, P_0 and P_{+1} are displayed in **figure 7.11(a), (b), (c) and (d)** respectively.

P_{-2}

Strong southerly wind anomalies are observed south of Africa and are associated with the ridge over the southern Oceans. An inflow is over Angola. Easterly flow anomalies occur over South Africa.

P_{-1}

Diffluent easterly flow anomalies are over most parts of the subcontinent and north-westerlies to westerlies over midlatitudes. A large anticyclone lies south of Madagascar.

P_0

Anticyclonic south-easterlies to easterlies dominate the southern African subcontinent. Strong easterlies are evident over Angola.

P_{+1}

Similar flow as in P_0 is over southern Africa but becoming north-easterlies over the area east of 25°E and south of 15°S. Southerly flow anomalies prevail over the midlatitudes.

Composite of 200 hPa Divergence

In order to understand the upper air circulation, divergence at 200hPa was composited. **Figure 7.12(a), (b), (c) and (d)** show the composite maps for 200

hPa divergence anomalies for P_{-2}, P_{-1}, P_0 and P_{+1} respectively.

P_{-2}

There is large-scale convergence west of 30°E and divergence east of 30°E. Centres of high divergence (>2.0 x $10^{-4}s^{-1}$) are found over south Atlantic (5°E, 35°S), off the coast of Namibia (15°E, 25°S), Mozambique Channel and central Indian Ocean. Over the continent the areas of convergence coincide with areas of higher pressure at 850 hPa. The target box is under upper-level convergence.

P_{-1}

The areas of positive divergence are south of 15°S with the largest values (>3 x $10^{-4}s^{-1}$) over the former Transvaal, East Africa (35°E, 10°S) and east of Madagascar (52.5°E, 25°S). There is an eastward propagation of convergence in the equatorial latitudes (0° - 5°S).

P_0

Continued eastward moving convergence zones are noted north of 10°S. The OLR -index box is under large positive anomalies (>3.0 x $10^{-4}s^{-1}$) and the structure is zonal. There are large-scale positive anomalies stretching from central parts of the subcontinent (Zambia), through northern Mozambique, Madagascar and south Indian Ocean. Convergence is found over southern parts of the Mozambique Channel. This pattern is in agreement with the 850 hPa geopotential composite anomalies, OLR, and temperature anomalies.

P_{+1}

Largest positive values (>3.0 x $10^{-4}s^{-1}$) are found over northern Mozambique (35°E, 10°N) and off the coast of Gabon (10°E, 3°S). The target area is under convergence which is to the west of 20°E. The convergence zone over the midlatitudes propagates eastwards at a rate of 15°/pentad.

Outgoing Longwave Radiation (OLR)

In order to understand the horizontal structure associated with Angola convective anomalies (OLR - Index) over southern Africa the composite technique is applied to OLR data. It should be noted that OLR can be expressed

as a heating function and is related to horizontal divergence (D) through an empirical formula derived by Lau (1992)($D = (-0.05\times10^{-6}) \cos^4\phi\times OLR$). This empirical formula is relevant in the tropics where ϕ is the latitude and OLR is the outgoing longwave radiation.

Figure 7.13(a), (b), (c) and (d) show composite maps of P_{-2}, P_{-1}, P_0 and P_{+1} for OLR anomalies. In the discussion, the Index box will be referred to as the Angola index and the key points are points with largest sums of positive or negative anomalies.

P_{-2}

At P_{-2}, there is a large-scale pattern of positive anomalies over most parts of the subcontinent (**figure 7.13(a)**). Generally there are positive values everywhere which refer to below normal convection. The pattern is similar to the classical case of easterly waves as explained by Asnani (1993). Easterly waves may arise due to the interaction between easterly trades and the orography. A high pressure occurs on the eastern side of Madagascar and a trough of low pressure over the Mozambique Channel. Another high pressure develops over the eastern subcontinent with low pressure over southern Angola. The approximate wavelength is between 1500 -2000 km.

P_{-1}

The precursor stage is dominated by negative anomalies over most parts of the subcontinent (**figure 7.13(b)**). Large anomalies are found over Angola and over the Indian Ocean (55°E, 25°S). This pattern suggests a sudden development of the negative anomalies. Lowest values occur in the central Indian Ocean (40°E, 14°S). The structure of this pattern is similar to PC 2 mode (see figure 7.3(b)).

P_0

The Angola OLR Index key box has negative anomalies. The principal features remain similar to P_{-1} but the intensity is decreased to the north of 15°S (**figure 7.13(c)**). Positive anomalies appear over the eastern parts of South Africa. PC3 mode (see figure 7.3(c)) corresponds to this pattern. The negative anomaly is orientated in a northwest to southeast axis. There are positive anomalies north of Madagascar.

P_{+1}

This pattern (**figure 7.13(d)**) is incoherent and similar to P_{-2} except for the positive anomalies over central Zimbabwe (30°E, 20°S). Generally, this pattern gives an impression of standing easterly waves as discussed for P_{-2}. The fact that P_{-2} and P_{+1} have similar structure would lead one to speculate that the convective anomalies may have a period of 20 days. This stage is a mixed bag with a decayed structure.

7.7 Thermal forcing field over southern Africa and adjacent oceans

The role of thermal forcing can be illustrated through investigation of relationships between temperature and pressure anomalies. The focus of this section is to demonstrate the relationship between temperature and pressure and the existence of a heating contrast between land and sea. Summer rainfall is a manifestation of the seasonal cycle of heating and cooling over southern Africa and adjacent oceans. The intensity of low pressure over the subcontinent during summer may control the summer circulation (Combined PC1 in chapter 6) and this low is in turn controlled by surface and tropospheric temperature over southern Africa and adjacent oceans. Evolution of a thermal low over southern Africa is important for the onset vortex of summer rainfall. A positive temperature anomaly during pre-rainy season induces a stronger heat low over southern Africa and supports larger amounts of moisture from the oceans and hence causes above normal rainfall. The opposite may be observed during below normal temperature. **Figure 7.14(a)** shows the mean September 850hPa-temperature field. Higher temperatures during the pre-rainy season support an increasing moisture content later in the season. Highest (> 26°C) temperatures are over the interior of the subcontinent and the lowest over the adjacent oceans. Note that in the tropical band (10°S-25°S), low values of temperature coincide with high-pressure regions and high temperature with low pressure. Stronger land-sea temperature contrasts are evident at latitude 18°S and this is used as the prescribed heating in the modelling.

In order to determine the relationship between standardised monthly temperature and mean sea level pressure (MSLP) anomalies, correlation

coefficients (r) were computed, using all the months (January 1980 to December 1993 i.e. 168 months). ECMWF data were used as discussed in chapter 3. Correlation coefficients between standardised monthly mean sea level pressure and 850hPa temperature anomalies are displayed in **figure 7.14(b).** Large values of correlation coefficients (r = -0.8) are found over southern Africa, Madagascar and the Sahara desert. Correlations coefficients greater than 0.25 are significant at 99.9%. In this case the autoregressive nature of the data is not taken into account when the significance test is computed (Greenhut, 1979). A positive relationship exists south of 45°S between temperature and pressure anomalies. Heating over southern Africa accounts for 36 - 64% of the mean sea level pressure anomalies. This further demonstrates that intense heating over southern Africa may result in development of intense heat lows.

In order to determine the spatial and temporal variability of near surface temperature (850hPa temperature) rotated PCA was applied to standardised monthly temperature anomalies. The PC pattern associated with differential heating between continent and oceans was retained. This pattern happened to be the first principal component. **Figure 7.15(a)** exhibits the first mode PC1 (20.8%) of monthly 850hPa standardised temperature anomalies and illustrates the thermal contrast between the oceanic and continental regions. The highest positive loadings are over southern Africa. Negative loadings arise over the Atlantic (15°S-40°S, 20°W-0°E) and Indian (20°S-50°S, 60°E-100°E) Oceans. The associated time series is displayed in **figure 7.15(b).** Large positive scores occurred in 1981, 1987 and 1989. Negative values were pronounced in 1980 and 1983.

In order to examine the area of influence of the thermally driven component of circulation, simultaneous temporal correlations between monthly 200-500 hPa geopotential thickness anomalies at grid point 20°S, 20°S and other grid points are done. The correlations are based on all months for the period 1980-1993. **Figure 7.16(a)** shows the correlation coefficient fields obtained between Northeast Namibia and the rest of the domain. The area of influence is confined

to most parts of southern Africa. The isoline of r = 0.7 is concentrated over Southern Africa and the eastern parts of the Atlantic Ocean. This shows that anomalous upper level heating over this region has an influence on southern African climate.

September vertical cross-section mean wind profiles are shown in **figure 7.16(b)** and display a sharp transition at 500hPa level between low level easterlies and upper level westerlies. In the model (to be discussed later), low-level easterlies and upper level westerlies are assumed to be constant in space and time to make the mathematics easier.

7.8 Mechanism of formation continental trough

In southern Africa, little work has been done on the thermal low due to lack of data. Many meteorologists have cited the thermal low when describing the weather in this region (Acharya and Bhalotra, 1981). In this section, the dynamics of the low are presented using the linearised equations of motion. The focus is on the interaction between the mean flow and surface heating. Although the linearised equations give a valid description of only the earliest stages of the development of motion, it is reasonable to believe that the effects of the non-linear terms are merely to check the growth rate by adjusting the flow pattern. Thus the flow at the later stages of the development should be determined largely by initial growth-rate. It seems valid; therefore to assume that the mechanism which converts available potential energy into kinetic energy can be determined through a study of the linearised equations. Thus it is possible to remove the complex, time consuming non-linear terms in the equations of motion and then build a model that will produce the broad features of the southern African circulation and associated Angola thermal low.

7.8.1 A two layer quasi-geostrophic model of trough formation

Introduction

The purpose of this section is to investigate the effect of surface heating on a vertically sheared zonal current. The model theory is based on quasi-geostrophic assumptions of Fandry and Leslie, (1984) who used it to simulate the formation of a trough over Australia. The next part deals with the

formulation of the quasi-geostrophic vorticity equation for two layers. The normal mode solutions are assumed and the vorticity equation is reduced to the inhomogeneous Helmholtz elliptic equation. Solutions decay away from the disturbance and thus they are confined to the region. Wave-like solutions are also obtained under certain conditions so they do not decay away from the obstacle. Hence two solutions are determined. In this case, the general solution is determined in terms of Green's functions (Abramowitz et al., 1970). Numerical integration is used to evaluate the double integrals and NAG subroutines are called to evaluate the Bessel functions (Abramowitz et al., 1970). The model is applied to the southern African situation where the heating is applied at the lower boundary. In this study a simple quasi-geostrophic model is applied to investigate the effect of surface heating on low level easterlies and upper westerlies over the subtropical region of southern Africa during spring and early summer. The following assumptions are made to make the mathematics simpler: βeta approximation, two-layer vertical structure, mean zonal winds are constant in each layer and quasi-geostrophic disturbances are considered

Basic model and equations

During the early summer season, there is a large land-sea temperature contrast over Southern Africa region and the adjacent oceans. The main objective of this study is to investigate the effects of surface heating due to land-sea temperature contrasts on a vertically sheared uniform zonal current.

Geometry of the model

Figure 7.16(c) displays the geometry of the model which consists of two mixed layers of constant potential temperature θ_1, θ_2. The subscript (1) and (2) refer to upper and lower layers. D_1 and D_2 are undisturbed depths; U_1 and U_2 are the constant zonal flow and upper and lower levels respectively. The surface orography or surface heating is parameterised through the function z = S (x, y) is the surface irregularity.

Vertical meridional cross-section along 15°S.

The vertical east-west cross-section of the mean September zonal flow through

15°S is given in figure 7.16(b). Along 15°S westerly flow prevails above 500 hPa and easterlies in lower troposphere.

Quasi-geostrophic model

The derivation of the equation of the potential vorticity has already been discussed. For the two layered flow, the quasi-geostrophic potential vorticity (full deviation of these equations can be found in Gill (1982)) equation can be written as:

$$\frac{D_1}{Dt}\left[\nabla^2\psi_1 - F_1(\psi_1 - \psi_2) + \beta y\right] = 0 \qquad (7.1)$$

$$\frac{D_2}{Dt}\left[\nabla^2\psi_2 - F_2(\psi_2 - \psi_1) + \beta y + R_s\right] = 0 \qquad (7.2)$$

The total derivative is

$$\frac{D_i}{Dt} = \frac{\partial}{\partial t} + U_i\frac{\partial}{\partial x} + V_i\frac{\partial}{\partial y}$$

$$\text{for i} = 1, 2 \quad U_i = -\frac{\partial \psi_i}{\partial y} \qquad V_i = \frac{\partial \psi_i}{\partial x}$$

x and y are eastward and northward co-ordinates, subscript 1 and 2 represent the upper and lower layer. ψ_i is the pressure field, β is the gradient of the coriolis parameter.

$$\nabla^2 = \frac{\partial^2}{\partial x^2} + \frac{\partial^2}{\partial y^2}$$

$R_s = \dfrac{S}{\varepsilon D_2}$ is the nondimensional function, S(x,y) is the surface irregularity $h_B(x,y)$ and can also represent the heating term $T_B(x,y)/\gamma$. D_2 is the depth of the undisturbed depth of the lower layer.

$\varepsilon = \dfrac{\overline{U}}{f_o L}$ is the Rossby number

$\overline{U}$ is velocity scale, f_o is the coriolis parameter, which is negative in the southern hemisphere, and L is the horizontal scale.

$F_1 = \dfrac{f_o^2 L^2}{g' D_1}$ is the constant and g′ is the reduced gravity.

$F_2 = \dfrac{f_o^2 L^2}{g' D_2}$ is a constant

$g' = g\frac{\Delta\theta}{\bar{\theta}}$, $\Delta\theta$ is the change in potential temperature across the interface and $\bar{\theta}$ is the mean potential temperature.

The amplitude of the interface perturbation is:

$\varsigma_2 = \varepsilon D_2 F_2(\psi_2 - \psi_1)$ where ψ_1 and ψ_2 are stream functions for upper and lower layers. Assuming steady flow i.e. $\frac{\partial}{\partial t} = 0$ and a solution of the form

$\phi_i = \psi_i + U_i y$ and substitute it in equation (7.1) and (7.2) for I = 1,2.

The equation in (7.1) and (7.2) become:

$$\nabla^2\phi_1 + F_1\phi_2 + \beta y = \gamma_1\phi_1 + (F_1U_2 - \gamma_1U_1)y \qquad (7.3)$$

$$\nabla^2\phi_2 + F_2\phi_1 + \beta y + R_S = \gamma_2\phi_2 + (F_2U_1 - \gamma_1U_{12})y \qquad (7.4)$$

where:

$$\gamma_1 = \frac{(F_1U_2 - \beta)}{U_1}, \gamma_2 = \frac{(F_2U_1 - \beta)}{U_2}$$

Adding equation (7.3) to α x (7.4) and simplifying results into:

$$\nabla^2\Phi - \lambda\Phi = -\alpha R_s \qquad (7.5)$$

This is the Helmholtz equation and depends on the sign of λ. If $\lambda > 0$, then an evanescent solution (confined to the obstacle) exists and if $\lambda < 0$ then it is a wave-like solution.

where:

$\lambda = -\alpha F_2 + \gamma_1$ satisfies the quadratic equation.

$$\alpha^2 - \alpha(\gamma_1 - \gamma_2)/F_2 - F_1/F_2 = 0,$$

and the normal modes are given by $\Phi^{(i)} = \phi_1 + \alpha^{(i)}\phi_2$

for i = 1, 2

Solving for α

$$\alpha_1 = (\gamma_1 - \gamma_2)/2F_2 + \left\{\left[(\gamma_1 - \gamma_2)/2F_2\right]^2 + \frac{F_1}{F_2}\right\}^{0.5}$$

$$\alpha_2 = -(\gamma_1 - \gamma_2)/2F_2 + \left\{\left[(\gamma_1 - \gamma_2)/2F_2\right]^2 + \frac{F_1}{F_2}\right\}^{0.5}$$

The normal mode solution are given as :

$$\phi_1 = [\alpha^{(1)}\Phi^{(2)} - \alpha^{(2)}\Phi^{(1)}]/(\alpha^{(1)} - \alpha^{(2)}) \quad (7.6)$$

$$\phi_2 = [\Phi^{(1)} - \Phi^{(2)}]/(\alpha^{(1)} - \alpha^{(2)}) \quad (7.7)$$

7.8.2 Solution to the quasi-geostrophic model

The solutions of equation (7.5) with the following boundary conditions:

If $\lambda > 0$, the boundary condition $|\Phi| \to 0$ as $x^2 + y^2 \to \infty$

But if $\lambda < 0$, the wave -like solutions are not uniquely determined

A radiation condition is applied: $(x^2 + y^2)^{.25}\Phi \to 0$, $x \to -\infty$

The general solutions of equation (7.5) with appropriate boundary conditions are determined in terms of Green's Function.

$$\Phi(x,y) = \alpha \int_{-\infty}^{\infty} d\xi \int_{-\infty}^{\infty} R_S(\xi,\eta) G(x,y;\xi,\eta) d\eta \quad (7.8)$$

where the Green's function G(x,y; ξ,η) is given by

$\lambda > 0$

$G(x,y;\xi,\eta) = (1/(2\Pi))*K_0(\lambda^{0.5}r)$

and for $\lambda < 0$

$$G = (x,y;\xi,\eta) = -.25\left\{ Y_0[(-\lambda)^{.5}r] + \frac{4}{\pi}\sum_{n=1}^{\infty} J_{2n-1}[(-\lambda)^{.5}r] Cos[2n-1)\theta]/(2n-1) \right\}$$

where $r^2=(x-\xi)^2+(y-\eta)^2$

$\theta = \tan^{-1}(y-\eta)/(x-\xi)$

K_0, Y_0 and J_{2n-1} are Bessel functions, which are obtained by calling the NAG subroutines. Thus the general solutions can be used to investigate the effects of arbitrary functions of heating/orography distributions. Numerical integration was utilised to evaluate the double integrals.

Surface Heating

As has been illustrated in the paper of Fandry and Leslie (1984) the surface heating can be represented by:

$$S(x,y) = h_B(x,y) + \frac{T_B(x,y)}{\gamma}, \quad (7.9)$$

where h_B is orography, T_B is temperature distribution, and γ is the lapse rate (γ = -6.5 x 10^{-3} °C m^{-1}). The function S(x,y) represents elevation and surface heating. In this case $h_B(x,y) = 0$. Thus surface heating is applied at the lower

boundary. The temperature distribution can be given as an arbitrary function.

Wind Flow

The wind cross section suggests that in the upper level westerly flow prevails ($U_1>0$) and below 500 hPa we have easterly flow ($U_2<0$). **Figure 7.16(c)** is a schematic diagram of the model showing upper level westerlies and lower level easterlies.

Scaling Parameters

Scaling parameters for Southern Africa are given as:

$$L = 10^6\, m, D_1 = 8km, \overline{U} = 10ms^{-1}, f_o = -.426392 \times 10^{-4} S^{-1} \text{ at } 17°S$$

$f_0 = -0.6\ X10^{-4}\ s^{-1}$ at 22.5°S, $D_2 = 3000$ m, $\beta_0 = 2 \times 10^{-11}\ m^{-1}\ s^{-1}$,

$g \cong 10\ m\ s^{-2}$ $\quad \frac{\Delta\theta}{\theta} = 0.1$

The level at which easterlies change to westerlies is assumed to be at 500hPa

$\varepsilon = 0.23452$, $F_1 = 0.22726$, $F_2 = 0.363616$, $U_2 = -1$, which is the easterly current in the lower level $U_1 = 1$ which is westerly in the upper level

$\gamma_1 = -2.22726$, $\gamma_2 = 1.63638$, $\alpha_1 = 10.6636$, $\alpha_2 = 0.02466$, $\lambda_2 = -2.13826$

Equation: $\nabla^2\Phi + \lambda\Phi = \alpha R_s$ (7.10)

7.8.3 Results of numerical experiments

From observations, the continental trough is seen to vary on daily to interannual scales. The trough may be strong in some years and weak in others, with consequences for the behaviour of summer rainfall. In some ENSO years, strong lows develop over the western Indian Ocean where high SST are observed (Mason, 1992; Rocha ,1992). The behaviour of the continental trough may depend on differential heating between land and the adjacent oceans. In order to explore this, four numerical experiments were set up. The first experiment deals with isolated heating over the 'continent', the second one involves cooling the adjacent 'oceans' and heating the 'continent' (e.g. increased differential) and the third one is cooling the Atlantic 'Ocean' and warming Indian 'Ocean' (asymmetric). The fourth experiment allows for a varying circulation. Generally, disturbances are expected to be much larger in the lower levels where localised heating (cooling) is associated with cyclonic

(anticyclonic) circulation.

Effects of isolated continental heating

The effects of localised heat sources are investigated. **Figure 7.17(a)** shows the heating of the western parts of the subcontinent. This heating represents a land-sea temperature contrast with maximum temperature at the western parts of the subcontinent (x = -1). In terms of orography the heating can be represented by T_B/γ. The solution is found for $U_1 = 1$, $U_2 = -1$. From **figure 7.17(b)** and **7.17(c)** the perturbations are much larger in the lower layer than in the upper layer. A trough has formed over the Angola region due to localised heating. In the upper layer wave like streamlines are observed in the solution. **Figure 7.18(a)** shows an idealised heating anomaly over the Kalahari Desert. The heating anomalies are greatly amplified in order to have large response. The response of the heating is displayed in **figure 7.18(b) and 7.18(c)** for lower and upper layers respectively. In the lower layer the disturbance is confined to the heating anomaly.

Effect of cool Oceans and warm continent

Figure 7.19(a) shows an idealised heating anomaly distribution with cool Atlantic and Indian 'oceans'. Maximum heating is over the continent. Low level easterly winds and upper level westerly winds are assumed with equal strength. The low-level streamline patterns indicate that a trough is developed over the 'continent' as a result of localised heating (see **figure 7.19(b).** Ridges are formed over the cooler 'oceans' in response to the negative temperature anomalies. At the upper level where the flow is westerly, weak troughs develop over cooler areas and a weak ridge over the heated 'land' area (see **figure 7.19(c).**

Effect of Asymmetric heating

The influence of warming the Indian 'Ocean' and subcontinent and cooling the Atlantic Ocean was investigated by applying the heating anomaly as shown in **figure 7.20(a)**. Warming to the east is weaker but extends over a larger area than for the 'continent'. Low level troughs develop over the heated areas in proportion to the anomaly imposed (see **figure 7.20(b)).** A ridge forms over the

Atlantic 'Ocean' and in the region between the troughs. The areas under this anticyclonic flow may be linked to below normal rainfall.

Varying circulation

In order to investigate the effect of varying the circulation with a large differential heating (e.g. cool oceans and warm continent), the low-level winds were assumed to be westerly and upper level winds easterly. **Figure 7.21(a)** shows the imposed heating. Advection of anticyclonic flow is observed over the tropics outside of the heating anomaly (see **figure 7.21(b).** Strong anticyclonic flow develops west of the 'continent' and over the Indian 'Ocean'. A pronounced cyclonic flow develops polewards of the heating anomaly. The upper circulation is unperturbed and remains easterly (see **figure 7.21(c)).**

7.9 Discussion and summary

Many local meteorologists have observed the importance of the Angola low. This thermal low has been associated with recurving of Atlantic southeasterly flow into Congo air. However, its physical explanation has been speculated to be surface heating, but the dynamical modelling of this feature has not been done. The surface heating which has been parameterised as orography in the linear quasi-geostrophic model has successfully explained the existence of the Angola low. Thus large land-sea temperature contrasts could play an important role in influencing the low-level flow over Southern Africa.

The plateau with maximum springtime heating over Angola may maintain a large-scale thermally driven vertical circulation, which is distinct from the planetary circulation. The heat source (warming) over the plateau and heat sink (cooling) in surrounding oceans can enhance the regional circulation with low and high pressure over land and ocean respectively. Sensible heat flux from the surface may provide the major source of heating on the plateau. Additional heating from condensation heating can further deepen the low over the subcontinent and thus allows more moisture convergence. Insufficient moisture e.g. in early spring can result in decay of the large-scale convective system. Thus sensible heating by the elevated plateau feeds the Angola low which maintains a large-scale thermally driven vertical circulation. The Angola low

may play an important part in determining the onset of the summer circulation. The interaction process between the plateau-induced circulation and large-scale NE monsoon circulation is important. Sensible heating of the elevated plateau surface and radiative cooling in the environment maintain the horizontal temperature contrast that drives the thermally direct vertical circulation.

Summary of intraseasonal oscillations

The dynamic and thermal characteristics of the atmosphere associated with deep convective anomalies over Angola have been presented in section 7.7. The convective anomalies have periods ranging from 10-30 days. It is suggested that the period may due to local or regional factors. In summary, the anomalous convective activities are characterised by the following features:-

(a) Before the onset a cold low is well established over the southern Indian Ocean and this is later transformed into a warm high at the time of deep convection. Over land a broad-trough develops between 10°S and 25°S with an intense low over eastern parts of Madagascar and the Indian Ocean (50°E, 30°S). A frontal system appears over the western coast during the convective period. Thus there is an interaction between the tropics and midlatitudes. Moisture comes from both the Indian subtropics and the equatorial Atlantic Oceans.

(b) Baroclinic structure is observed at P_0 in the wind and divergence anomalies over the tropical regions, but a barotropic structure over the midlatitudes. Low level westerlies and upper level easterlies are observed in the equatorial band. Cold and warm core fields are observed in lower and upper levels respectively. Mid and upper-tropospheric warming imply an eastward propagating feature (Chang and Lim 1988). Maximum moisture convergence is over Angola and this reduces the need for strong shear for the disturbance to develop (Lau and Peng 1990). Upward motion is strong over southeastern Angola and the Zambezi valley in the lower and midtroposphere, with downward motion over the mid-latitudes Southwest Indian and the eastern Atlantic Oceans. An indirect circulation in the low levels and direct circulations in the middle and upper troposphere are found where the energy is created to maintain the deep

convection through the release of latent heat. Strong easterlies in the upper levels create vertical easterly shear, which intensifies the disturbance in the tropics (Lau and Lim 1984). The easterly wind shear confines the unstable waves to the lower troposphere (Xie and Wang, 1996). The 200hPa-divergence field suggests a westward propagating feature in the upper levels.

(c) Along 17°S, there is strong convergence at 20°E, and divergence at 55°E, suggesting an out-of-phase pattern for the convective anomalies in these two areas. OLR PC1, PC2 and PC3 support out-phase convective activities between central Southern Africa (17°S, 21E°) and the Indian Ocean region (17°S, 52°E). The dipole structure is best depicted in pentad OLR PC2.

(d) The anchoring is well depicted in the OLR, precipitable water, 200hPa divergence fields at P_0 and in pentad OLR PC3.

The dynamic and temporal structure of convective activities associated with Angola low has been presented. Through numerical modelling and the use of quasi-geostrophic theory, it has been demonstrated that surface heating plays an important role in the formation of the inland thermal low. Quasi-geostrophic linear theory suggests that localised heating and cooling is associated with cyclonic and anticyclonic anomalous flow in low levels respectively. In easterly low level flow, the perturbation is confined to the heated area, but under low-level westerly flow the disturbance is not confined. This is consistent other modelling results (Xie and Wang, 1996; Lau and Lim, 1984).

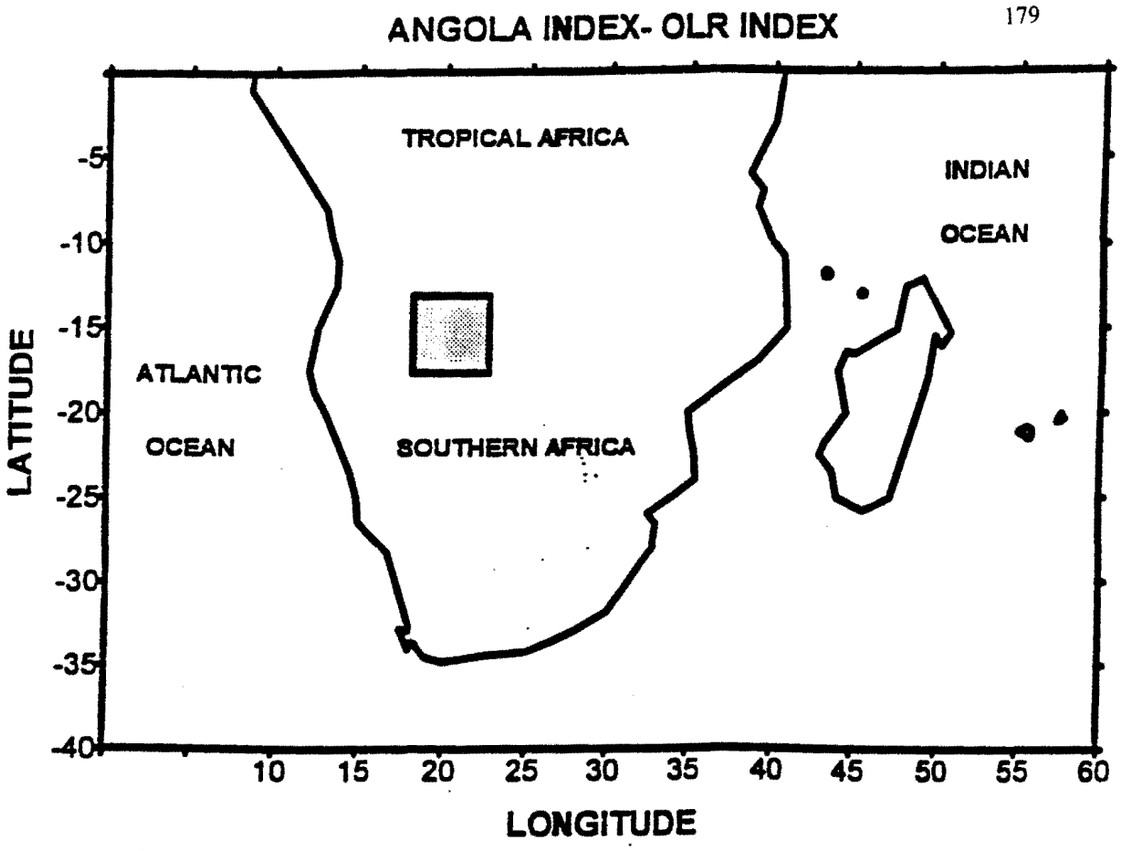

Figure 7.1 (a) Map of study domain and the shaded rectanlgle is the area where the OLR-index (Anglola) was extracted.

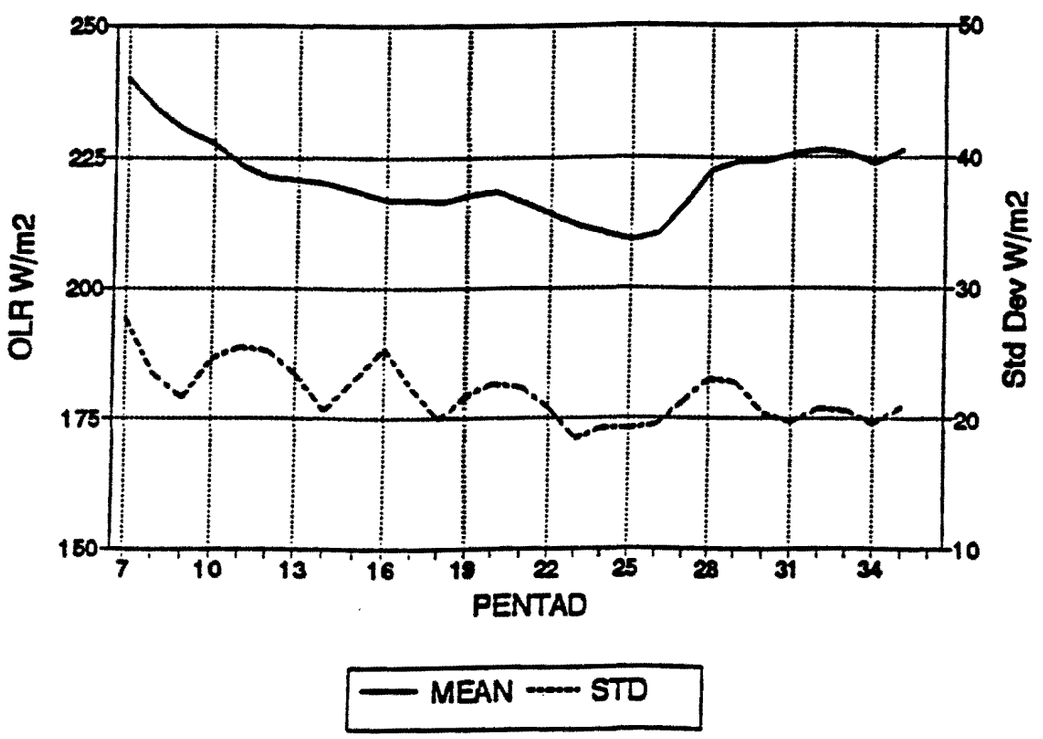

Figure 7.1 (b) Historical mean and standard deviation of Angola Index.

a

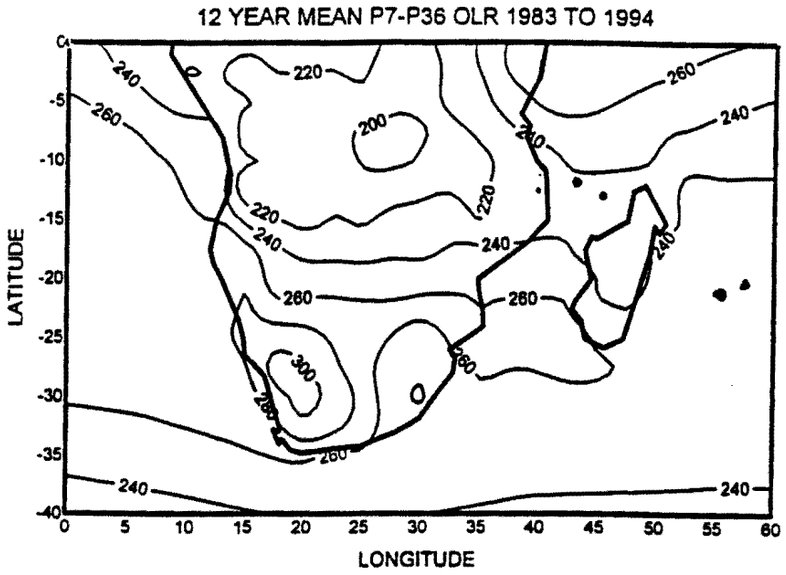

Figure 7.2 (a) Spatial distribution of the mean P7-P36 OLR from 1983 to 1994.

b

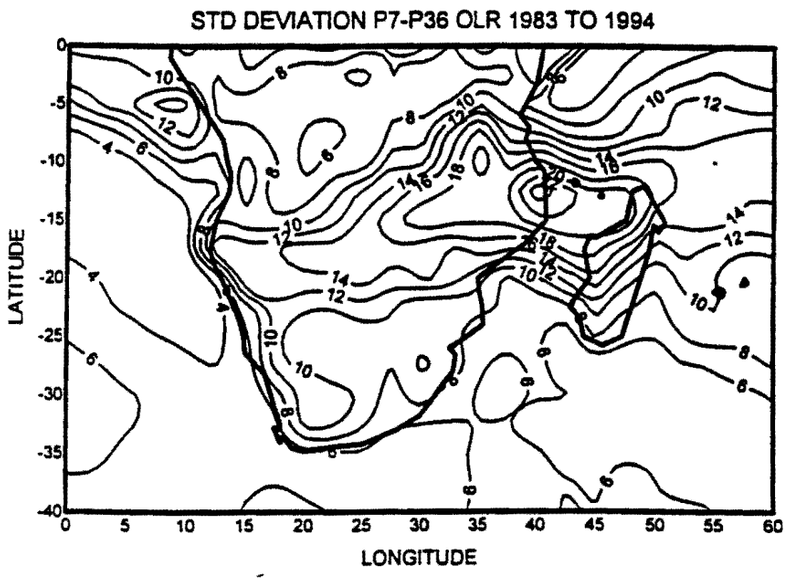

Figure 7.2 (b) Spatial distribution of the standard deviation.

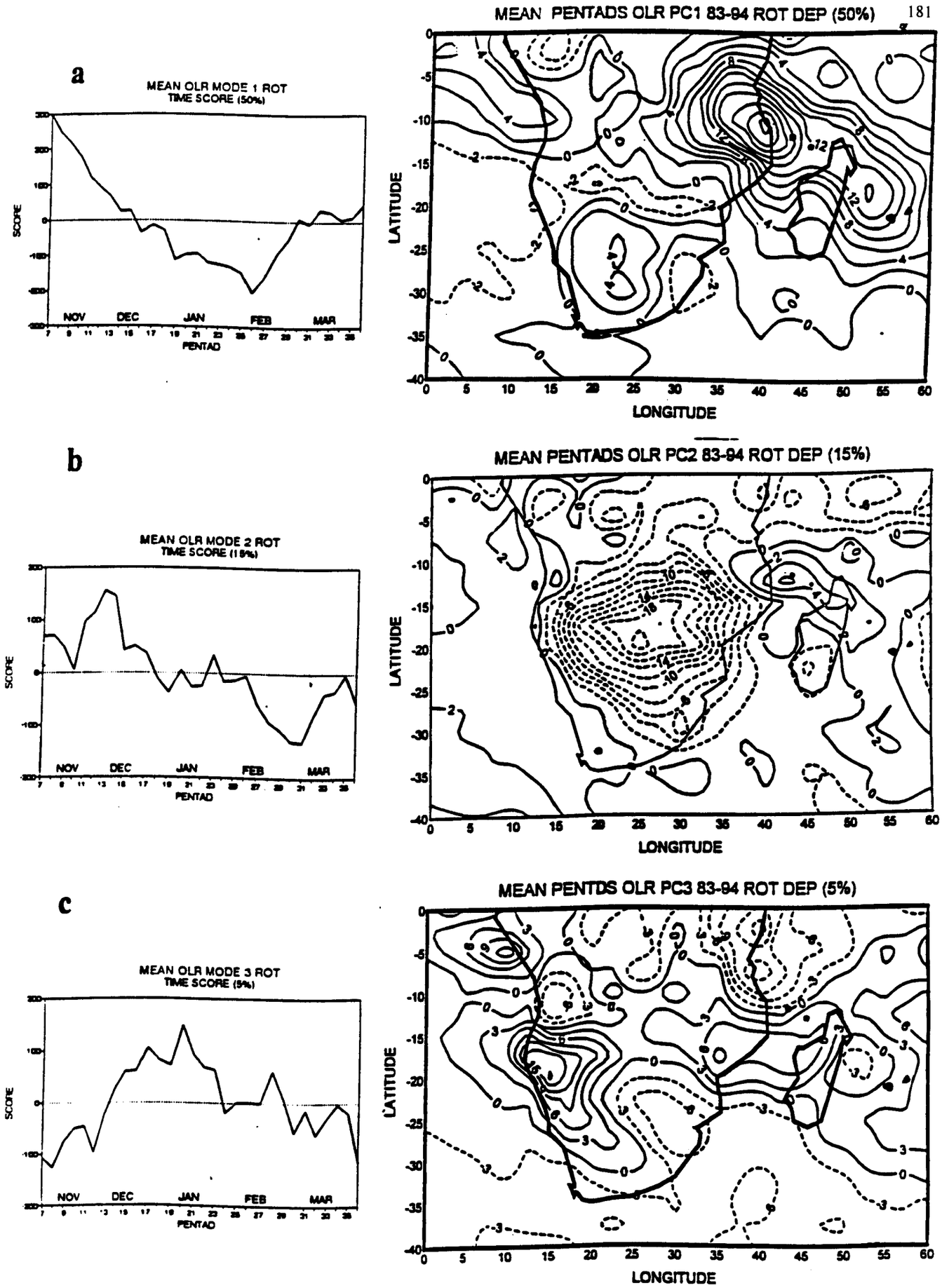

Figure 7.3 (a) Distribution of the first PC of mean OLR pentads for the period 1983 to 1994 and the associated time series. (b) Same as figure (a) but for PC2. (c) Same as figure (a) but for PC3.

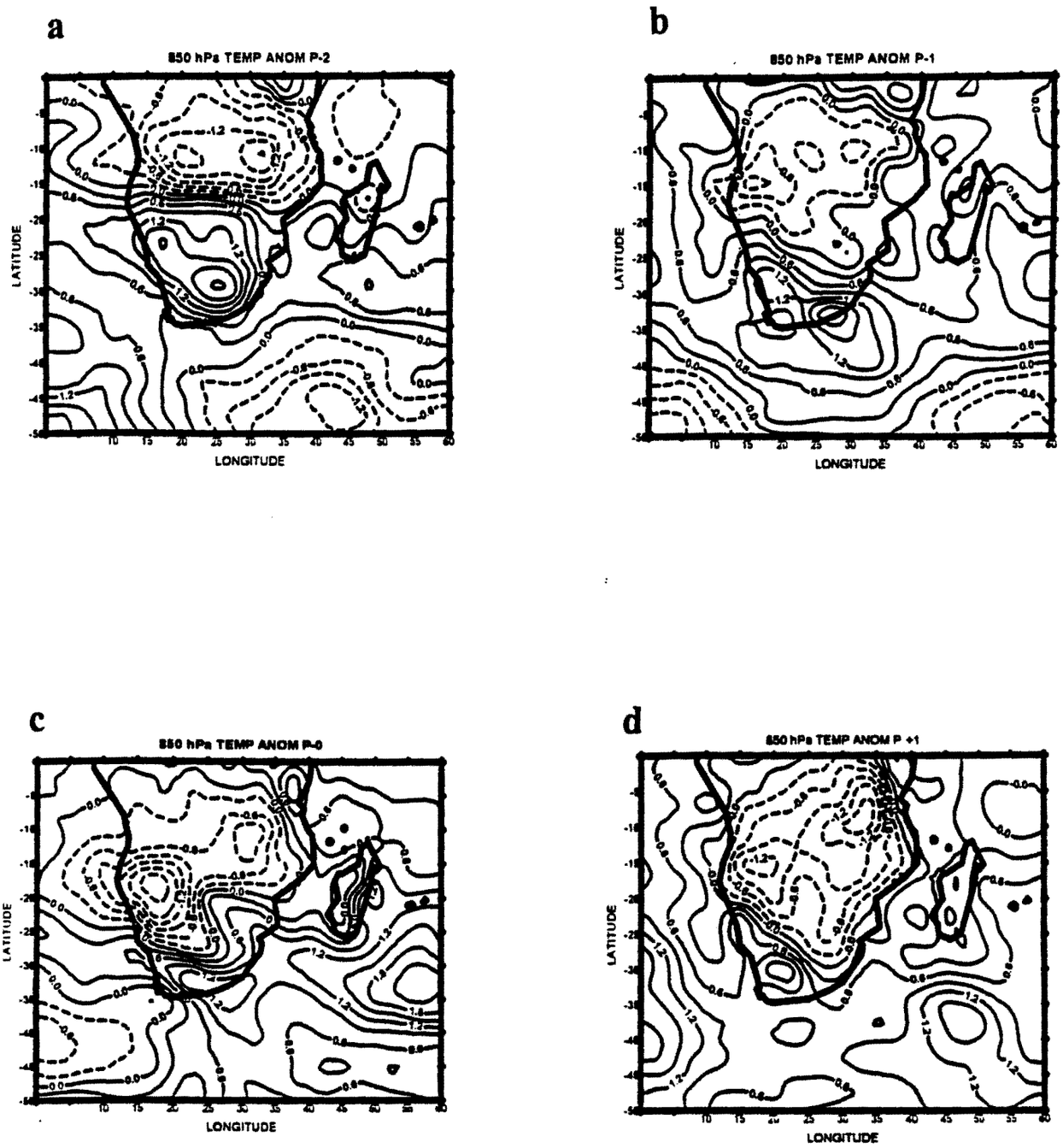

Figure 7.4 (a) Composite anomaly for 850 hPa temperature at P_{-2}. (b) Same as in figure (a) but for P_{-1}. (c) As in figure (a) but for P_0. (d) Similar to (a) but for P_{+1}. Contour interval is 0.3°C.

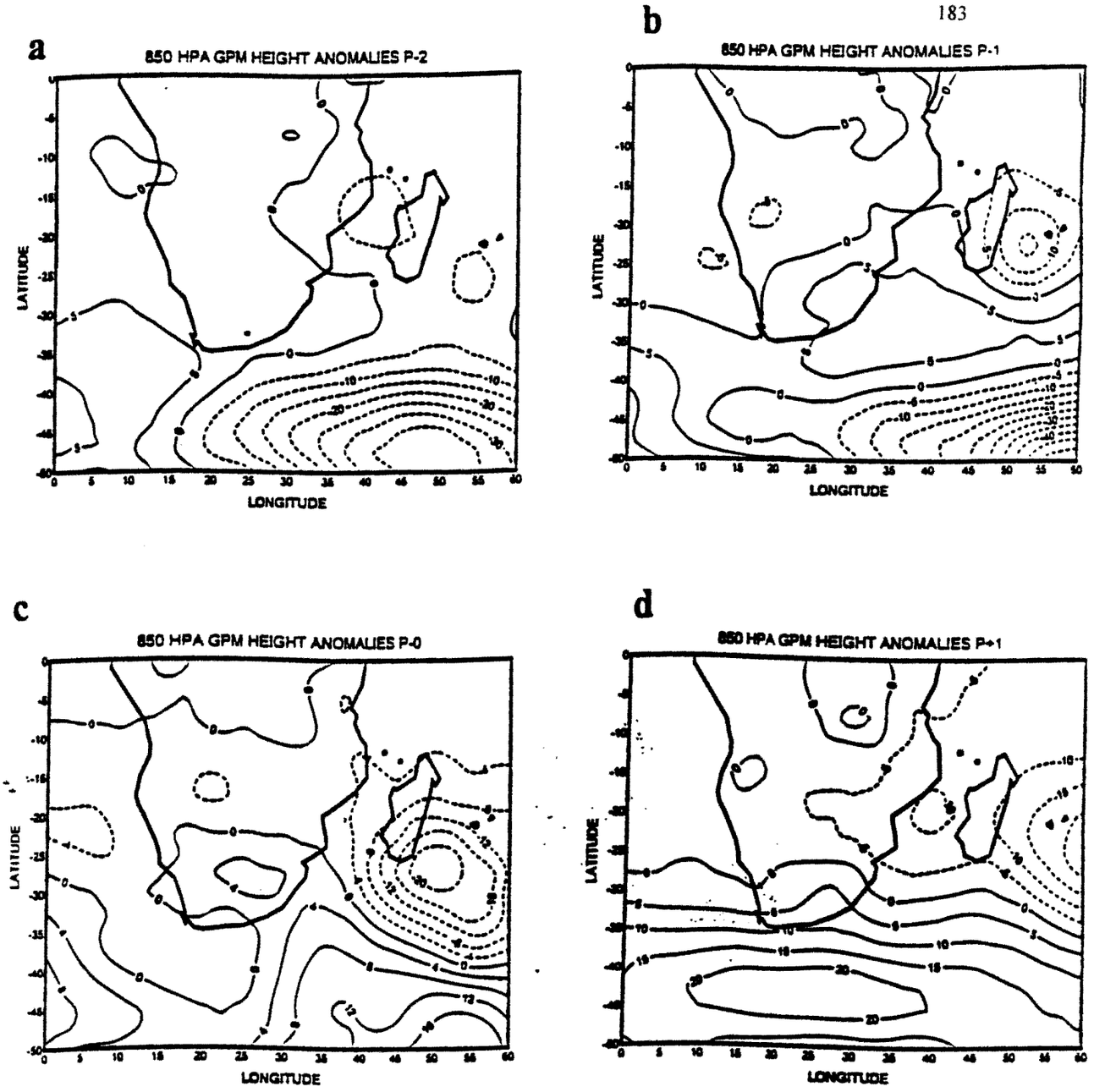

Figure 7.5 (a) Composite anomaly for 850 hPa geopotential height at P_{-2}. The contour interval is 5 meters. (b) Same as in figure (a) but for P_{-1}. (c) As in figure (a) but for P_0. (d) Similar to (a) but for P_{+1}.

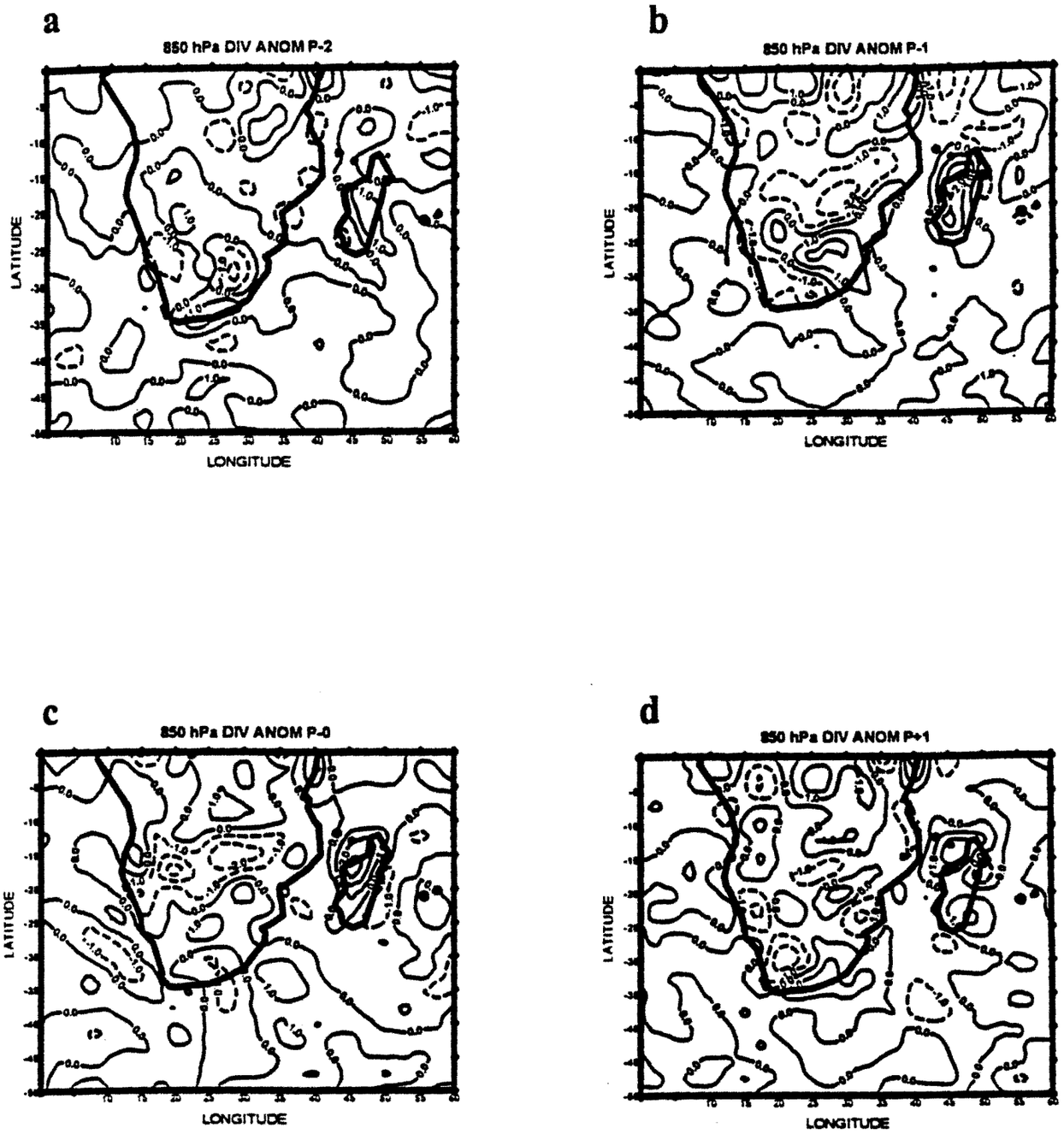

Figure 7.6 (a) Composite anomaly for 850 hPa divergence at P_{-2}. (b) Same as in figure (a) but for P_{-1}. (c) As in figure (a) but for P_0. (d) Similar to (a) but for P_{+1}.. Contour interval is 1.0 x $10^{-5}s^{-1}$.

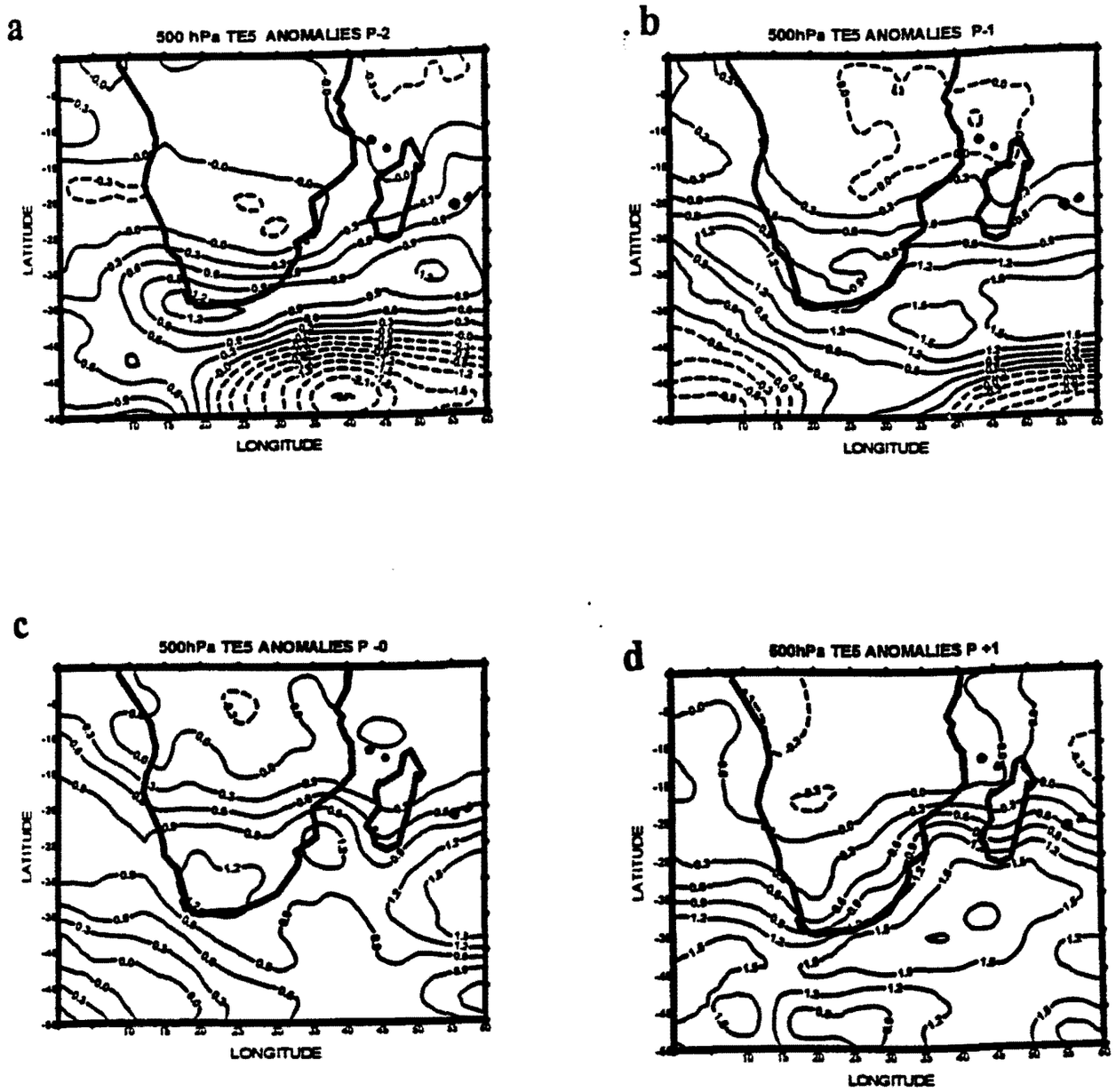

Figure 7.7 (a) Composite anomaly for 500 hPa temperature at P_{-2}. (b) Same as in figure (a) but for P_{-1}. (c) As in figure (a) but for P_0. (d) Similar to (a) but for P_{+1}. The contour interval is 0.3°C.

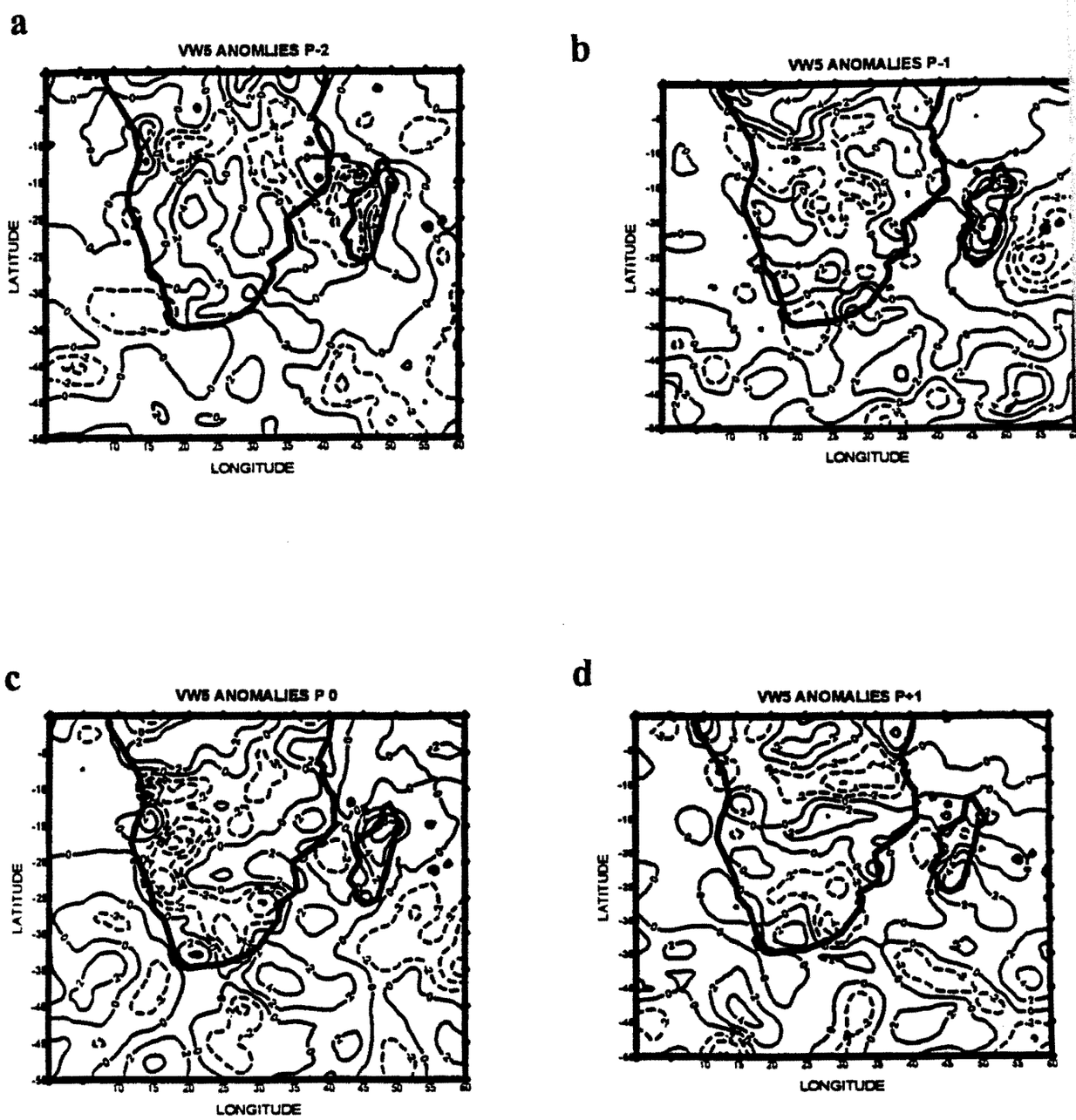

Figure 7.8 (a) Composite anomaly for 500 hPa vertical velocity at P_{-2}. (b) Same as in figure (a) but for P_{-1}. (c) As in figure (a) but for P_0. (d) Similar to (a) but for P_{+1}. The contour interval is 2.0 x 10 Pa s^{-1}

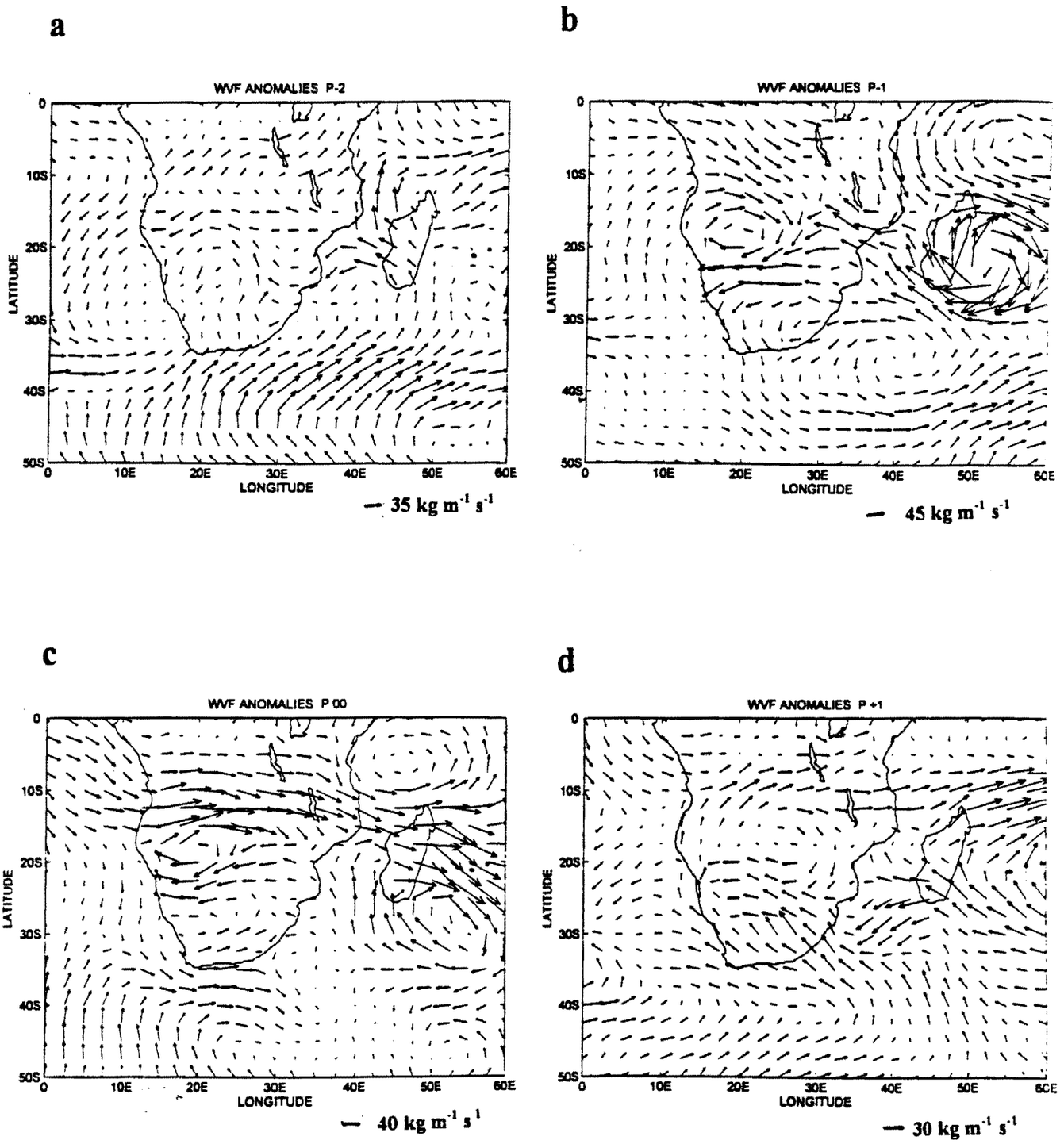

Figure 7.9 (a) Composite anomaly for Water Vapour Flux at P_{-2}. (b) Same as in figure (a) but for P_{-1}. (c) As in figure (a) but for P_0. (d) Similar to (a) but for P_{+1}.

a

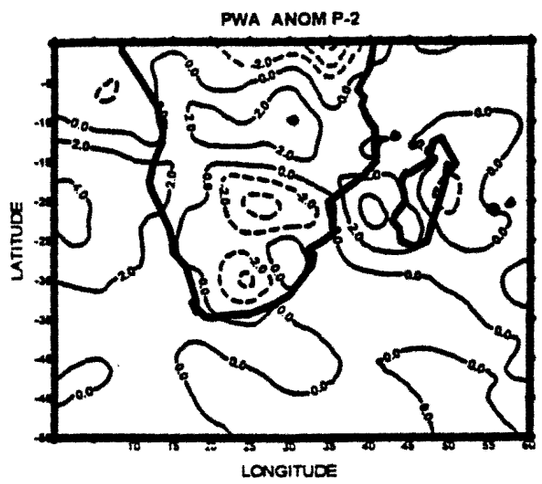

b

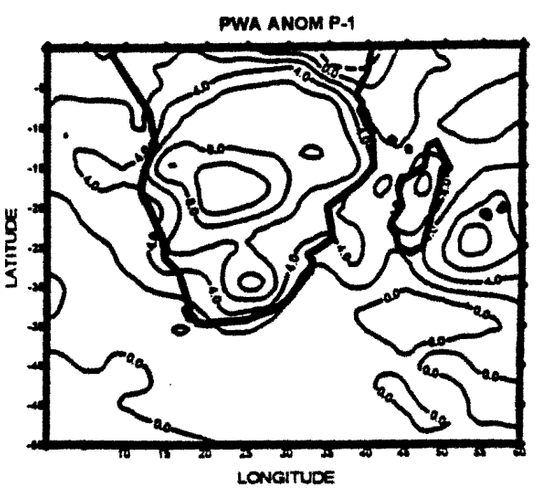

c

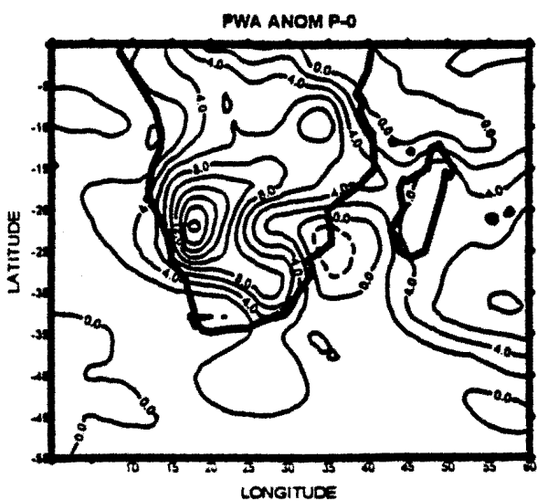

d

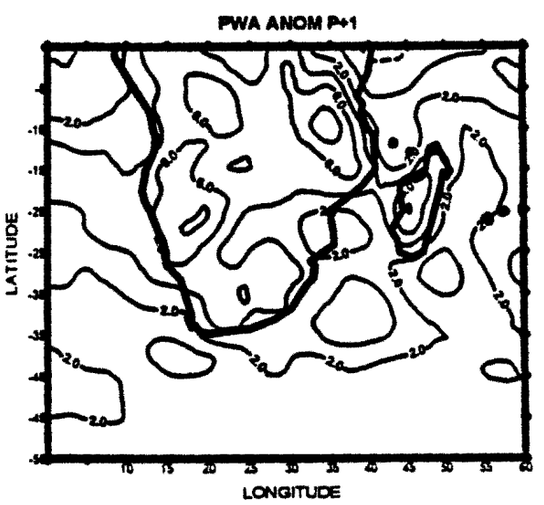

Figure 7.10 (a) Composite anomaly for Precipitable Water at P_{-2}. (b) Same as in figure (a) but for P_{-1}. (c) As in figure (a) but for P_0. (d) Similar to (a) but for P_{+1}. The contour interval is 2.0mm

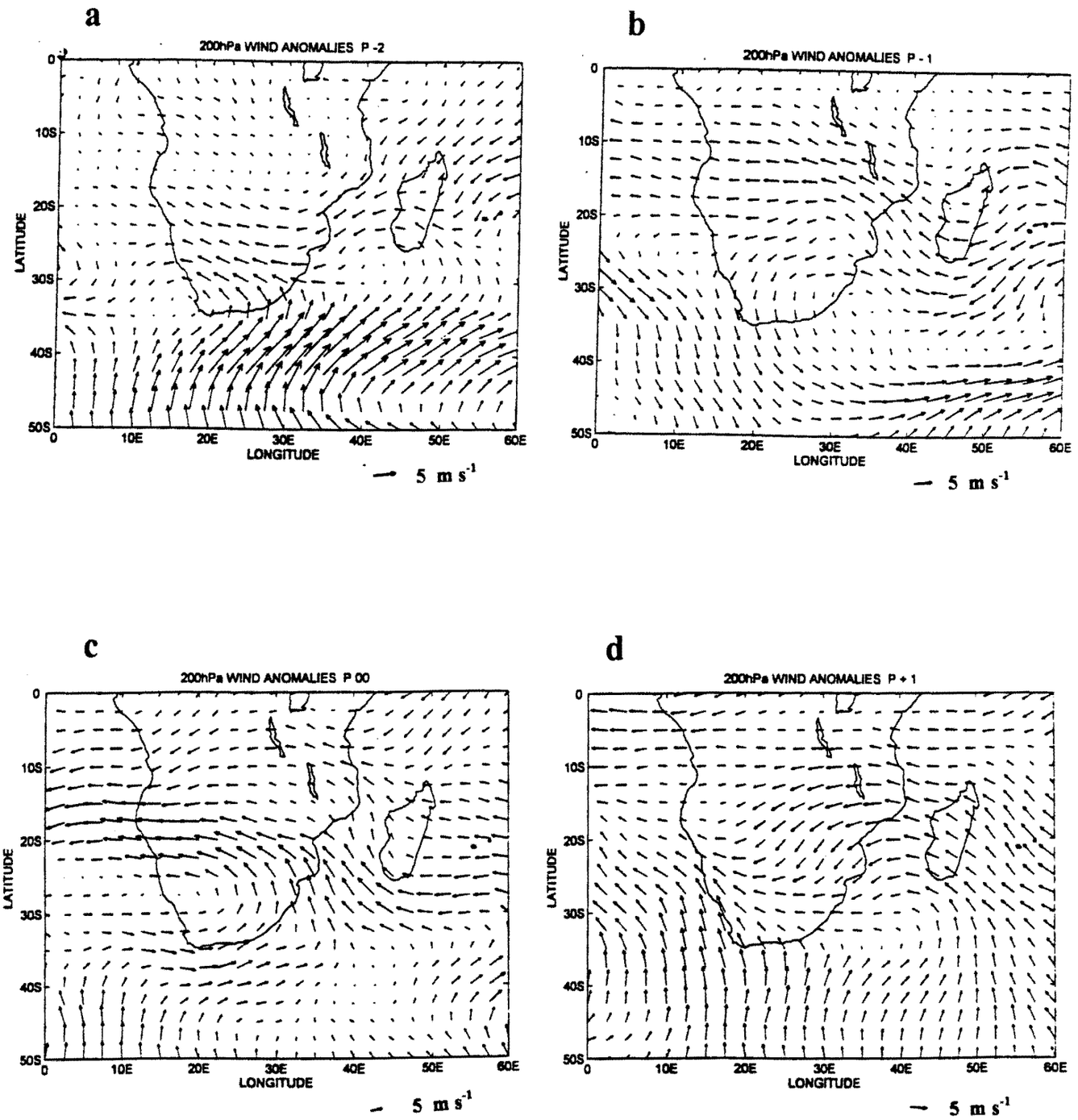

Figure 7.11 (a) Composite anomaly for 200 hPa zonal winds at P_{-2}. (b) Same as in figure (a) but for P_{-1}. (c) As in figure (a) but for P_0. (d) Similar to (a) but for P_{+1}.

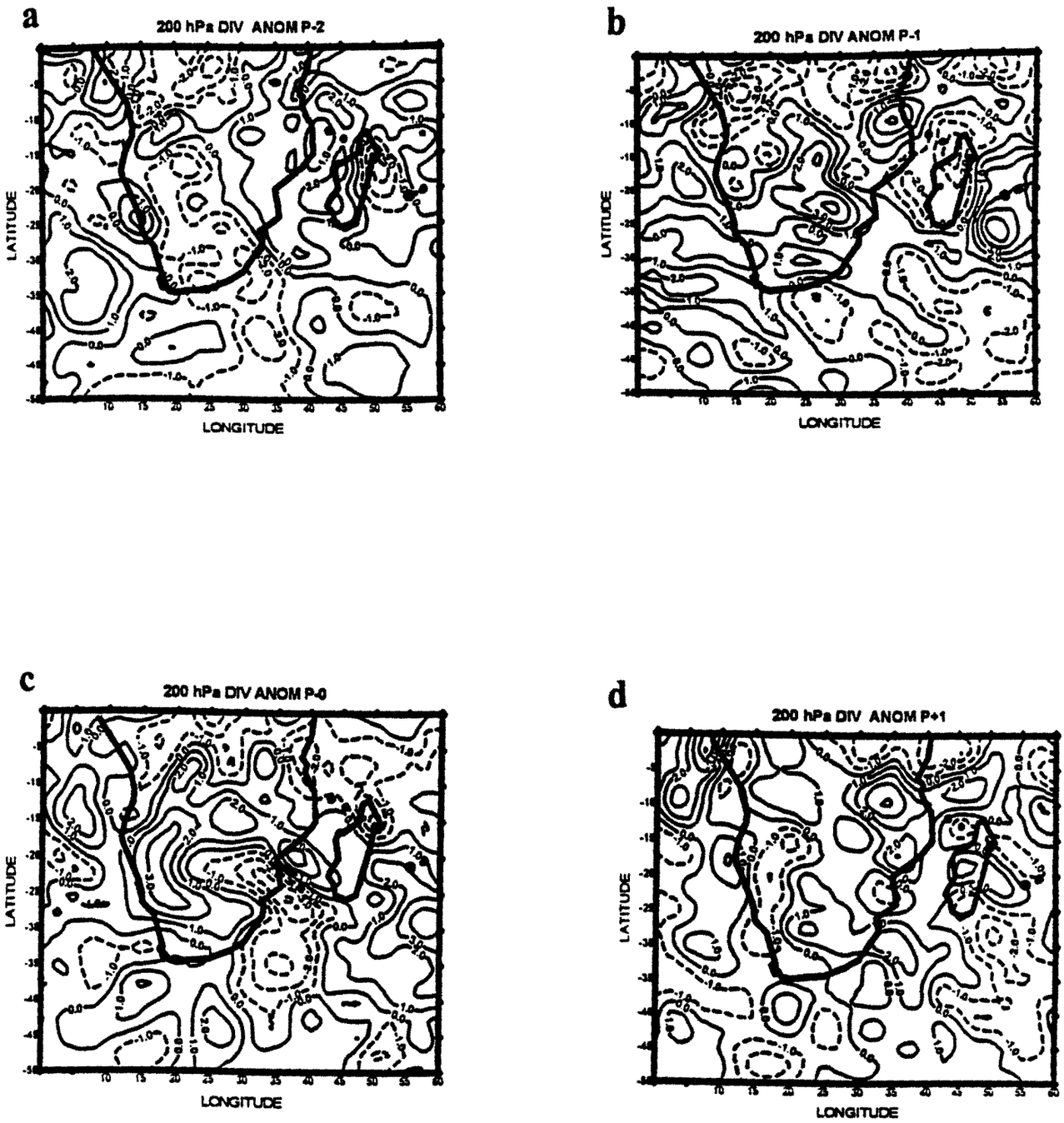

Figure 7.12 (a) Composite anomaly for 200 hPa divergence at P_{-2}. (b) Same as in figure (a) but for P_{-1}. (c) As in figure (a) but for P_0. (d) Similar to (a) but for P_{+1}. The contour interval is 1.0 x 10^{-5} s^{-1}.

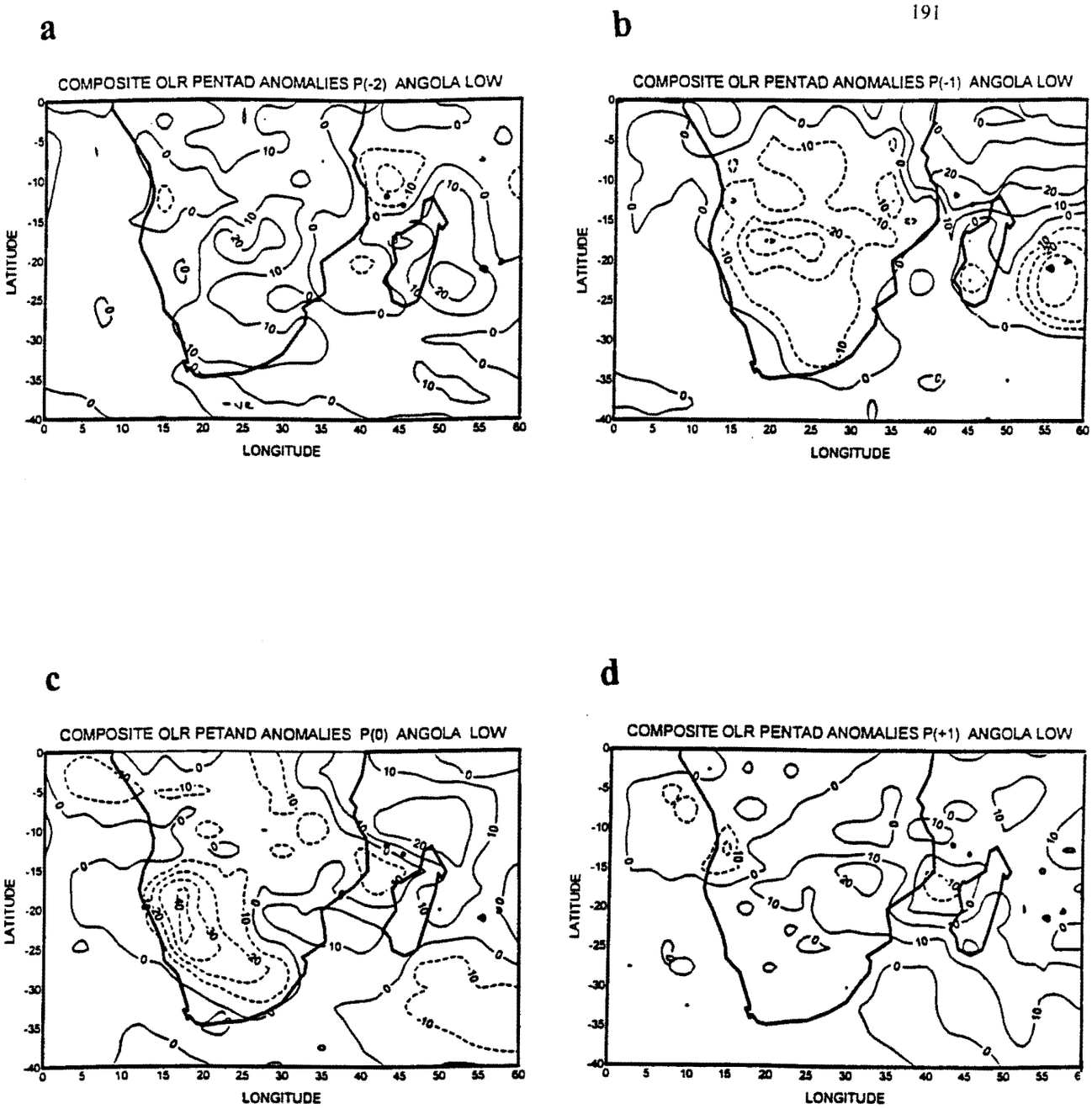

Figure 7.13 (a) Composite anomaly for OLR at P_{-2}. (b) Same as in figure (a) but for P_{-1}. (c) As in figure (a) but for P_0. (d) Similar to (a) but for P_{+1}. The contour interval is 10Wm^{-2}.

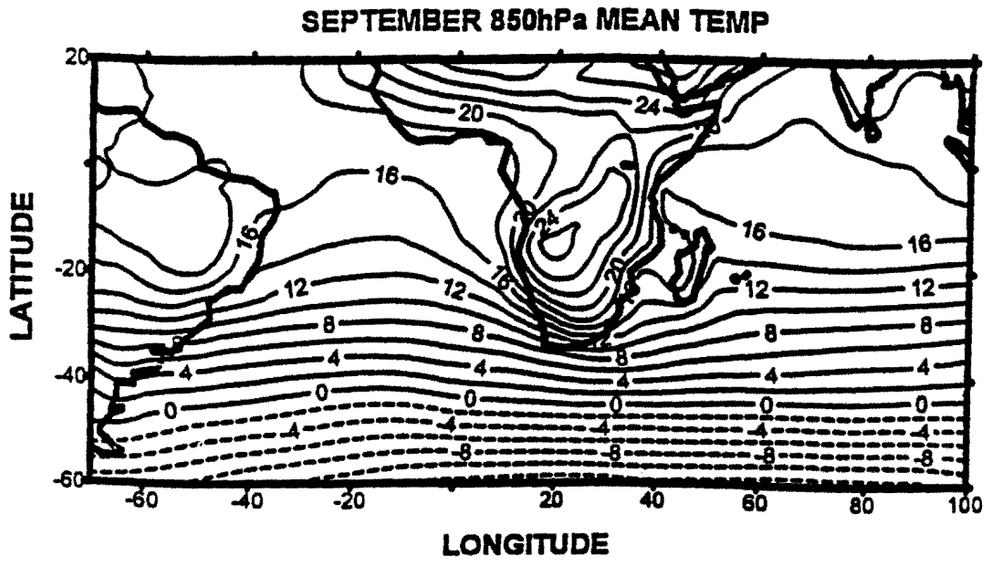

Figure 7.14 (a) Mean September 850 hPa temperature. Contour interval is 2°C.

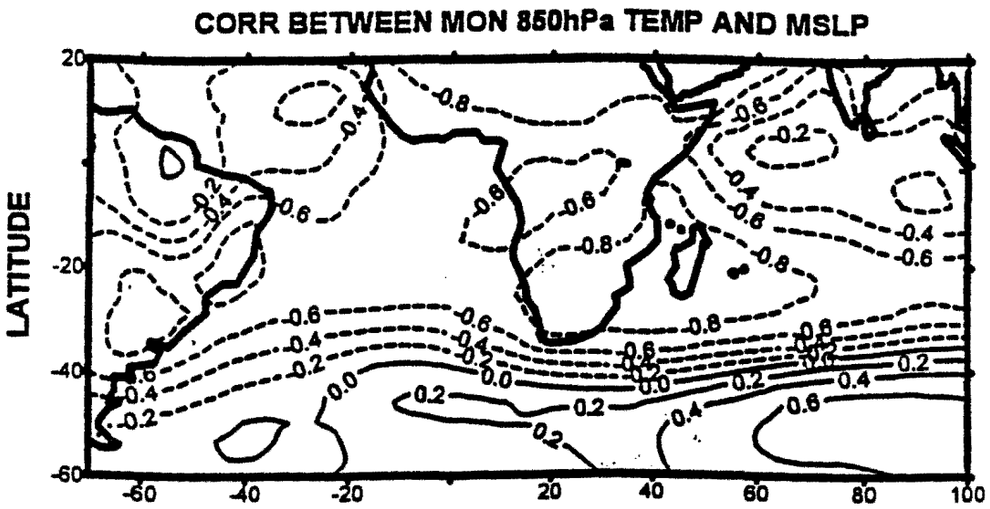

(b)Simultaneous temporal correlations between 850 monthly temperature and mean sea level. Contour interval is 0.2

c

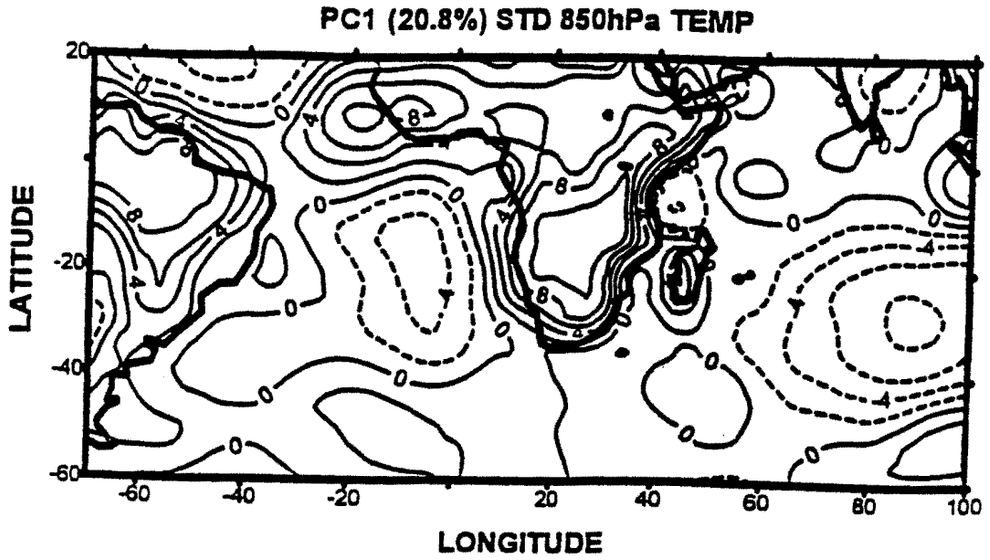

Figure 7.15 (a) Distribution of the first PC (20.8%) of standardised monthly mean 850 hPa temperature anomalies for all months based on the data described in chapter 2. Contour interval is 2 (arbitrary units).

d

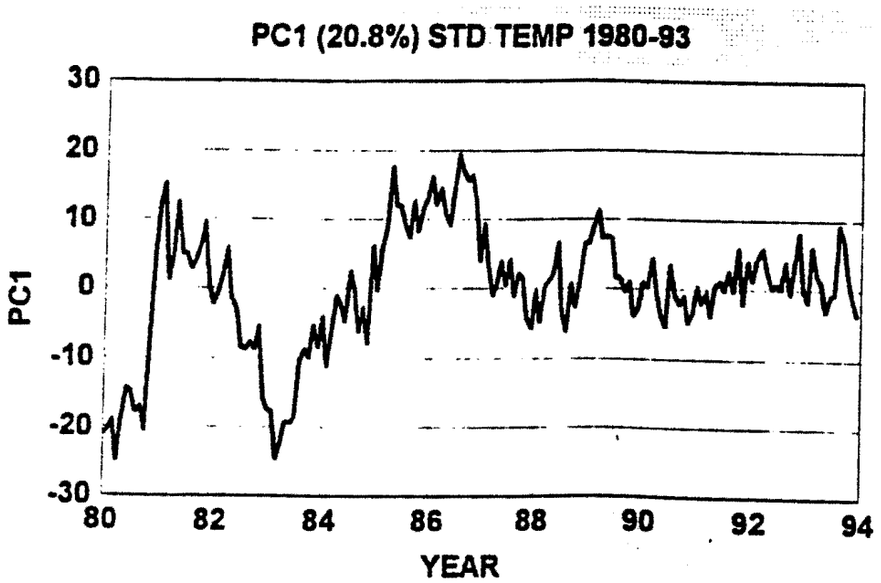

Figure 7.15 (b) Time series of the coefficients assocated with the first PC in figure 7.15(a)

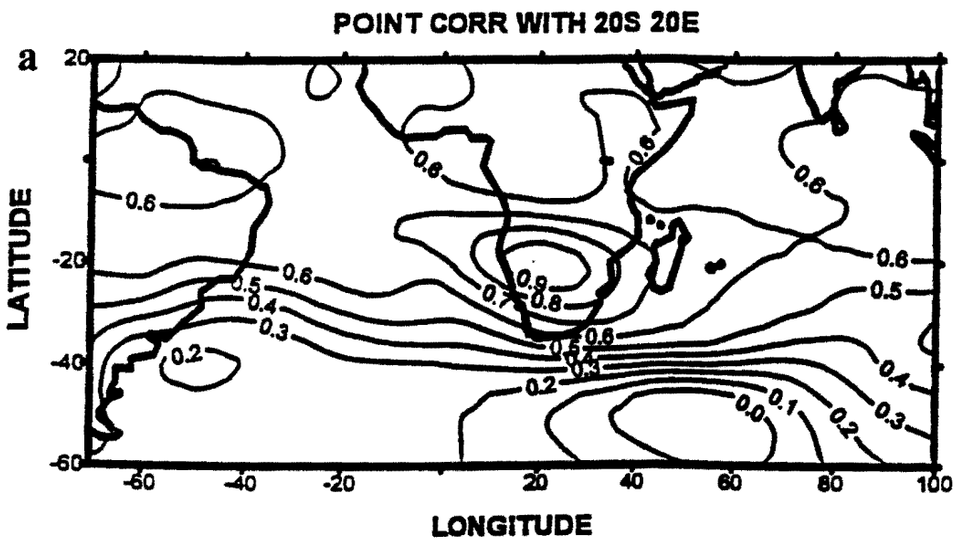

Figure 7.16 (a) Simultaneous temporal correlations between 500-200 hPa thickness monthly anomalies at grid point 20°S, 20°E and other grid points based on the data set described in chapter 2. Contour interval is 0.1.

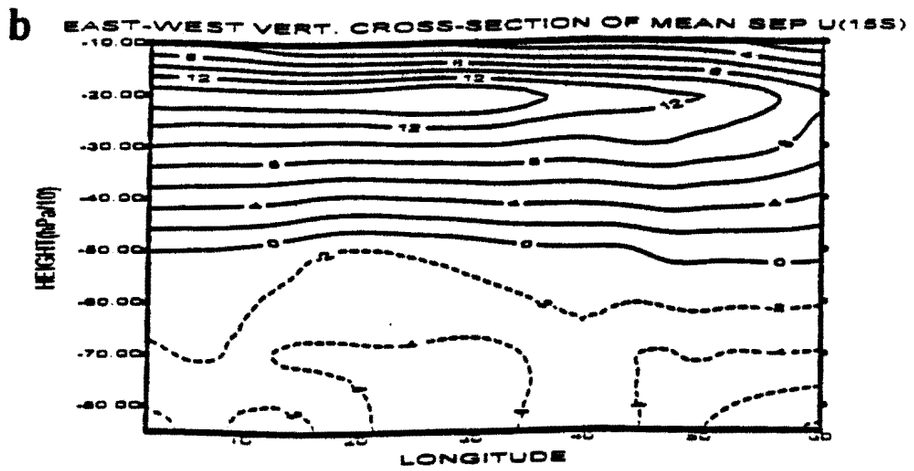

Figure 7.16 (b) Zonal vertical cross section of mean September zonal wind component. Contour interval is 2 m s^{-1} .

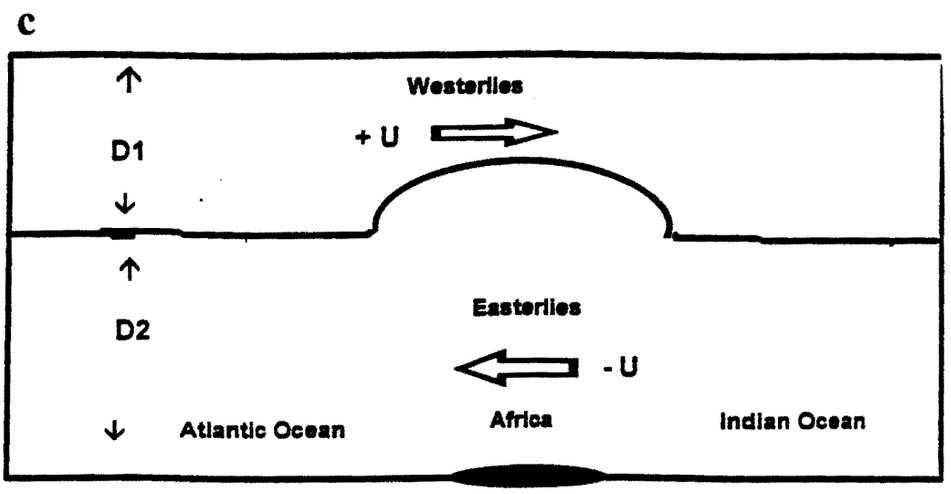

Figure 7.16 (c) Schematic diagram of the model depicting upper level westerlies and low level easterlies.

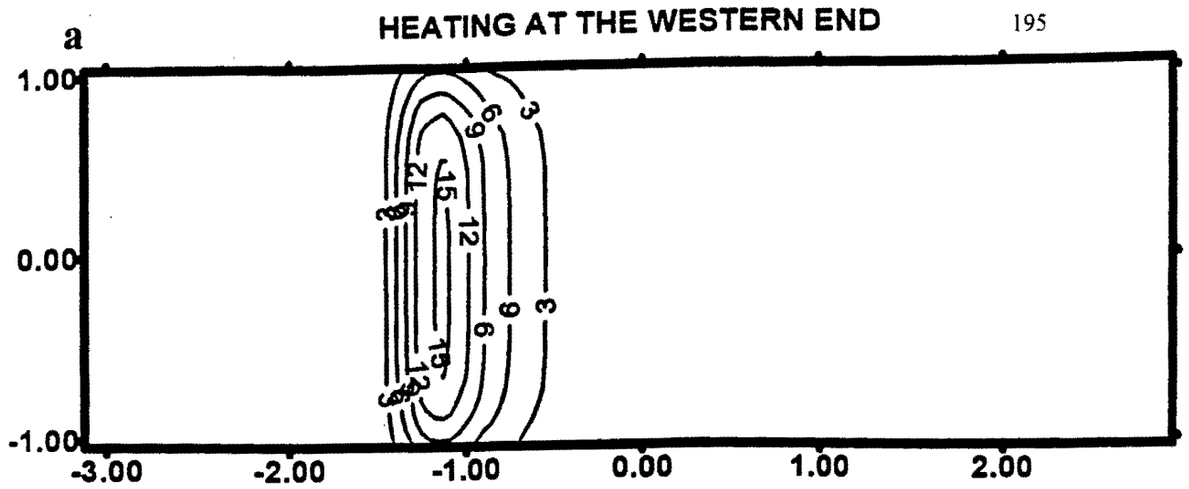

Figure 7.17 (a) Spatial distribution of prescribed surface heating

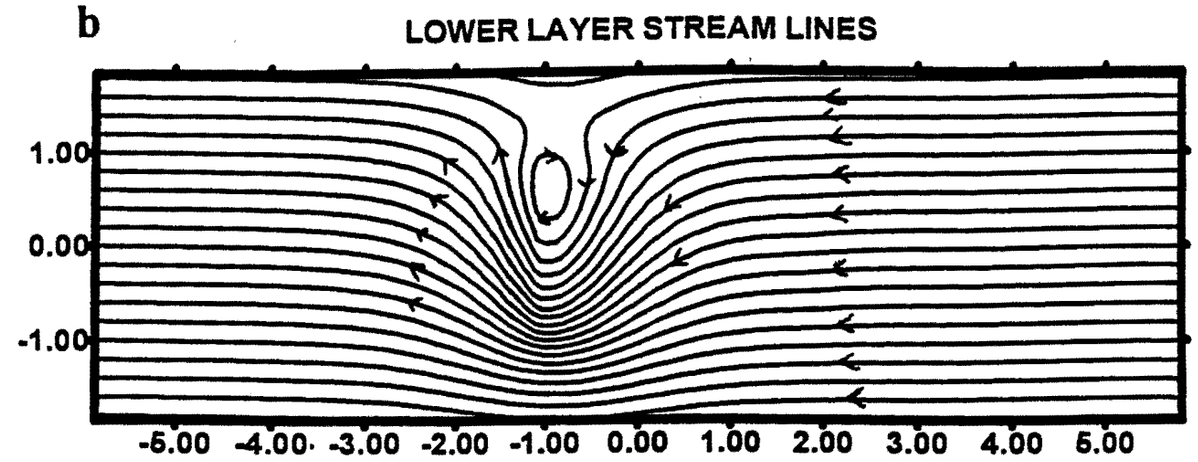

17.17 (b) Lower layer flow due to surface heating in a basic flow of upper level westerlies (U_1=1) and lower level easterlies (U_2=-1).

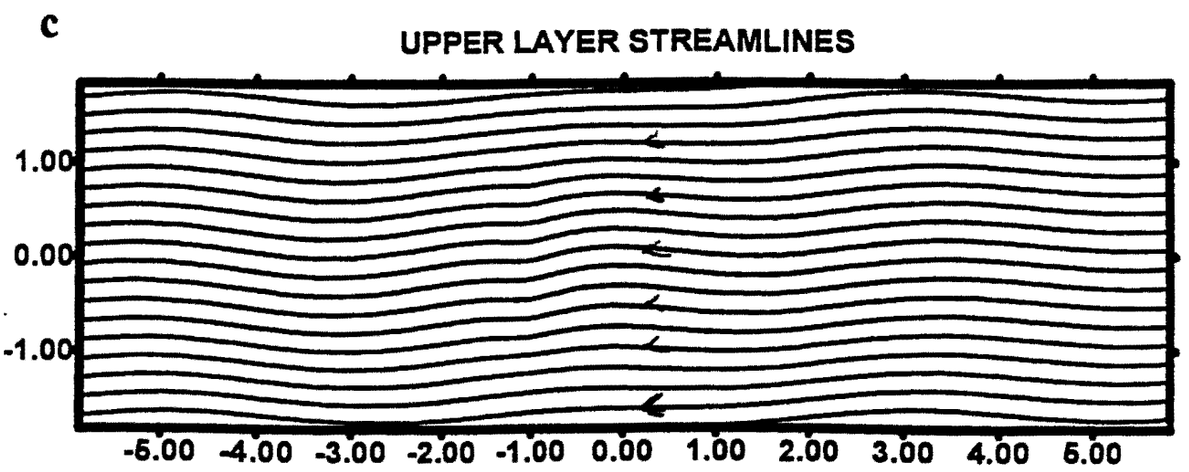

17.16 (c) Same as in figure 7.17 (b) but for upper level.

SCALE : 1 unit = 12.5 degrees, center (0, 0) corresponds to (22.5°S, 25°E)

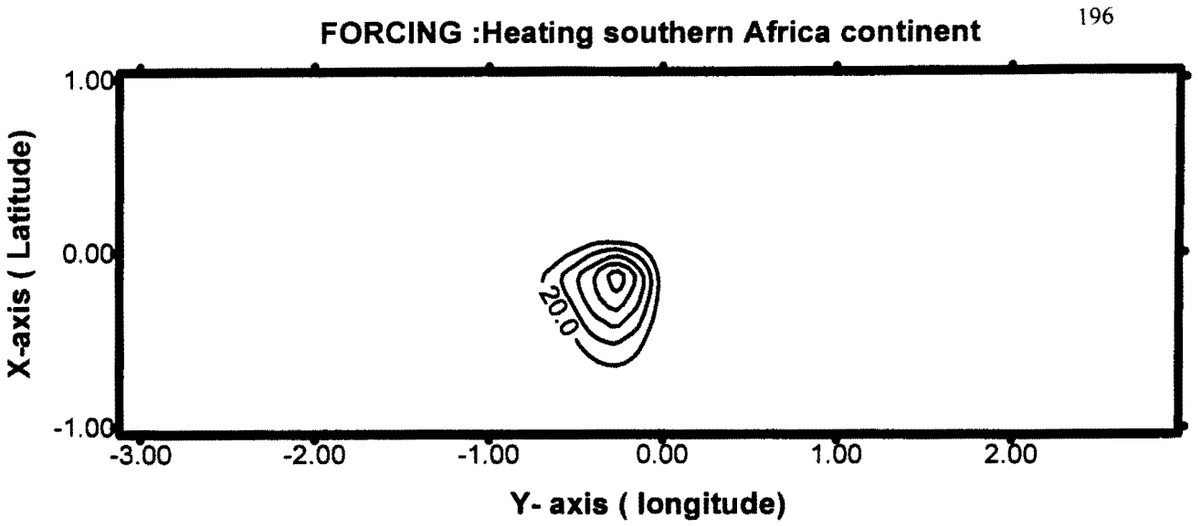

Figure 7.18 (a) **Idealised heating maximum over Kalahari desert**

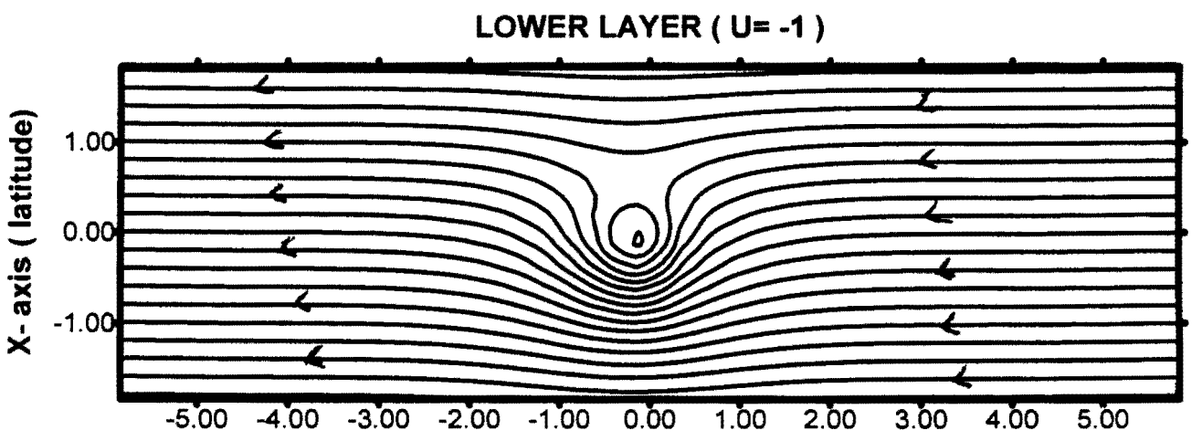

Figure 7.18 (b) **Lower layer flow due to above surface heating with lower level easterlies**

Upper layer flow due to idealised surface heating with upper level westerlies

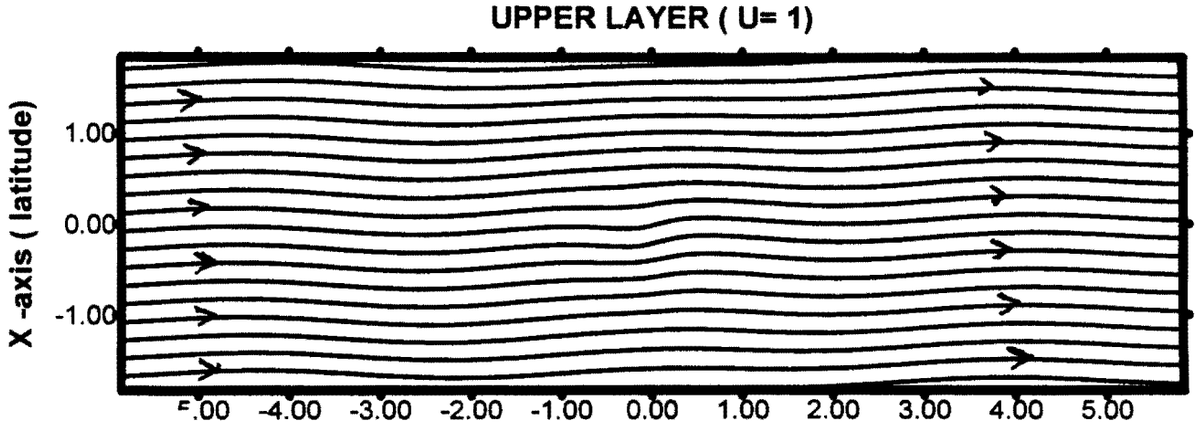

Figure 7.18 (c)

SCALE : 1 unit = 12.5 degrees, center (0, 0) corresponds to (22.5°S, 25°E)

FORCING :Cooler 'Atlantic ' warm ' southern Africa' and cool 'Indian'

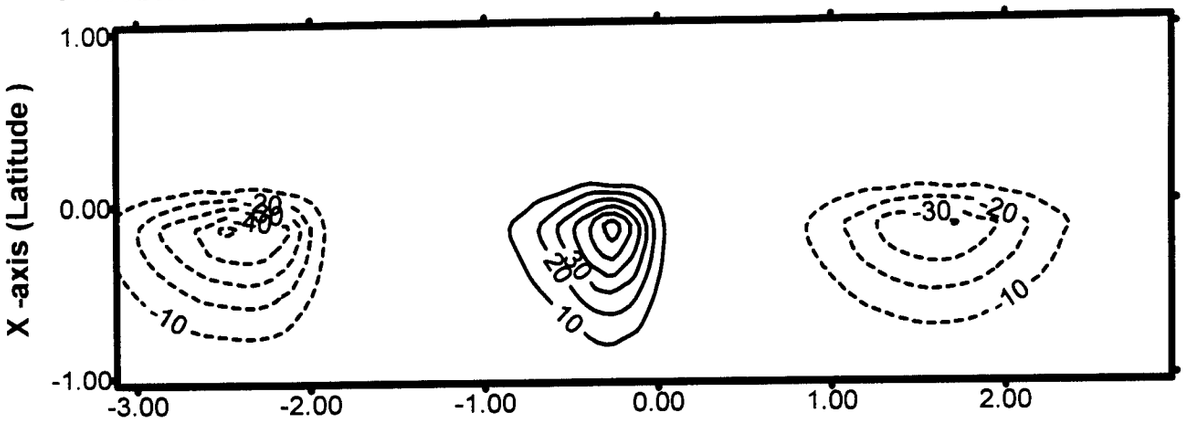

Figure 7.19(a)

Idealised heating maximum over Kalahari desert

LOWER LAYER (U = -1)

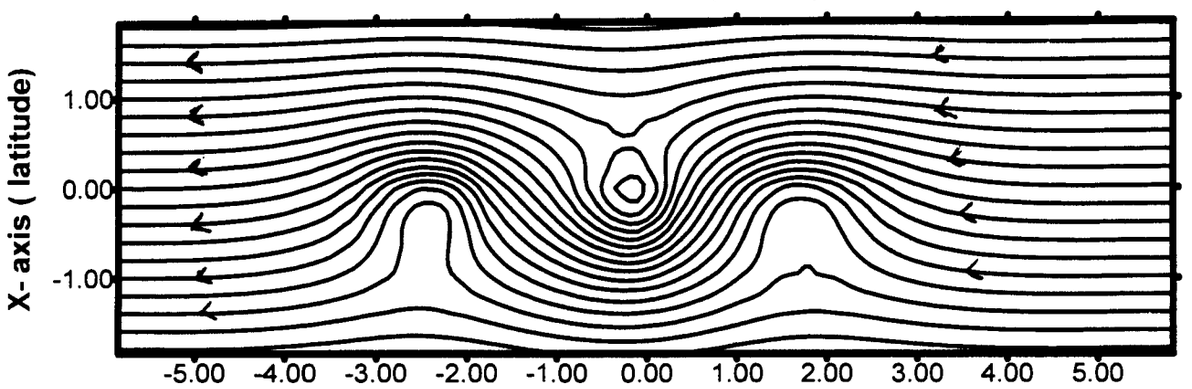

Figure 7.19(b)

Lower layer flow due to idealised surface heating with lower level easterlies

Upper layer flow due to surface heating in a basic flow with upper level westerlies

UPPER LAYER (U= 1)

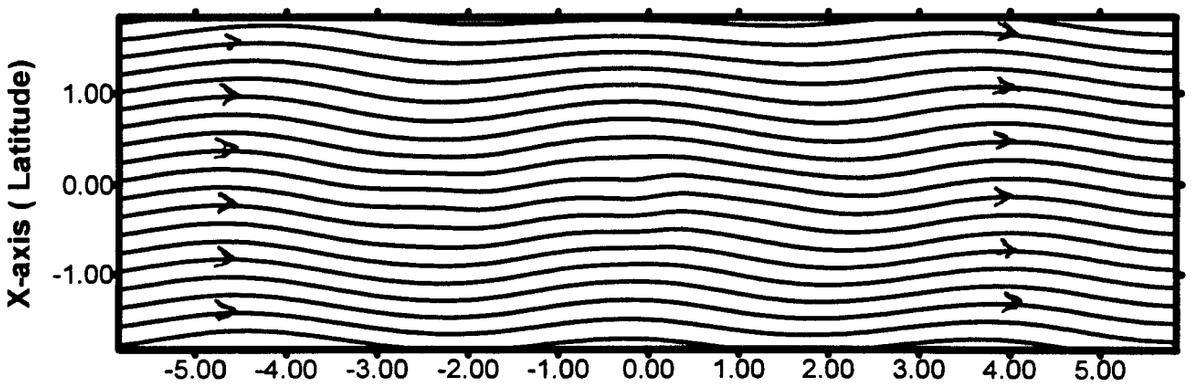

Figure 7.19(c)

SCALE : 1 unit = 12.5 degrees, center (0, 0) corresponds to (22.5°S, 25°E)

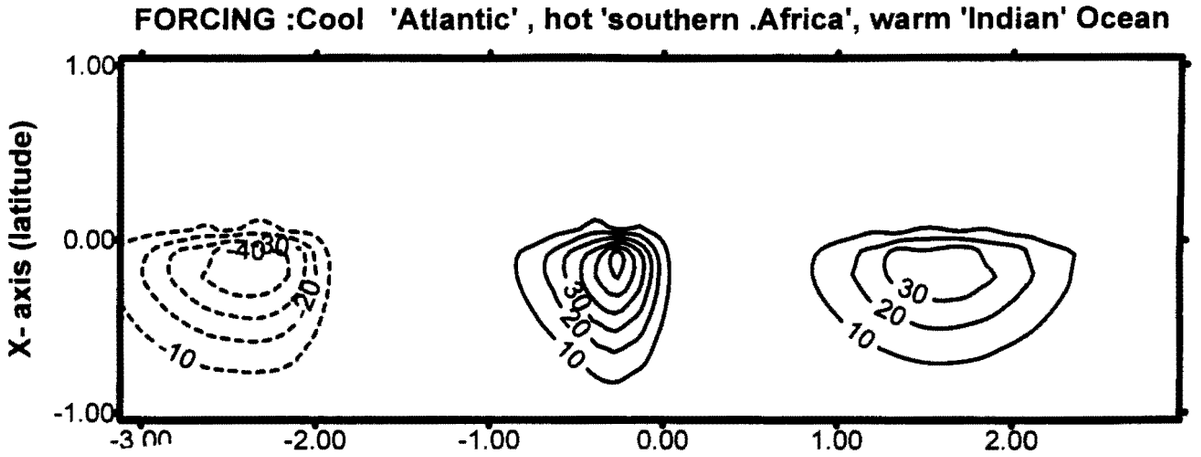

Figure 7.20 (a)

Idealised heating maximum over Kalahari desert and Indian Ocean

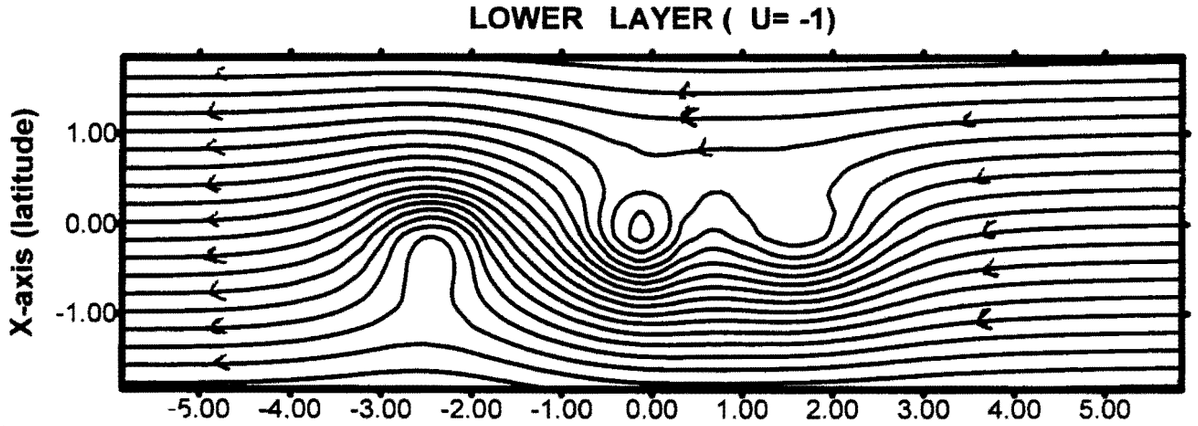

Figure 7.20 (b)

Lower layer flow due to above idealised heating with low lwvel easterlies

Upper layer flow with upper level westerlies

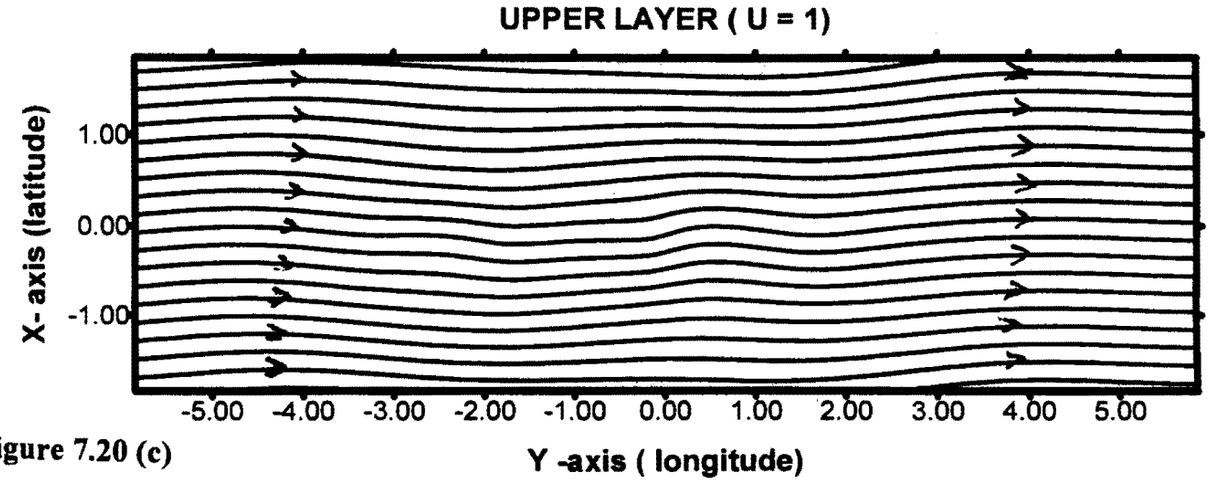

Figure 7.20 (c)

SCALE : 1 unit = 12.5 degrees, center (0, 0) corresponds to (22.5°S, 25°E)

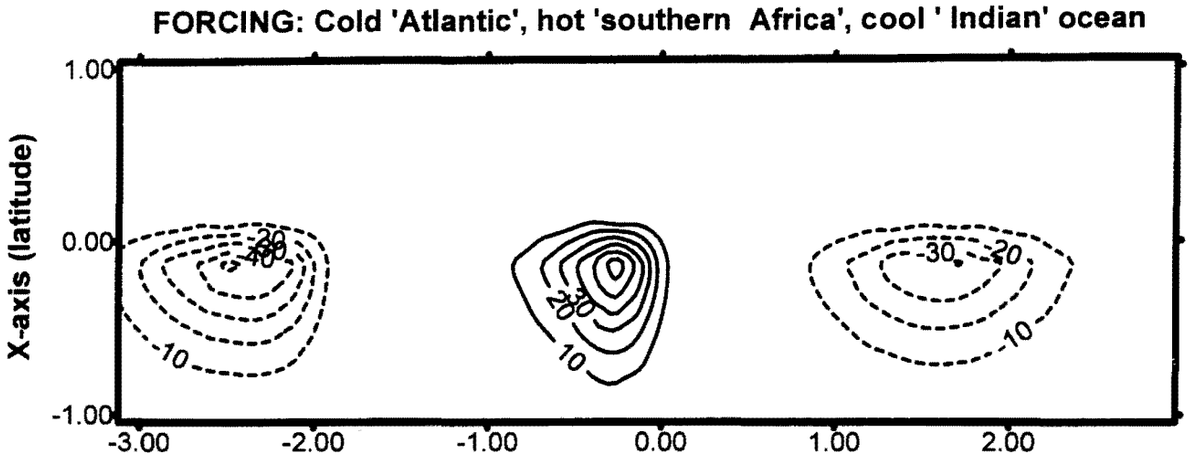

Figure 7.21 (a) **Idealised heating maximum over Kalahari desert**

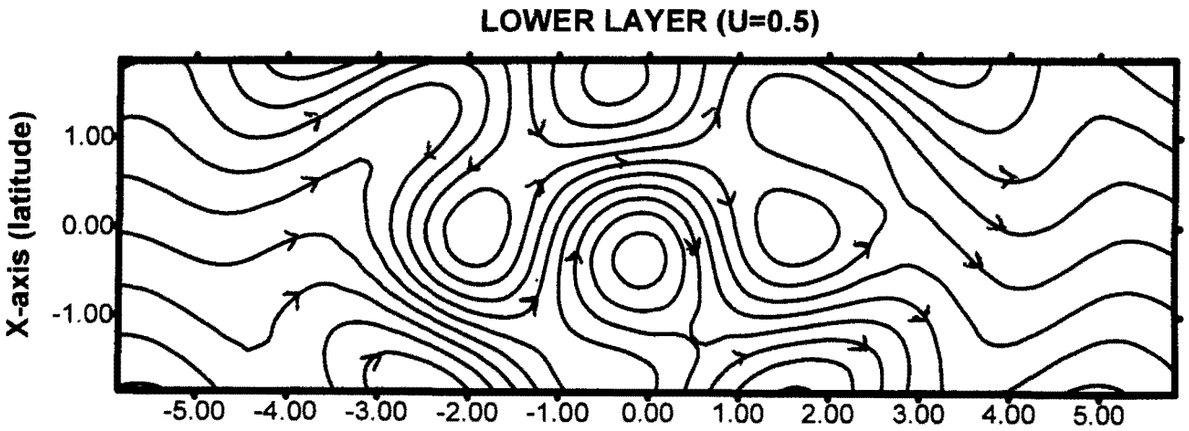

Figure 7.21 (b)

Lower layer flow due to idealised surface heating with lower level westerlies

Upper layer flow due to idealised surface heating with upper level easterlies

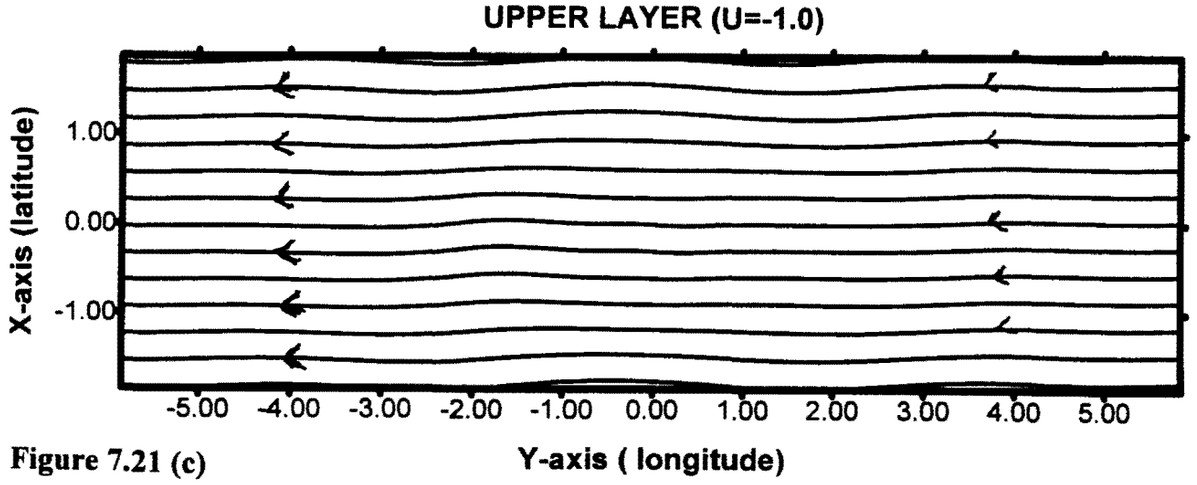

Figure 7.21 (c)

SCALE : 1 unit = 12.5 degrees, center (0, 0) corresponds to (22.5°S, 25°E)

CHAPTER 8

SUMMARY OF FINDINGS AND CONCLUSIONS

Roles of remote and local forcing of summer rainfall over southern Africa have been investigated through empirical and modelling studies. Objective and subjective analysis techniques have been used to determine the spatial and temporal structure of inter-annual and intra-seasonal variability of the southern African climate system. Mean characteristics of the summer circulation over southern Africa and adjacent Indian and Atlantic Oceans have been presented. Important features of variability in summer rainfall anomalies and sea surface temperature anomalies have been documented. Empirical relationships between rainfall anomalies and sea surface temperature anomalies have been found. One of the objectives of the thesis was to identify concurrent circulation anomalies in order to separate direct and indirect forcing of SST anomalies and this has been achieved through combined PCA. Teleconnections of the atmospheric circulation patterns over Africa and adjacent oceans were a focus of study. Therefore, PCA was applied to continuous monthly convective, kinematic and thermodynamic data in order to identify the tropical teleconnection patterns.

The mechanisms of rainfall variability over southern Africa have been linked to SST anomalies and most previous attempts have explained the rainfall variability by contrasting atmospheric conditions associated with dry and wet periods. Adjacent Indian, Atlantic SST anomalies and the global ENSO circulations are related to southern African summer rainfall. Here these have been linked to regional dynamics through the effect of zonal wind anomalies and heating over Angola. The ENSO phase has strong influence on southern African climate. In order to get a better picture on the workings of ENSO; correlations between SOI and regional circulations have been presented. Further investigation of ENSO effects was accomplished by computing lag correlation between SOI and selected PC modes as continuous time series. In previous attempts to explain seasonal

rainfall over South Africa, multiple regression and correlation analyses have been used and there has been no attempt to use combined PCA. In this thesis combined PCA was utilised in order to reveal coherent structures of summer between rainfall, OLR, SST and tropospheric wind anomalies. Tropical features have been found to be one of the controls of interannual rainfall variability. Extended Empirical Orthogonal Functions has been applied to investigate propagating features.

One of the stated objectives in this thesis was to demonstrate that intraseasonal variability in summer rainfall is linked to local forcing by the Angola low. Modelling of the formation of the Angola heat low using the quasi-geostrophic theory was carried out to prove the stated hypothesis. Previous studies on intraseasonal oscillations of southern Africa have utilised local rainfall indices, and no attempt was made to examine intra-seasonal convective activities associated with the Angola low. In the process of analysing the data in order to satisfy the stated aims and testing the ideas of the Angola low, insights have been gained on the variability of the summer circulation, Angola low convective activities, summer rainfall variability, tropical SST variability near Africa, and atmospheric teleconnection patterns. The main findings are summarised below.

8.1 Mean circulation characteristics over southern Africa and adjacent oceans

The thesis has documented a detailed description of southern African summer circulation by presenting the 14-year mean circulation features. The description of Southern African and oceans' circulation has been achieved via the ECMWF, NCEP OLR, UK Meteorological Office SST data sets and historical rainfall. A three dimensional structure of the summer circulation has been presented indicating the mean distribution of selected atmospheric variables. Mean significant meteorological features have been found.

For the period 1950 to 1990 a positive SST trend was observed over most parts of the oceans with highest values over the eastern and southwestern Atlantic,

southern and central parts of the Indian Oceans. High persistence in SST anomalies was found over the eastern Atlantic and northern parts of the Indian Oceans. The SST in these areas may be useful for long-range rainfall forecasting

8.2 Angola low

The Angola low has been identified in the mean field as one of the controlling factors of rainfall over southern Africa through cyclonic moisture convergence. The DJF 850hPa temperature mean thickness pattern for standard layer 850-500hPa indicates maximum values over southern Angola and northern Namibia. A vortex is found over Angola in the low-level circulation and water-vapour flux field and this proves the existence of the Angola thermal low. The inland low (Angola low) is maintained by radiative forcing, moisture convergence and higher surface temperature enhancing surface evaporation and low pressure at 850hPa. The supply of moisture over southern Africa reduces the role of vertical shear and without moisture the atmosphere may be stable. Thus absence of this continental low pressure may result in less moisture convergence and reduced rainfall over the subcontinent. High surface temperatures, evaporation and moisture convergence over the subcontinent maintain convective activities. Heating due to release of latent heat further results in the deepening of the thermal low and enhancement of moisture convergence. Upper level easterlies associated with convection may enhance the barotropic instability. The north-south temperature gradient is observed in the 850hPa temperature, 850-500hPa thickness and 500-200hPa thickness fields south of 25°S. These strong gradients support baroclinic modes which may influence the basic summer circulation. Significant convection occurs over the interior of the subcontinent (7°S-18°S, 18°E-40°E) where the mean OLR amounts to ~ 230 W m^{-2}. This area can be considered as the monsoon domain. Convective activity is associated with relatively high thickness, precipitable water and high values of upper level divergence. Tropospheric warming and ascending motion (due to release of latent heat and large-scale convergence) imply a direct

circulation over the subcontinent summer. Warm air is ascending over the subcontinent and cool air sinking over the adjacent oceans. Figure 8.1 shows how the repetitive CISK process may enhance the convective activities over land and dry zones over the adjacent oceans. The above findings emphasise the importance of heating (sensible and latent heat) over Angola and cooling of the adjacent ocean for the wet summer cases (figure 8.1).

8.3 Interannual variations of summer (DJF) rainfall over southern Africa

Before linking rainfall anomalies to SST anomalies, PCA was applied to summer (DJF) rainfall anomalies in order to identify temporal and spatial characteristics. Four regional scale, spatially coherent areas were identified. The centres of action of the four modes are found over Angola, southern Tanzania, eastern Botswana and Eastern South Africa. The first mode, which explains about 24% of the total variance, is the Angola mode, which exhibits ENSO temporal characteristics. Evidence of quasi-biennial oscillations (2-3 years) in rainfall is found to be strong in all the PC modes' time series. The long-term DJF rainfall trend is in decline over an area extending from Angola to southeastern parts of South Africa (KwaZulu Natal); a positive trend is evident over the north-east of the subcontinent and south-western parts of South Africa (Cape province). It should be noted that Angola rainfall PC pattern contributes most to inter-annual variability of summer rainfall.

8.4 SST temporal and spatial fluctuations in the Atlantic and Indian Oceans

In order to investigate the mechanism behind rainfall variability, one needs to understand inter-annual variations of SST anomalies within the Indian and Atlantic Oceans. Well-defined patterns of SST anomalies have been identified, but further analysis is required. The role of SST anomalies in the Atlantic and Indian Oceans on southern African climate was investigated by first revealing the spatial and temporal characteristics. Nine PC modes of standardised monthly SST anomalies have been extracted by the use of PCA. The first mode is spatially concentrated

over the central Indian Ocean and is closely identified with ENSO. Its time series contains an increasing trend. The rising SST there could explain the declining rainfall over southern Africa. The second mode focuses on the eastern equatorial Atlantic. It exhibits decadal oscillations, which are also found in PC8 near Brazil. The 3 to 5 year periods are quite evident in most SST modes. PC3 represents the Atlantic dipole, which is linked to West African rainfall. PC4 is located over the Agulhas warm current. PC5 to PC9 are midlatitude modes and can influence baroclinic disturbances and standing wave trains which in turn affect the circulation over southern Africa.

8.5.Statistical links between southern African summer rainfall features and SST anomalies

The summer rainfall PC modes and SST anomalies were lag correlated in order to investigate the mechanisms behind the different summer rainfall patterns. DJF PC1 rainfall Angola mode was linked to tropical SST in the central Atlantic and Indian Ocean SST. DJF PC2, PC3 and PC4 rainfall modes were also linked to central Indian Ocean SST anomalies. Periods of high anomalous SSTs in the tropical central Atlantic and Indian Ocean were identified with decreased rainfall in most of the PC modes. This work re-confirms the importance of tropical SST forcing on interannual oscillations of rainfall over Southern Africa.

Combined PCA shows that different summer rainfall anomalies over southern Africa were linked to different summer sea surface temperature patterns. The role of central Indian Ocean SST anomalies is quite evident in most of the rainfall anomalies. For the period 1950 to 1989 warm water over the Mozambique Channel, Agulhas current and cold waters over the central Indian Ocean was associated with wet summers over southern Africa. Reversal of the north-south SST gradient (equator and subtropics) enhances wet summers through thermal easterly winds.

8.6 Linkage between summer SST, convection and circulation anomalies

Identification and documentation of coherent summer circulation, SST and convection anomalies was achieved through analyses of concurrent variations. Identification of circulation anomalies directly (external SST-forced) or indirectly (internal dynamics) forced by SST anomalies was done. Four major features, which accounted for 61% of total variance, have been described. The first PC pattern (20%) demonstrated the role of internal dynamics. The pattern was associated with anomalous high SST and anticyclonic circulation over the subtropical regions with low-level convergence and upper level divergence over southern Africa. The second PC pattern (16%) was associated with SST-driven circulation anomalies and linked to ENSO. Large scale upper-tropospheric easterly wind anomalies co-occurred with a decreased north-south SST gradient over the Indian Ocean in wet summers due to this PC mode. This suggests that ENSO and southern African summer rainfall are linked together through the Walker circulation. The third feature (14%) was SST-forced over the Indian Ocean and internally forced over Atlantic Ocean. It indicates dry summers over southern Africa being associated with negative SST anomalies over most parts of both oceans. The fourth PC mode (11%) was SST-forced, with an increased north-south temperature gradient over the Indian Ocean. Warming in the south-west Indian Ocean led to dry summers over southern parts of southern Africa.

The combined PCA of summer SST, circulation and convection anomalies has demonstrated that different rainfall regimes are caused by different SST and circulation anomalies. Both internal and external forcing are important but the internal forcing shown by the first PC mode dominates.

8.7 Atmospheric anomaly patterns over southern Africa

The influence of tropospheric circulation anomalies on southern African climate was achieved by investigating first the characteristics of upper level features and identifying the major PC modes of selected atmospheric data. A Barotropic structure has been identified in the vertical structure of monthly geopotential anomalies with strong barotropicity over the midlatitudes and the Gulf of Guinea.

Time and space structures of interannual fluctuations of selected atmospheric dynamic and thermodynamic variables have been described by applying PCA to monthly standardised data. Tropical and midlatitude PC modes of variability have been found in 850-500 hPa thickness heights, 500 hPa geopotential heights, water vapour flux, winds and OLR anomalies. In most cases, the first three modes were retained. Tropical modes are dominant over midlatitude modes, probably due to the standardisation process. Some of the results are:

(i) Thickness (850-500hPa layer) and 500hPa geopotential height PC modes had almost similar spatial patterns. The first modes of lower thickness and 500 hPa geopotential had their centre of action located over the equatorial tropical Atlantic Ocean. The second PC mode of 500hPa geopotential heights had maximum loading over the tropical Indian Ocean. Extended Empirical Orthogonal Analysis (EEOF) was applied to 500hPa standardised monthly geopotential height in order to identify moving features as stated in the preface. Four modes of EEOF have been presented and account for 46% of the total variance. The first mode suggests a south-westward movement of pressure anomalies from the central Indian Ocean to the south Atlantic. The second PC mode shows westward movement of negative anomalies in the tropical band from the Indian Ocean to the tropical Atlantic, while positive anomalies are observed to shift from the equator to the South Atlantic Ocean. The third mode indicates an eastward movement of negative anomalies from the Equatorial tropical Atlantic to western parts of the Indian Ocean.

(iv) The first three modes of vector water vapour flux are centered over tropical oceans, with PC1 focusing on the western equatorial Atlantic explaining 10% of total variance. The first PC of OLR anomalies accounts for 11% of the total variance and has maximum loadings over the continental deserts. The second mode is over the Indian Ocean monsoon trough. The third mode is the tropical South Atlantic and the fourth mode is identified with southern Africa and accounts for 3.9% of the total variance.

8.8 Association between SOI and regional circulation features

In order to investigate the role of ENSO in southern African climate, correlation coefficient fields between SOI and regional circulations were presented. The relationship between DJF 500 hPa geopotential height anomalies and SOI show that cold events (high SOI) are associated with positive pressure anomalies in midlatitudes and negative anomalies in tropical bands. The SOI explains up to 36% of the DJF 500 hPa geopotential height anomalies over most parts of Africa and the midlatitudes (east of 20°E and west 40°E). During warm events (low SOI) a positive pressure anomaly is found over most parts of Africa and negative pressure anomalies in the midlatitudes. These relationships hold even six months before the peak rainfall (DJF). The correlation patterns reveal a 'see-saw' between midlatitudes (south of 35°S and east of 30°W) and the rest of the tropical band (including Africa and the Equatorial Indian Ocean).

The spatial distribution of zero lag correlation coefficients between DJF SOI and DJF OLR shows that the convective activities over southern African are out of phase with those over the south-west Atlantic and central Indian Oceans. Warm events are associated with below normal convective activities over southern Africa and above normal convection over eastern Africa and the central Indian and western Atlantic Oceans. Highest correlation coefficients (> 0.4) are found over the tropical Atlantic and southern Africa where the SOI explains 16% - 36% of the DJF OLR variability.

Lag/lead time correlations between SOI and the first two modes of 500hPa geopotential height anomalies suggest that there may be a feedback mechanism over West African and the central Indian Ocean. The SOI is correlated with PC1 mode time series of 850-500hPa thickness, 500hPa geopotential heights and PC4 of OLR. This result suggests that the Equatorial Atlantic Ocean and Southern African convective activities are closely associated with ENSO events on time scale of 2-4 years in the 1980-1993 period. Spectral analysis of SOI time series 1980-1993 reveals a 3.5 year period of oscillation.

8.9 Role of the Angola low in southern African climate evolution

Spectral analysis of the Angola OLR index reveals 10-30 day periods of oscillation in convective activities. After the identification of the Angola low from the mean fields, the composites of selected atmospheric variables associated with wet spells over Angola have been presented in order to document the thermo-dynamical and kinematic structures as stated in chapter 1. The Angola low and the extended zonal trough pattern are observed during the wet spells (Po composite for 850hPa temperature, 500hPa vertical velocity, precipitable water, 200hPa divergence and OLR. These patterns show the presence of the Angola low and the anchoring of the ITCZ over the subcontinent. It is also observed in PC3 of mean pentads. The anchoring is thus well documented. The other findings of the composite analysis are:

(i). Ten days before the onset of the wet spell, a deep cold low is observed over the southern Indian Ocean and moisture over southern Africa originates from the southern Indian ocean. During this time, high precipitable water is observed over southern Congo, Zambia and Mozambique Channel where convective activities occur. Surface heating leads the convection by 10 days. A direct circulation is observed at 500hPa level with warm air rising over Zambia and cold air sinking over the Kalahari Desert in southern Botswana. The large scale setting of the

pressure field requires pressure to rise over the Atlantic and falls over the Indian Oceans.

(ii). One pentad before the wet spell, a meridional pressure gradient is evident over southern Africa and the adjacent oceans. A high-pressure anomaly is observed over the southwest Indian Ocean which, controls easterly flow over areas south of 20°S. Southern African moisture is advected from the Atlantic and Indian Oceans. Two vortices with high precipitable water develop over Angola and east of Madagascar. Convective activities are observed over most parts of the subcontinent. The OLR and precipitable water anomalies suggest a southwestward movement of convection during the 10 days before the wet spell. Upper level divergence anomalies also suggest a westward shift.

(iii). During the wet spell, a meridional pressure gradient is maintained with a positive pressure anomaly over the south Indian Ocean and a negative pressure anomaly over the region east of Madagascar. Low level convergence over Angola during the wet spell is associated with large values of surface divergence anomalies over Madagascar and the Mozambique Channel. The inland vortex remains in the same position. South of 20°S, anomalous moisture comes from the Indian Ocean and north of 20°S, it originates from the Atlantic Ocean. High precipitable water is found over northern Namibia and southern Angola. Convective activities occur over most parts of the subcontinent except Swaziland and southern Mozambique. Direct circulation dominates in the middle and upper troposphere with an indirect circulation in lower troposphere. Both meridional and zonal gradients of temperature are observed. A baroclinic structure in winds and divergence is noted over tropical regions. Maximum upper level easterly anomalies are associated with areas of deep-convective activities.

(iv). Five days after the wet spell, a high-pressure anomaly is observed south of 30°S and the centre of the inland vortex is found over Zimbabwe. High precipitable water is confined to northern Namibia and Mozambique. A decline in

convective activities is evident by positive OLR anomalies over most parts of Southern Africa.

8.10 Thermal forcing and modelling of the continental trough

The local low level thermal forcing explains approximately 36% to 64% of the mean sea level pressure over southern Africa and the adjacent oceans. The local heating may reduce the static stability so that the tropical disturbance will not require much vertical wind shear to become unstable. Sensible heat flux from the surface provides the source of heating over Angola and is important in pre-rainy season since it may influence the long term mean moisture content of the atmosphere. For the period 1980 to 1993 the land/sea temperature contrast contributes 21% of the total temperature variance.

The effect of imposing different heating functions on southern Africa and adjacent oceans was investigated by using a two-layer quasi-geostrophic model. The solutions of the model show a large disturbance in the lower layer compared to the upper layer. It is seen from the solution that a low pressure develops over an area of maximum heating.

Numerical results show that a trough forms over the heating anomaly and is proportional to heating intensity. Ridges form over cooling anomaly areas. Under low level easterly winds the disturbance is confined to the anomaly but with low level westerly shear the anomaly spreads to other regions. It is seen that land-sea temperature contrasts play an important role in determining the low-level flow over southern Africa and the location of the heat low. The observed temperature contrast between land and ocean results in low pressures over the subcontinent and high pressures over adjacent oceans.

In conclusion the major features, which may influence summer rainfall variations over southern Africa are:

(a) Intensity of low level heating and development of the inland low,

(b) Various SST (remote) features especially over the central Indian Ocean,

(c) Tropospheric circulations either driven by internal or external forcing. In ENSO events external forcing dominates.
(d) Mid-level tropospheric pressure anomalies over the equatorial Atlantic Ocean.

In conclusion the summer rainfall anomalies have been found to be a function of several modes of SST and atmospheric circulation anomalies. It has been found that the heating over Angola plays the important role in determining the behaviour of the summer rainy season (figure 8.2). ENSO effects are identified with external (direct SST) forcing associated with large-scale zonal flow in the upper level. ENSO has also been linked to mid-tropospheric pressure anomalies over equatorial latitudes and a feedback mechanism exists. Thus, the heating over Angola, land/sea temperature contrast, tropical, subtropical SST anomalies and equatorial mid-tropospheric pressure anomalies should be considered when selecting predictors for long range-forecast models. The contribution of external dynamics can make seasonal forecasts possible while internal dynamics create problems on inter-annual time scales. Given the importance of SST forcings, modelling of SST may offer useful guidance in rainfall forecasts, to reduce environmental and societal vulnerability to climate fluctuations.

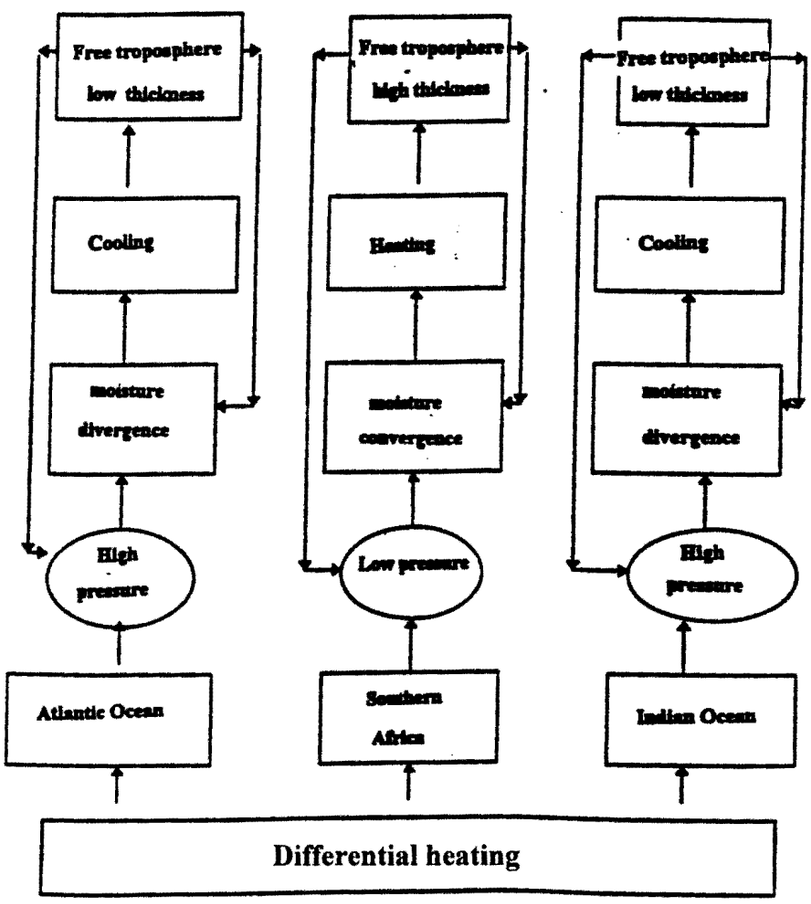

Figure 8.1 Schematic diagram showing the major summer mechanisms over southern Africa and the adjacent Indian and Atlantic oceans.

ROLE OF INTERNAL(INDIRECT FORCING BY SST) DYNAMICS

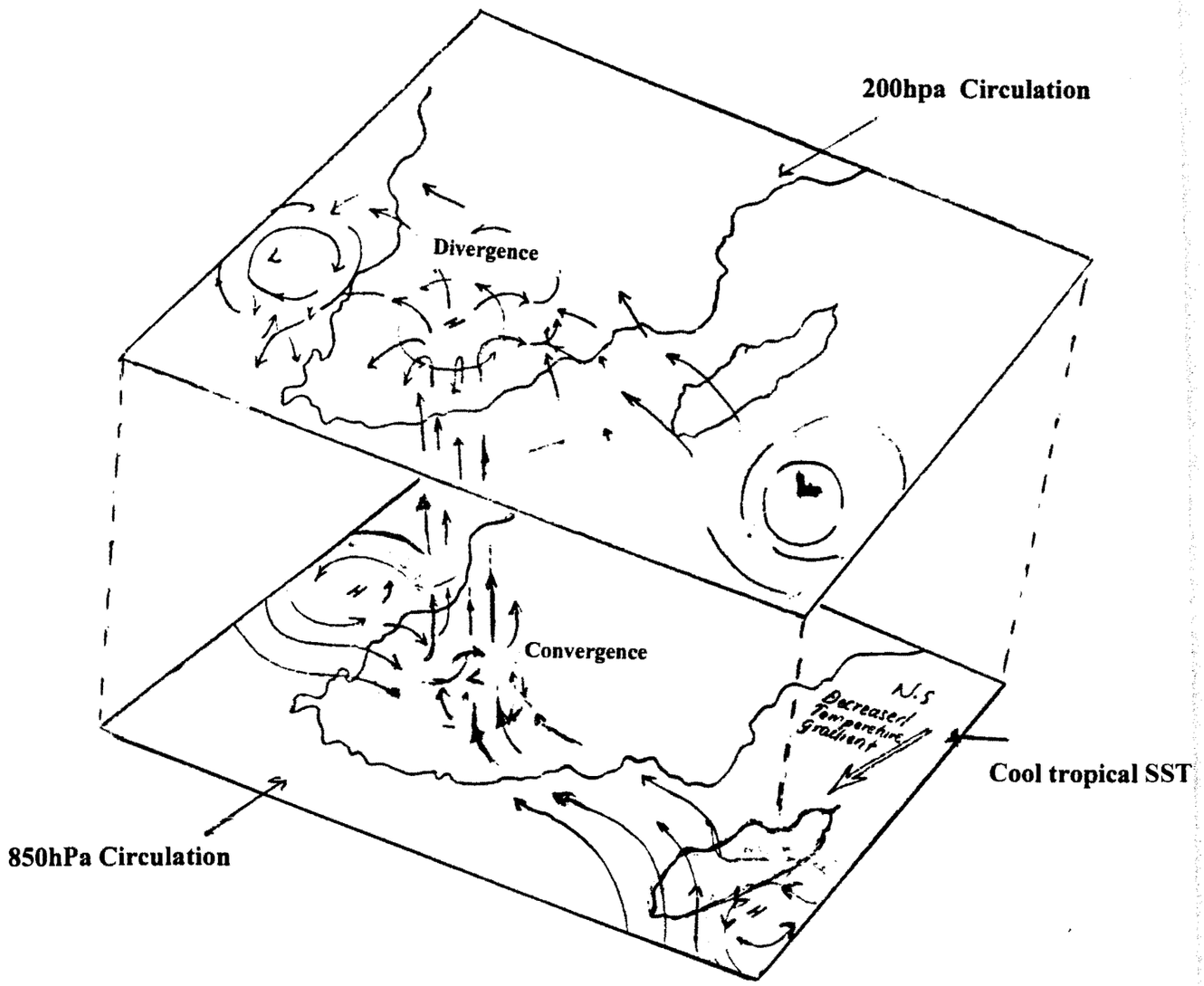

Figure 8.2 A schematic representation of 850hPa and 200hPa circulation associated with combined PC1 (21%) in figure 6.1 . This shows the contribution of internal dynamics. Note the low level convergence depend on the intensity of the inland low or Angola low.

Annex 1 : Table of pentad calender used in chapter 7

The below displays the pentad calendar, for reference

Pentad Number	Date	Month
14	07 - 11	December
15	12 - 16	December
16	17 - 21	December
17	22 - 26	December
18	27 - 31	December
19	01 - 05	January
20	06 - 10	January
21	11 - 15	January
22	16 - 20	January
23	21 - 25	January
24	26 - 30	January
25	31 - 04	February
26	05 - 09	February
27	10 - 14	February
28	15 - 19	February
29	20 - 24	February
30	25 - 01	March

Appendix

Annex 2

List of mathematical symbols used in chapter 4 .

$\frac{\partial}{\partial t}$ local rate of change

$V = (u,v)$ horizontal velocity in lower free atmosphere

$\vec{V}_B$ non dimensional horizontal boundary velocity

x, y *x and* y cordinate

$\vec{k}$ vertical unit vector

∇ $\nabla = i\partial/\partial x + j\partial/\partial y$, i and j are unit vectors

ϕ non-dimensional geopotential in lower free atmosphere

ε Rayleigh friction coefficient

δ kronecker delta function, switch-on parameter determined by the sign of precipitation and other conditions

N Newtonian cooling coefficient

G Coefficient of longwave radiational forcing

T_s, surface temperature

ρ_s air density in the boundary layer

d Depth of the boundary

B Heating coefficient due to boundary-layer moisture convergence

r Ratio of the equilibrium temperature deviation at the midtroposphere to SST deviation

F Coefficient of evaporation

T_* is 293.2° K

ε_* Rayleigh friction for free troposphere

β the meridional gradient of the coriolis parameter

C_0 the gravity wave-speed for the gravest baroclinic mode

R Gas constant

L_c Latent heat

b Efficiency of condensation heating

C_p Specific heat at constant pressure

S_2 Static stability at the middle of the free troposphere

μ the reciprocal of the Newtonian cooling

Δp Half pressur depth of the free troposphere

q_3, q_1, q_e specific humidity at the lower, the upper and the boundary layers respectively

p_s, p_e,p_2, g represent surface , boundary layer, mid-level pressure and the gravity respectively

C_E Coefficient of turbulent vertical moisture flux

K_q $6.95\text{x}10^{-4}\text{K}^{-1}$

A Coefficient of SST gradient forcing

K_D Surface friction coefficient

I Heating coefficient due to free-troposphere moisture convergence

E Ekman number of the boundary layer

REFERENCES

Abramowitz, M. and Stegun, I.A., (Eds) 1970: *Handbook of Mathematical functions,* Dover, 1043pp.

Acharya U. R and Rao N.S.B., 1981: Meteorology of Zambia Part 1 Meteorological Department , Lusaka, Zambia, 21pp.

Asnani G.C. Prof., 1993: *Tropical Meteorology.* Noble Printers Pvt Ltd., Pune India, Vol.1 and 2, 1202pp.

Baghare, M.M., 1978: Tropical cyclones over southern Africa with special reference to Weather over Zambia. *Meteorological notes*, Series A, 15, Zambia Meteorological Department.

Bengtsson, L. and Shukla, J., 1988: Integration of space and in situ observations to study global climate change. *Bulletin of American Meteorological Society.* **69**, 1130-1143.

Blackmon, M.L., Lee, Y. H. and Wallace J.M., 1983: Horizontal structure of 500mb height fluctuations with short intermediate and long time scales. In Hoskins B.J. and Pearce R.P (Editors), 1983: *Large-scale dynamical processes in the atmosphere* 57-91. Academic Press, London, 397pp.

Blade, E. and Hartman, D.L., 1995: The linear and non-linear extratropical response of the atmosphere to the tropical intra seasonal oscillations. *Journal of Atmospheric Science*, **52,** 4448-4471.

Bloomfield, P., 1976: *Fourier analysis of time series: An introduction.* Wiley and Sons, Inc. New York. 258pp.

Burroughs W., 1986: Randomners Rules the Weather. *New Scientist*, 10th July, 36-40.

Casey, T. M., 1997: Characteristics Anomaly pattern and equatorial East African rainfall, Fifth International Conference on southern hemisphere Meteorology and Oceanography, *American Meteorological Society*, 7-11 April, 1997, Pretoria, South Africa, 95.

Cavalcanti, I.F.A., 1997: Southern Hemisphere Climate Variability and Anomalies over South America, Fifth International Conference on southern hemisphere

Meteorology and Oceanography, *American Meteorological Society*, 7-11 April, 1997, Pretoria, South Africa, 93-94.
Chang, C.P. and Lim, H., 1988: Kelvin Wave CISK : A possible mechanism for 30-50 day oscillations. *Journal of Atmospheric Science.* **45**, 1, 1709-1720.

Chang, C.P., 1977: Viscous internal gravity waves and low frequency oscillations in the tropics. *Journal of Atmospheric Science.* **34,** 901-910.

Chang, J.H., 1972: *Atmospheric Circulation Systems and Climates.* Oriental Publishing Co. Honolulu; Hawaii, 298-319.

Charney, J. and Eliassen, A., 1964: On growth of the hurricane depression, *Journal of Atmospheric Science.* **21**, 68-75.

CLIVAR, 1995: World Climate Research Programme, Initial Science Plan, Draft, January, 1995.

CLIVAR, 1998: World Climate Research Programme, Initial Implementation Plan, WCRP, No 103, WMO/TD No 869 ICPO, 14, 145-160.

D'Abreton, P.C., 1992: The dynamics and energetics of tropical temperate tranfer over Southern Africa. Unpublished *PhD Thesis, University of Witswatersrand,* Johannesburg, South Africa. 231pp.

Das, P.K., 1986: *Monsoons,* Fifth IMO lecture, WMO-No-613 , World Meteorlogical Organization, 155pp.

Diaz, H.F., 1996: Precipitation monitoring for Climate change detection. *Meteorological Atmospheric Physics.* **60**. 179-190.

European Centre for Medium Range Weather Forecasts:(1994) The description of ECMWF/WCRP Level III-A. Global Atmospheric Data Archive.

Fandry, C.B. and Leslie, L.M., 1984: A Two Layer Quasi-Geostrophic Model of Summer Trough Formation in the Australian Subtropical Easterlies. *Journal of Atmospheric Sciences.* **41**, 5, 806-817.

Folland, C., Owen, J., Ward, W.M. and Colman, A. 1991: Prediction of seasonal rainfall in the Sahel region using empirical and dynamical methods. *Journal of Forecasting.* **10**, 21-56.

Fullard, H., Darby, H.C., O.B.E., Litt, D., 1975: The University Atlas, George Phillip and Son, London, Great Britain, 117.

Gadgil, S. and Srinivasan, J., 1996: Meridional migration of Tropical Convergence Zone. *Journal of Applied Meteorology*. **35**, 1189-1202.

Genstat 5 Committee, 1993: *Genstat 5 Release 3*. Statistics Dept., Rothamsted Experimental station. Clarendon Press and Oxford University Press, 1796pp.

Gershunov, A. and Michaelsen, J., 1996: Climatic-scale space time variability of tropical precipitation. *Journal of Geophysical Research*. **101**, D21, 297-307.

Gill, A.E., 1980: Some simple solutions for heat induced tropical circulations. *Quartlerly Journal of Royal Meteorological Society*. **106**, 447-462.

Gill, A.E., 1982: *Atmosphere-Ocean dynamics*. Academic Press, London, 662pp.

Goddard, L. and Graham N.E., 1997: GCM based Climate Forecasts over southern Africa, Fifth International Conference on southern hemisphere Meteorology and Oceanography, *American Meteorological Society*, 7-11 April, 1997, Pretoria, South Africa, 87-88.

Greenhut, G.K. 1979: Reply to Sciremammano F. "Comments on Correlations between rainfall and sea surface temperature during GATE" Journal of Physical Oceanography, **9**, 1298-1299.

Greenhunt, G.K., 1978: Correlations between rainfall and sea surface temperature during GATE. Journal of Physical Oceanography, **8**, 1135-1138

Harrison, M.S.J., 1983: The Southern Oscillation, Zonal equatorial circulation cells and South African rainfall, First International Conference on Southern Hemisphere Meteorology, *American Meteorological Society*. 302-305.

Harrison, M.S.J., 1984: A generalised classification of South African Summer rain bearing synoptic systems. *Journal of Climatology*. **4**, 547-560.

Harrison, M.S.J., 1986: A synoptic climatology of South African rainfall variations. Unpublished *PhD Thesis. university of the Witswatersrand*, Johannesburg, South Africa. 341pp.

Hastenrath, R., 1986: On Climate Predictions in the Tropics. *Bulletin of American Meteorological Society*. **67**, 6, 696-702.

Hastenrath, S, Nicklis A, and Greischar., 1993: Atmospheric-Hydrospheric mechanisms of climate anomalies in western equatorial Indian ocean, *Journal of Geophysical Research*. **98**, C11, 20219-20235.

Hayashi, Y.Y. and Sumi, A., 1986: The 30-60 day Oscillations simulated in an aqua-planet model . *Journal of Meteorological Society of Japan.* **64**, 451-467.

Holton, J.R., 1972: *An Introduction to Dynamical Meteorology*. Academic Press, New York. 319pp.

Hoskins, B. and Ambrizzi, T., 1993: Rossby wave propagation on a realistic longitudinally varying flow, *Journal of Atmospheric Sciences*, **50**, 12, 1661-1671.

Hoskins, B.J. and Karoly, D.J., 1981: The steady linear response of a spherical atmosphere to thermal and orographic forcing. *Journal of Atmospheric Sciences,* **38,** 1179-96.

Hoskins, B.J. and Pearce, R.P., 1983: *Large-scale Dynamical Processes in the atmosphere*. Academic Press, London. 397pp.

Hoskins, B.J., Hsu, H.H., James, I.N., Masutani, M., Sardeschmukh, P.D. and White, G.H., 1989: Diagonistics of the global atmosphere circulation based on ECMWF analyses; 1979-1989.

Hulme, M. and Kelly M., 1993: Exploring the Links Between Desertification and Climate Change. *Environment*, **35**, 6, 5-11, and 39-45.

Hulme, M., J.Arntzen, T.Downing, R.Leemans, J.Malcolm, N.Reynard, S.Ringrose, D.Rogers, E.Chiziya, D.Conway, A.Joyce, P.Jain, C.Markham, and H.Mulenga, 1996: *Climate change in Southern Africa; an exploration of some potential impacts and implications in the SADC region,* Report to WWF International , University of East Anglia, Climate Research Unit and WWF International,Gland Switzerland, 104pp.

Hulme, M., 1992: A 1951-1980 Global land and precipitation climatology for the evaluation of general circulation models. *Climate Dynamics*. **7**, 57-72.

Hulme, M., 1994: GU23WLD0093.DAT, version 1.0, December, 1994. Climatic Research Unit, School of Environmental Sciences, University of East Anglia, U.K. 1-5.

Hulme, M., and Jones P.D. 1993: A historical monthly precipitation dataset for global land areas: application for climate monitoring and climate evaluation. ppA/14-A/17 in *Analysis methods of precipitation on global scale.* Report of a GEWEX Workshop, 14-17 September 1992, Koblenz, Germany, *WMO/TD* No. 558, Geneva.

Hurrel, J.W. and Trenberth, K.E., 1992: An evaluation of monthly mean MSU and ECMWF Global atmospheric temepratures for monitoring climate. *Journal of Climate*. **5**, 1424-1440.

Janowiak, J.E., 1988: An investigation of interannual rainfall variability in Africa. *Journal of Climate*. **1**, 240-255.

Jenkins, G.M. and Watts, D.G., 1968: *Spectral analysis and its application,* Holden-Day, San Francisco, 525pp.

Johnston, R.J., 1992: *Multivariate Statistical Analysis in Geography*. Longman Scientific Technical. John Wiley and Sons, Inc. New York, 280pp.

Jury, M.R. , B. Parker and Waliser, D., 1994: Evolution and variability of the ITCZ in SW Indian Ocean : 1988-90, *Theoretical Applied Climatology.* **48**, 187-194.

Jury, M.R. and Pathack, B.M.R., 1991: A study of Climate and Weather variability over tropical SW Indian Ocean, *Meteorological Atmospheric Physics.* **47**, 37-48.

Jury M.R., 1992: A climatic dipole governing the interannual variability of convection over SW Indian Ocean and SE Africa region. *Trends in Geophysical Research,* **1**, 165-172.

Jury, M.R., 1995: Ocean atmosphere interaction research in the context of Southern Africcan climate variability. Oceanography Dept., University of Cape Town. Draft Report, 14pp.

Jury, M.R., 1996: Long-Range Climate Forecasting and User Needs in Southern Africa, Workshop on Reducing Climate-Related Vulnerability in Southern Africa,

1-4 October 1996 Victoria Falls, Zimbabwe, National Oceanic and Atmosspheric Administration, Office of Global Programs, 35-41.

Jury, M.R., Pathack, B. Rautenbach, C.J. deW. and van Heerden, J., 1996: Drought over South Africa and Indian Ocean SST: Statistical and GCM results. *Global Atmosphere and Ocean Systems*. **4**, 47-67.

Kabanda T.A., 1995: Seasonal and intraseasonal dynamics and precursors of rainfall over northern Tanzania. *Msc thesis , University of Cape-Town*, Cape Town, South Africa.

Karoly, D.J., 1985: An atmospheric climatology of southern hemisphere based on ten years of daily numerical analyses(1972-82); Standing wave climatology, *Australian Meteorological Magazine*. **33**, 105-116.

Keshavamurty, R.N. and Rao S.M., 1992: *The Physics of Monsoons*. Allied Publishers Ltd, New Delhi, 199pp.

Kiladis, G.N., 1997: Interannual variability of southern hemisphere circulation related to the southern oscillation, Fifth International Conference on southern hemisphere Meteorology and Oceanography, *American Meteorological Society*, 7-11 April, 1997, Pretoria, South Africa, 236-237.

Kiladis, G.N. and Diaz H.F., 1989: Global Climatic Anomalies Associated with Extremes in Southern Oscillation. *Journal of Climate*, **2**, 1069-1089.

Knutson, T.R., Weickman, K.M and Kutzbach J.E., 1986: Global scale intraseasonal oscillation of outgoing long wave radiation and 250mb zonal wind during the Northern Hemisphere summer. *Monthly Weather Review*. **114**, 605-623.

Krishnamurti, T.N. and Subrhmanyam, D., 1982: The 30-50 day mode at 850 mb during MONEX, *Journal of Atmospheric Science*. **39**, 2088-2095.

Kumar, S., 1978: Interaction of upper westerly waves with intertropical convergence zone and their effect on weather over Zambia during the rain season, Government Printers, Lusaka, 36pp.

Kuo, H. L., 1978: Two-layer model study of the combined barotropic and baroclinic instability in the tropics '*Journal of Atmospheric Science*. **35**, 1840-1860.

Kuo, H.L., 1989: Long-term oscillations in coupled atmosphere -ocean system and El-Nino phenomenon, *Journal of Climate.* 1989, **12**, 1421-1437.

Kushnir, Y., 1994: Interdecadal variations in the North Atlantic seas-surface temperature and associated atmospheric conditions. *Journal of Climate.* **7**, 141-157.

Kwon J.H., 1989: A Re-examination of the Genesis of African Waves. *Journal of the Atmospheric Sciences*, **46**, 24, 3621-3631.

Lau, K.M and Peng L., 1987: Origin of low frequency (intraseasonal) oscillations in the tropical atmosphere Part 1: Basic theory. *Journal of Atmospheric Science.* **44**, 6, 950-972.

Lau, K.M and Peng L., 1990: Origin of low frequency (intraseasonal) oscillations in the tropical atmosphere Part III: Monsoon Dynamics. *Journal of Atmospheric Science.* **47**, 12, 1443-1462.

Lau, K.M., 1992: East Asian Summer Monsoon Rainfall Variability and Climate Teleconnection. In Murakami, M. (Ed) 1992: *Asian Monsoon,* Universal Academy Press, Meteorological Society of Japan, Tokyo, 211-241pp.

Lau, K.M. and Lim, H., 1984: On the dynamics of equatorial forcing of climate teleconnections. *Journal of Atmospheric Science.* **41**, 161-176.

Lau, K.M. and Sheu, P.J., (1988): Annual cycle, Quasi-Biennial oscillation and southern oscillation in global precipitation. *Journal of Geophysical Research.* **93**. D9 10975-10988.

Legler, D.M., 1983: Emperical orthogonal function analysis of wind vectors over the tropical Pacific region. *Bulletin of American Meteorological Society.* **64**, No.3, 234-241.

Leslie, L.M., 1980: Numerical modelling of summer heat lows over Australia. *Journal of Applied Meteorology.* **19**, 381-387.

Levey, K.M., 1993: Intra-seasonal Oscillations of Convection over Southern Africa. *MSc. Thesis*, University of Cape Town. 236pp.

Levey, K.M. and Jury, M.R., 1996: Composite Intra-seasonal oscillations of convection over Southern Africa. *Journal of Climate*, **9**, 1910-1920.

Liebmann, B. and Hartmann, D.L., 1982:Interannual variations of outgoing IR associated with tropical circulation changes during 1974-78, *Journal of the Atmospheric Sciences, 39, 1153-1162*

Lim, H. and Chang, C.P., 1983: Dynamics of teleconnections and weather circulations forced by equatorial heating. *Journal of Atmospheric Science*. **40**, 1897-1915.

Lindesay, J. A., 1988: The Southern Oscillation and flow fields over southern Africa. Unpublished Ph.D. Thesis. University of Witwaterssrand, 284 pp.

Lindesay, J.A. and Jury, M.R., 1991: Atmospheric circulation controls and characteristics of a flood event in Central South Africa, *International Journal of Climatology*. **11**, 609-627.

Lutjeharms, J.R.E. and Van Ballegooyen, R.C., 1988: Retroflection of the Agulhas Current. *Journal of Physical Oceanography,* **18**, 1570-1583.

Madden, R.A. and Julian, P.R., 1971: Detection of a 40-50 day oscillation in the zonal wind in tropical pacific. *Journal of Atmospheric Science*. **28**, 702-708.

Madden, R.A. and Julian, P.R., 1994: Observations of the 40-50-Day Tropical Oscillation- A Review. *Monthly Weather Review,* **122**, 814-837

Majodina M., 1995: Composite analysis of winter storms south of Africa, *Honours thesis,* University of Cape Town, Cape Town, South Africa.

Majodina, M. and Jury, M.R., 1996: Composite winter cyclones south of Africa: Evolution during eastwards transit over Agulhas warm pool. *South African Journal of Marine Science*. **17**, 241-252

Makarau, A., 1995: Intra-seasonal oscillatory modes of Southern Africa summer circulation. *PhD thesis. University of Cape Town*, Cape Town, South Africa.

Mason J.M., 1992: Sea surface temperatures and South African rainfall variability, *PhD thesis, University of the Witwatersrand*, Johannesburg, South Africa. 235pp

Mass, C., 1979: A linear primitive-equation model of African wave disturbances. *Journal Atmospheric Science, **36**, 2075-2092.*

Matarira C.H. and Jury M.R., 1992: Contrasting Meteorological Structure of Intra-seasonal Wet and Dry Spells in Zimbabwe. *International Journal of Climatology*, **12**, 165-176.

Matarira, C.H. and Unganai, L.S., 1995: A rainfall prediction model for Southern Africa based on Southern Oscillation phenomena. FAO/SADC Regional Early Warning System Project, Harare, Zimbabwe.

Matsuno T.,1966: Quasi-Geostrophic Motions in the Equatorial Area. *Journal of the Meteorological Society of Japan*, **44,** 25-43.

Miron, O. and Tyson, P.D., 1984: Wet and dry conditions and pressure anomaly fields over South Africa and adjacent oceans 1963-1979. *Monthly Weather Review.* **112**, 2127-2132.

Mo K.C. and Higgin, W., 1997: The Pacific South American Modes and Tropical Intraseasonal Oscillations, Fifth International Conference on southern hemisphere Meteorology and Oceanography, *American Meteorological Society*, 7-11 April, 1997, Pretoria, South Africa, 218.

Montgomery, R.B., 1940: Report on the work of G.T. Walker, *Monthly Weather Review*, **39**, (supplement), 1-22.

Mudenda, O.S. and Mumba, Z.L.S., 1997: The unusual Tropical storm of January, 1996 over Zambia. In Fifth International Conference on Southern Hemisphere Meteorology and Oceanography. *American Meteorological Society* 7-11th April, 1997. Pretoria, South Africa. 332-333.

Murakami T., Wang B and Lyons S.W., 1992: Contrasts Between Summer Monsoons over the Bay of Bengal and the Eastern North Pacific. *Journal of the Meteorological Society of Japan*, **70**, 61-67.

Mumba, Z.L.S. and Chipeta, G.B., 1984: Synoptic aspects of rainfall in Zambia. *Zambia Meteorological Notes*; Series A, **20**. Zambia Meteorological Department, Lusaka, Zambia. 66pp.

Murakami, T., Wang, B. and Lyons S.W., 1992: Contrast Between Summer Monsoons over the Bay of Bengal and the eastern North Pacific. In Murakami M. (Ed) 1992: *Asian Monsoon*. Universal Academy Press, Meteorological Society of Japan, Tokyo. 61-79.

Nanjundiah, R.S., Srinivasan, J. and Gadgil, S., 1992: Intra-seasonal variation of the Indian summer Monsoon: In Mukarami M. (Ed) 1992: *Asian Monsoon.* Universal Academy Press, Meteorological society of Japan, Tokyo. 529-550.

Neelin J.D, Held I.M and Cook K.H., 1987: Evaporation-wind feedback and low frequency variability in tropical atmosphere . *Journal of Atmospheric Science.* **44**, 2341-2348.

Nicholson S.E., 1986: The Spatial Coherence of African Rainfal Anomalies. Inter-hemispheric Teleconnections. *Journal of Climate and Applied Meteorology*, **25**, 1365-1381 .

Nicholson, S.E. and Entekhabi, D., 1986b: The Quasi-periodic behaviour of rainfall variability in Africa and its relationship to the southern oscillation. *Archives of Meteorology of Geophysics*. Bioklimatol., Series **A.34**, 311-348.

Nicholson, S.E. and Nyenzi, B.S., 1990: Temporal and Spatial variability of SST's in the Tropical Atlantic and Indian Ocean. *Meteorology and Atmospheric Physics*, **42**, 1-17.

Nicholson, S.E.,1997: An analysis of the ENSO signal in the tropical Atlantic and Western Indian Oceans. *International Journal of Climatology*, **17**, 345-375.

Nigam, S. and Shen H.S., 1993: Structure of Oceanic and atmospheric low-frequency variability over the Tropical Pacific and Indian Oceans. Part 1: COADS Observations, *Journal of Climate*, **6,** 657-676.

North, G.R., Bell, T.L., Cahalan, R.F. and Moeng, F.J., 1982: Sampling errors in estimation of empirical orthogonal functions. *Monthly Weather Review.* **110**, 699-706.

Numerical Algorithm Group Ltd 1990: NAG Fortran Library, Introductory Guide Mark, 14, Wilkinson House Oxford UK.

Ogallo L.J., 1988: Relationships Between Seasonal Rainfall in East Africa and Southern Oscillation. *Journal of Climatology*, **8**, 31-43.

Okoola, R.E., 1989: Westwards moving disturbances in south-west Indian Ocean. *Physics Meteorological Atmospheric*. **41**, 35-44.

Pathack, B.M.R., 1993: Modulation of South African summer rainfall by global climatic processes. PhD thesis, University of Cape Town, Cape Town, South Africa. 261 pp.

Preisendorfer, R.W. and Mobley, C.D., 1988: Principal component analysis in meteorology and oceanography. Elsevier Science Publishers, New York USA 425pp.

Preston-Whyte, R.A and Tyson P.D, 1988: *The atmosphere and weather of Southern Africa*, Oxford University Press , Cape Town, 374pp.

Quinn, W.H and Neal V.T., 1983: Long -term variations in the Southern Oscillation, El-Nino and Chilean subtropical rainfall, *Fishery Bulletin* **81**, 363-374.

Ramage, C.S., 1971: *Monsoon Meteorology*, Academic Press; New York, 296pp.

Rashid, M.H.A., 1997: Some aspects of low-frequency variability of the southern hemisphere oscillation, in Fifth International Conference on Southern Hemisphere Meteorology and Oceanography, 7-11 April 1997 Pretoria South Africa. 89-90.

Rautenbach, C J deW., 1997: A GCM describing teleconnections between global SST anomalies and the Copious summer rainfall over Southern Africa (1995/1996). Fifth International Conference on southern hemisphere meteorology on Southern Hemisphere Meteorology and Oceanography, *American Meteorological Society*, 7-11th April 1997, Pretoria, South Africa 1-2.

Reason, C.J.C, Allan, R.J, Lindesay J.A. and Spenning, G.C.R, 1997: Mechanism associated with low frequency climate variability in the south Indian Ocean region, Fifth International Conference on southern hemisphere Meteorology and Oceanography, *American Meteorological Society*, 7-11 April, 1997, Pretoria, South Africa, 3-4.

Reason, C.J.C., 1996: Topography and the Dynamical Response to easterly flow in Southern Hemisphere West Coast regions. *Meteorological Atmospheric Physics*. **61**, 187-199.

Reason, C.J.C., Allan, R.J. and Lindesay, J.A., 1996: Evidence for the influence of remote forcing on interdecadal variability in Southern Indian Ocean. *Journal of Geophysical Research.* 1996: **101**, C5, 11867-11882.

Reason, C.J.C., Godfred-Spenning, C.R., Allan, R..J. and Lindesay J.A., 1998: Air-sea interaction mechanisms and low frequency climate variability in the south Indian ocean region. *International Journal of Climatology* **18,** 91-3405.

Reason, C.J.C., and Lutjeharms, J.R.E., 1998: Variability of South Indian Ocean and implications for southern African rainfall, *South African Journal of Science,* **94,** 115-123.

Richman, M.B., 1986: Rotation of principal components. *Journal of Climatology.* **6,** 293-335.

Rinker, D.K. Jnr. and Young, G.S., 1996: Use of obliquely rotated principal component analysis to identify coherent structures. *Boundary Layer Meteorology.* 80, 19-47.

Rocha, A. and Simmonds, I., 1997a: Rainfall variability over the Sahel and Kalahari regions and its associations with sea surface temperature, Fifth International Conference on southern hemisphere Meteorology and Oceanography, *American Meteorological Society*, 7-11 April, 1997, Pretoria, South Africa, 7-8.

Rocha, A. and Simmonds, I., 1997b: Distinct modes of SST -forced rainfall variability over southern hemisphere continents, Fifth International Conference on southern hemisphere Meteorology and Oceanography, *American Meteorological Society*, 7-11 April, 1997, Pretoria, South Africa, 91-92.

Rocha, A.M.C. 1992: The influence of global sea surface temperature on southern African summer climate, *PhD thesis*, University of Melbourne, Melbourne, Australia, 249pp.

Rocha, A. and Simmonds, I., 1997d: Interannual variability of south-eastern African summer rainfall. Part II. Modelling the impact of sea-surface temperatures on rainfall and circulations. *International Journal of Climatology.* **17**, 267-290.

Rocha, A., and Simmonds, I., 1997c: Interannual variability of south-eastern African summer rainfall. Part I: Relationships with air-sea interaction processes. *International Journal of Climatology.* **17**, 235-265.

Ropelewski, C.F. and Halpert, M., 1996: Quantifying Southern Oscillation-Precipitation relationships. *Journal of Climate*. **9**, 5 May, 1996. 1043-1059.

Rowson, D.R. and Coloucci, S.J., 1992: Synoptic Climatology of Thermal low-pressure systems over south-western north America. *International Journal of Climatology*. **12**, 529-545.

Rui, H. and Wang, B., 1990: Development characteristics and dynamic structures of tropical intraseasonal convectional anomalies. *Journal of Atmospheric Science*. **47**, 357-379.

Semazzi, F.H.M. and Sun, L., 1997: The Role of orography in determining the Sahelia Climate. *International Journal of Climatology*. **17**, 581-596.

Semazzi, F.H.M., Burns, B. and Schemm, J.K., 1996: A GCM study of teleconnections between the continental climate of Africa and global sea surface temperature anomalies. *Journal of Climate*. **9**, 10, 2480-2497.

Semazzi, H.F.M., 1980: Stationary barotropic flow induced by a mountain over a tropical belt. *Monthly Weather Review*. **108**, 922-930.

Sheng, J. and Hayashi, Y., 1990a: Estimation of atmospheric energetics in the frequency domain during the FGGE year. *Journal of Atmospheric Science* **47** 1255-1268.

Sheng, J. and Hayashi, Y., 1990b: Observed and simulated energy cycles in the frequency domain. *Journal of Atmospheric Science*. **47**, 1243-1254.

Smith, E.A., 1986: The Structure of the Arabian heat low. Part 1. Surface energy budget. *Monthly Weather Review*. **114,** 1067-1083.

Srinivasan, J. and Smith, G.L., 1996: Meridional Migration of Tropical Convergence Zone. *Journal of Applied Meteorology*, **35,** 1189-1202.

Statistica , 1995: *Statistica for Windows Quick reference*, StatSoft, Inc, 2325 East 13th street, Tulsa, OK, USA. 197pp.

Sui, C.H. and Lau, K.M., 1989: Origin of lower frequency (intraseasonal) oscillations in the tropical atmosphere. Part II. Modification of mobile wave CISK modes by boundary forcings. *Journal of Atmospheric Science*. **46,** 37-56.

Tennant, W.J., 1996: Influence of Indian Ocean sea surface temperature anomalies on the general circulation of southern Africa. *South African Journal of Science*. **92**, 289-295

Theron, G.F. and Harrison, M.S.J., 1990: Thermodynamic properties of the mean circulation around Southern Africa, *Theoretical and Applied Climatology*, **43**, 161-174.

Thiao, W., 1996: Summary of lessons learned from climate predictions for Southern Africa in 1992-95, Workshop on Reducing Climate-Related Vulnerability in Southern Africa, 1-4 October 1996 Victoria Falls, Zimbabwe, National Oceanic and Atmosspheric Administration, Office of Global Programs, 43-54.

Trenberth, K.E., 1980: "Planetary Waves at 500 hPa in Southern Hemisphere" *Monthly Weather Review,* **108**, 1378-1389.

Trenberth, K.E.and Olson, J.G., 1988: An evaluation and inter comparison of global analyses from the National Meteorological Centre and European Centre for Medium Range Weather Forecasts. *Bulletin of American Meteorological society.* **69**, 1047-1057.

Tyson, P.D., 1980: Temporal and spatial variation rainfall anomalies in Africa south of latitude 22° during the period of meteorological record. *Climate Change* **2**, 363-371.

Tyson, P.D., 1981: Atmospheric circulation variations and the occurrence of extended wet and dry spells over Southern Africa. *Journal of Climatology*. **1**, 115-130.

Tyson, P.D., 1984: The atmospheric modulation of extended wet and dry spells over South Africa 1958-1978, *Journal of Climatology,* **4**, 621-635.

Underhill L.G., 1981: *Introstat* (3rd ed), Juta and Company, Ltd, Creda Press, Cape Town, South Africa. 383pp .

van Loon, H., 1972: Temperature, pressure and wind in southern hemisphere. Meteorological Monograph. *American Meteorological Society*. **13**, 25-100.

Walker, G.T. and Bliss, E.W., 1932: World Weather, *Royal Meteorological Society*, **4**, 53-84.

Walker, N.D., 1989b: Sea surface temperature - rainfall relationships and associated ocean atmosphere coupling mechanisms in the southern African region. Unpublished *PhD. thesis, University of Cape Town*, Cape Town South Africa. 171pp.

Walker, P., 1989a: *Famine Early Warning Systems*: Victims and Destitution. London; Earthscan.

Wallace, J.M. and Gutzles, D.S., 1981: Teleconnections in the geopotential height field during northern hemisphere winter. *Monthly Weather Review*. **109**, 785-812.

Wang, B., 1992: Dynamics of tropical low frequency waves: The vertical structure and development of ENSO anomaly mode during 1979-1989 *Journal of Atmospheric Science* **49**, 9, 698-712.

Wang, B., 1988: Dynamics of tropical low frequency waves: An Analysis of the moist Kelvin wave. *Journal of Atmospheric Science* **45**, 14, 2051-2065

Wang, B. and Li, T., 1993: A simple tropical model of relevance to short -term climate variations. *Journal of Atmospheric Science* **50**, 2, 260-284

Wang, B. and Xie, X., 1997: A model for Boreal summer intraseasonal oscillation, *Journal of Atmospheric Science*, **54**, 1, 72-86.

Wang, B. and Rui, H., 1990: Synoptic Climatology of Transiet Tropical Intraseasonal Convection Anomalies: 1975-1985 *Meteorological Atmosphere Physics*. 43-61.

Weare, B. and Nasstrom, S., 1982: Examples of extended emperical orthogonal function analysis. *Monthly Weather Review*, **110**, 481-485.

Webster, P.J., 1981: Mechanisms determining the atmosphere response to sea surface temperature anomalies, *Journal of Atmospheric Sciences*, **38**, 554-571.

Webster, P.J., 1972: Response of the tropical atmosphere to local steady forcing. *Monthly Weather Review*. **100**, 518-540.

Webster, P.J., 1973: Remote forcing of time independent tropical atmosphere. *Monthly Weather Review*. **101**, 58-68.

Webster, P.J., 1983: Mechanisms of monsoon low frequency variability; surface hydrology effects. *Journal of Atmospheric Science,* **40**, 2110-2127.

William, J. E. and R.E. Thomson, 1997: *Data Analysis Methods in Physical Oceanography*, Gray Publishing, Tunbridge Wells, Kent, 634pp.

WMO Bulletin 1994; **43**, 3.

Woodruff, S.D., Slutz, R.J., Jenne, R.L. and Steuer, P.M., 1987: A Comprehensive Ocean Atmosphere Data Set. *Bulletin of American Meteorological Society.* **68**, 1239-1250.

WMO, 1996: *World Food Summit*, United Nations Food and Agricultural Organisation http://www.dpie.gov.au/dpie/conference/wfs/tech.html

Xie, X. and Wang, B., 1996: Low frequency equatorial waves in vertically sheared zonal flow Part II : Unstable waves, *Journal of Atmospheric Science* **53**, 23, 3589-3605.

Yuen, C.K. and Fraser, D., 1979: *Digital Spectral Analysis*, CSIRO, Pitman Publishing Ltd., and Fearon Pitman Publishers Inc., 156pp.